Principles and Basics of InSAR

Irena Hajnsek
*Earth Observation and Remote Sensing,
Institute of Environmental Engineering, ETH Zürich
*Microwaves and Radar Institut,
German Aerospace Center, Oberpfaffenhofen

Earth Observation and Remote Sensing

hajnsek@ifu.baug.ethz.ch
irena.hajnsek@dlr.de

ETH
Eidgenössische Technische Hochschule Zürich
Swiss Federal Institute of Technology Zurich

SAR Polarimetry (PolSAR)

Allows the identification / decomposition of different scattering processes occurring inside the resolution cell

SAR Interferometry (InSAR)

Allows the location of the effective scattering center inside the resolution cell

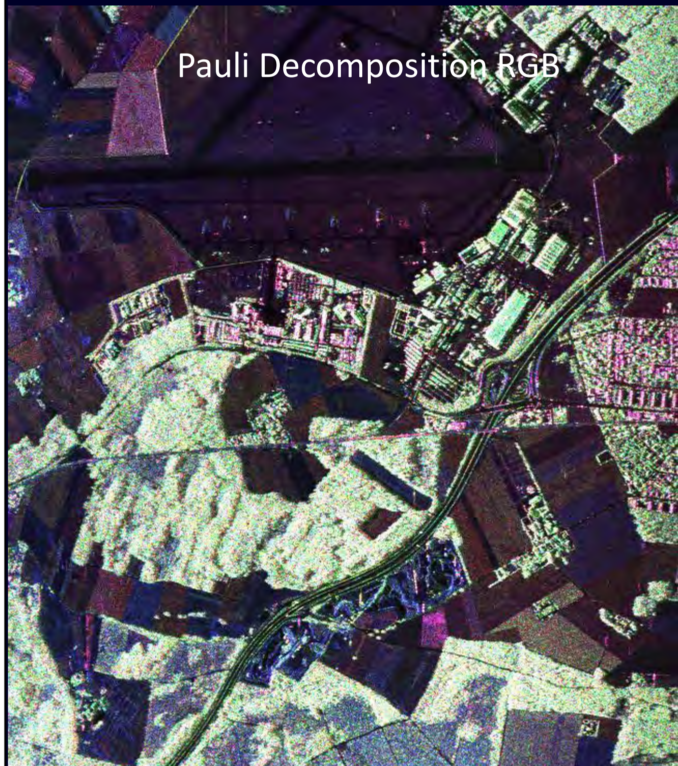

Polarimetric SAR Interferometry (Pol-InSAR)

Potential to separate in height different scattering processes occurring inside the resolution cell

Polarimeric SAR Interferometry: Concepts and Application

Irena Hajnsek

*Earth Observation and Remote Sensing,
Institute of Environmental Engineering, ETH Zürich
*Microwaves and Radar Institut,
German Aerospace Center, Oberpfaffenhofen

Earth Observation and Remote Sensing

hajnsek@ifu.baug.ethz.ch
irena.hajnsek@dlr.de

ETH
Eidgenössische Technische Hochschule Zürich
Swiss Federal Institute of Technology Zurich

SAR Interferometry

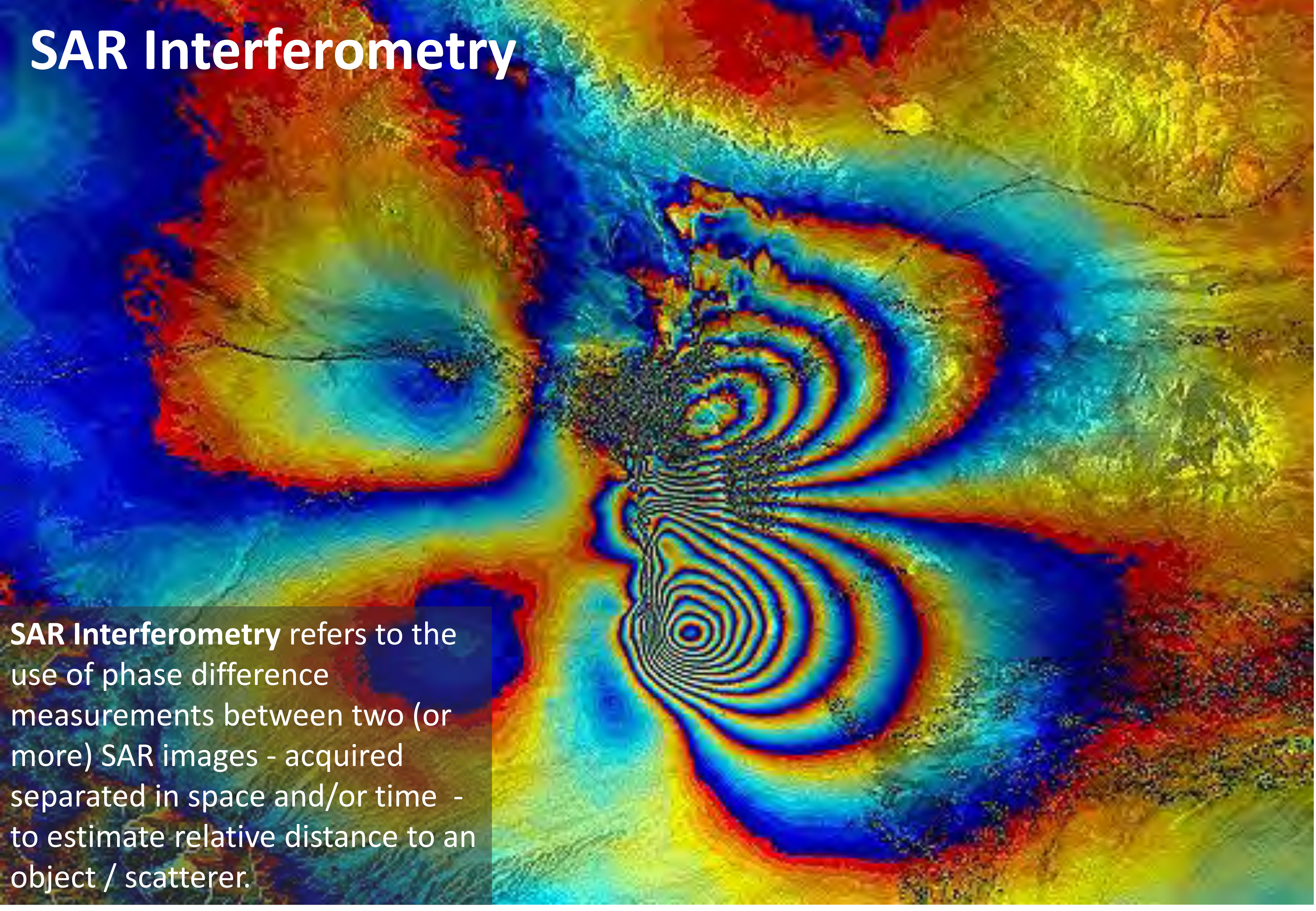

SAR Interferometry refers to the use of phase difference measurements between two (or more) SAR images - acquired separated in space and/or time - to estimate relative distance to an object / scatterer.

SAR Interferometry

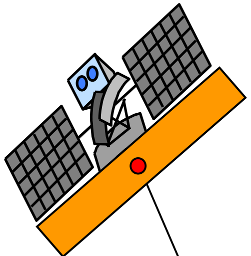

Signal from resolution cell P in Image 1: $i_1 = |i_1| \exp[-i(2\frac{2\pi}{\lambda}R_1) + \varphi_{S1}]$

Phase: $\varphi_1 = \arg(i_1) = \boxed{(2\frac{2\pi}{\lambda}R_1)} + \boxed{\varphi_{S1}}$

Term 1: Deterministic - proportional to the range distance R_1 of P

Term 2: Stochastic - induced by the scatterer (Speckle)

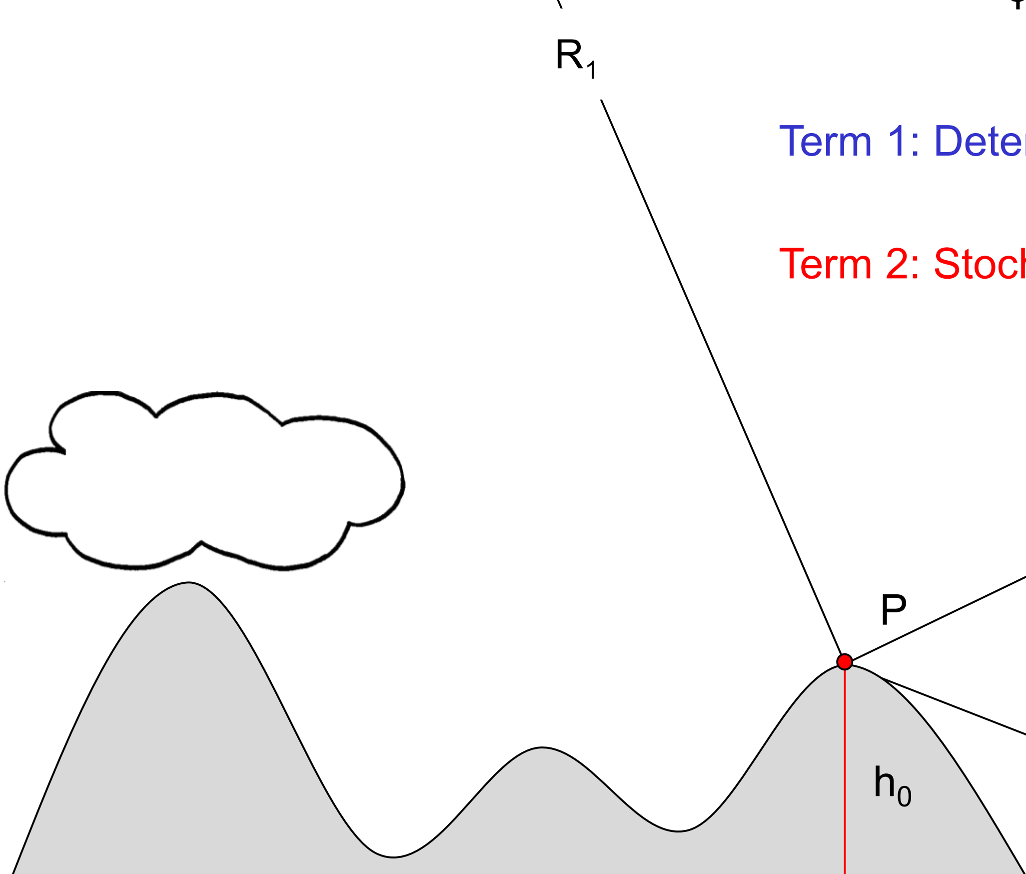

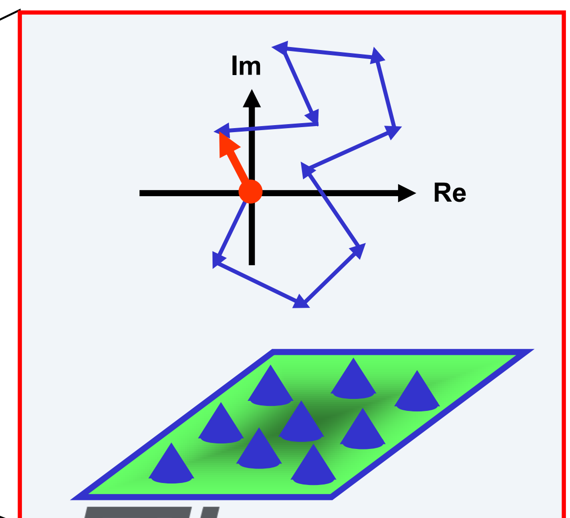

ERS – Bachu / China ~ 100 km × 80 km

Amplitude of Image 1

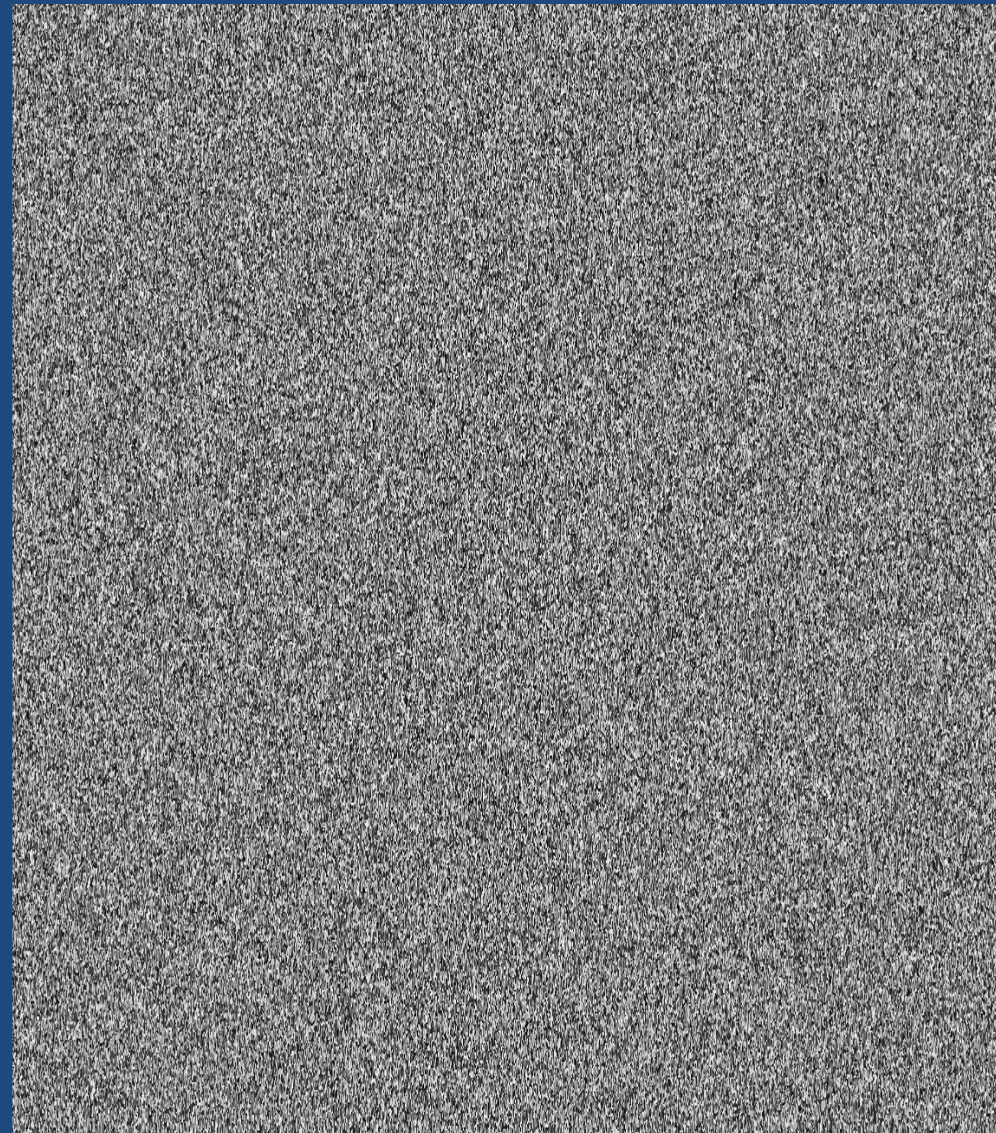

Phase of Image 1

SAR Interferometry

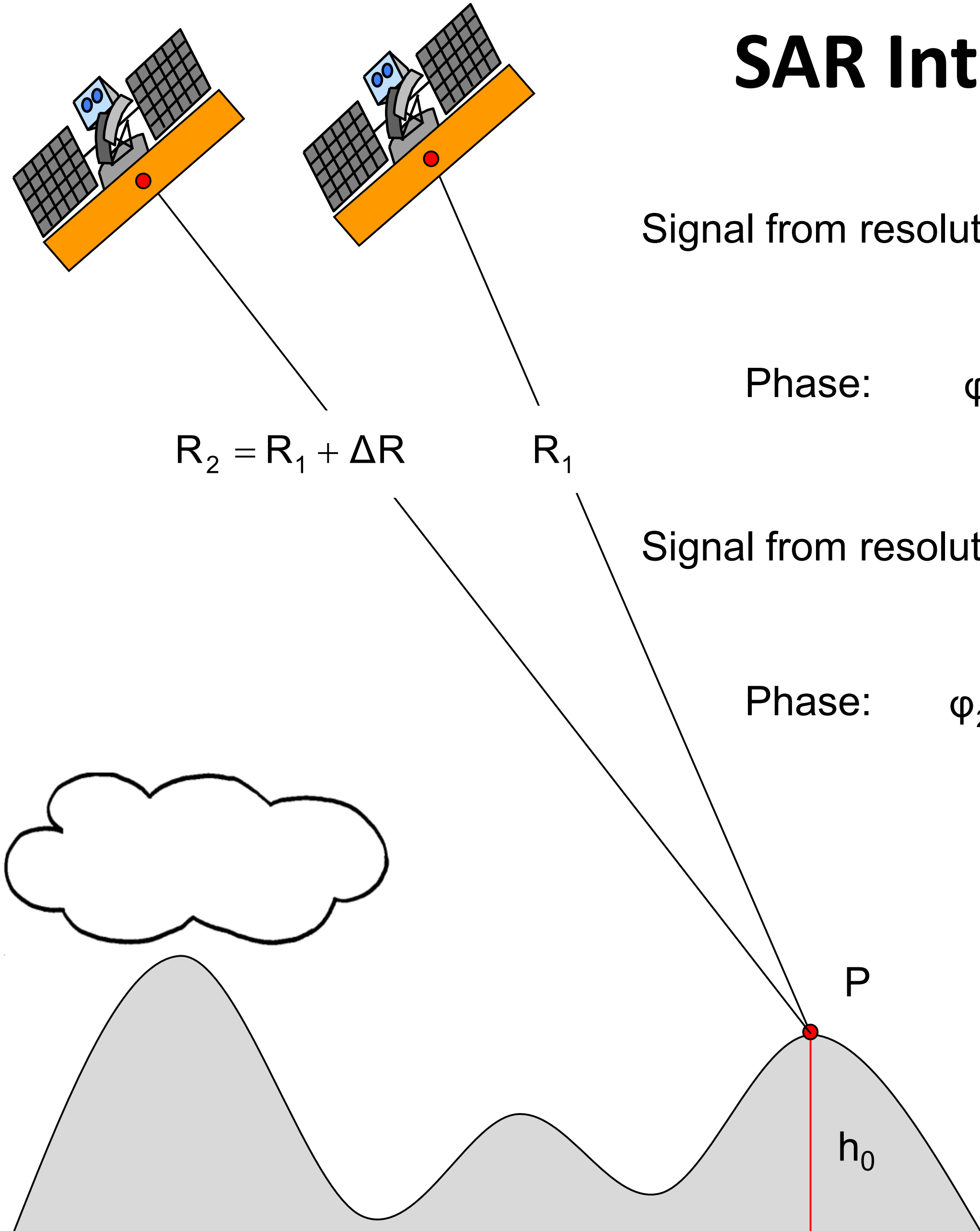

Signal from resolution cell P in Image 1: $i_1 = |i_1| \exp[-i(2\frac{2\pi}{\lambda}R_1) + \varphi_{S1}]$

Phase: $\varphi_1 = \arg(i_1) = \boxed{(2\frac{2\pi}{\lambda}R_1)} + \boxed{\varphi_{S1}}$

Signal from resolution cell P in Image 2: $i_2 = |i_2| \exp[-i(2\frac{2\pi}{\lambda}R_2) + \varphi_{S2}]$

Phase: $\varphi_2 = \arg(i_2) = \boxed{(2\frac{2\pi}{\lambda}R_2)} + \boxed{\varphi_{S2}}$

hajnsek@ifu.baug.ethz.ch
irena.hajnsek@dlr.de

SAR Interferometry

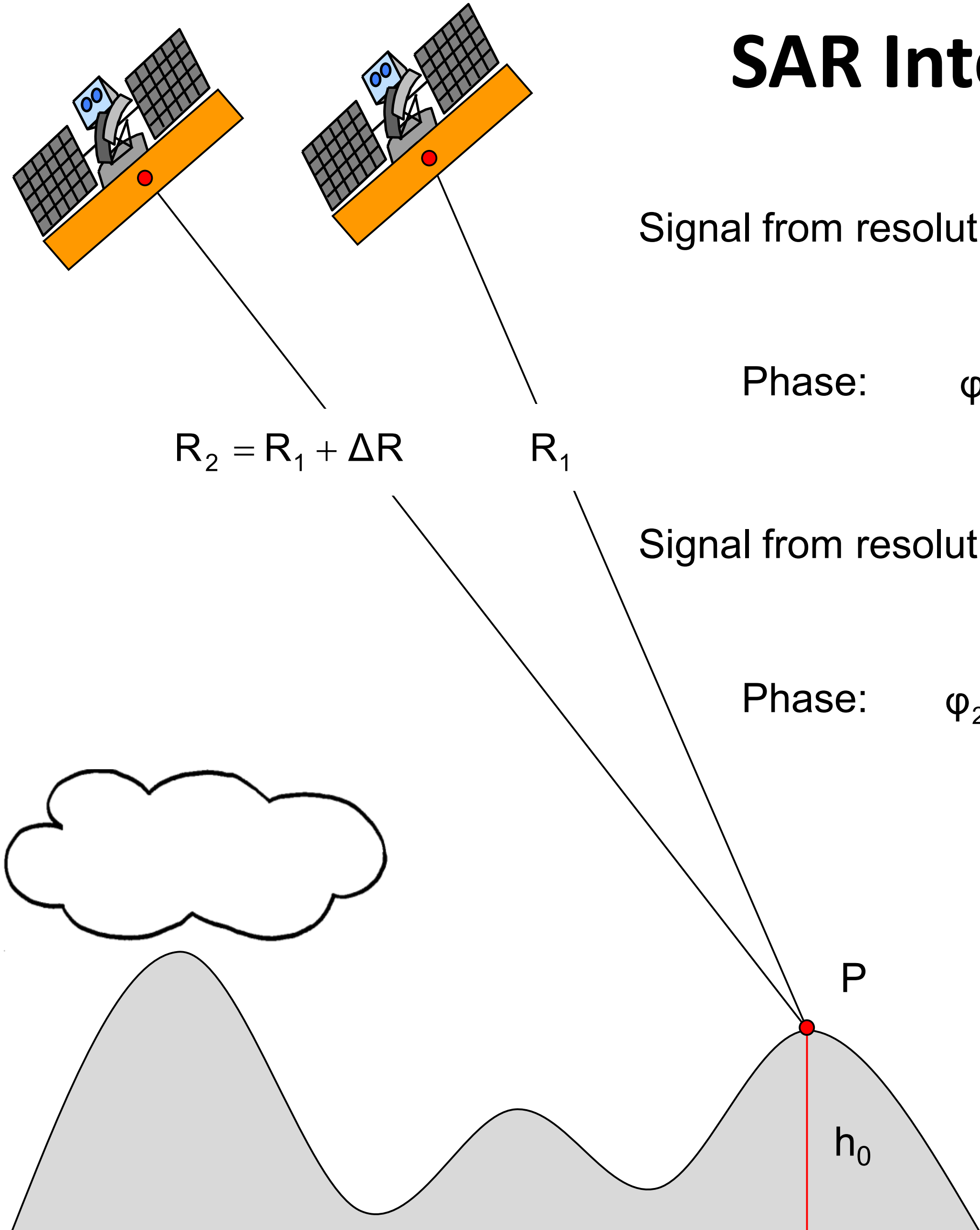

Signal from resolution cell P in Image 1: $i_1 = |i_1|\exp[-i(2\frac{2\pi}{\lambda}R_1) + \varphi_{S1}]$

Phase: $\varphi_1 = \arg(i_1) = \boxed{(2\frac{2\pi}{\lambda}R_1)} + \boxed{\varphi_{S1}}$

Signal from resolution cell P in Image 2: $i_2 = |i_2|\exp[-i(2\frac{2\pi}{\lambda}R_2) + \varphi_{S2}]$

Phase: $\varphi_2 = \arg(i_2) = \boxed{(2\frac{2\pi}{\lambda}R_2)} + \boxed{\varphi_{S2}}$

Assuming $\varphi_{S1} = \varphi_{S2}$!!!

Interferogram: $i_1 i_2^* = |i_1 i_2^*|\exp[-i(2\frac{2\pi}{\lambda}\Delta R)]$

Phase: $\varphi_{Int} = \frac{Re\{i_1 i_2^*\}}{Im\{i_1 i_2^*\}} = \boxed{2\frac{2\pi}{\lambda}\Delta R}$

Deterministic !!!

Earth Observation and Remote Sensing

hajnsek@ifu.baug.e
irena.hajnsek@d

ERS – Bachu / China ~ 100 km × 80 km

Amplitude of Image 1

Amplitude of Image 2

hajnsek@ifu.baug.ethz.ch
irena.hajnsek@dlr.de

ERS – Bachu / China ~ 100 km × 80 km

Amplitude of Image 1

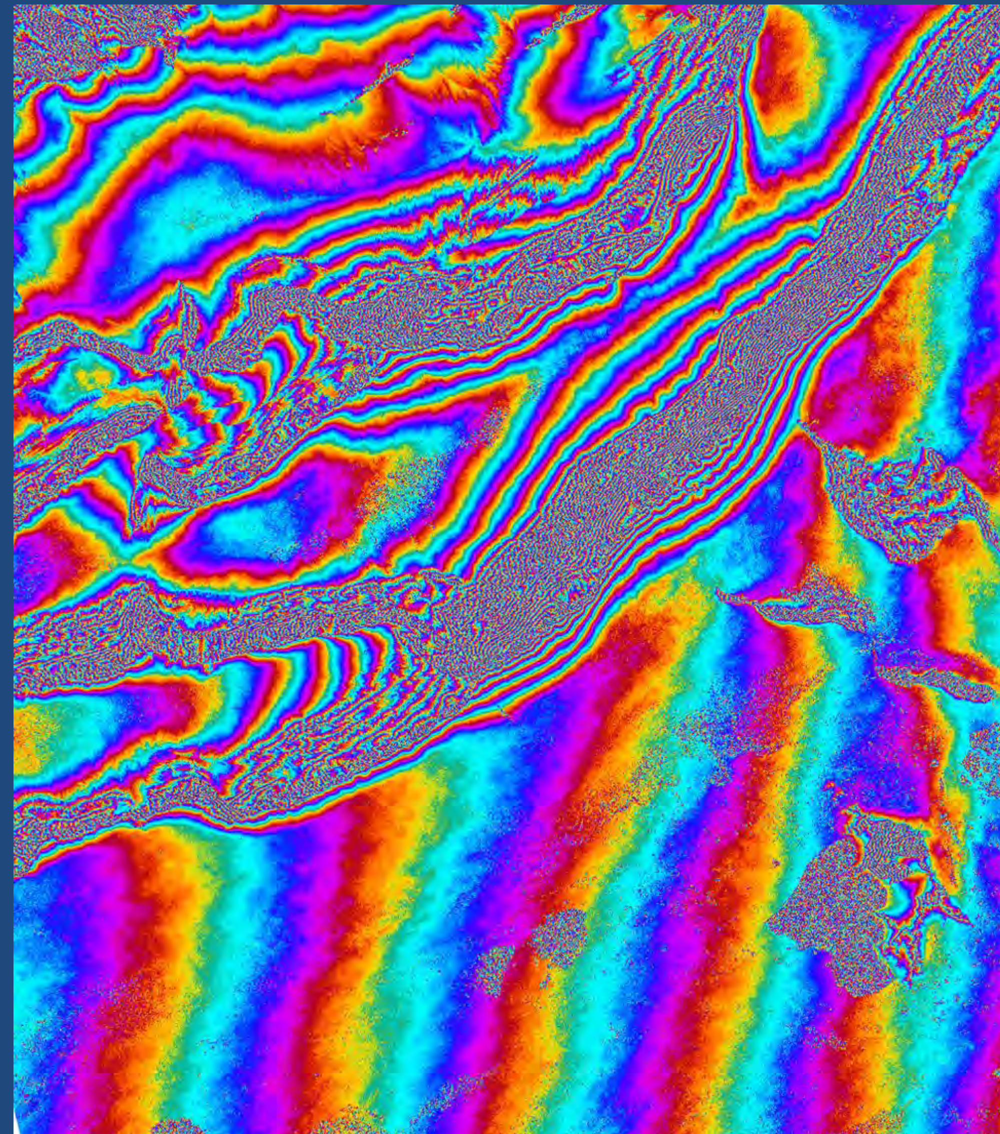

Interferometric Phase Image

hajnsek@ifu.baug.ethz.ch
irena.hajnsek@dlr.de

SAR Interferometry

Interferometric Phase: $\varphi = 2\frac{2\pi}{\lambda}\boxed{\Delta R}$

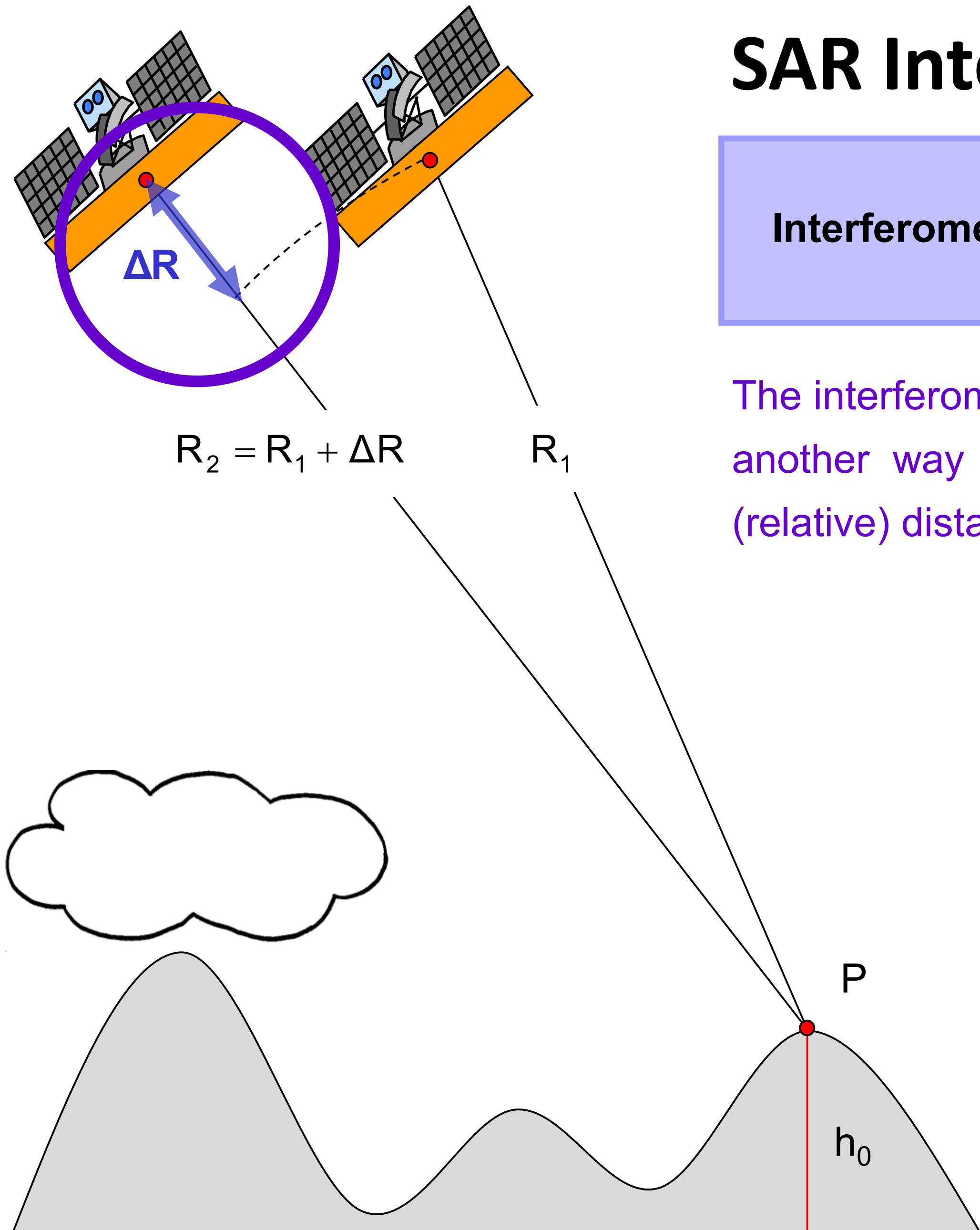

The interferometric phase φ is another way to measure the (relative) distance ΔR:

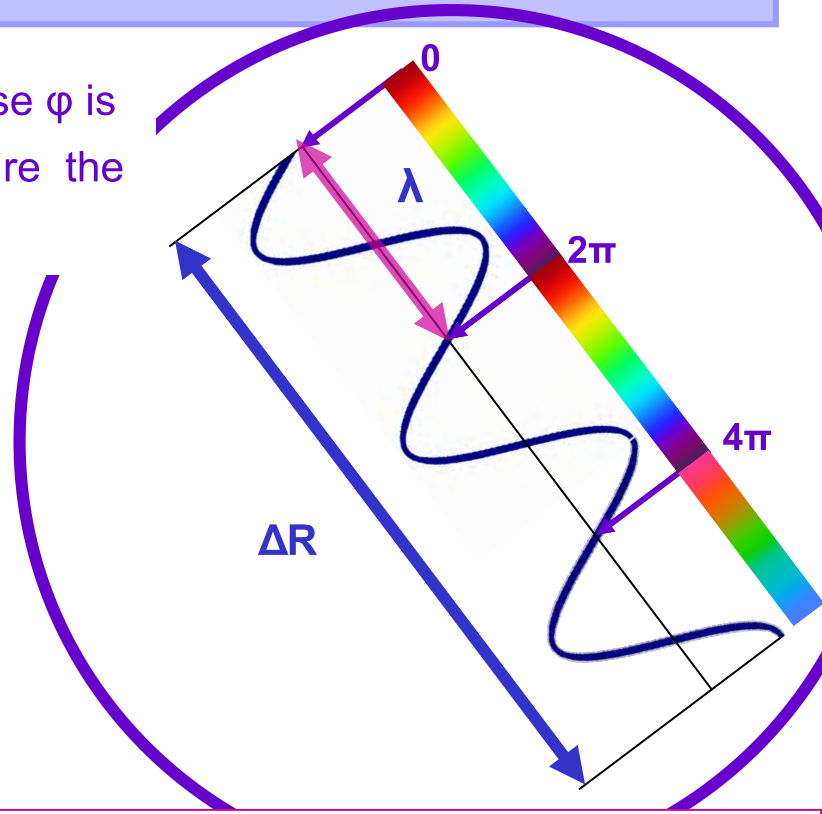

Phase measurements in interferometric systems can be made with a degree level accuracy. At radar wavelengths of 1-90cm (Ku to P-band) this corresponds to millimeter accuracy !!!

Earth Observation and Remote Sensing

hajnsek@ifu.baug.ethz.ch
irena.hajnsek@dlr.de

DEM Generation

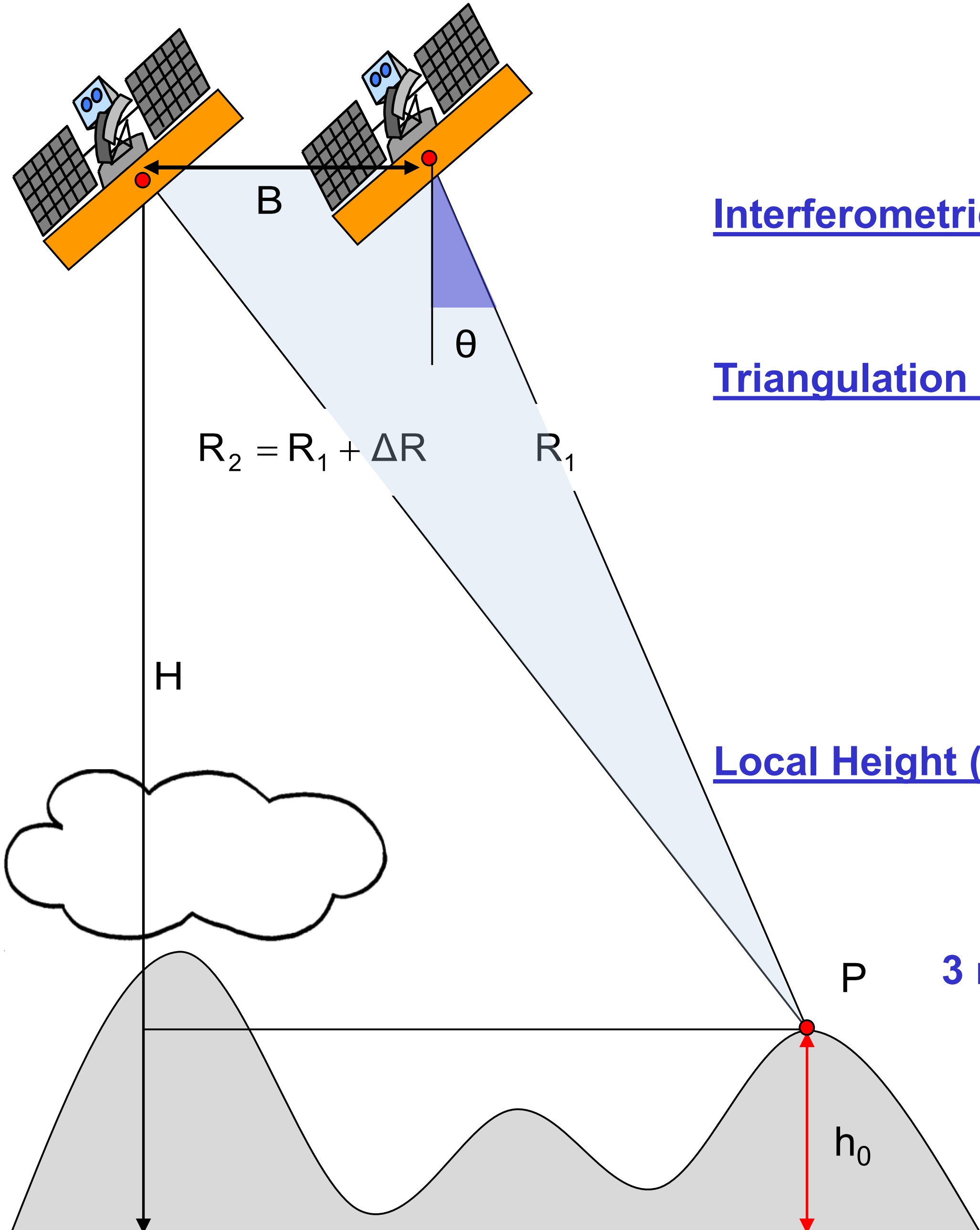

Interferometric Phase (1): $\varphi = 2\dfrac{2\pi}{\lambda}\boxed{\Delta R} + 2\pi\ N \qquad N = 0,\ \ \pm 1,\ \ \pm 2$

Triangulation (2): $(R_1 + \Delta R)^2 = R_1^{\ 2} + B^2 - 2R_1 B\cos(\pi/2 + \theta) \rightarrow$

$$\rightarrow\ \sin(\boxed{\theta}) = \frac{(R_1 + \Delta R)^2 - R_1^{\ 2} - B^2}{2R_1 B}$$

Local Height (3): $\boxed{h_0} = H - (R_1 + \Delta R)\cos(\theta)$

3 non-linear equations for 3 unknowns (h_0, θ, ΔR)

B … Spatial baseline and

R_1 … Range distance in Image 1 are known

Critical is the fact that the interferometric phase φ is initially measured modulo 2π ► Phase Unwrapping

hajnsek@ifu.baug.e
irena.hajnsek@d

ERS – Bachu / China ~ 100 km × 80 km

Amplitude Image

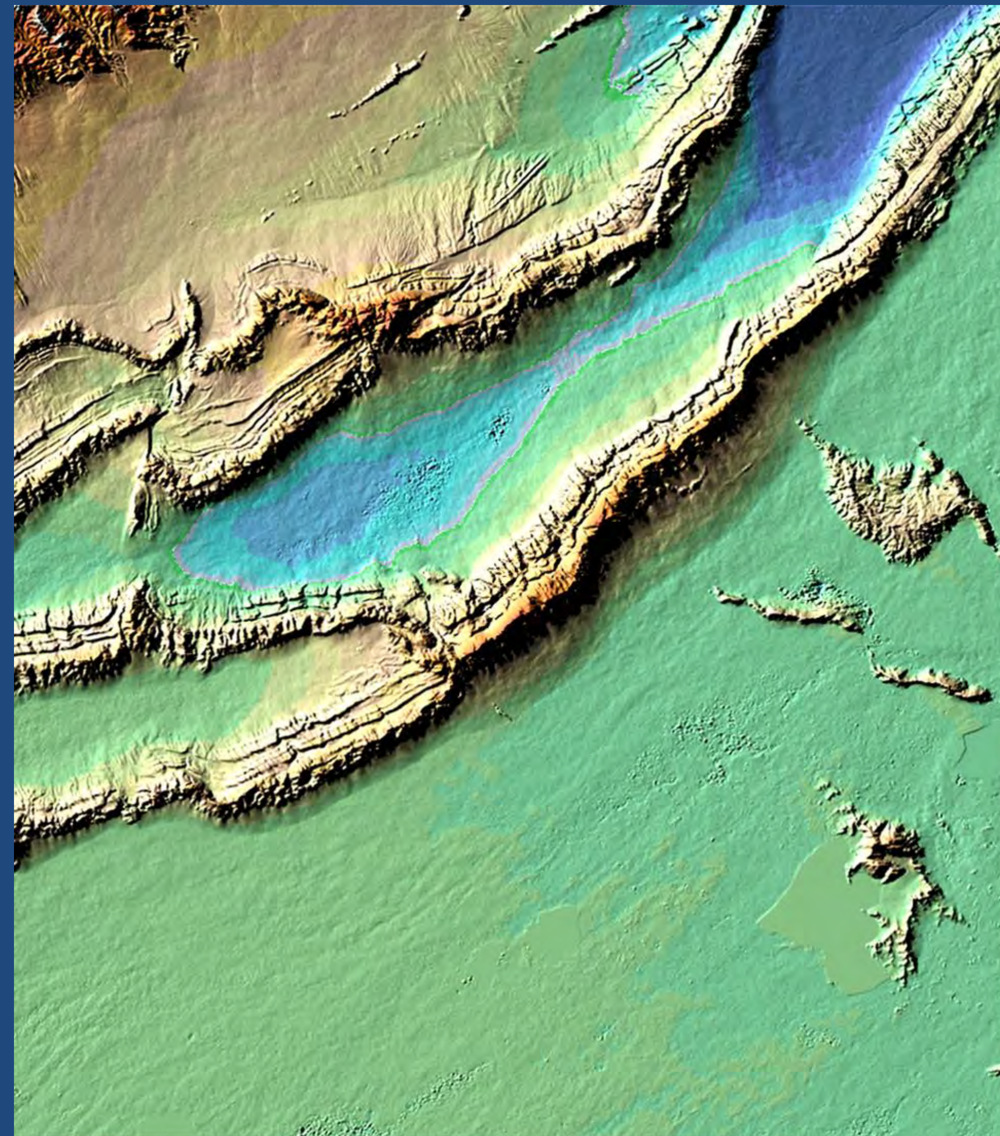

Digital Elevation Model with false colors

ERS – Bachu / China ~ 100 km × 80 km

Amplitude Image

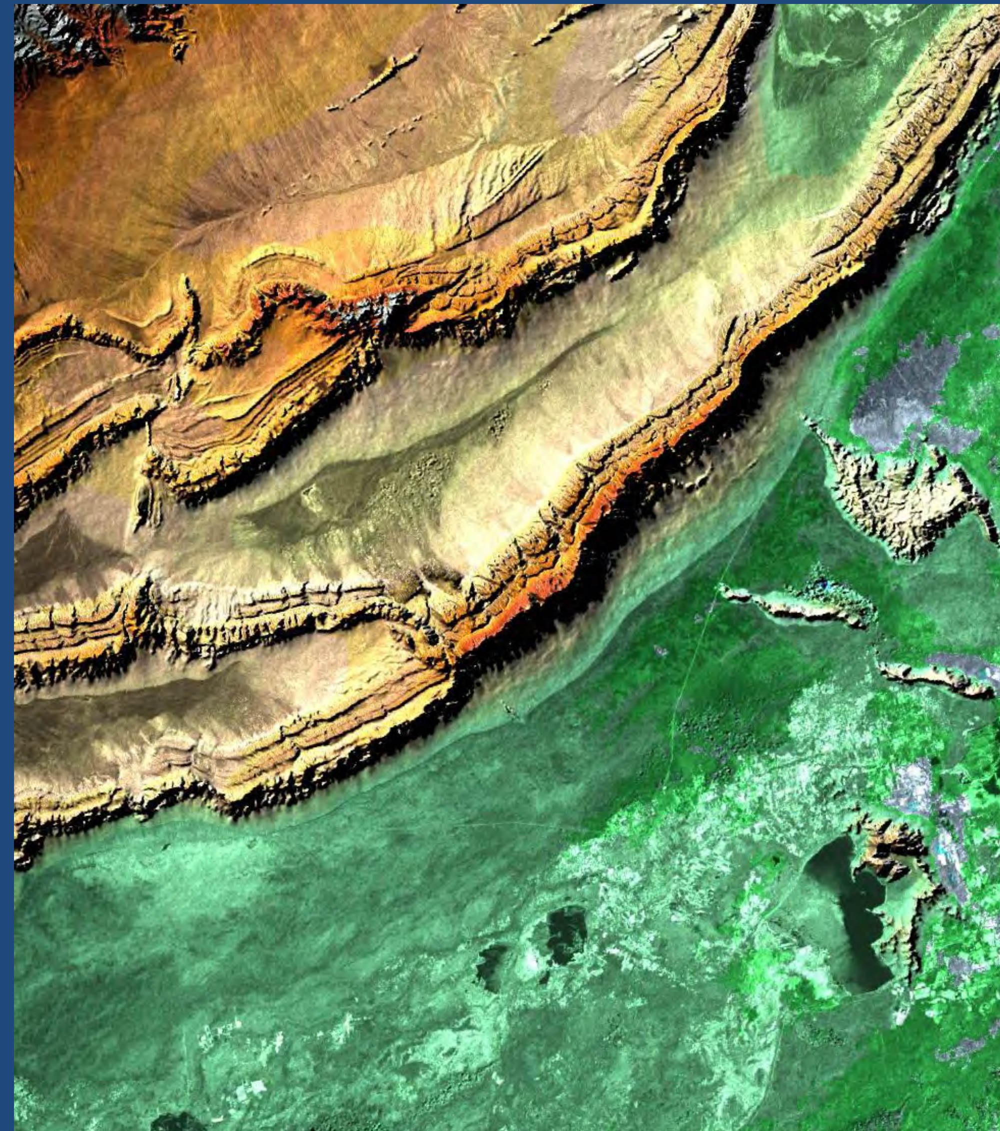

Digital Elevation Model and SAR image

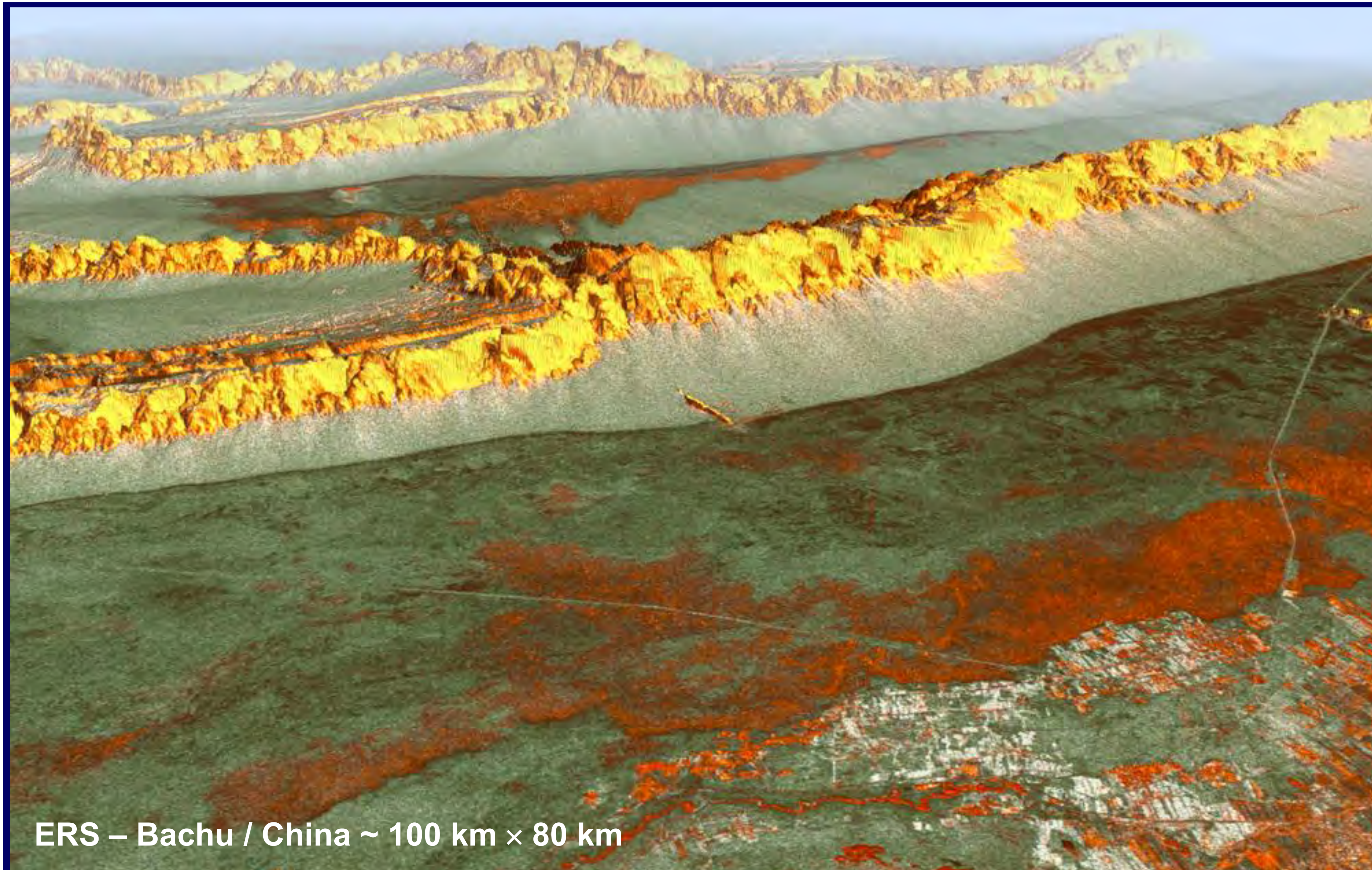

hajnsek@ifu.baug.ethz.ch
irena.hajnsek@dlr.de

InSAR Phase: Height Sensitivity

Interferometric Phase: $\varphi = 2\frac{2\pi}{\lambda}\Delta R + 2\pi N$ where $N = 0, \pm 1, \pm 2$

P_1 & P_2 : Two points at the same range but different heights h_1 & h_2 :

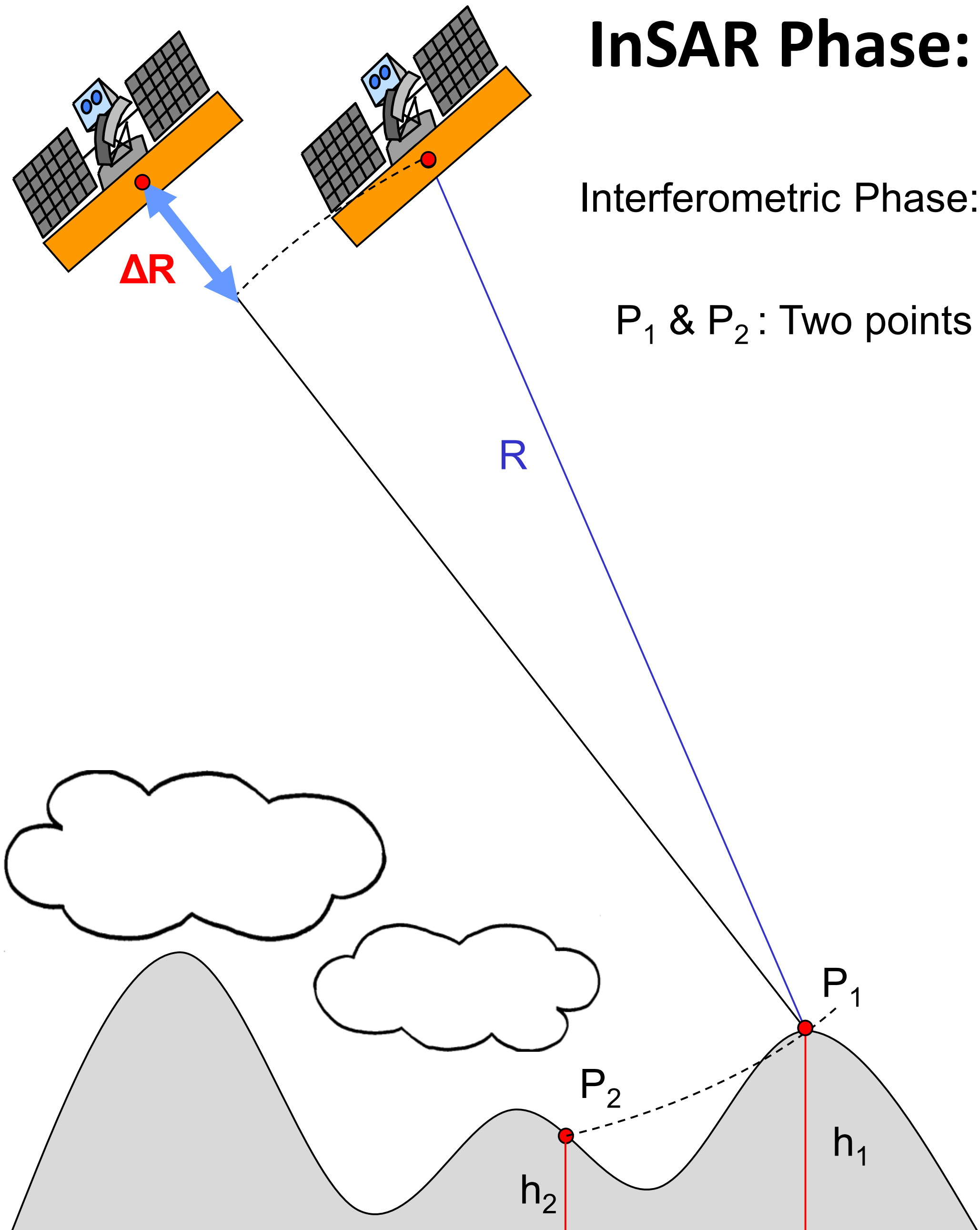

InSAR Phase: Height Sensitivity

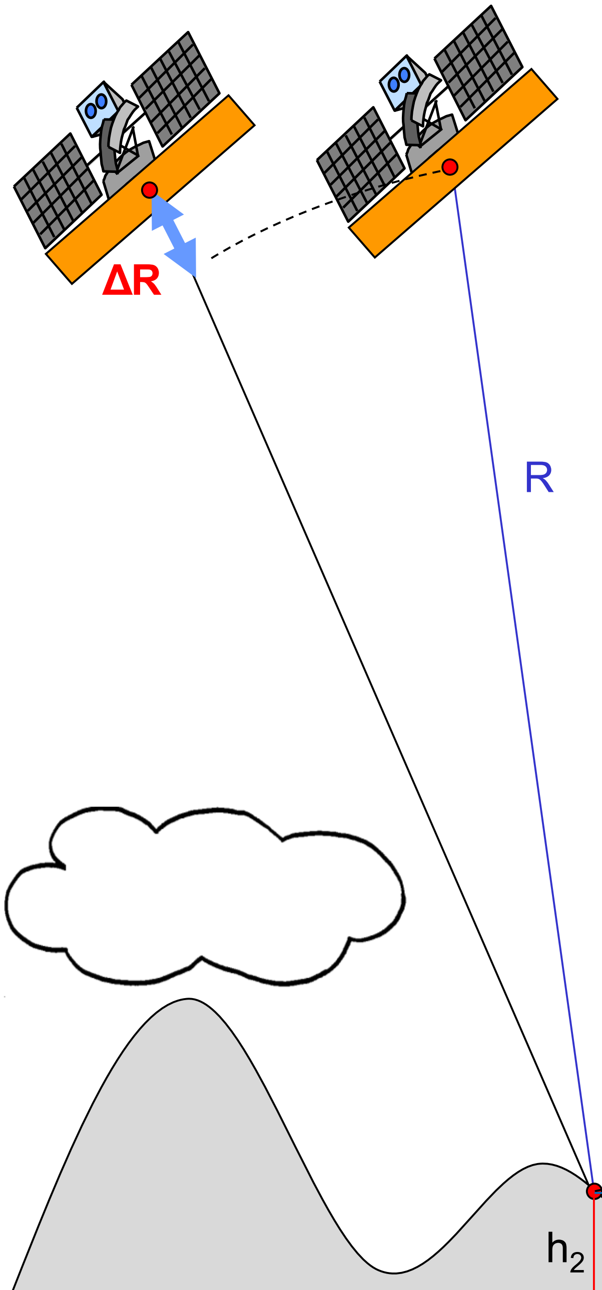

Interferometric Phase: $\varphi = 2\frac{2\pi}{\lambda}\Delta R + 2\pi\ N$ where $N = 0, \ \pm 1, \ \pm 2$

P_1 & P_2 : Two points at the same range but different heights h_1 & h_2

ΔR changes implying a different interferometric phase at each point

In other words: The height difference $\Delta h = h_1 - h_2$ causes an (interferometric) phase difference $\Delta\varphi$;

Phase-to-Height Sensitivity $\partial\varphi / \partial z$ [rad/m]: is defined by the (interferometric) phase difference caused by a given height difference (1m)

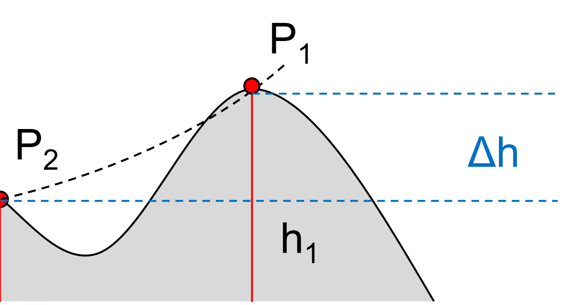

hajnsek@ifu.baug.ethz.ch
irena.hajnsek@dlr.de

InSAR Phase: Height Sensitivity

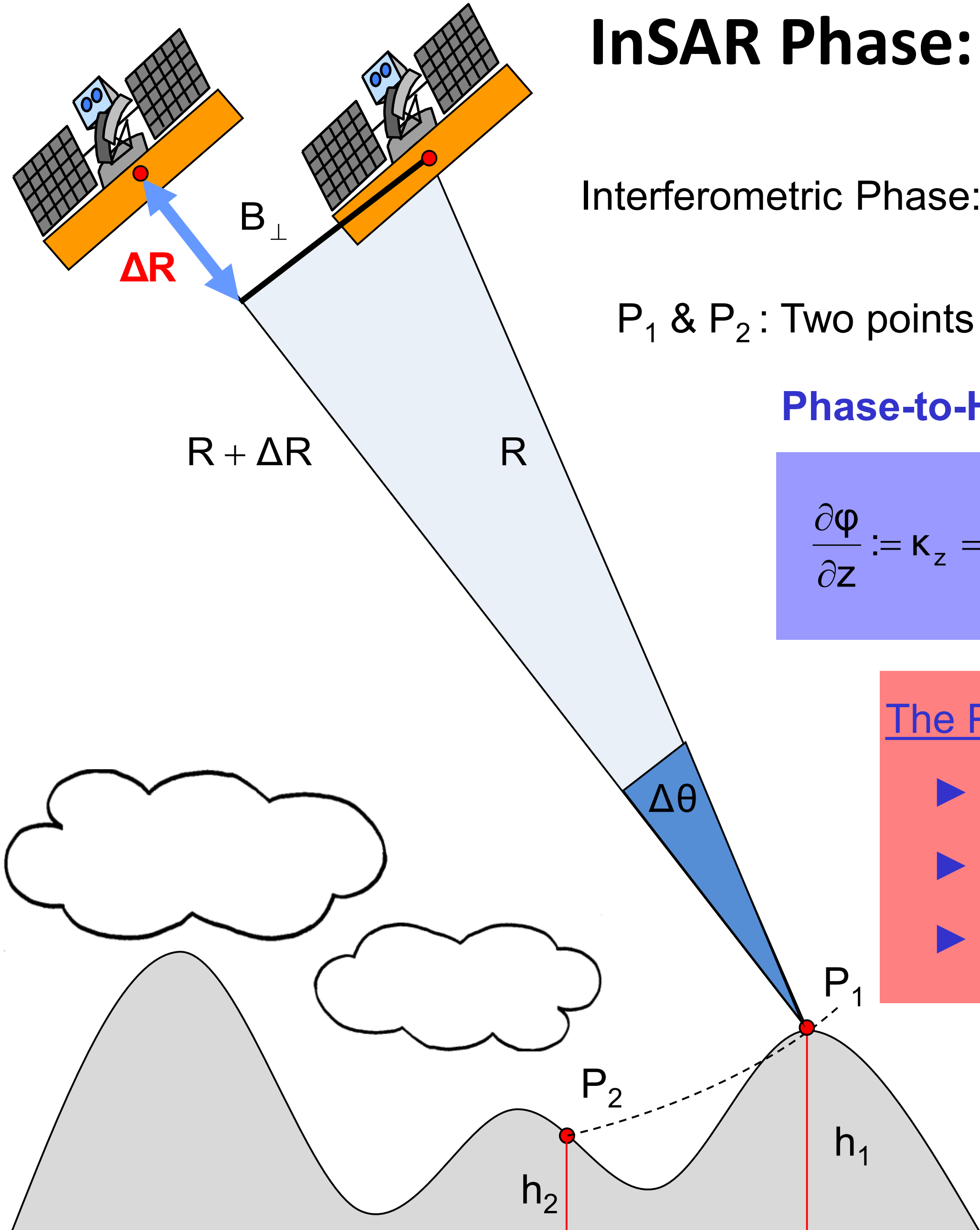

Interferometric Phase: $\varphi = 2\dfrac{2\pi}{\lambda}\boxed{\Delta R} + 2\pi N$ where $N = 0, \pm 1, \pm 2$

P_1 & P_2 : Two points at the same range but different heights h_1 & h_2 :

Phase-to-Height Sensitivity:

$$\frac{\partial \varphi}{\partial z} := \kappa_z = \frac{4\pi}{\lambda}\frac{\Delta\theta}{\sin(\theta)} \approx \frac{4\pi}{\lambda}\frac{B_\perp}{R\sin(\theta)} \quad \text{using} \quad \Delta\theta \approx \frac{B_\perp}{R}$$

<u>The Phase-to-Height Sensitivity increases with:</u>

- ► Increasing the spatial baseline (i.e. Δθ or $B_\perp$);
- ► Increasing the system frequency (<u>i.e. decreasing λ</u>);
- ► At steeper (i.e. smaller) incidence angles θ.

Height of Ambiguity (HoA):

the height that causes a 2π phase difference:

$$\text{HoA} = \frac{\lambda}{4\pi}\frac{R\sin(\theta)}{B_\perp}2\pi = \frac{\lambda}{2}\frac{R\sin(\theta)}{B_\perp}$$

Earth Observation and Remote Sensing

hajnsek@ifu.baug.ethz.ch
irena.hajnsek@dlr.de

Swiss Federal Institute of Technology Zurich

InSAR Phase: Height Sensitivity

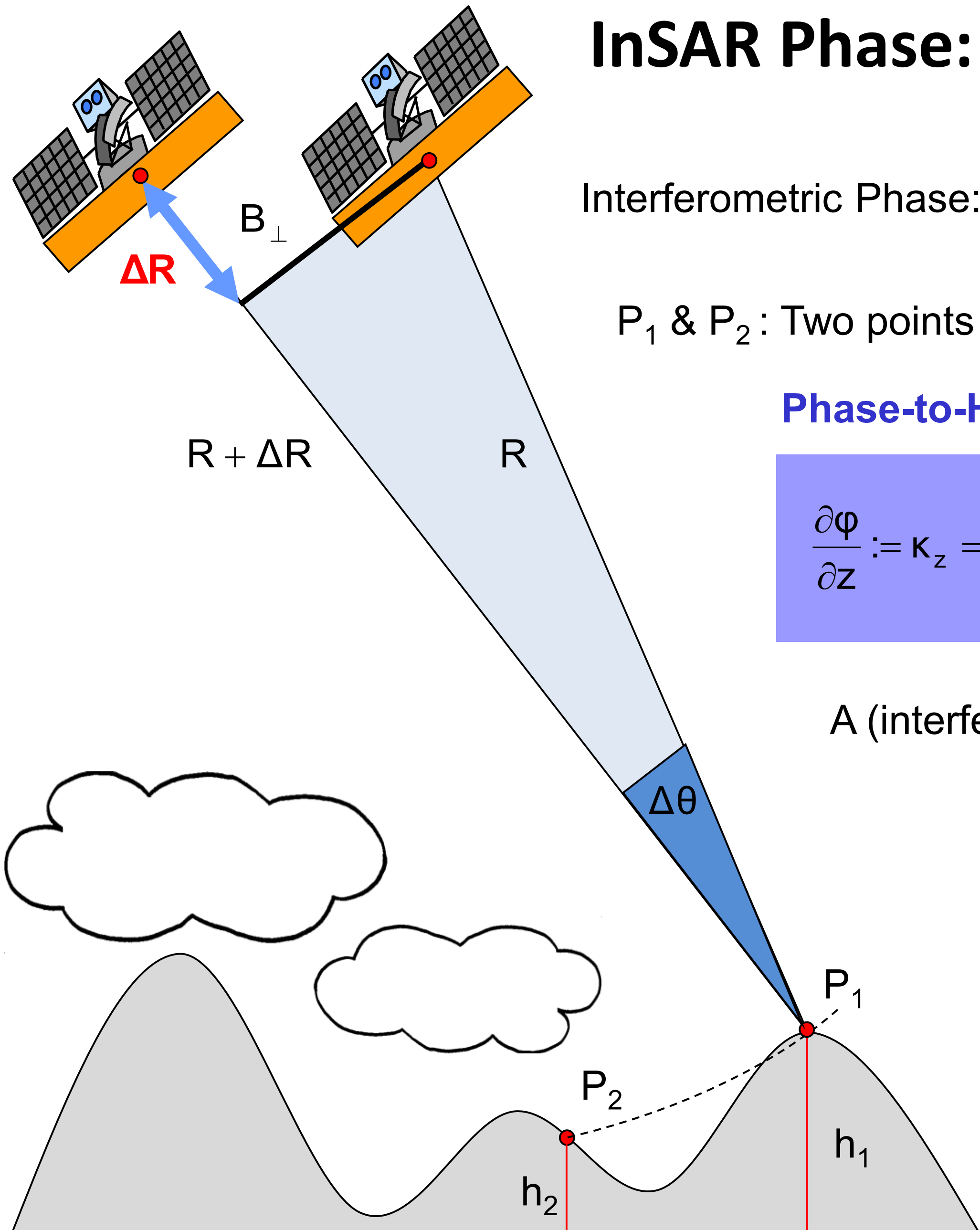

Interferometric Phase: $\varphi = 2\dfrac{2\pi}{\lambda}\boxed{\Delta R} + 2\pi\, N$ where $N = 0, \ \pm 1, \ \pm 2$

P_1 & P_2 : Two points at the same range but different heights h_1 & h_2 :

Phase-to-Height Sensitivity [rad/m]:

$$\frac{\partial \varphi}{\partial z} := \kappa_z = \frac{4\pi}{\lambda}\frac{\Delta\theta}{\sin(\theta)} \approx \frac{4\pi}{\lambda}\frac{B_\perp}{R\sin(\theta)}$$

using $\Delta\theta \approx \dfrac{B_\perp}{R}$

A (interferometric) phase error σ_φ induces a **height error σ_z:**

$$\sigma_z = \frac{1}{\partial\varphi / \partial z}\sigma_\varphi = \frac{1}{\kappa_z}\sigma_\varphi \approx \frac{\lambda}{4\pi}\frac{R\sin(\theta)}{B_\perp}\sigma_\varphi$$

For the same (interferometric) phase error σ_φ the induced height error decreases with:

- ► Increasing the spatial baseline;
- ► Increasing the system frequency;
- ► At steeper incidence angles θ.

hajnsek@ifu.baug.e
irena.hajnsek@dl

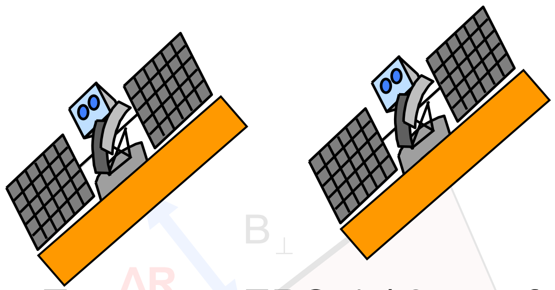

InSAR Phase: Height Sensitivity

Example: ERS-1 / 2 Interferometry at C-band λ=5.6 cm =0.056m , R=870km, θ=23º=23 π/180 rad

Phase-to-Height Sensitivity: $\frac{\partial\varphi}{\partial z} = \frac{4\pi}{\lambda}\frac{B_\perp}{R\sin(\theta)} \approx 2\pi\frac{B_\perp}{100^2}$

$B_\perp$	$\partial\varphi/\partial z$ [rad/m]	HoA
50 m	≈ 0.0314	≈ 200 m
100 m	≈ 0.0628	≈ 100 m
200 m	≈ 0.1256	≈ 50 m

… with increasing $B_\perp$ the Phase-to-Height Sensitivity increases

Height Error: $\sigma_z = \frac{1}{\partial\varphi/\partial z}\sigma_\varphi \approx \frac{1}{2\pi}\frac{100^2}{B_\perp}\sigma_\varphi$

Assuming that one can estimate the interferometric phase with an accuracy of 30º (σ_φ=30 π/180 rad)

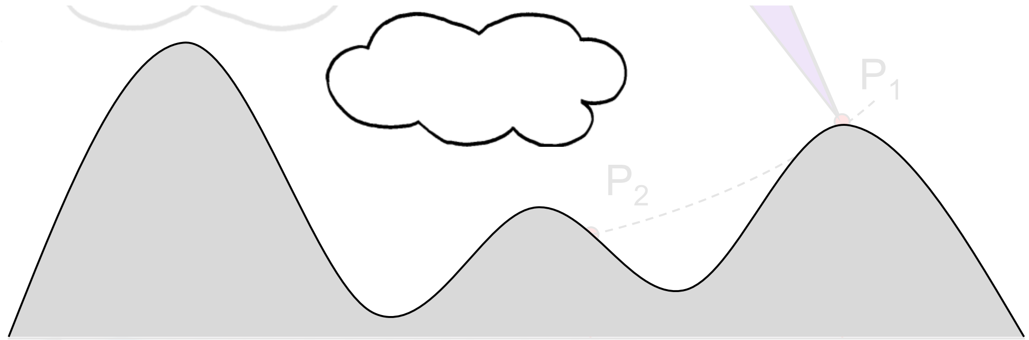

$B_\perp$	$\partial\varphi/\partial z$ [rad/m]	σ_z
50 m	≈ 0.0314	≈ 16.6 m
100 m	≈ 0.0628	≈ 8.3 m
200 m	≈ 0.1256	≈ 4.2 m

With increasing the spatial baseline ($B_\perp$) the height error decreases !!!

SAR Interferometry (InSAR)

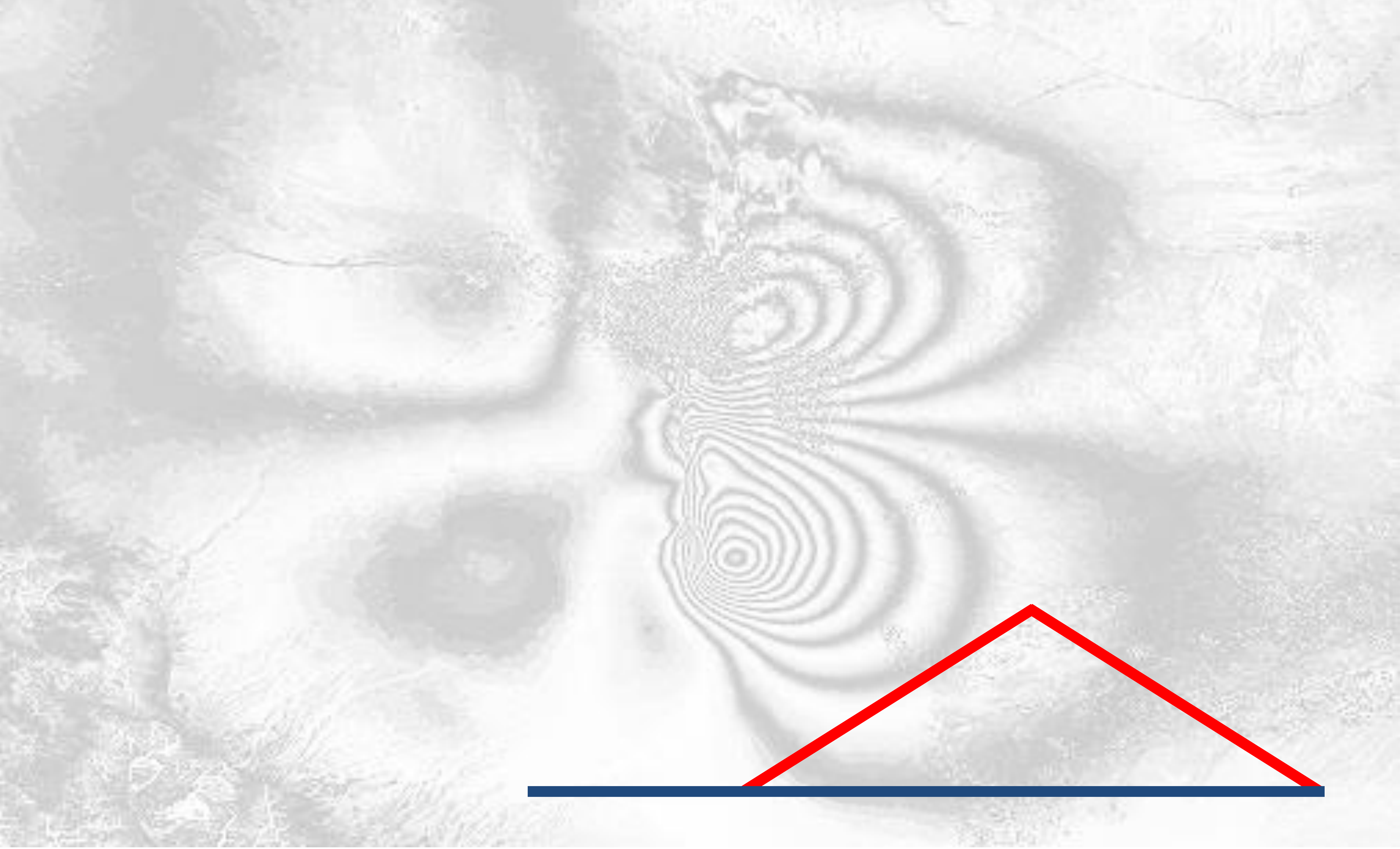

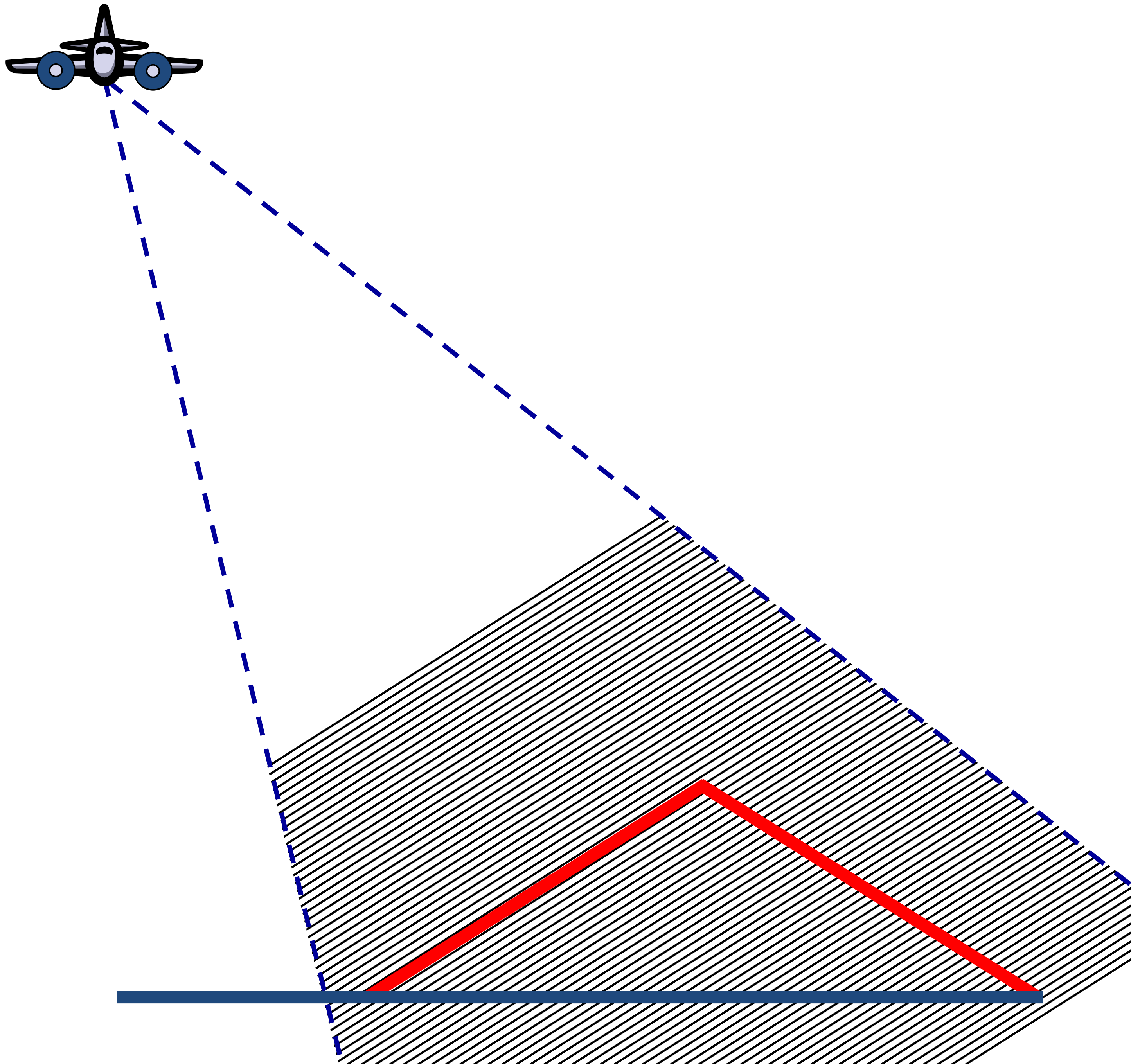

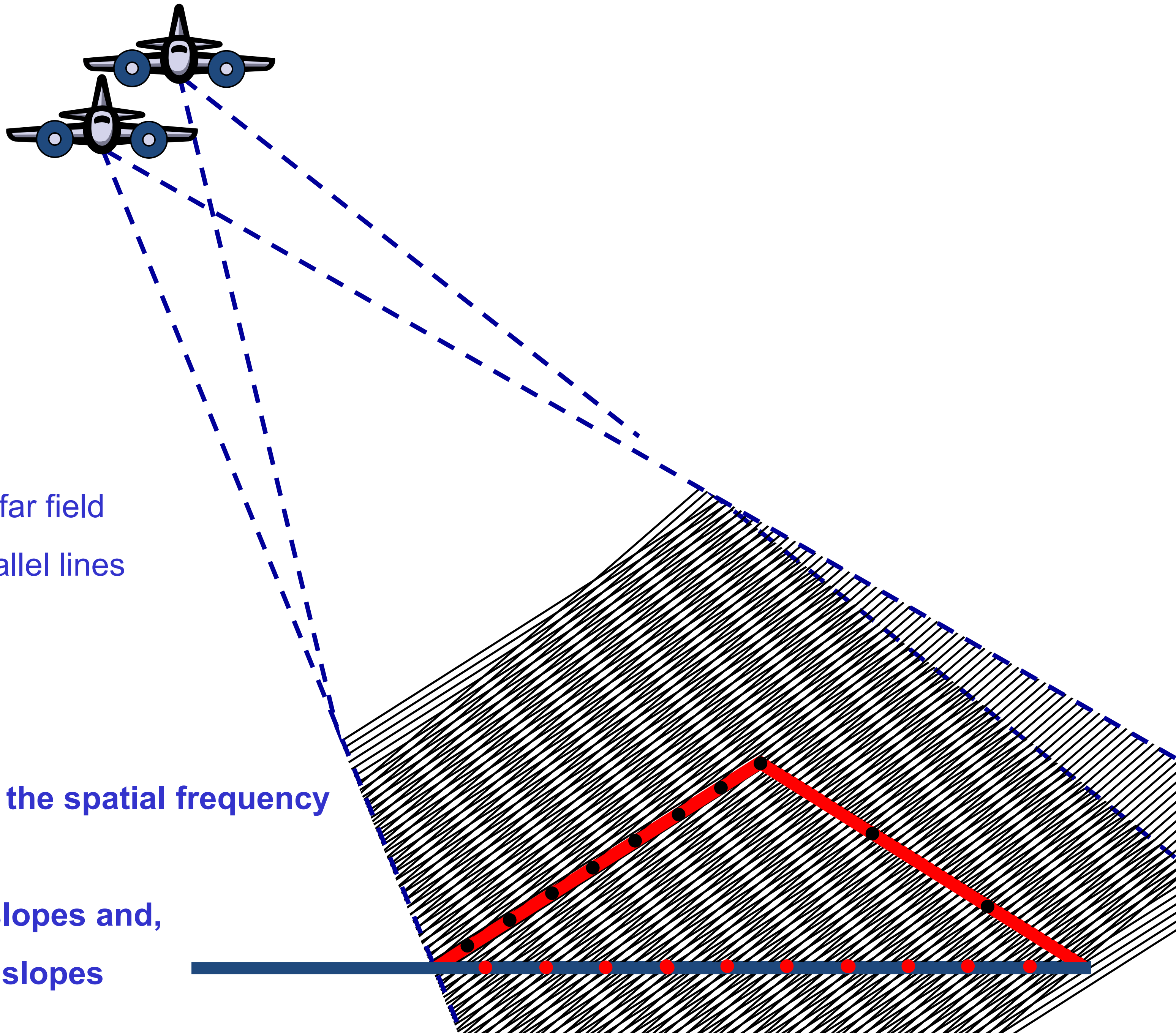

Interference pattern in the far field consists of equidistant parallel lines (parallel ray approx.).

With respect to flat terrain, **the spatial frequency** of the interference pattern

- **increases at positive slopes and,**
- **decreases at negative slopes**

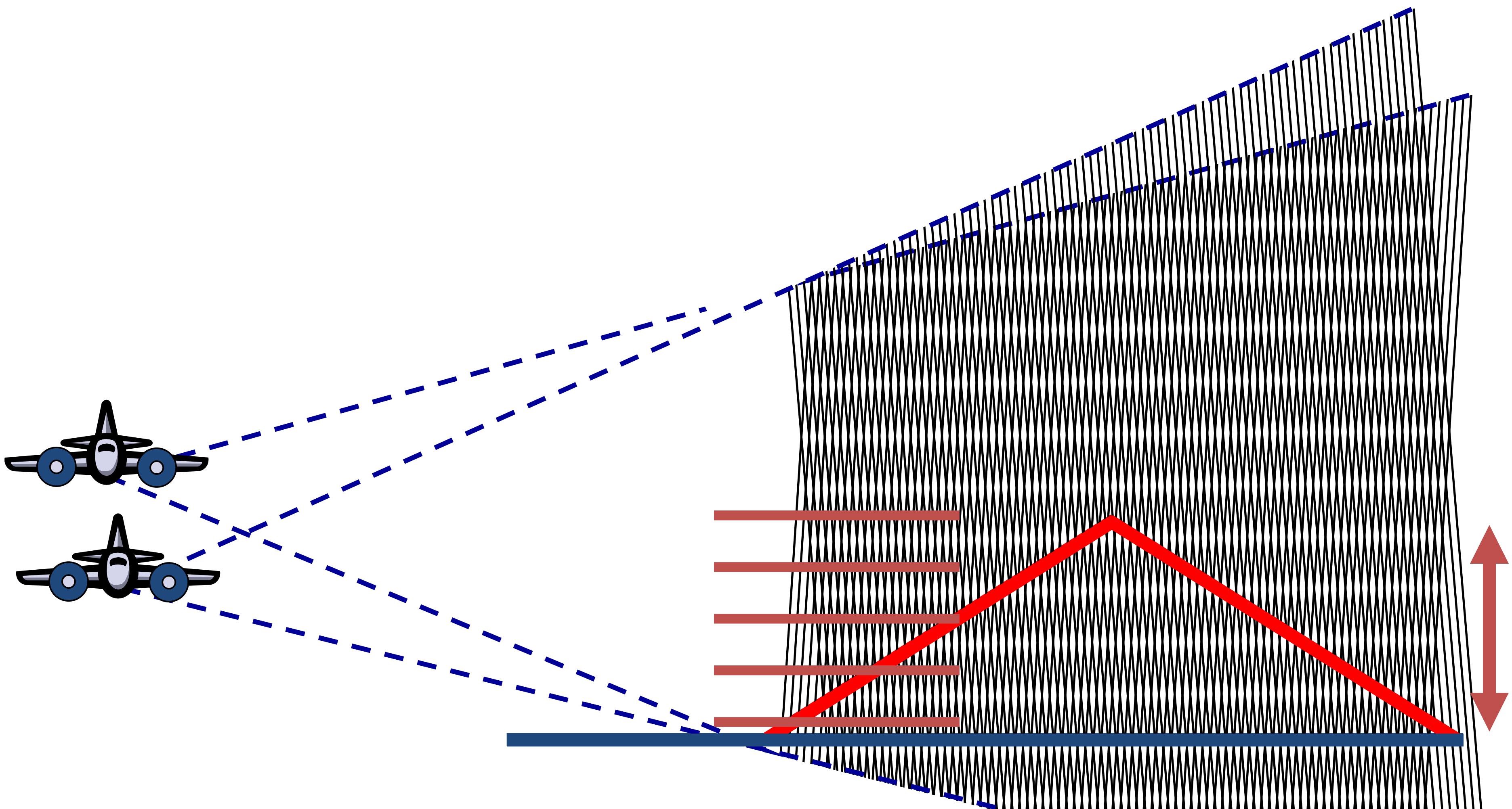

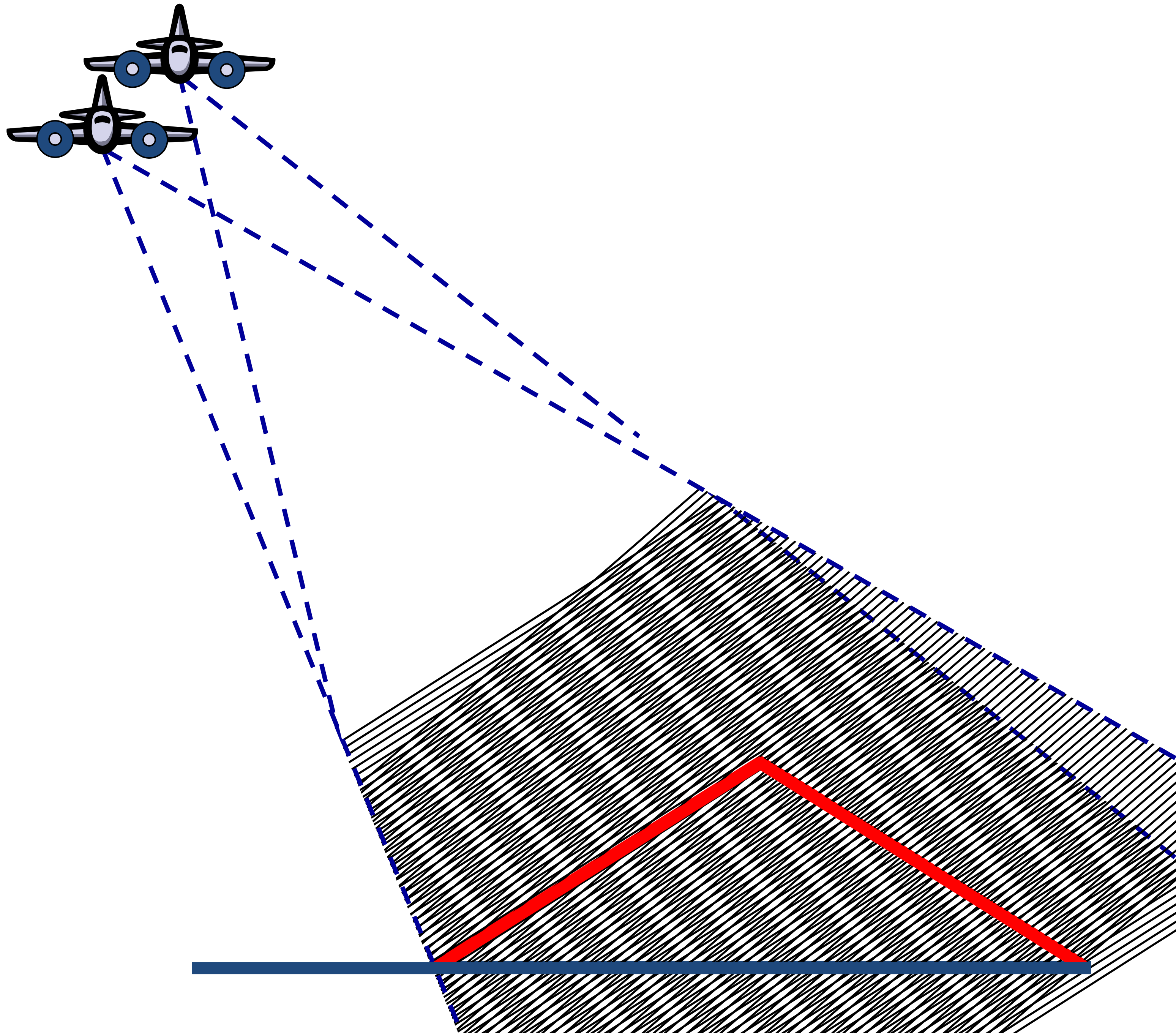

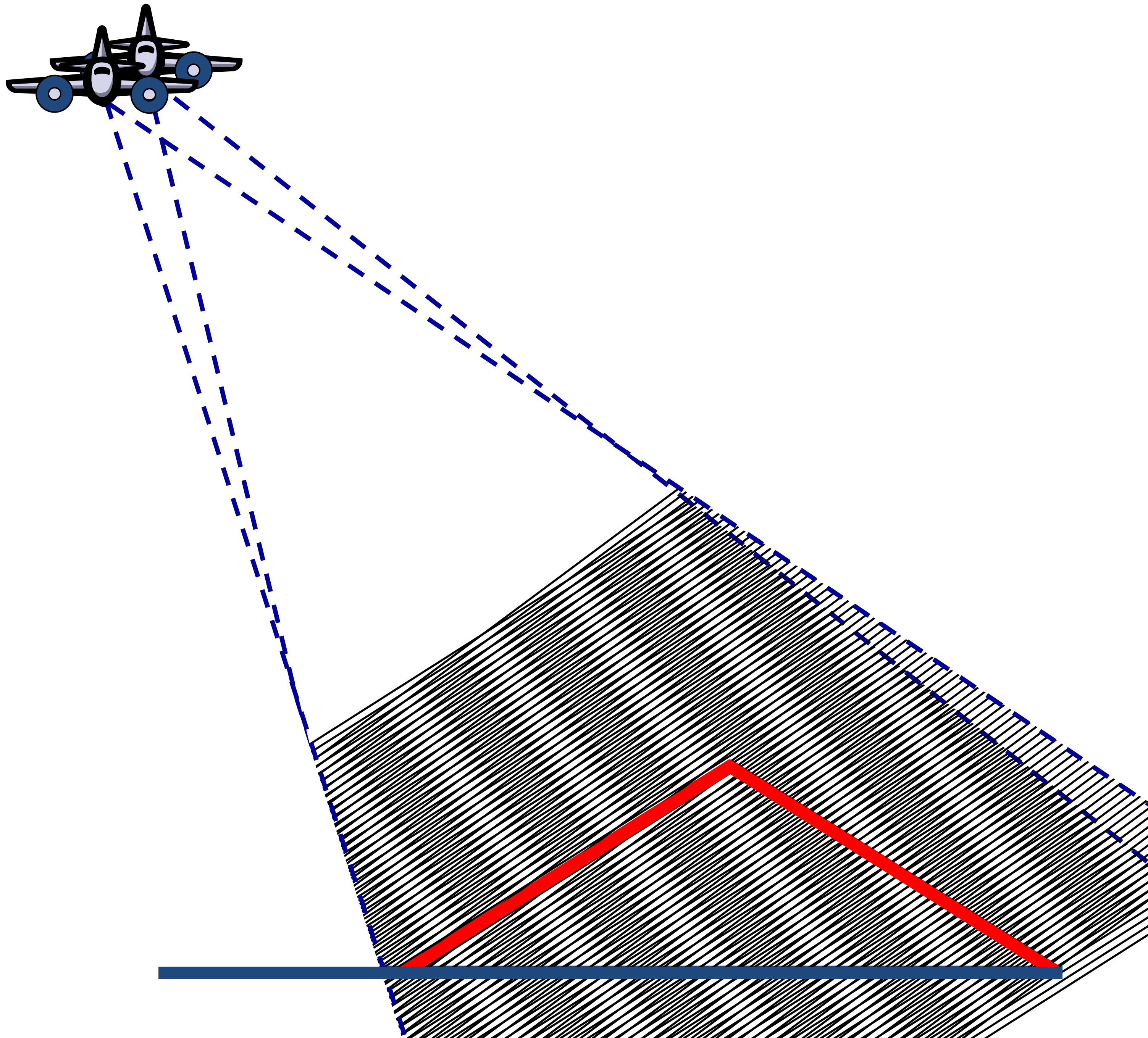

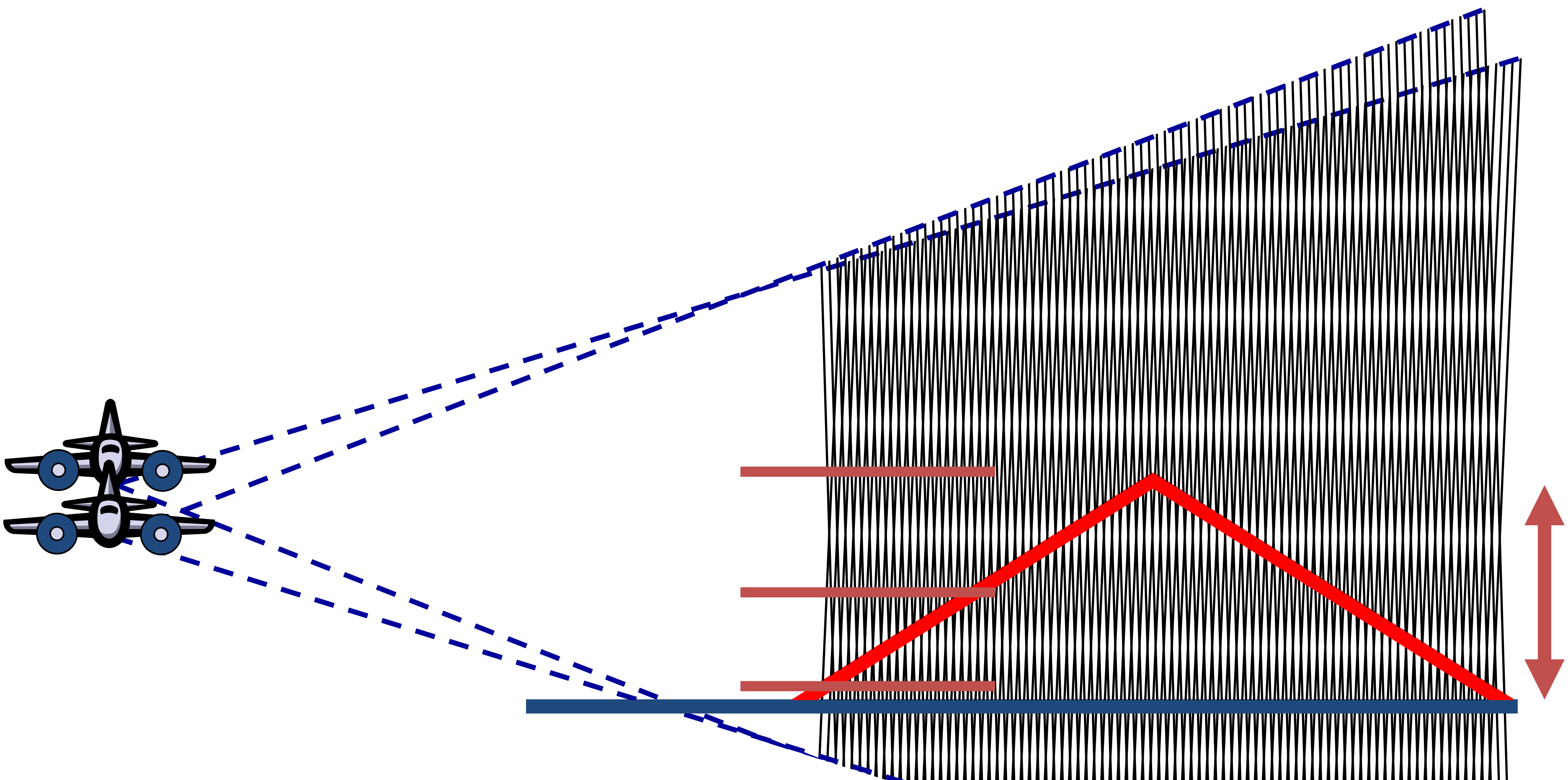

The Phase-to-Height Sensitivity increases with increasing the spatial baseline (i.e. Δθ or B⊥);

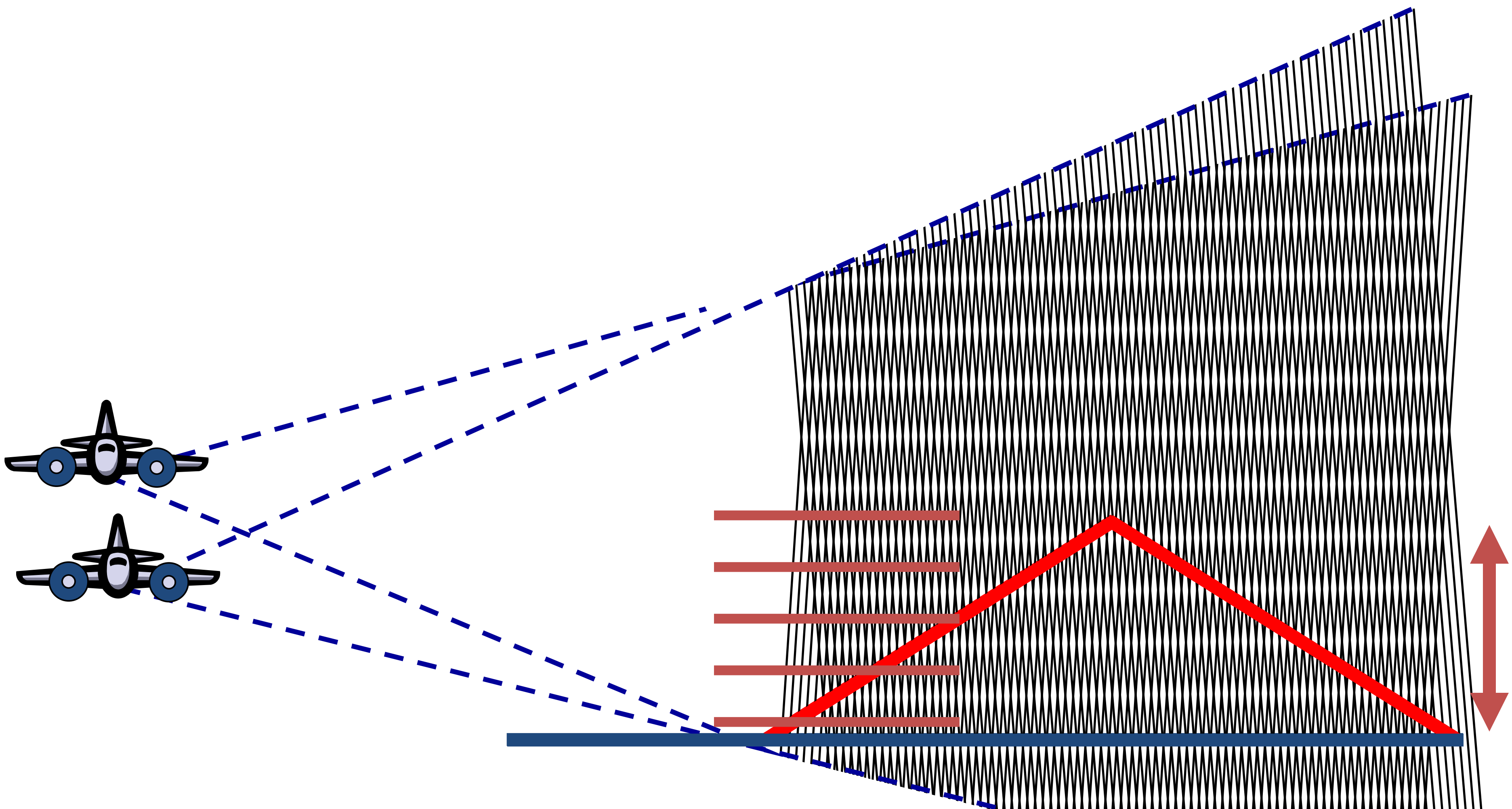

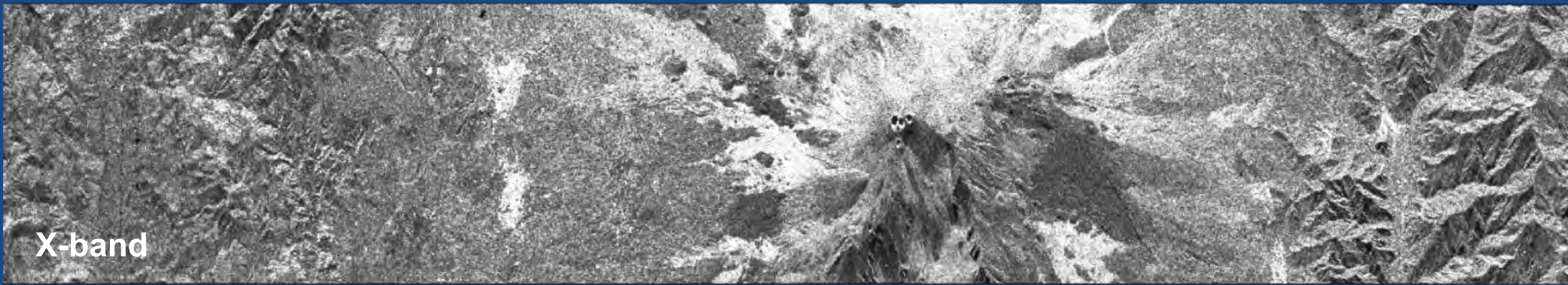

Amplitude Images

24 Hours Temporal Baseline

SIR-C / Test Site: Mt. Etna, Italy

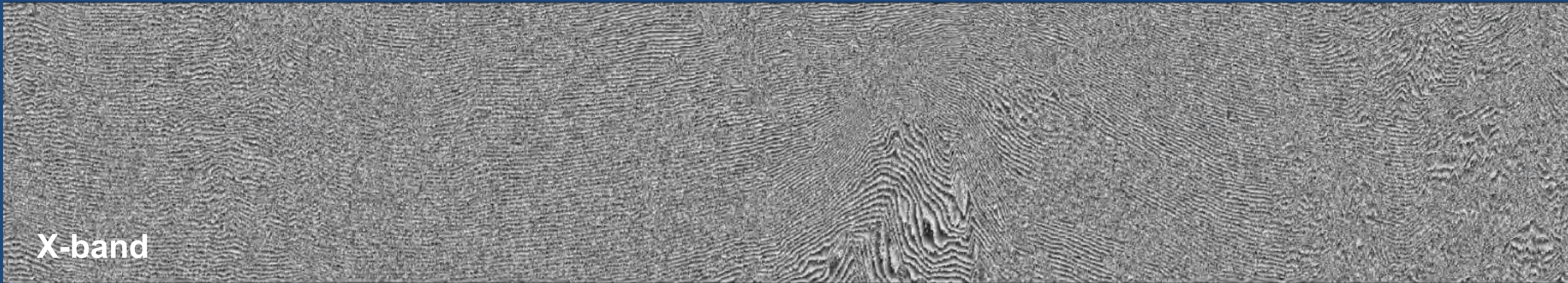

Phase Images

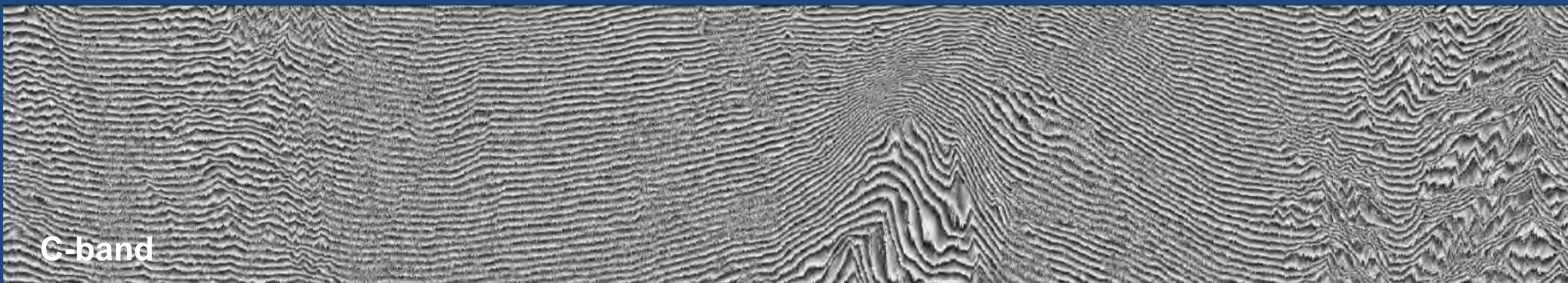

SIR-C / Test Site: Mt. Etna, Italy

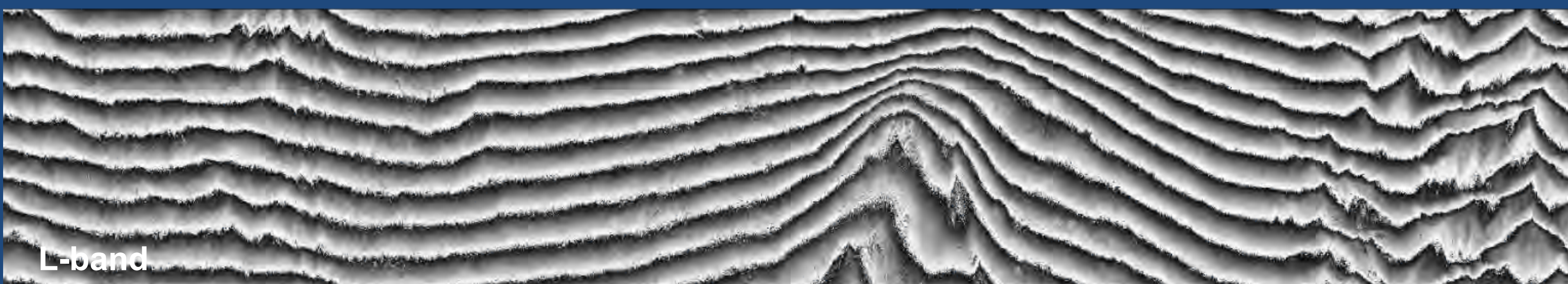

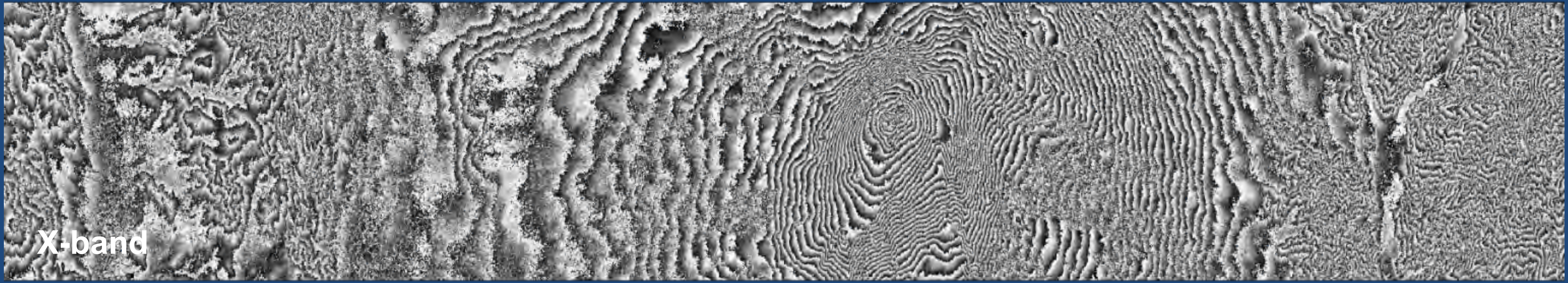

Phase Images

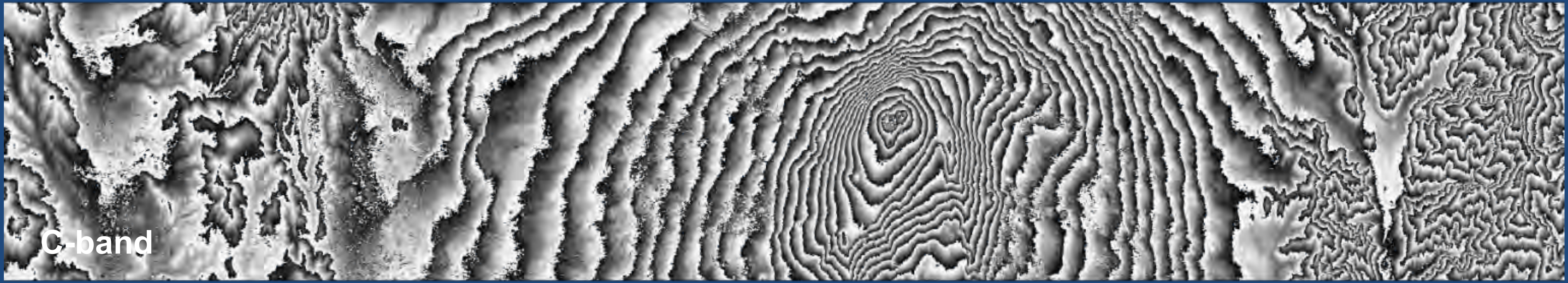

SIR-C / Test Site: Mt. Etna, Italy

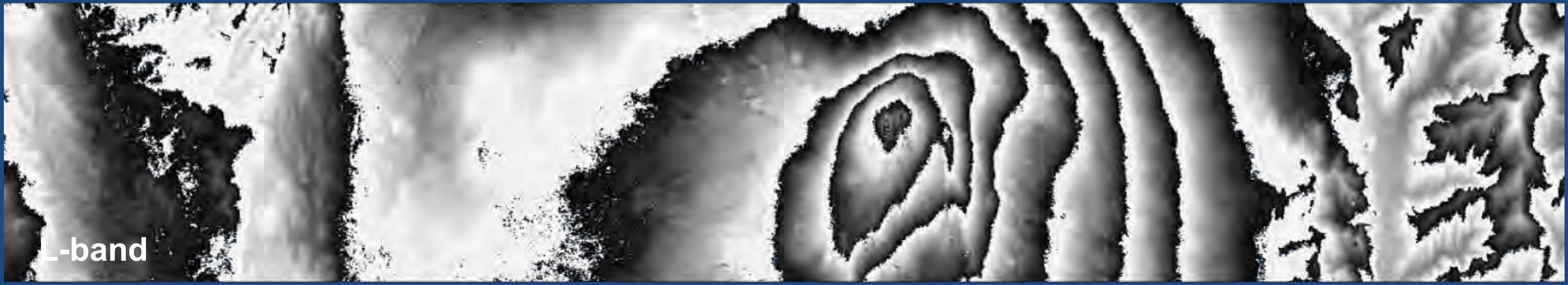

Interferometric Coherence

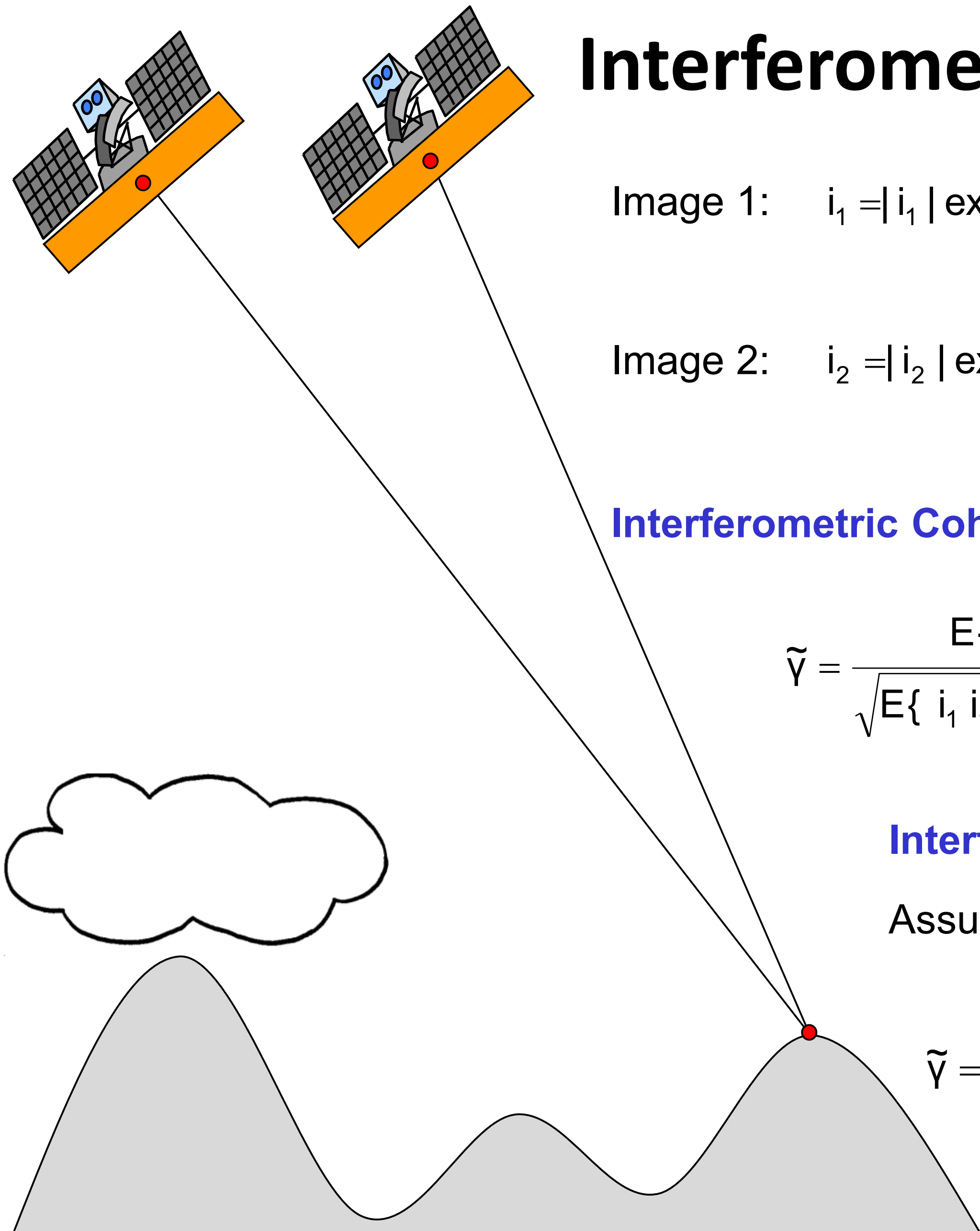

Image 1: $\quad i_1 = |i_1| \exp[-i(2\frac{2\pi}{\lambda}R_1) + \varphi_{S1}]$

Image 2: $\quad i_2 = |i_2| \exp[-i(2\frac{2\pi}{\lambda}R_2) + \varphi_{S2}]$

Interferometric Coherence: Normalised Complex Correlation Coefficient

$$\tilde{\gamma} = \frac{E\{\, i_1\, i_2^* \,\}}{\sqrt{E\{\, i_1\, i_1^* \,\}\; E\{\, i_2\, i_2^* \,\}}} = \frac{|\, E\{\, i_1\, i_2^* \,\}\,|\, \exp(i\varphi)}{\sqrt{E\{|\, i_1\,|^2\}\; E\{|\, i_2\,|^2\}}} \qquad 0 \leq |\, \tilde{\gamma} \,| \leq 1$$

Interferometric Coherence Estimation:

Assuming stationarity within the estimation window:

$$\tilde{\gamma} = \frac{\sum_{W} i_1[i,j]\; i_2^*[i,j]}{\sqrt{\sum_{W} |\, i_1[i,j]\,|^2 \sum_{W} |\, i_2[i,j]\,|^2}} = \frac{< i_1\, i_2^* >}{\sqrt{< i_1\, i_1^* >\; < i_2\, i_2^* >}}$$

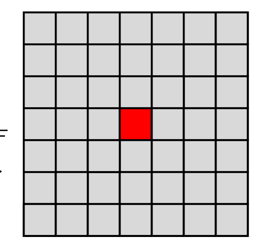

Typical window size: 10 (3x3) – >100 pixels

InSAR Coherence

… is a measure of interferogram quality:

Standard Deviation of the InSAR Phase φ:

$$\sigma_{\varphi} = \sqrt{\int_{-\pi}^{\pi} \varphi^2 \mathrm{pdf}(\varphi) \cdot d\varphi}$$

depends on ► the underlying coherence &

► the number of looks N.

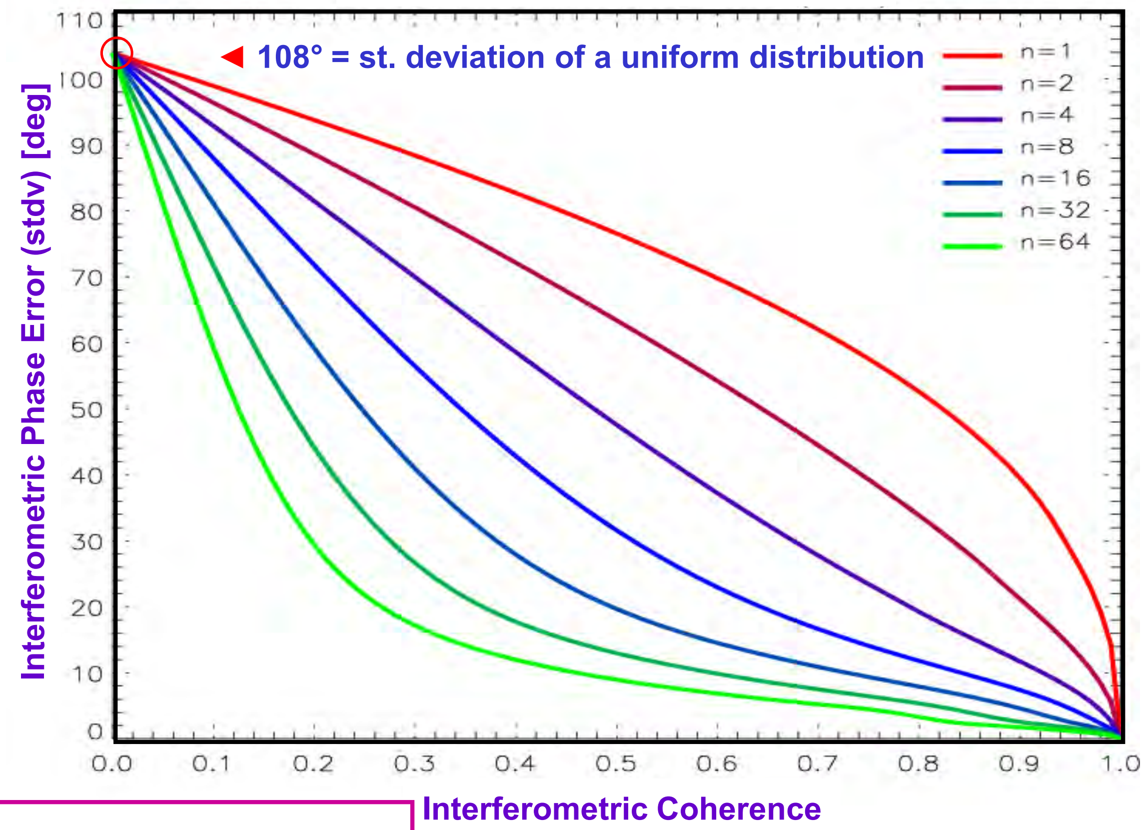

An increase in decorrelation (= loss in coherence) is associated with an increase in the phase variance;

► Increased phase variance leads to increased height errors.

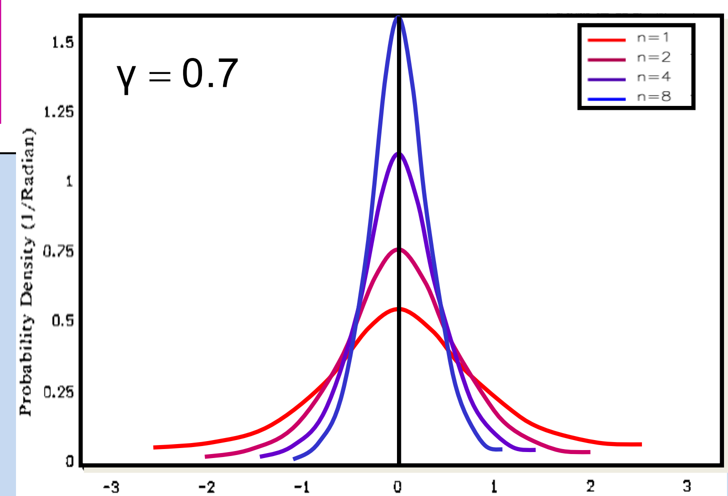

where: $$\mathrm{pdf}(\varphi, N) = \frac{\Gamma(N+1/2)(1-|\gamma|^2)^2\beta}{2\sqrt{\pi}\Gamma(N)(1-\beta^2)^{N+1/2}} + \frac{(1-|\gamma|^2)^N}{2\pi} F(N,1;1/2;\beta^2)$$

► F is a Gauss hypergeometric function and $\beta = |\gamma| \cos(\varphi - \overline{\varphi})$

► **N is the number of Looks**

Interferometric Phase Images

Simulation

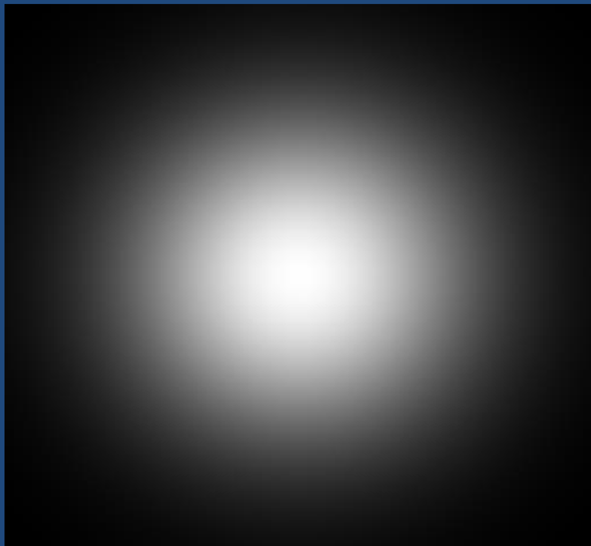

Absolute Phase

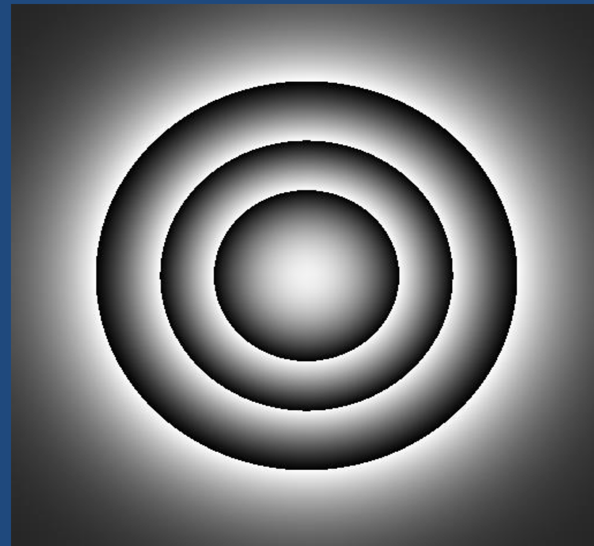

Coherence=1.0 Looks=1

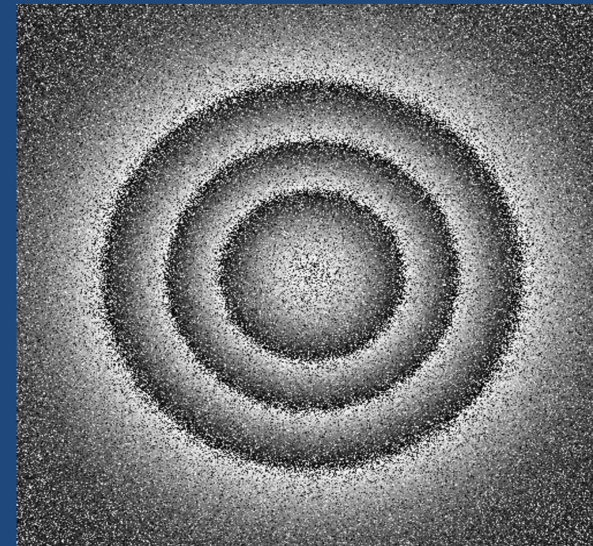

Coherence=0.8 Looks=1

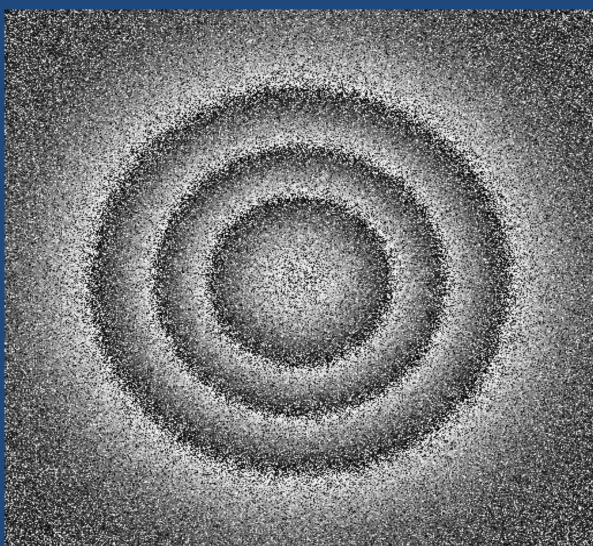

Coherence=0.6 Looks=1

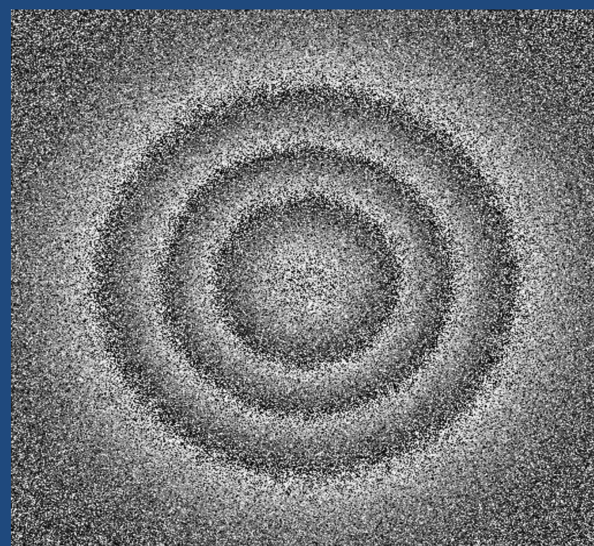

Coherence=0.4 Looks=1

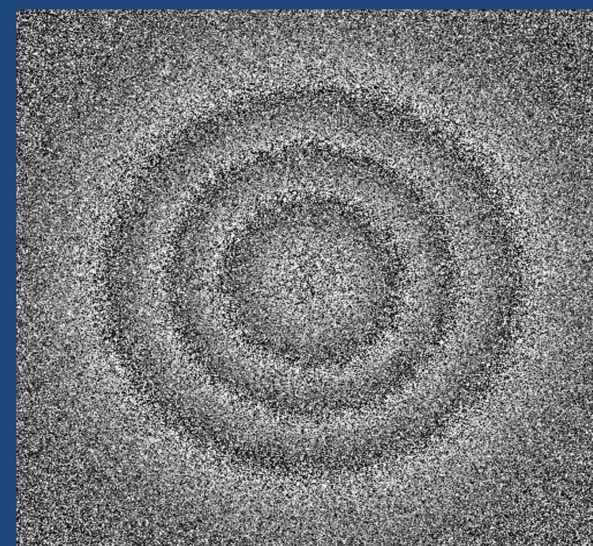

Coherence=0.2 Looks=1

hajnsek@ifu.baug.ethz.ch
irena.hajnsek@dlr.de

Interferometric Phase Images

Simulation

Absolute Phase

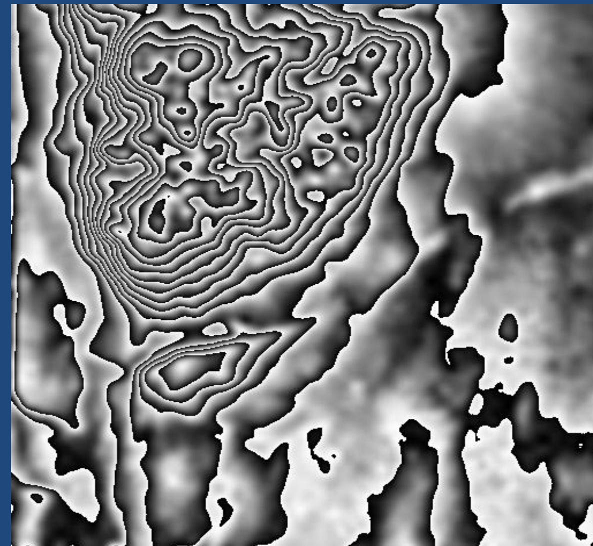

Coherence=1.0 Looks=1

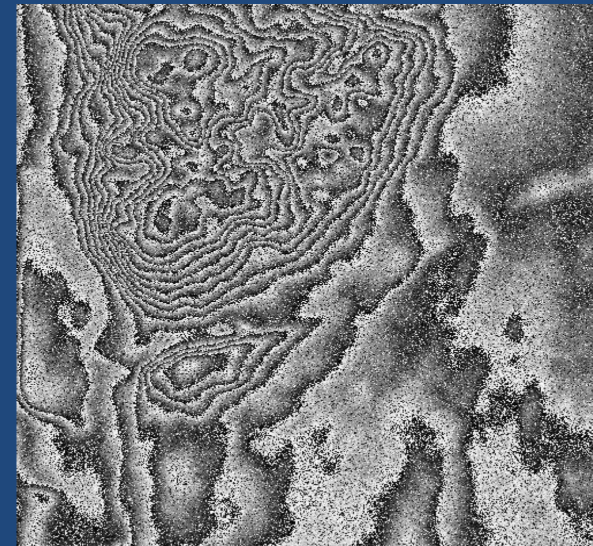

Coherence=0.8 Looks=1

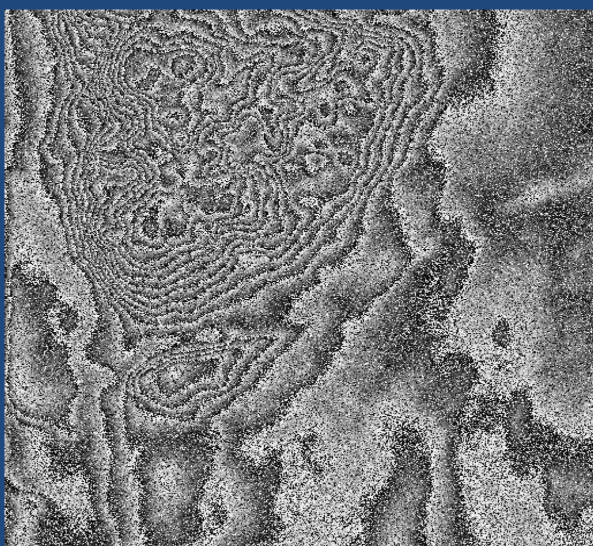

Coherence=0.6 Looks=1

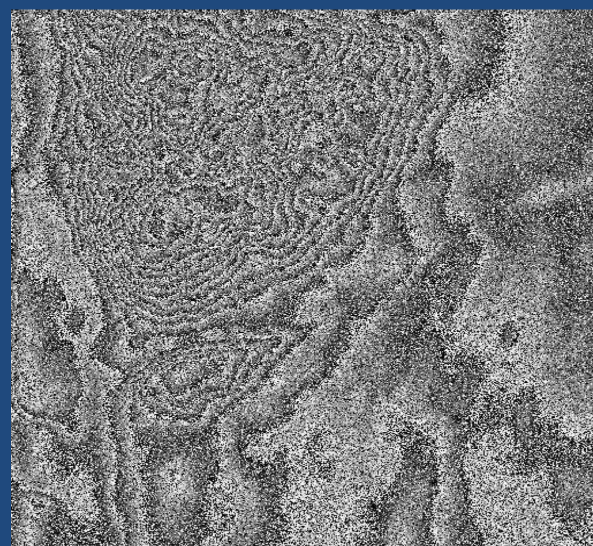

Coherence=0.4 Looks=1

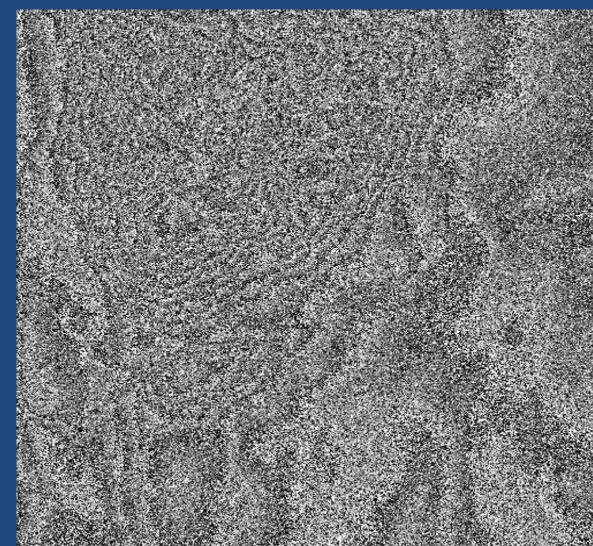

Coherence=0.2 Looks=1

hajnsek@ifu.baug.ethz.ch
irena.hajnsek@dlr.de

Repeat-Pass SAR Interferometry

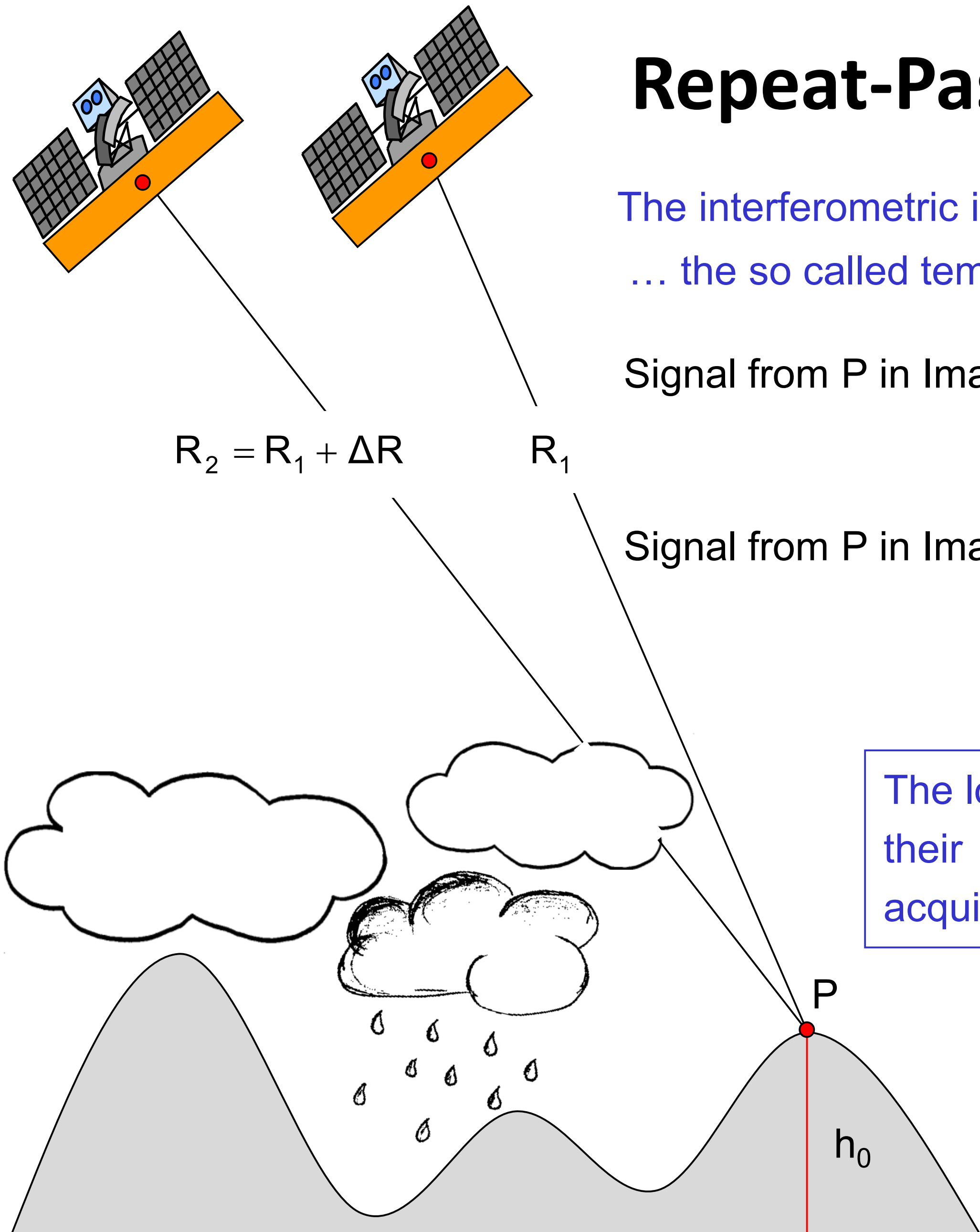

The interferometric images are acquired at different times

… the so called temporal baseline may range from seconds to years

Signal from P in Image 1 @ time t_1:

$$i_1 = |i_1| \exp[-i(2\frac{2\pi}{\lambda}R_1) + \varphi_S(t_1) + \varphi_{Prop}(t_1)]$$

Signal from P in Image 2 @ time t_2:

$$i_2 = |i_2| \exp[-i(2\frac{2\pi}{\lambda}R_2) + \varphi_S(t_2) + \varphi_{Prop}(t_2)]$$

The location of the scatterers in the resolution cell and/or their properties may change in the time between the two acquisitions: $\varphi_S(t_1) \neq \varphi_S(t_2)$ **Temporal decorrelation**

The phase induced by the propagation medium (atmosphere or ionosphere) varies in the time between the two acquisitions: $\varphi_{Prop}(t_1) \neq \varphi_{Prop}(t_2)$

Earth Ob
Remote

Reduced and variable quality but allows displacement measurements

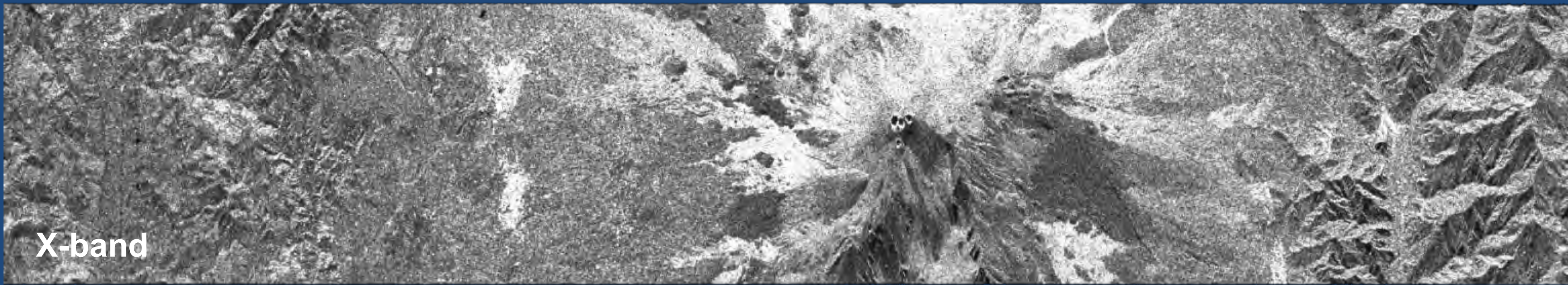

Amplitude Images

24 Hours Temporal Baseline

SIR-C / Test Site: Mt. Etna, Italy

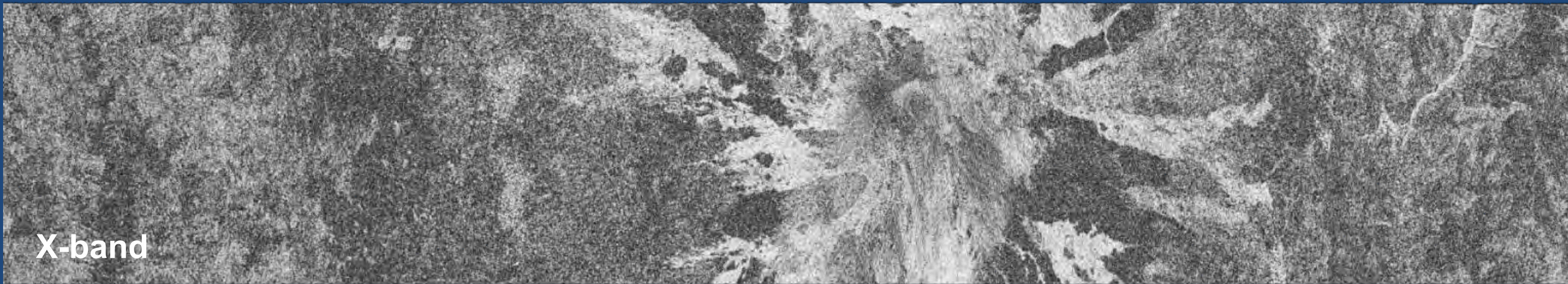

Coherence Images

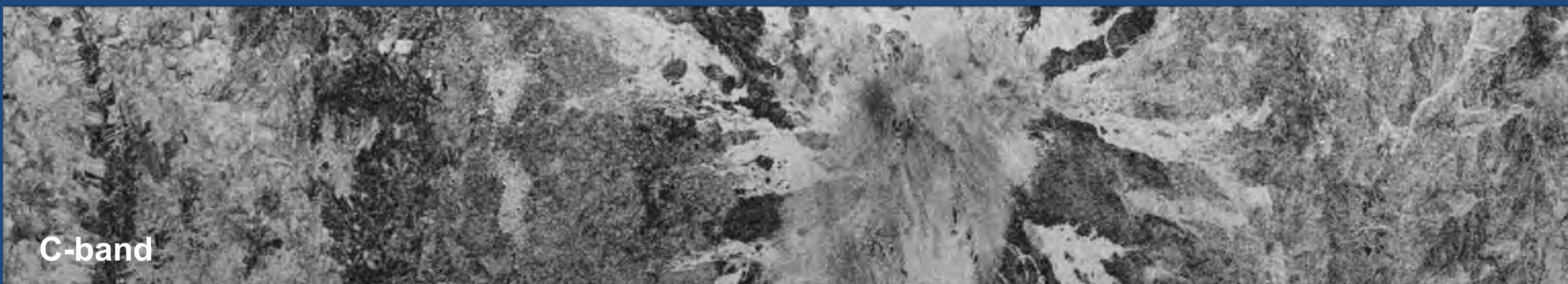

SIR-C / Test Site: Mt. Etna, Italy

Temporal Decorrelation

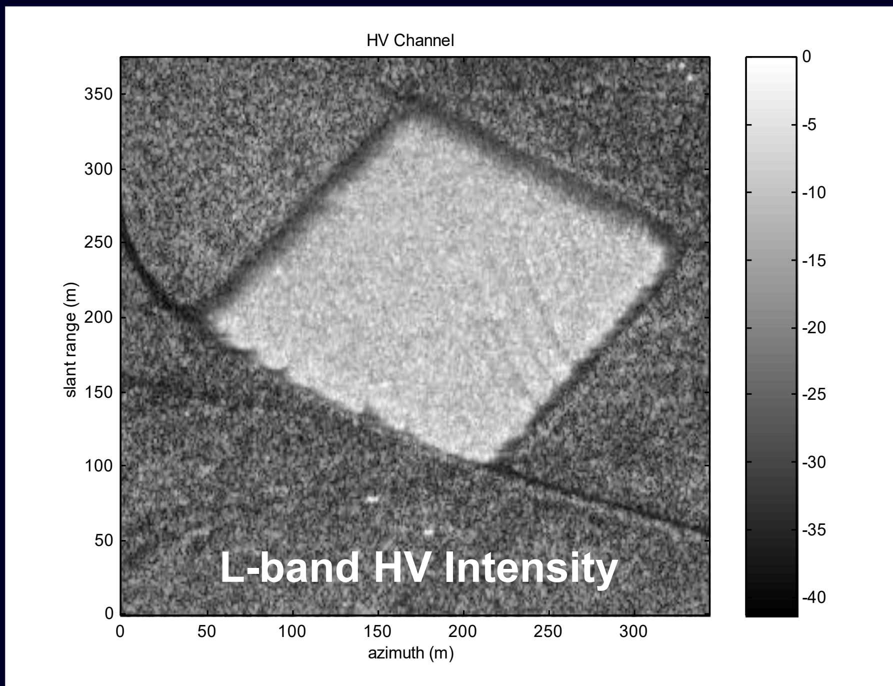

E-SAR / Test Site: Fox Covert,England

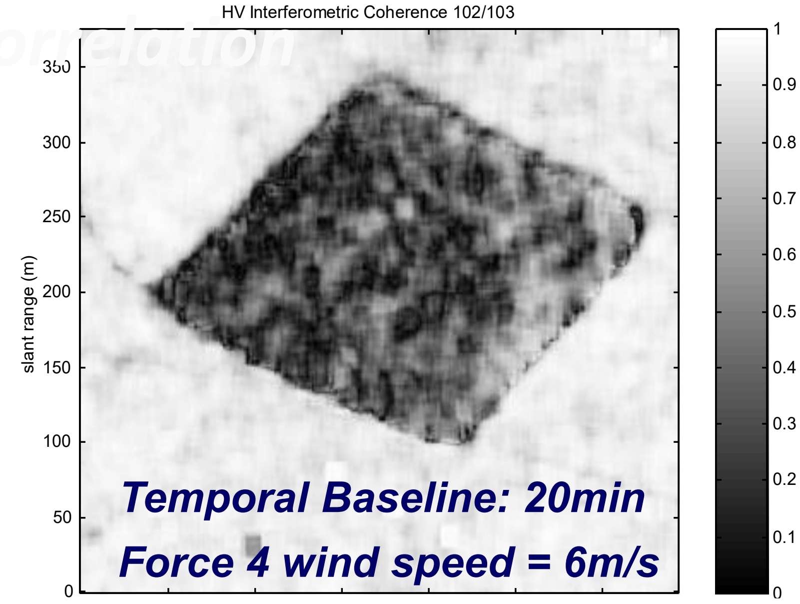

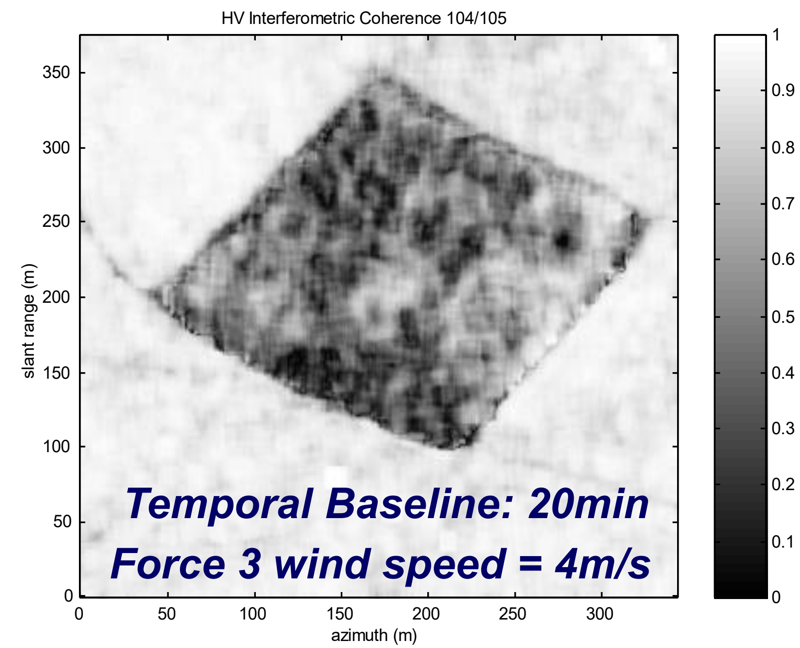

Temporal Decorrelation

E-SAR / Test Site: Fox Covert,England

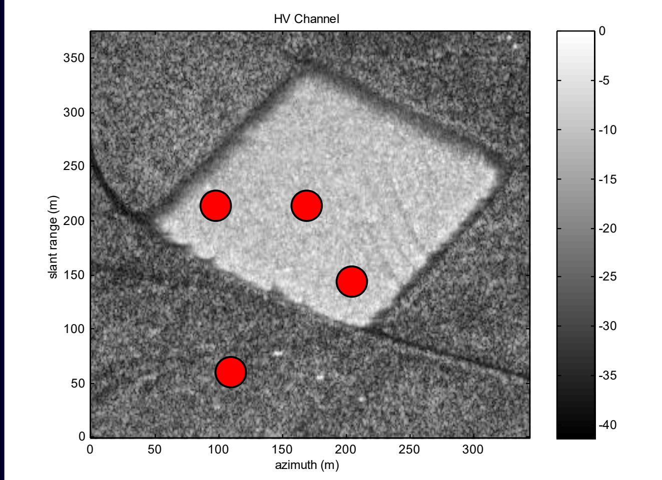

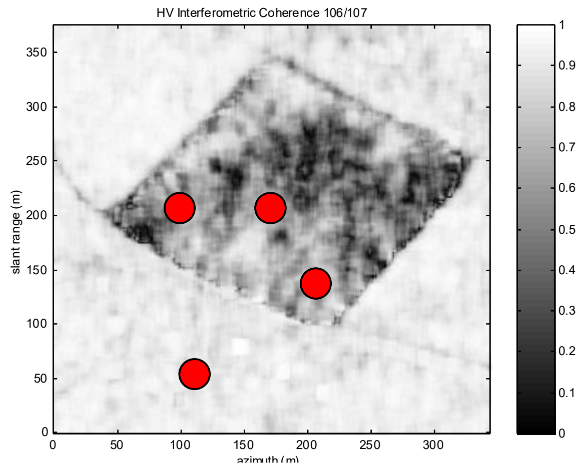

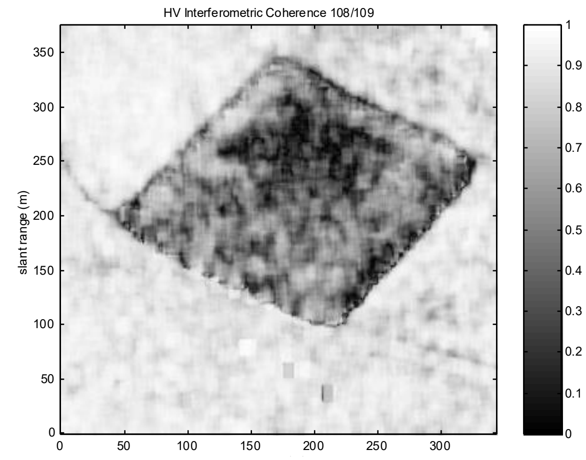

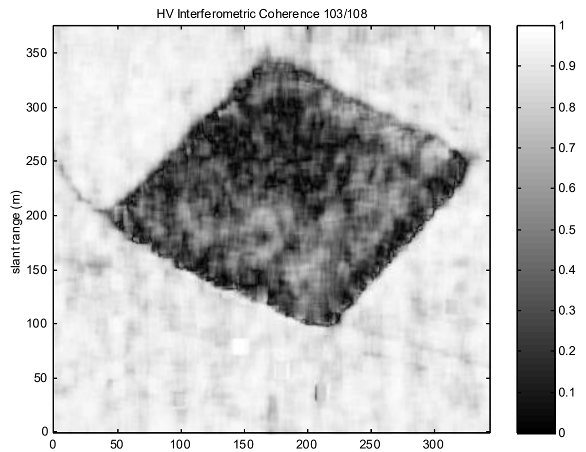

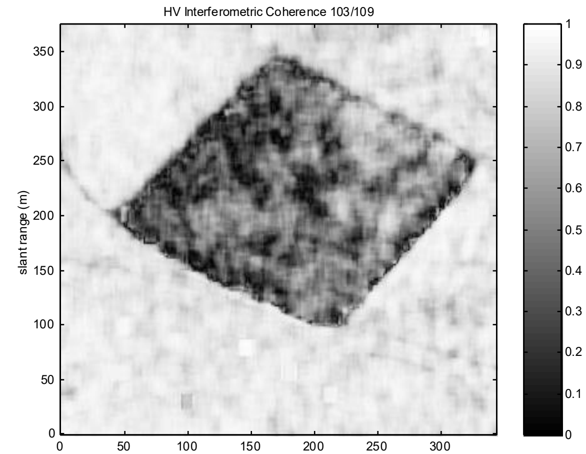

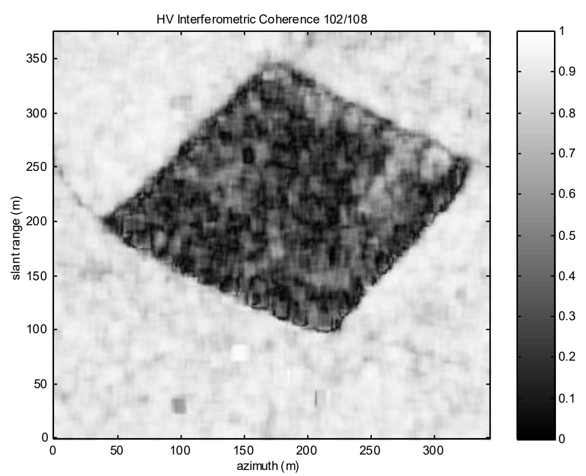

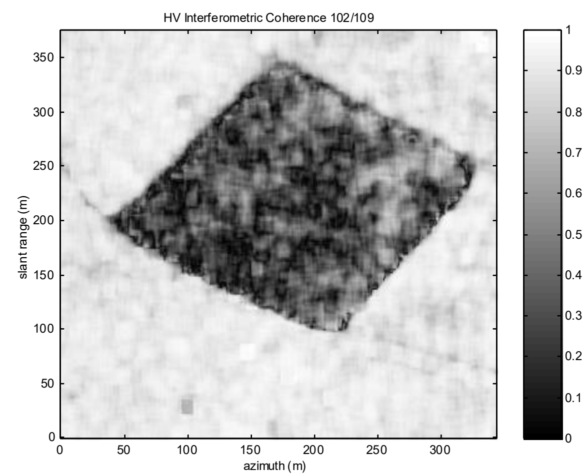

Data Courtesy QuinetiQ / UK

Forest Height Estimation – Decorrelation Effects

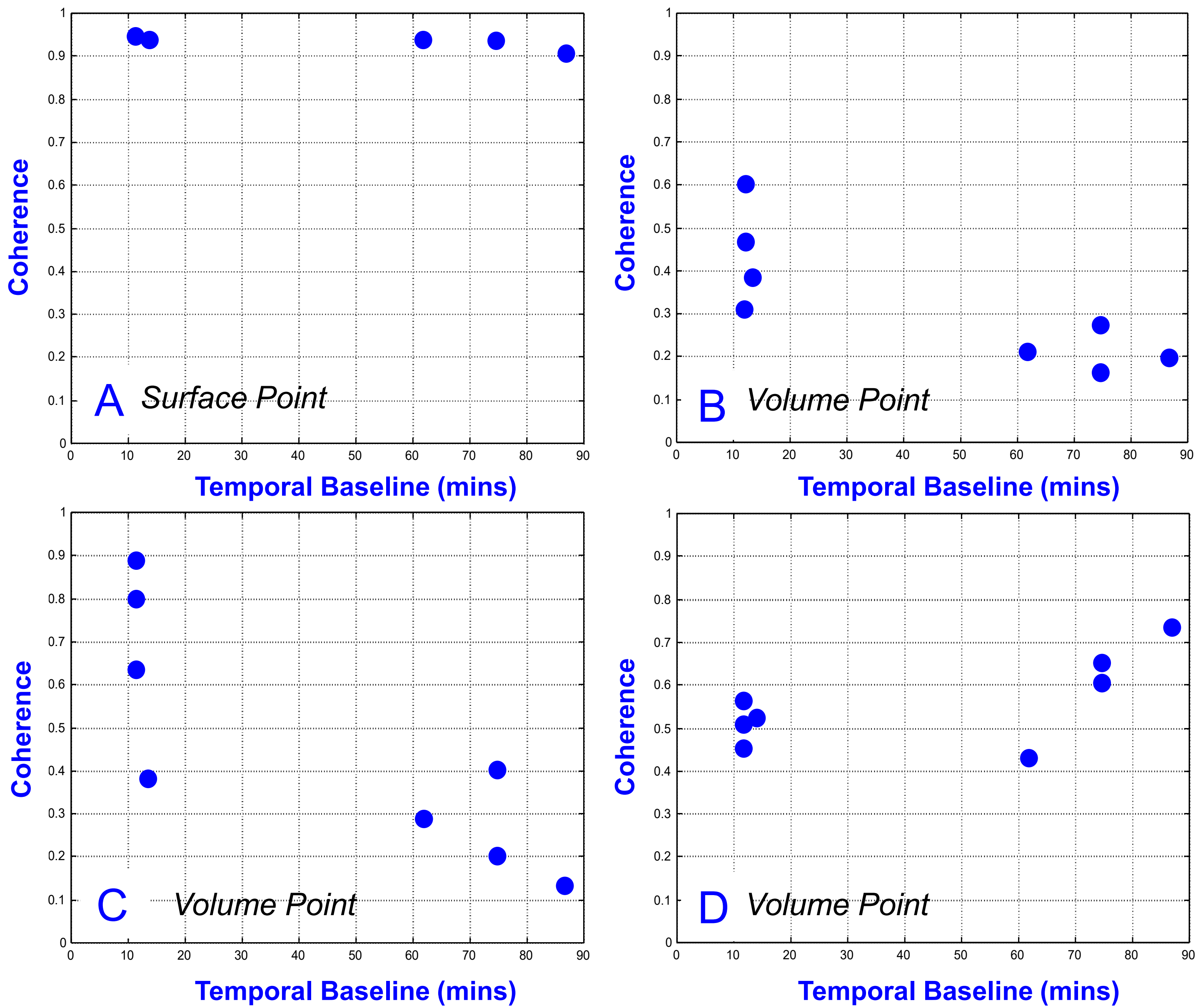

ETH
lgenössische Technische Hochschule Zürich
iss Federal Institute of Technology Zurich

TanDEM-X Data Acquisition Modes

Pursuit Monostatic	Bistatic	Alternating Bistatic
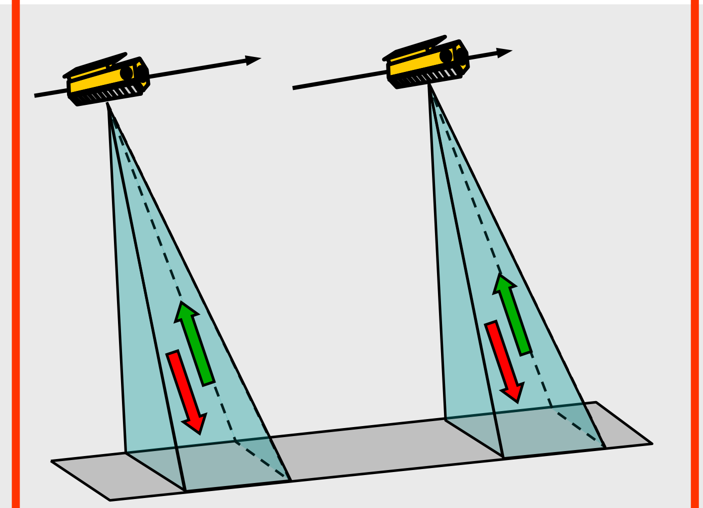	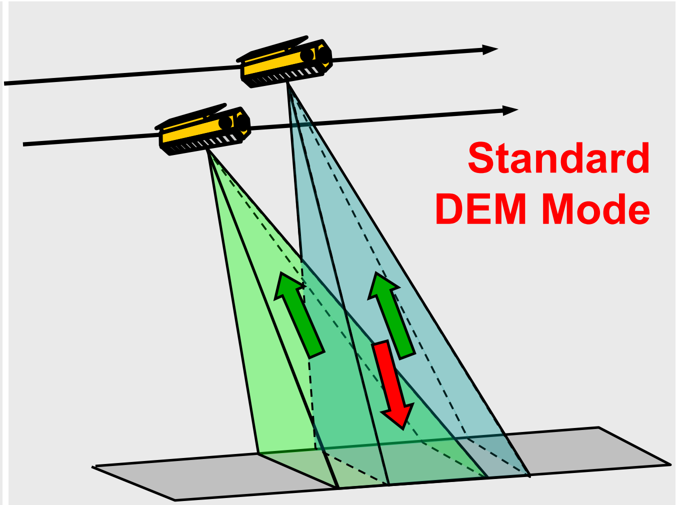	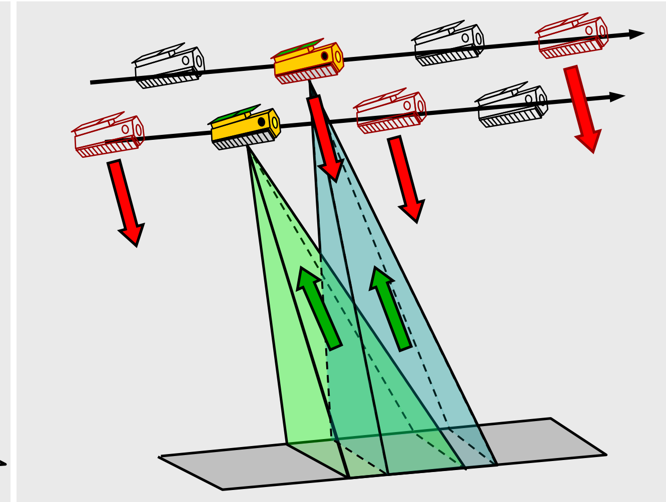
• **both satellites transmit and receive independently** • susceptible to temporal decorrelation and atmospheric disturbances • no PRF and phase synchronisation required (backup solution)	• **one satellite transmits and both satellites receive simultaneously** • small along-track displacement required for Doppler spectra overlap • requires PRF and phase synchronisation	• **transmitter alternates between PRF pulses** • provides three interferograms with two baselines in a single pass • enables precise phase synchronisation, calibration & verification

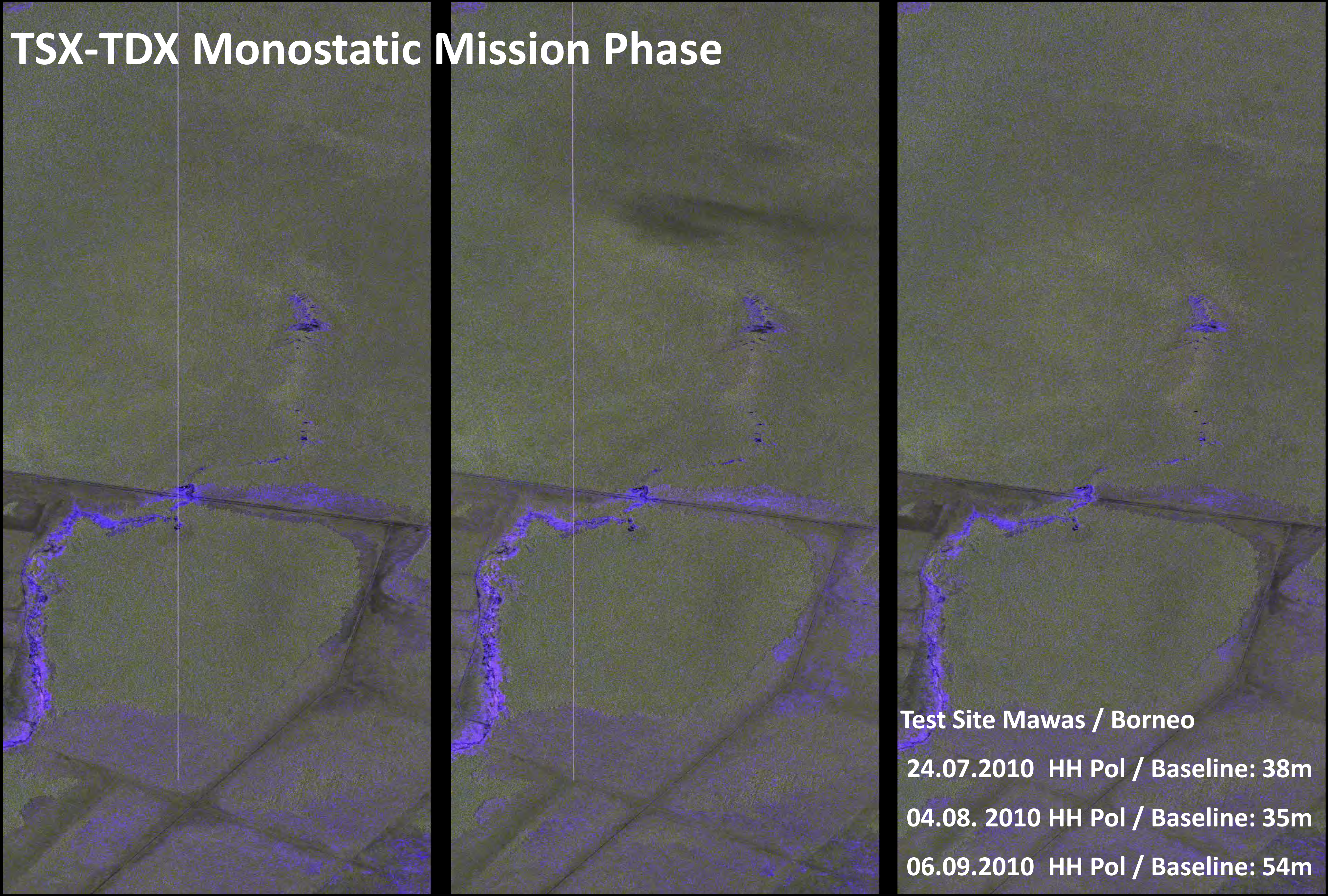
TSX-TDX Monostatic Mission Phase
Test Site Mawas / Borneo
24.07.2010 HH Pol / Baseline: 38m
04.08. 2010 HH Pol / Baseline: 35m
06.09.2010 HH Pol / Baseline: 54m

TSX-TDX Monostatic Mission Phase

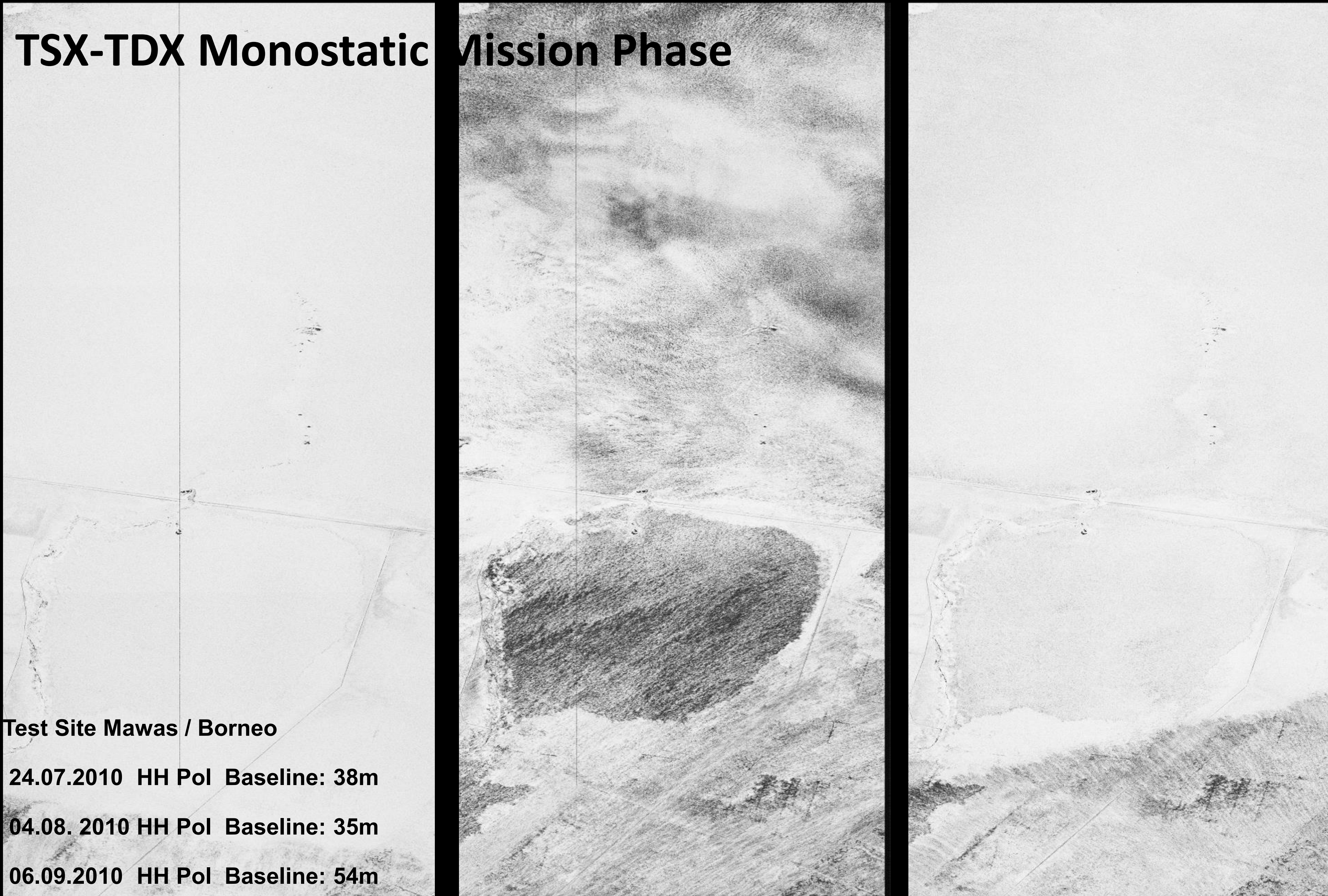

Test Site Mawas / Borneo

24.07.2010 HH Pol Baseline: 38m

04.08. 2010 HH Pol Baseline: 35m

06.09.2010 HH Pol Baseline: 54m

Single-Pass SAR Interferometry

The interferometric images are acquired at the same time

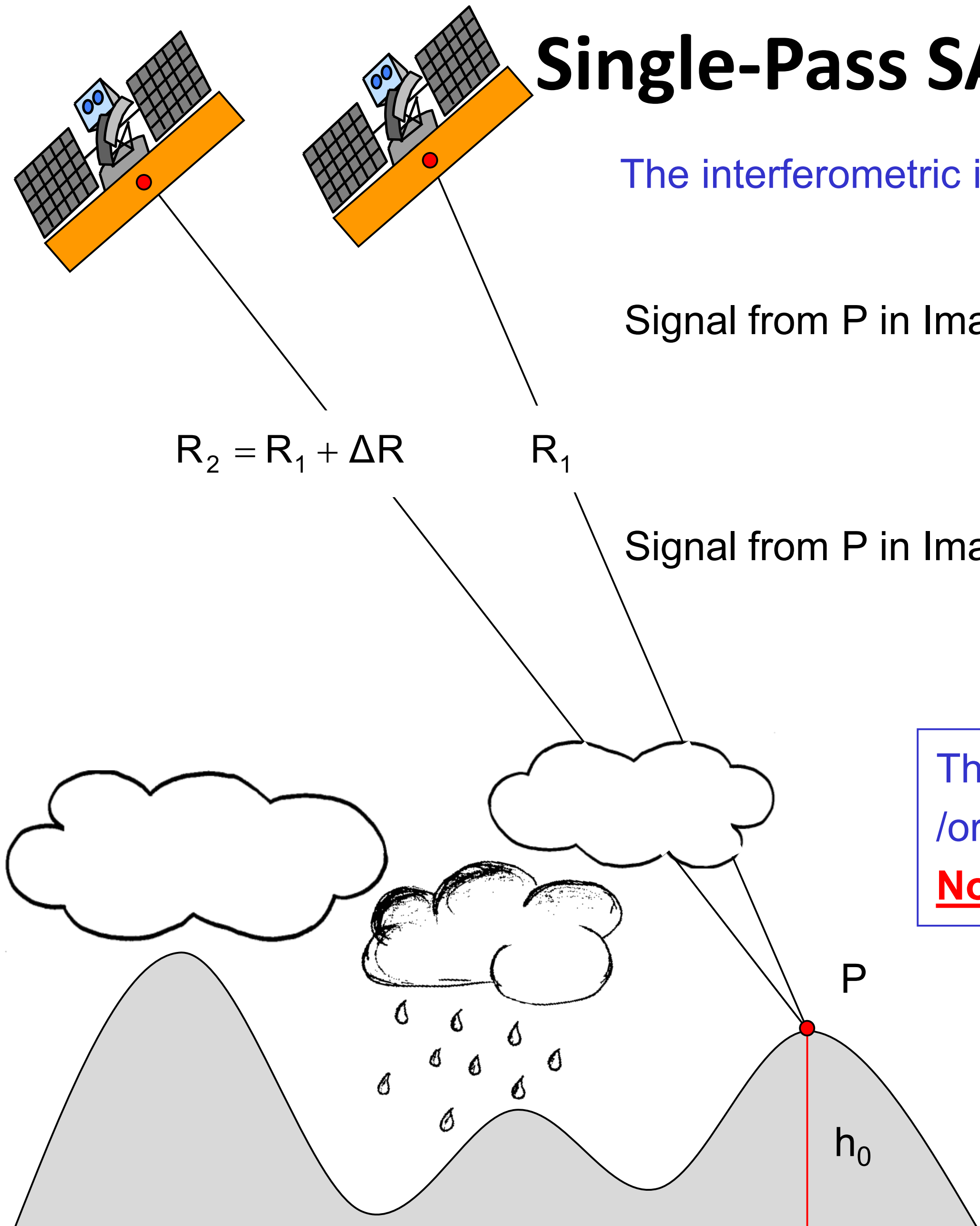

Signal from P in Image 1 @ time t_1:

$$i_1 = |i_1| \exp[-i(2\frac{2\pi}{\lambda}R_1) + \varphi_{S1}(t_1) + \varphi_{Prop}(t_1)]$$

Signal from P in Image 2 @ time t_2:

$$i_2 = |i_2| \exp[-i(2\frac{2\pi}{\lambda}R_2) + \varphi_{S1}(t_1) + \varphi_{Prop}(t_1)]$$

The location of the scatterers in the resolution cell and /or their properties are the same for both acquisitions: **No temporal decorrelation**

Both signals travel through the same atmosphere and ionosphere): $\varphi_{Prop}(t_1) = \varphi_{Prop}(t_1)$

hajnsek@ifu.baug.ethz.ch
irena.hajnsek@dlr.de

TanDEM-X Data Acquisition Modes

Pursuit Monostatic	Bistatic	Alternating Bistatic
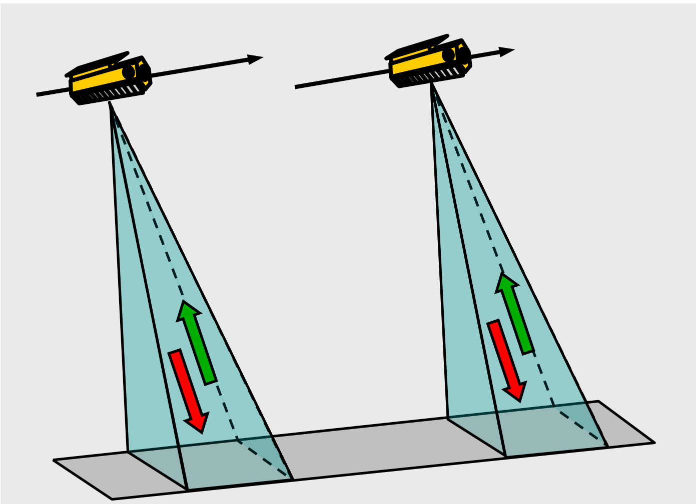	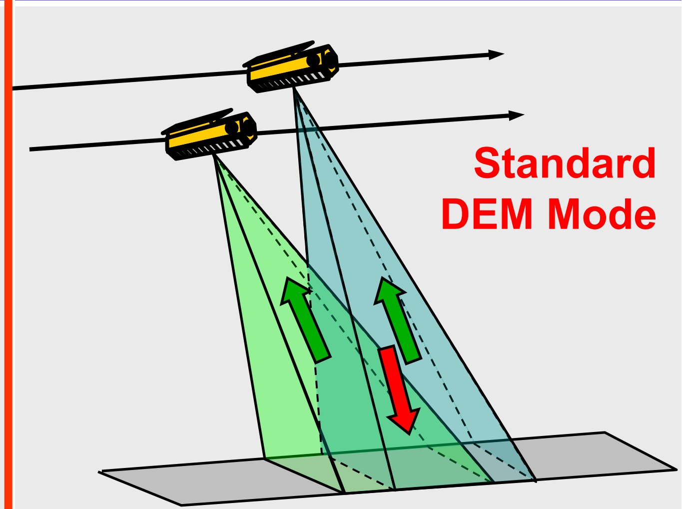	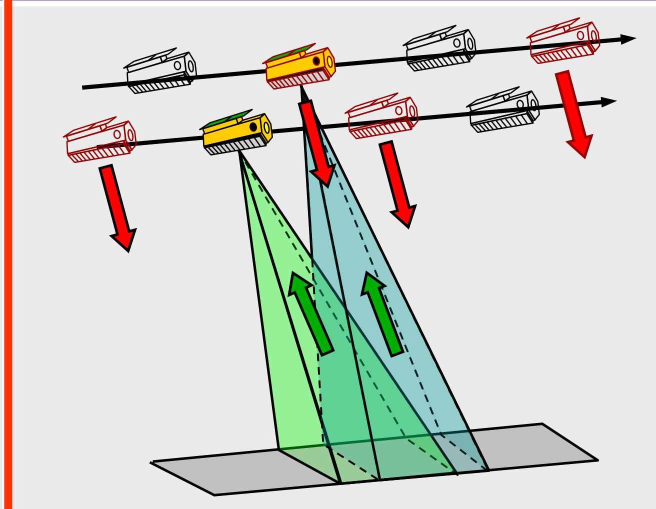
• **both satellites transmit and receive independently** • susceptible to temporal decorrelation and atmospheric disturbances • no PRF and phase synchronisation required (backup solution)	• **one satellite transmits and both satellites receive simultaneously** • small along-track displacement required for Doppler spectra overlap • requires PRF and phase synchronisation	• **transmitter alternates between PRF pulses** • provides three interferograms with two baselines in a single pass • enables precise phase synchronisation, calibration & verification

Large Baseline DEM with TanDEM-X

- first TanDEM-X DEM (acquired before reaching 20 km formation)
- large effective baseline (~ 2 km) from Earth rotation
- squint angle ensures coherence

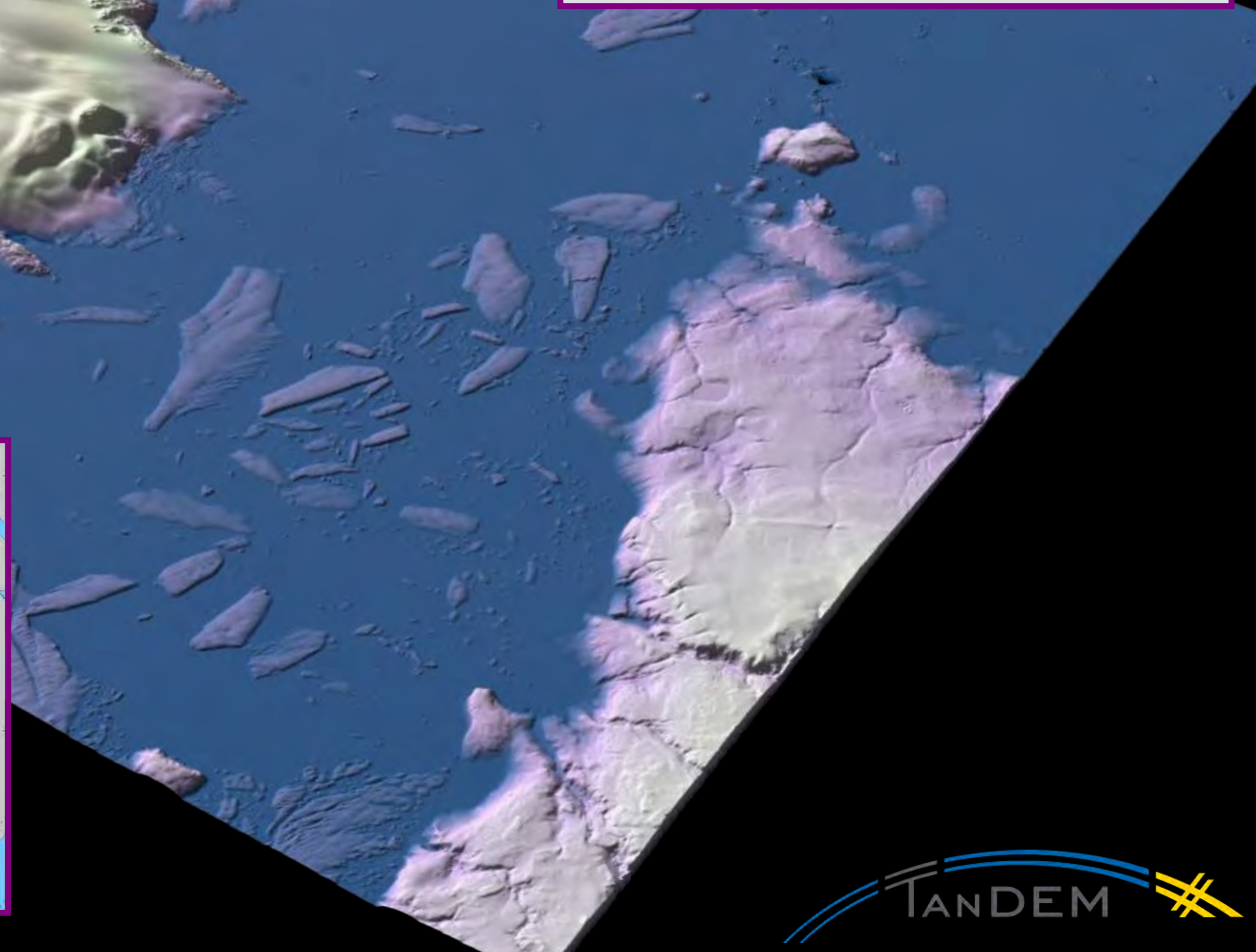

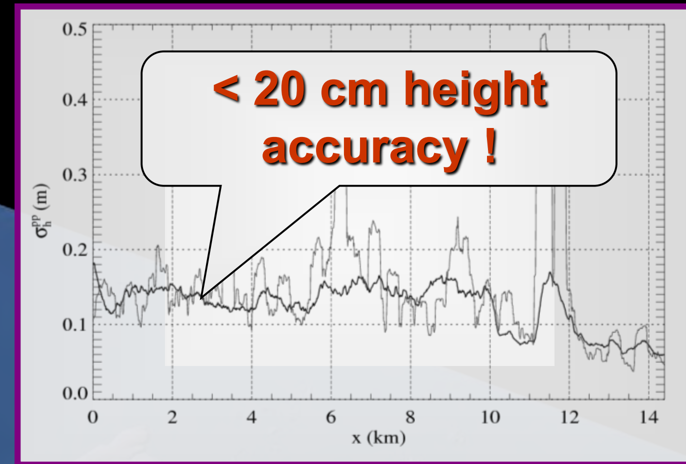

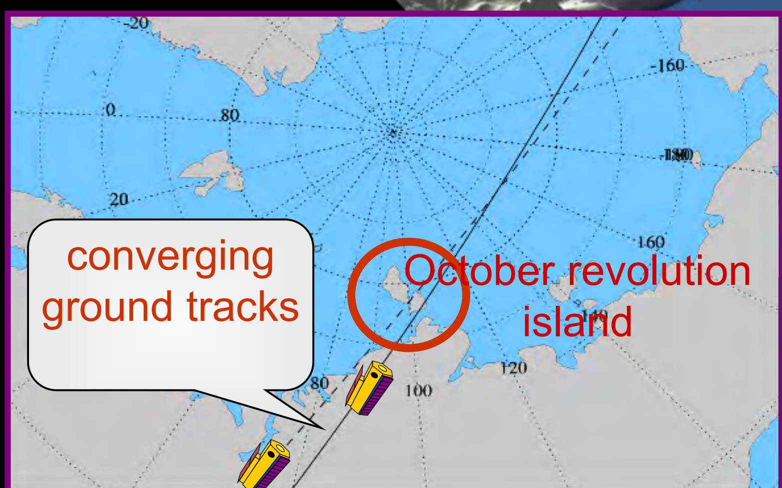

TanDEM-X: Ice loss of Aletschgletscher

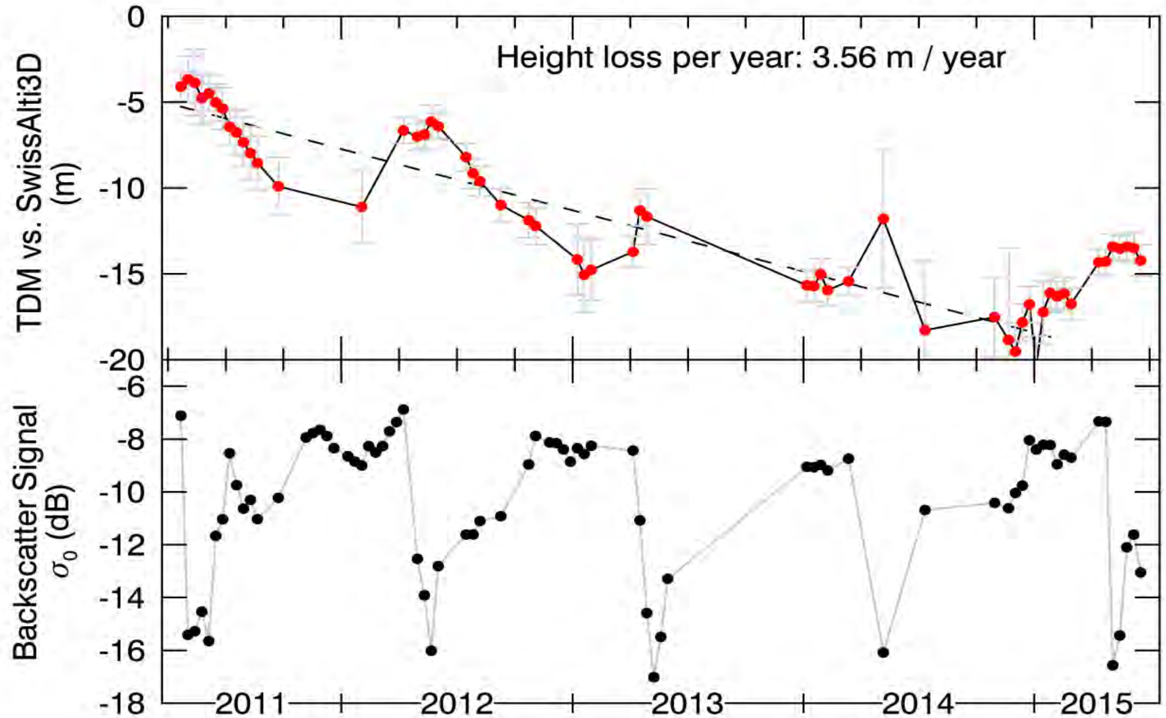

- Results consistent with IceSat data.
- In winter, the apparent elevation stays constant or even decreases(-) during snow accumulation(+) Elevation jumps up at snow melt.

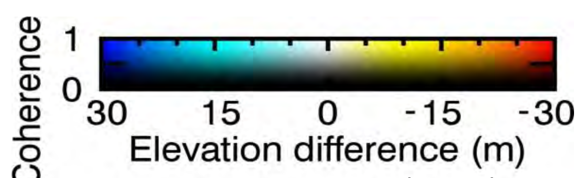

vs. SwissAlti3D (2009)

hajnsek@ifu.baug.ethz.ch
irena.hajnsek@dlr.de

ETH
Eidgenössische Technische Hochschule Zürich
Swiss Federal Institute of Technology Zurich

Snow Depth determined by DEM Differencing I

dry snow
vs.
wet snow

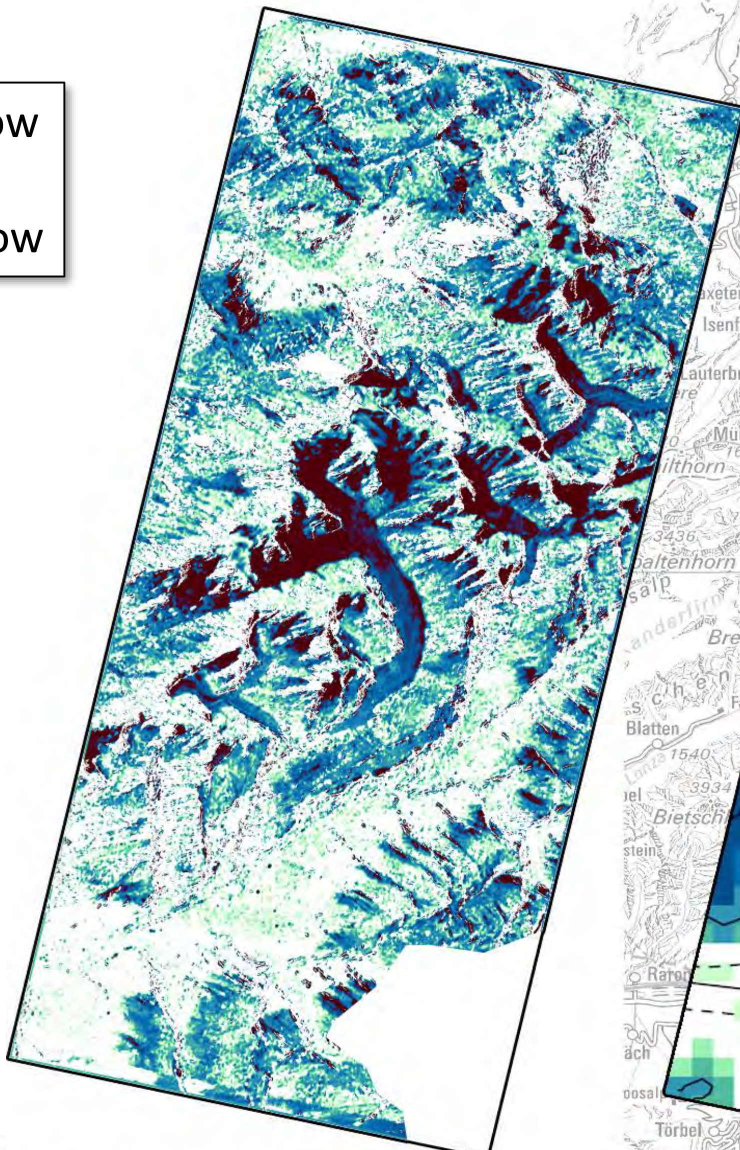

TanDEM-X elevation difference,
17.04.2013 vs. 06.04.2013

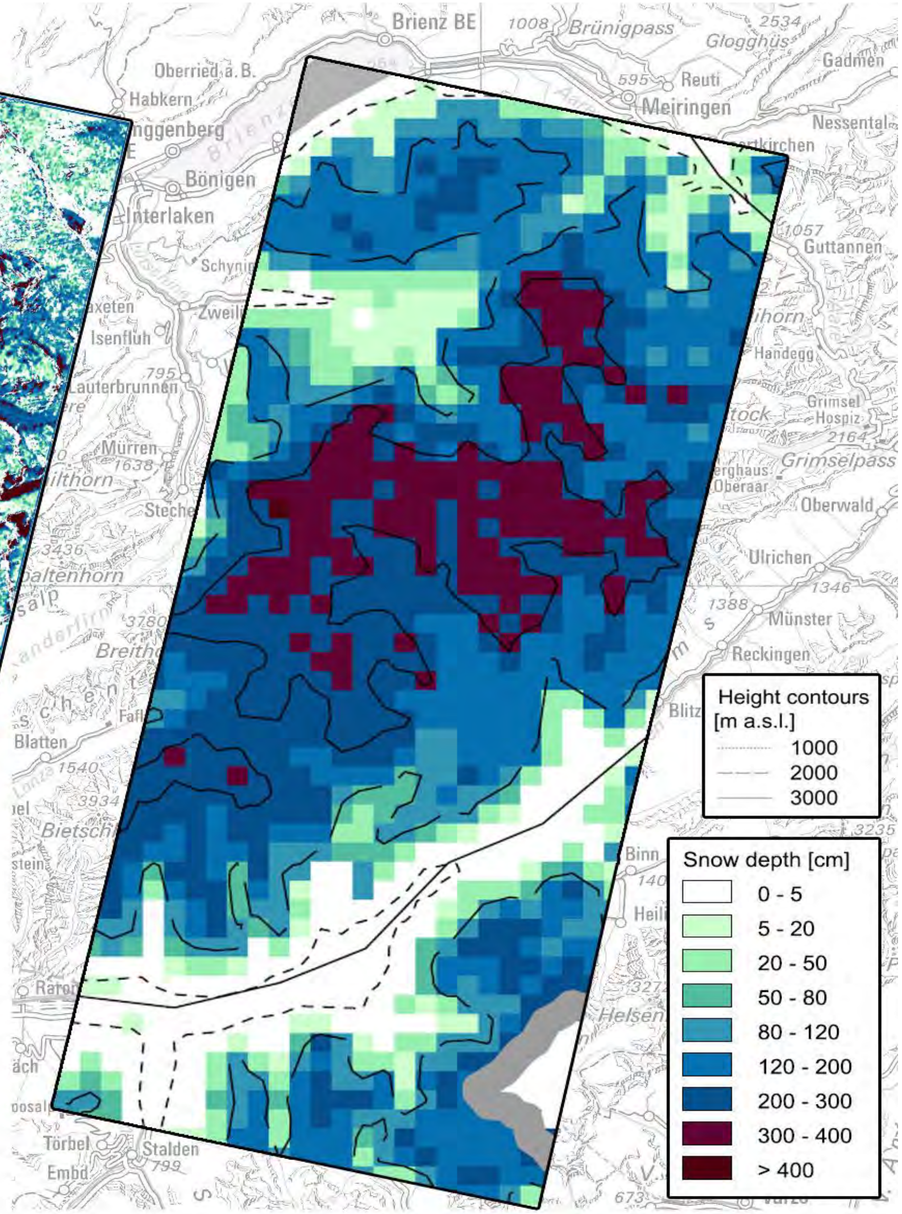

SLF, snow depth map, 18.04.2013

Snow Depth determined by DEM Differencing II

summer
vs.
wet snow
in spring

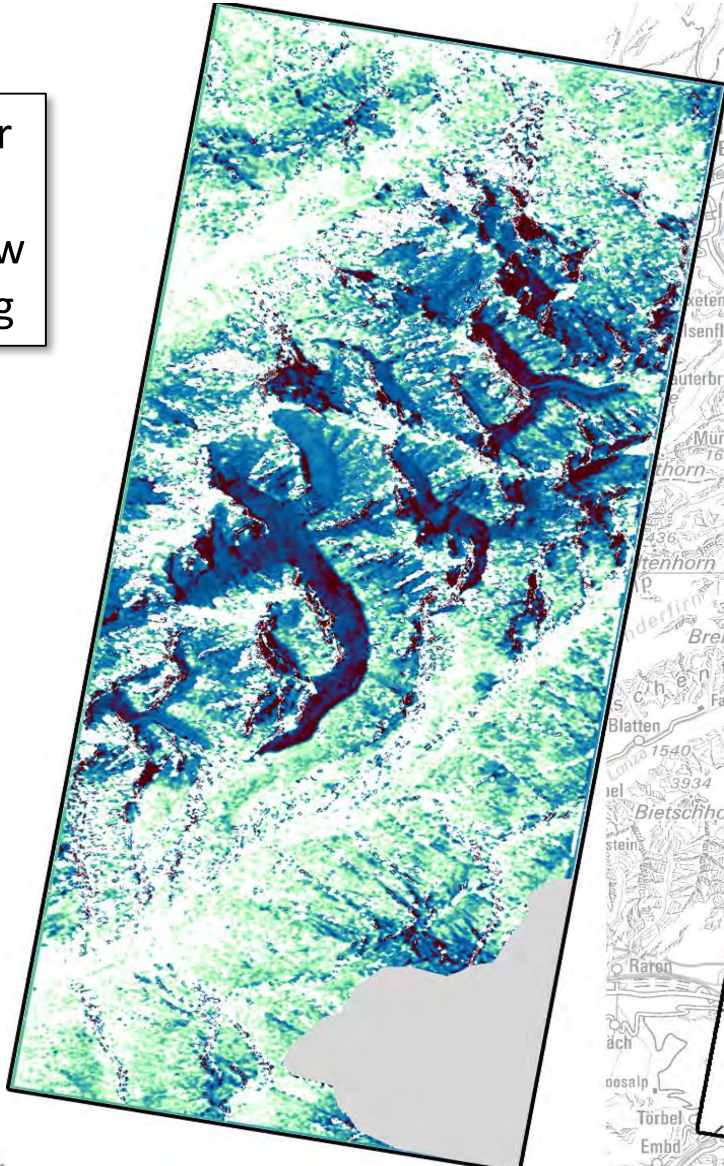

TanDEM-X elevation difference,
02.06.2012 vs. 27.07.2012

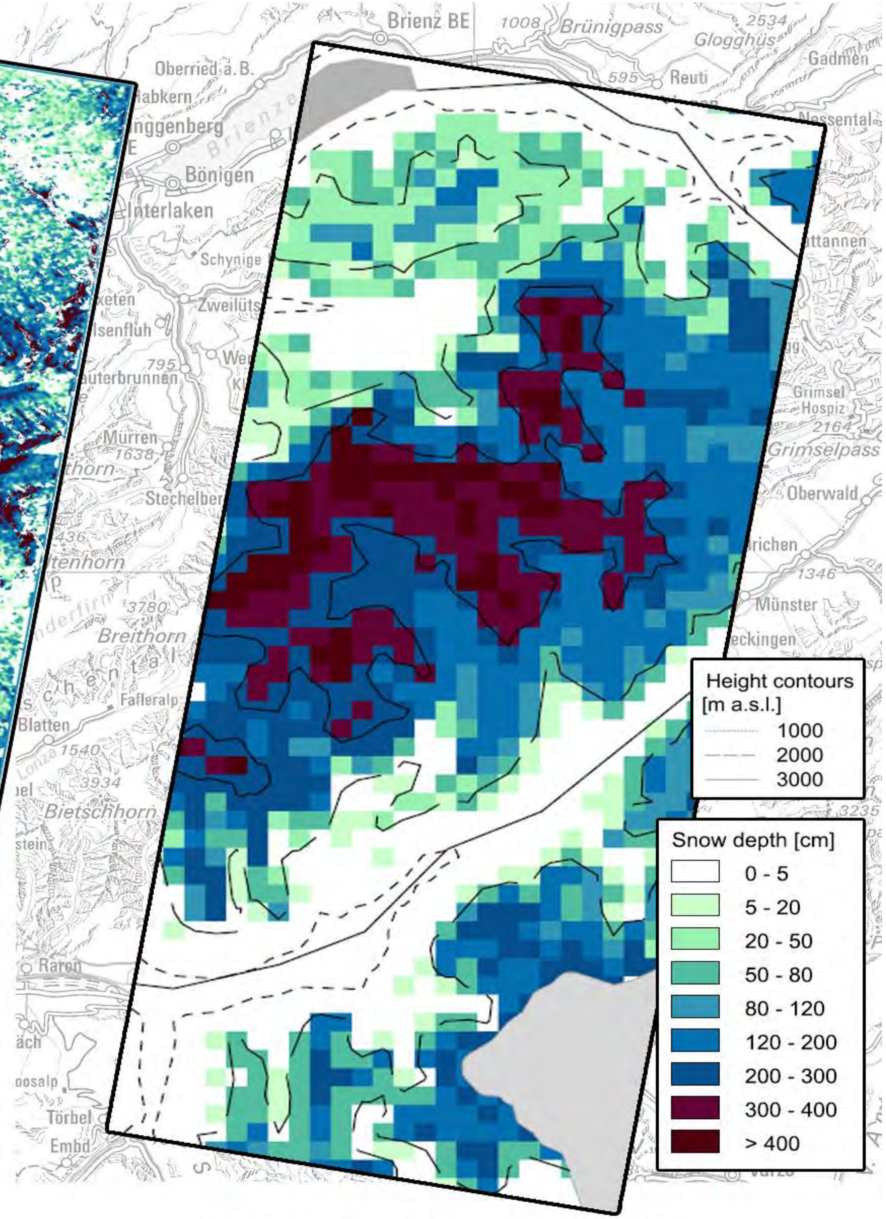

SLF, snow depth map, 31.05.2012

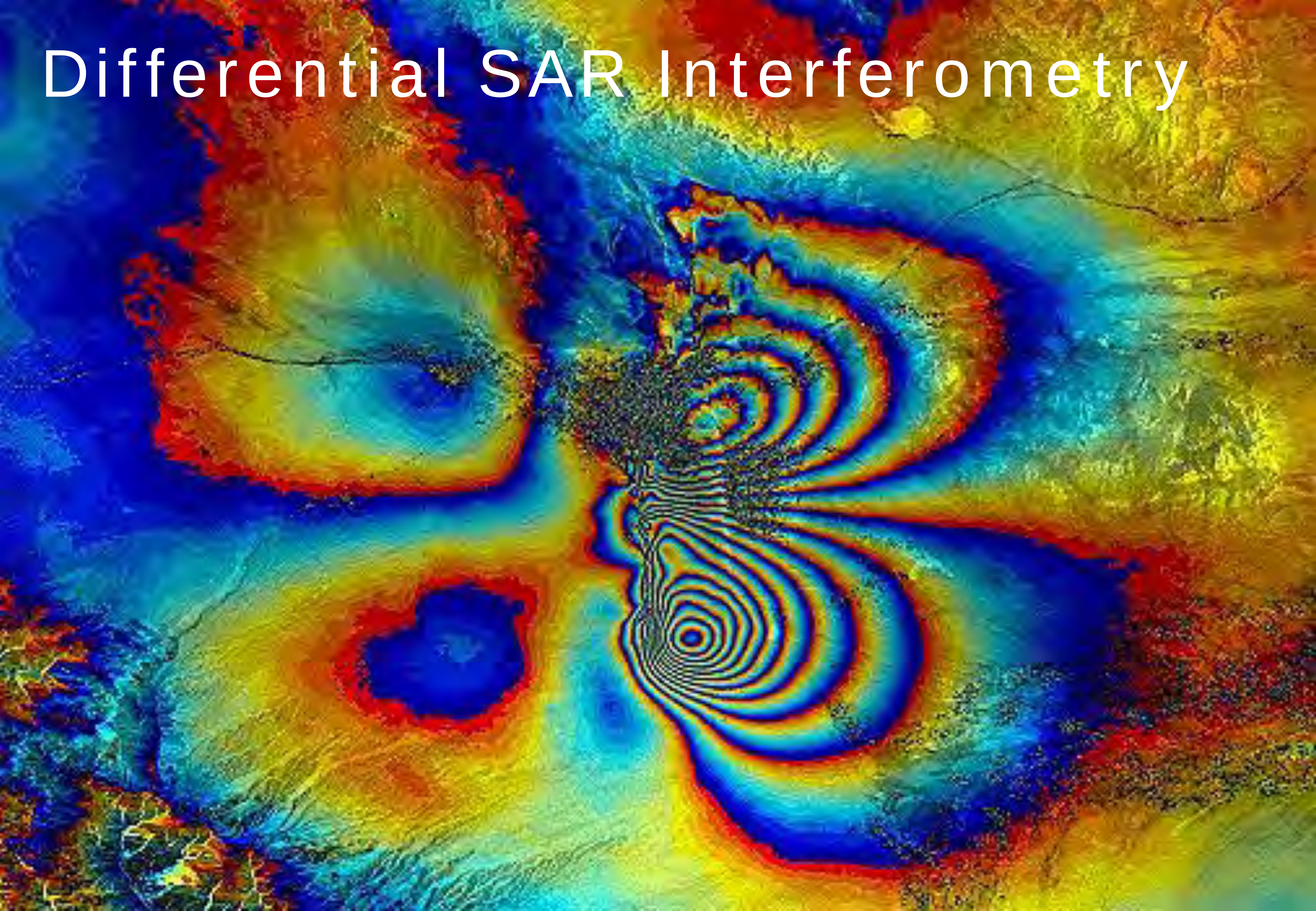
Differential SAR Interferometry

SAR Interferometry

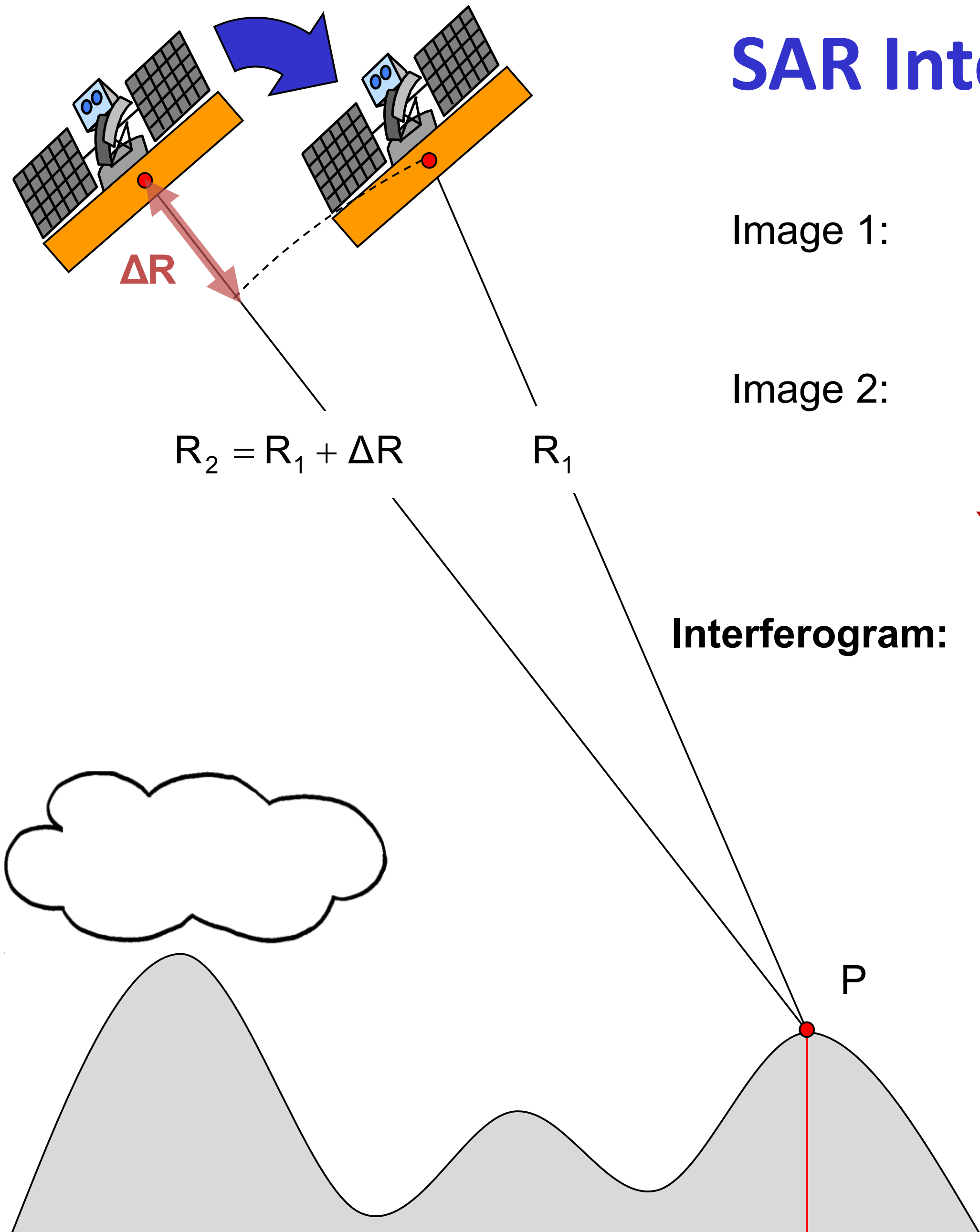

Image 1: $i_1 = |i_1| \exp[-i(2\frac{2\pi}{\lambda}R_1) + \varphi_{S1}]$

Image 2: $i_2 = |i_2| \exp[-i(2\frac{2\pi}{\lambda}R_1) + \varphi_{S2}]$

Assuming $\varphi_{S1} = \varphi_{S2}$!!!

Interferogram: $i_1\, i_2^* = |i_1\, i_2^*| \exp[-i(2\frac{2\pi}{\lambda}\Delta R)]$

hajnsek@ifu.baug.e
irena.hajnsek@d

Differential SAR Interferometry (D-InSAR)

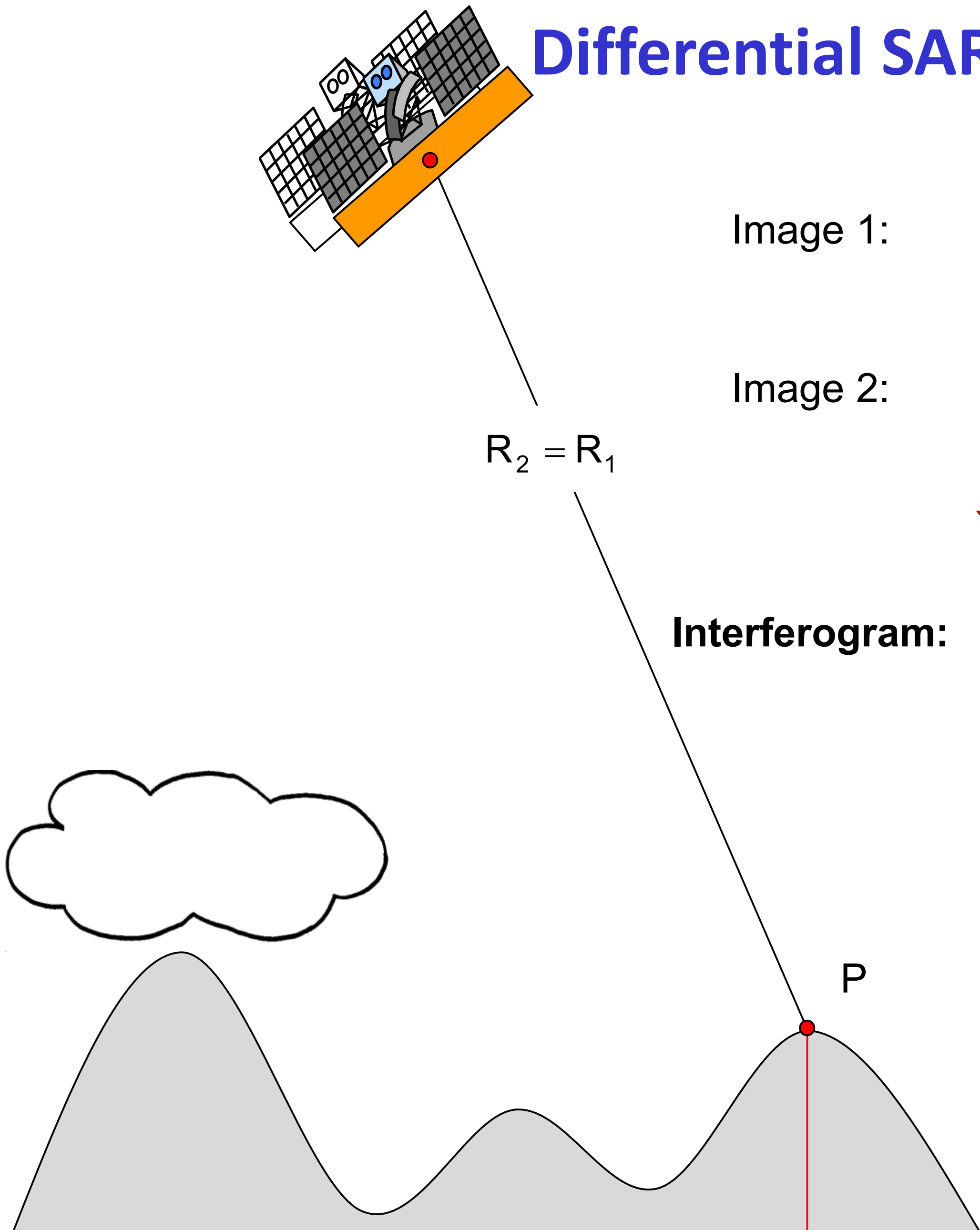

Image 1: $$i_1 = |i_1| \exp[-i(2\frac{2\pi}{\lambda}R_1) + \varphi_{S1}]$$

Image 2: $$i_2 = |i_2| \exp[-i(2\frac{2\pi}{\lambda}R_1) + \varphi_{S2}]$$

Assuming $\varphi_{S1} = \varphi_{S2}$!!!

Interferogram: $$i_1 i_2^* = |i_1 i_2^*| \exp[-i(2\frac{2\pi}{\lambda}\Delta R)] \xrightarrow{\Delta R = 0} i_1 i_2^* = |i_1 i_2^*|$$

When the images are acquired from the same location i.e. the spatial baseline becomes zero, $\Delta R = 0$, and the intererometric phase loses its sensitivity to terrain elevation.

Differential SAR Interferometry (D-InSAR)

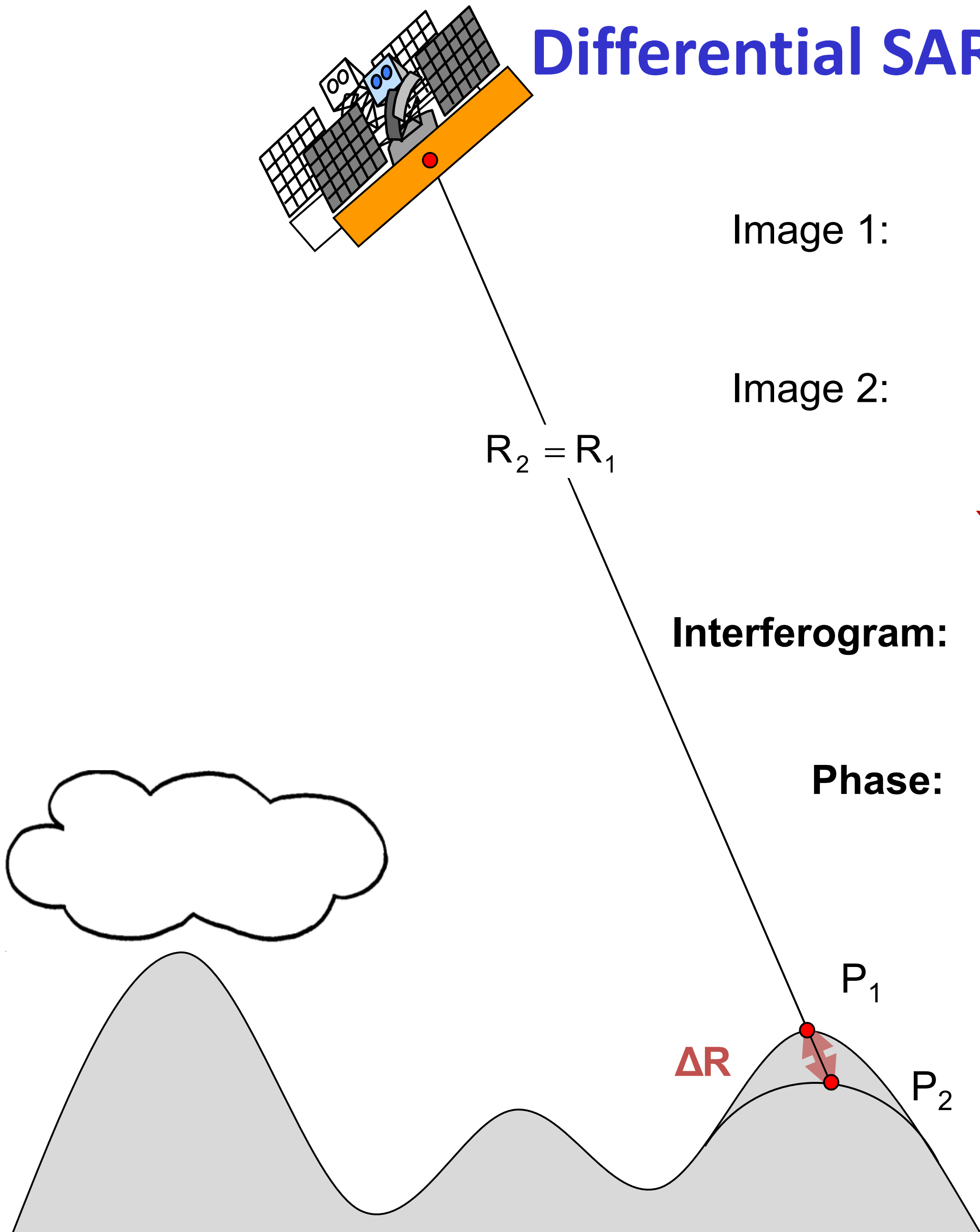

Image 1: $i_1 = |i_1| \exp[-i(2\frac{2\pi}{\lambda}R_1) + \varphi_{S1}]$

Image 2: $i_2 = |i_2| \exp[-i\ 2\frac{2\pi}{\lambda}(R_1 + \Delta R) + \varphi_{S2}]$

Assuming $\varphi_{S1} = \varphi_{S2}$!!!

Interferogram: $i_1\, i_2^* = |i_1\, i_2^*| \exp[-i(2\frac{2\pi}{\lambda}\Delta R)]$

Phase: $\varphi = \arg(\ i_1\, i_2^*) = 2\frac{2\pi}{\lambda}\Delta R$

When the two images are acquired from the same location but at different times, i.e. with zero spatial & non-zero temporal baseline, **the intererometric phase** is **proportional** to the **change in the slant range distance** occurring in the time between the two acquisitions.

Differential SAR Interferometry

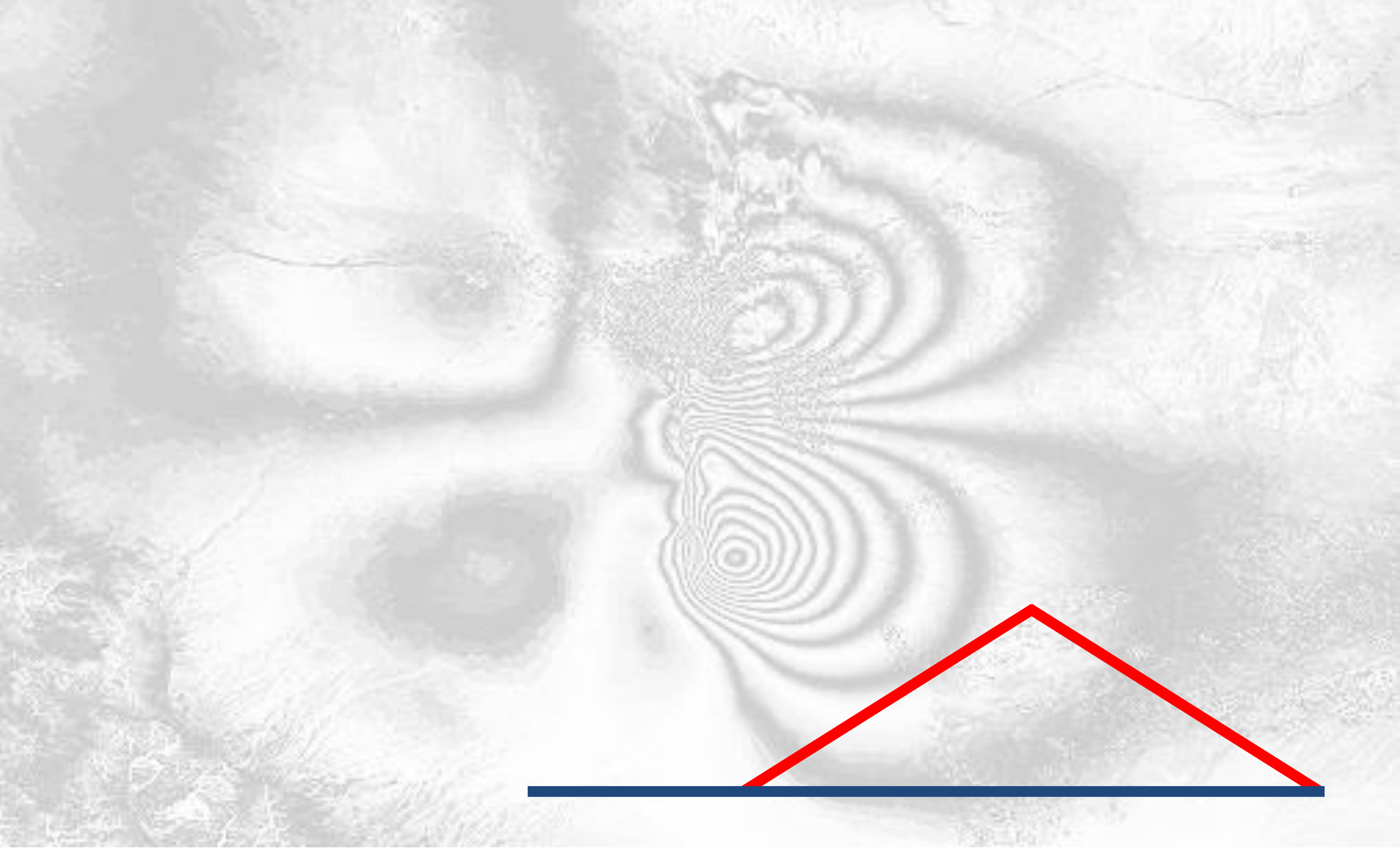

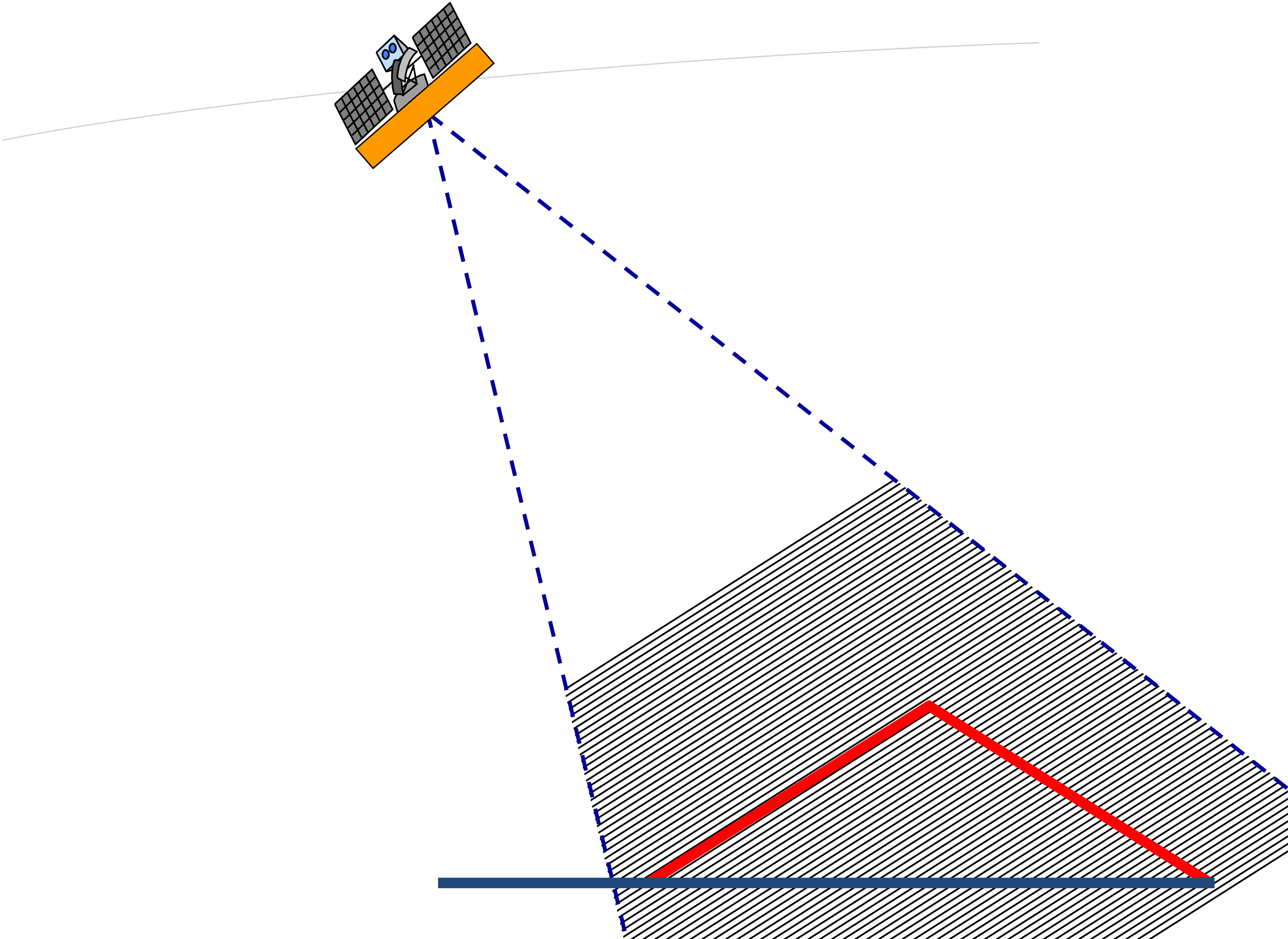

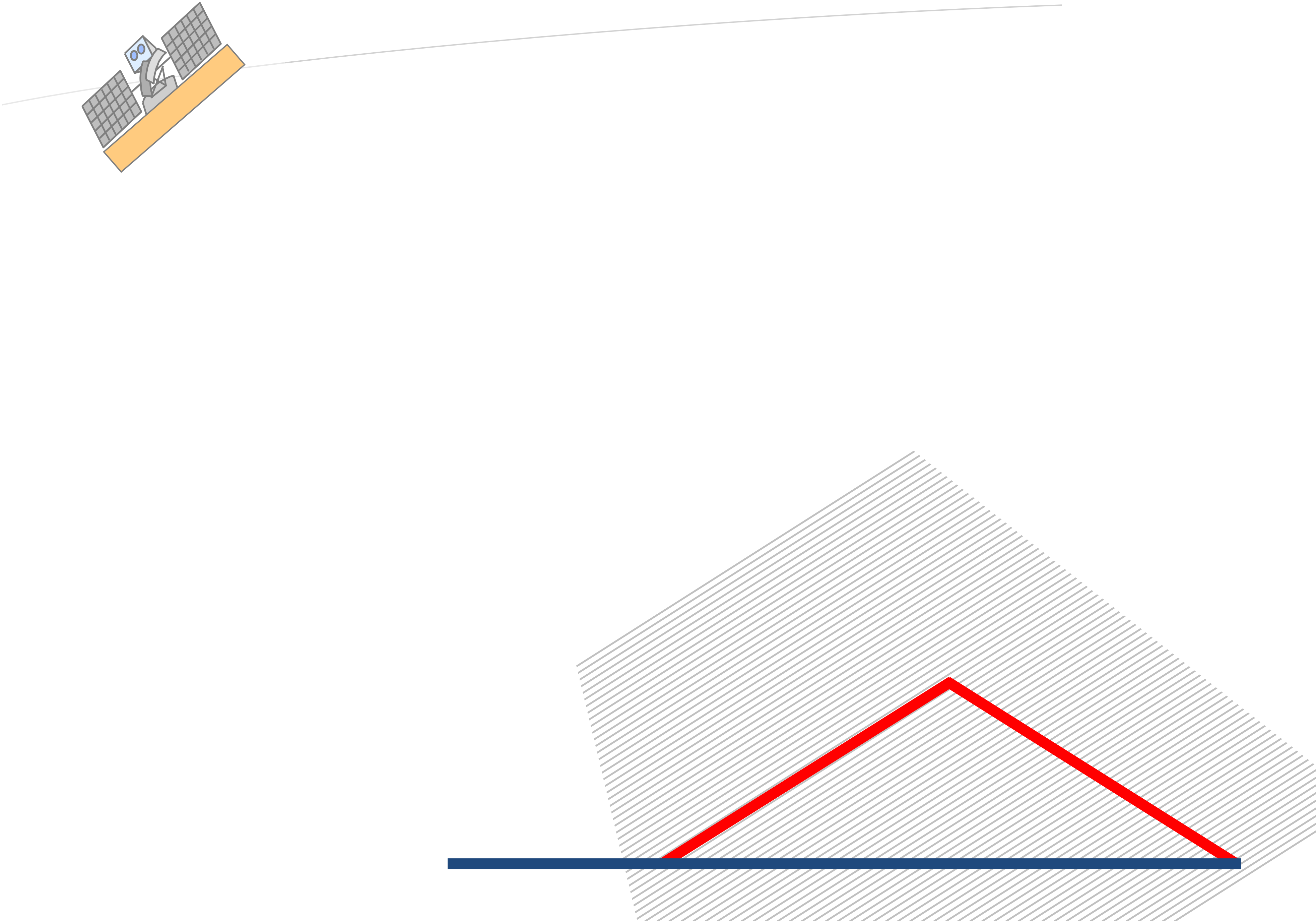

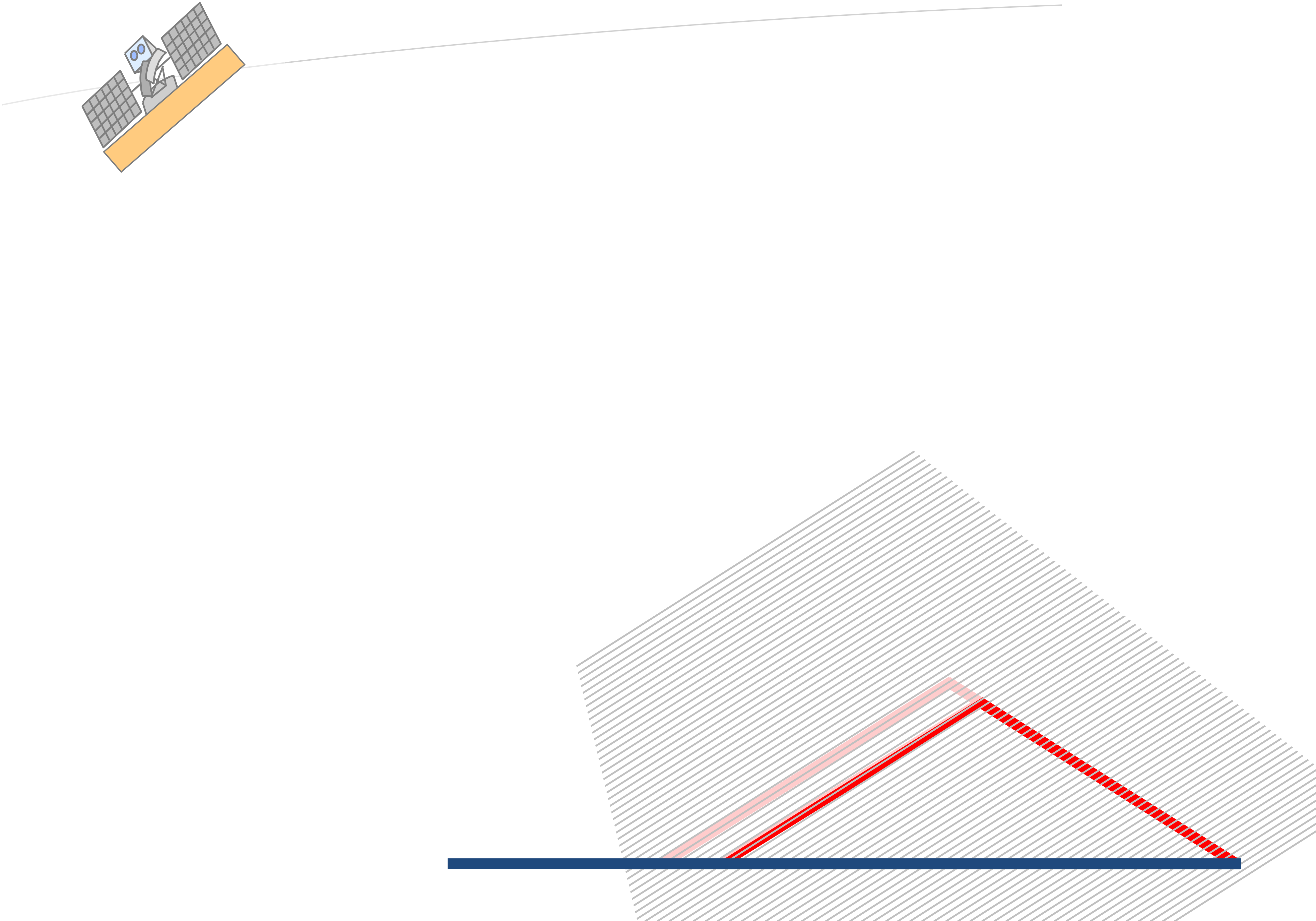

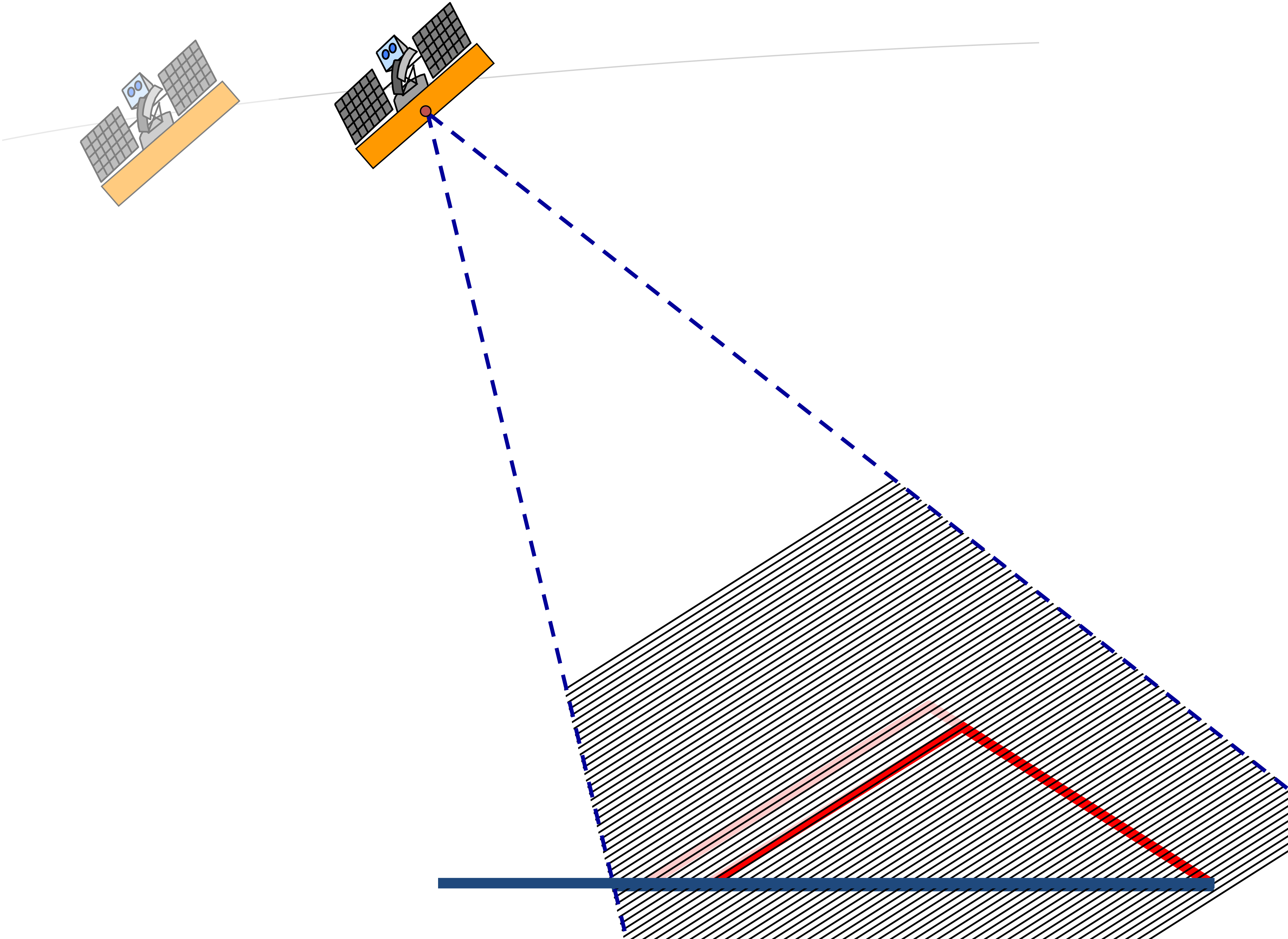

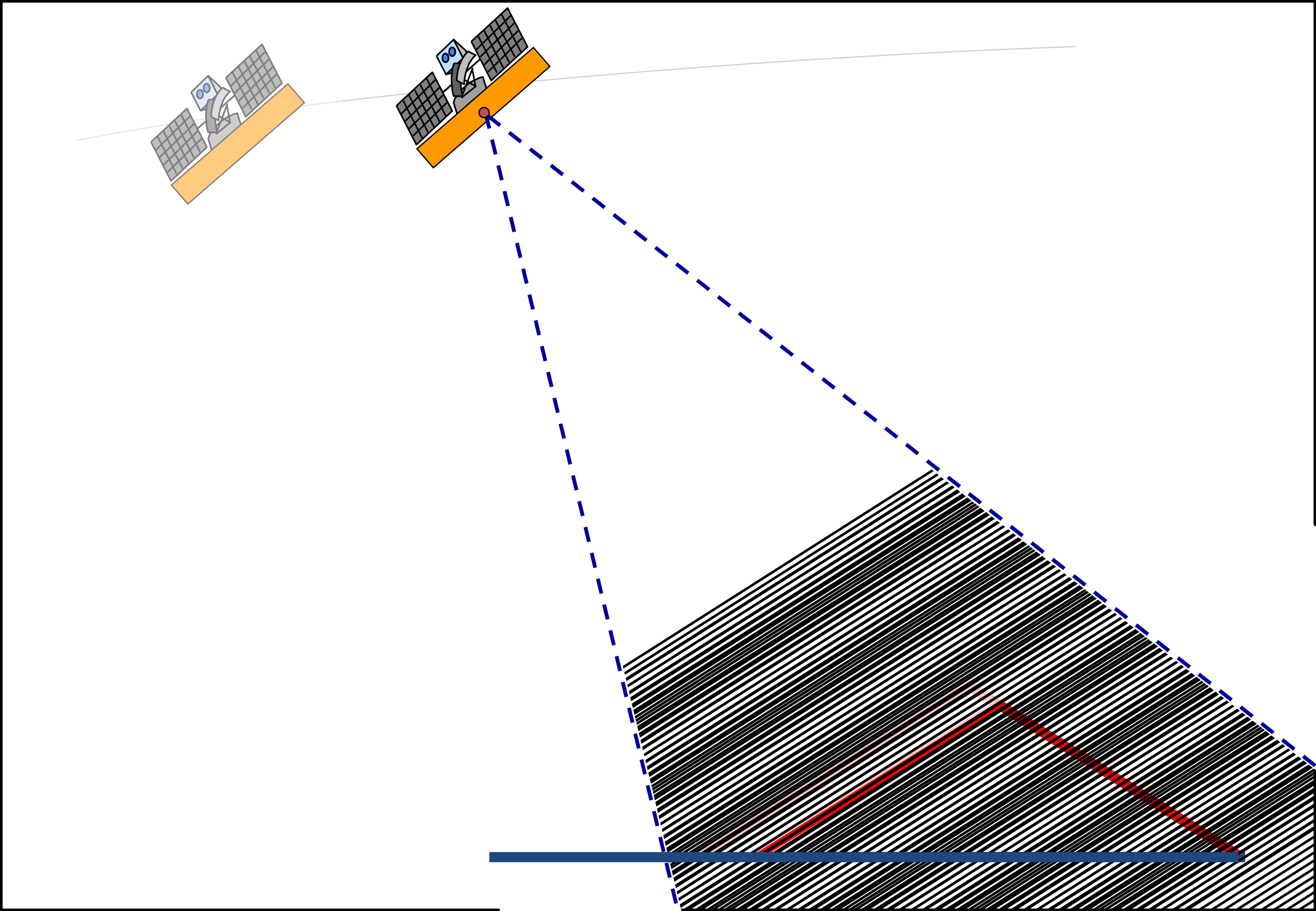

D-InSAR Phase: Height Sensitivity

Interferometric Phase: $\varphi = 2\frac{2\pi}{\lambda}\Delta R + 2\pi\ N$ where $N = 0, \ \pm 1, \ \pm 2$

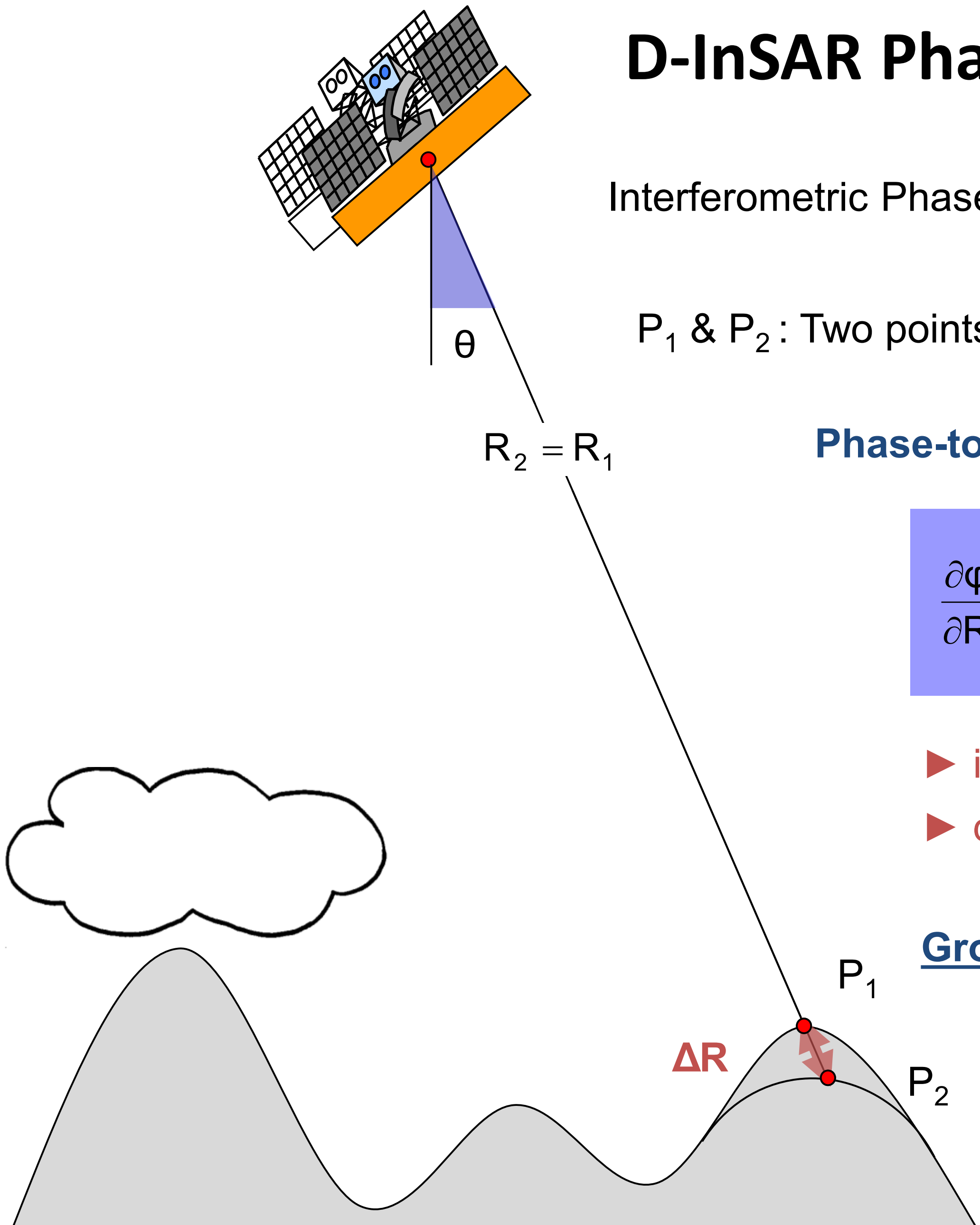

P_1 & P_2: Two points at different slant range distance:

Phase-to-Slant-Range Distance Sensitivity:

$$\frac{\partial \varphi}{\partial R} := \frac{4\pi}{\lambda} \longrightarrow \sigma_R = \frac{\lambda}{4\pi}\sigma_\varphi$$

height error σ_R

- ▶ independent on the acquisition geometry
- ▶ depends only on the system wavelength

Ground range (hor.-) & **Height** (ver.- displacement):

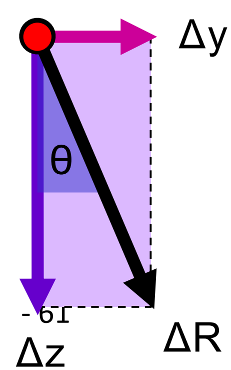

$$\Delta R = \Delta y \sin(\theta) + \Delta z \cos(\theta)$$

Earth Observation and Remote Sensing
hajnsek@ifu.baug.ethz.ch
irena.hajnsek@dlr.de
ETH
Eidgenössische Technische Hochschule Zürich
Swiss Federal Institute of Technology Zurich

InSAR vs D-InSAR

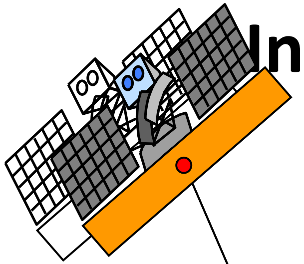

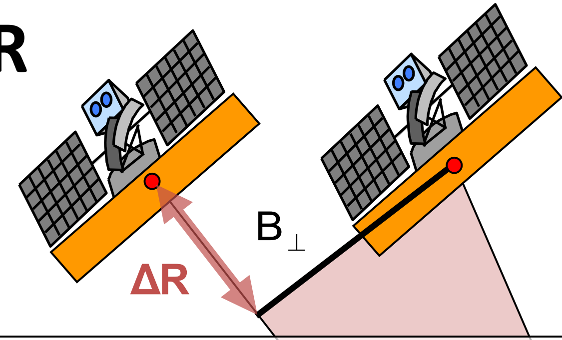

Example ERS: Space-borne C-band (λ=0.056m) interferometer with incidence θ=23° at range R=870km

1 (2π) phase cycle (i.e. 1 fringe) corresponds to:

D-InSAR

$$\sigma_R = \frac{\lambda}{4\pi}\sigma_\varphi = \frac{\lambda}{4\pi}2\pi = 0.028\ \text{m}$$ (in LOS)

$$\sigma_z = \frac{1}{\cos(\theta)}\sigma_R = 0.030\ \text{m}$$ (vertical)

$$\sigma_y = \frac{1}{\sin(\theta)}\sigma_R = 0.072\ \text{m}$$ (horizontal)

InSAR

$$\sigma_z = \frac{\lambda}{4\pi}\frac{R\sin(\theta)}{B_\perp}\sigma_\varphi = \frac{\lambda}{4\pi}\frac{R\sin(\theta)}{B_\perp}\frac{10}{360}2\pi$$

At perp. baseline $B_\perp$=100m: σ_z=100m terrain elevation

At perp. baseline $B_\perp$=200m: σ_z= 50m terrain elevation

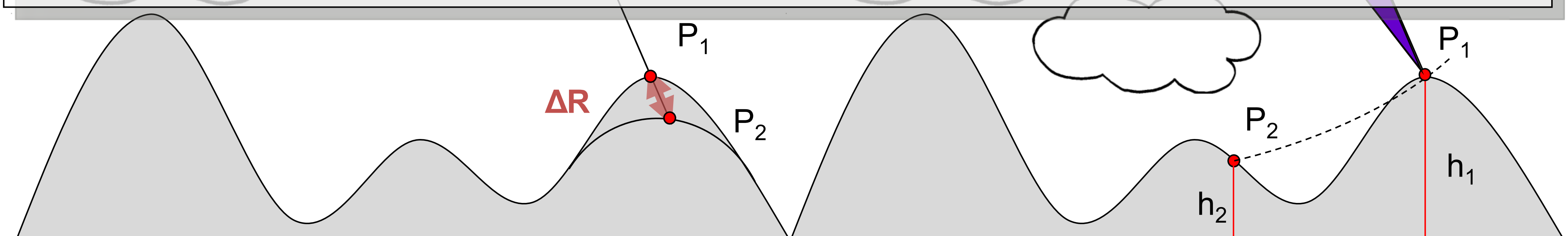

hajnsek@ifu.baug.e
irena.hajnsek@dl

InSAR vs D-InSAR

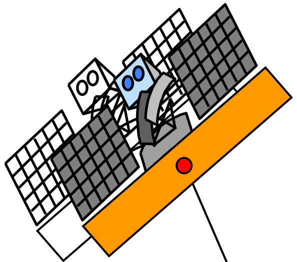

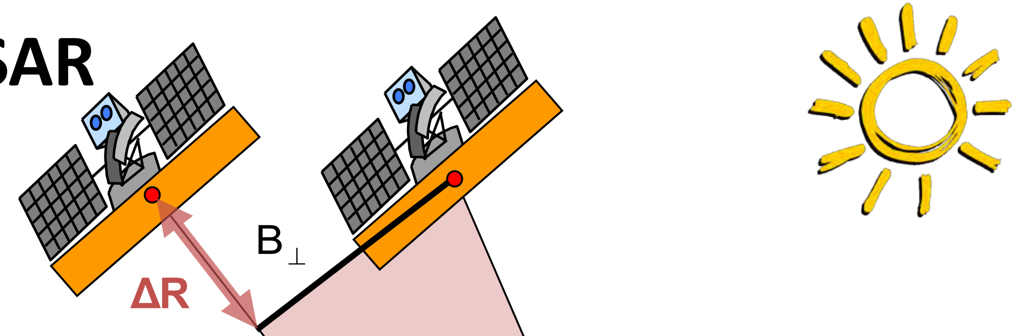

Example ERS: Space-borne C-band (λ=0.056m) interferometer with incidence θ=23° at range R=870Km

Assuming the ability to measure the interferometric phase with an accuracy of 20°:

D-InSAR

$$\sigma_R = \frac{\lambda}{4\pi}\sigma_\varphi = \frac{\lambda}{4\pi}\frac{20}{360}2\pi \approx 1.5\ \text{mm} \quad \text{(in LOS)}$$

$$\sigma_z = \frac{1}{\cos(\theta)}\sigma_R = 1.6\ \text{mm} \quad \text{(vertical)}$$

$$\sigma_y = \frac{1}{\sin(\theta)}\sigma_R = 4.0\ \text{mm} \quad \text{(horizontal)}$$

InSAR

$$\sigma_z = \frac{\lambda}{4\pi}\frac{R\sin(\theta)}{B_\perp}\sigma_\varphi = \frac{\lambda}{4\pi}\frac{R\sin(\theta)}{B_\perp}\frac{20}{360}2\pi$$

At perp. baseline $B_\perp$=100m: σ_z= 5.50m terrain error

At perp. baseline $B_\perp$=200m: σ_z= 2.75m terrain error

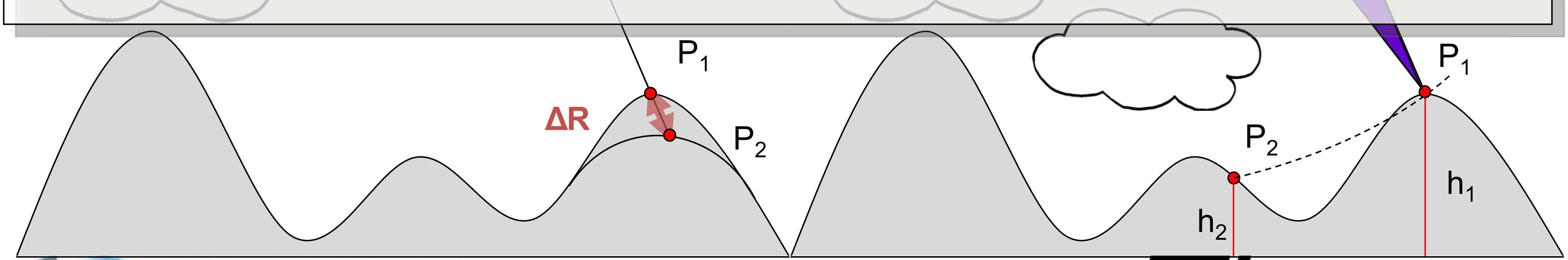

hajnsek@ifu.baug.e
irena.hajnsek@d

Seismic Faults: The Bam Earthquake by Envisat ASAR

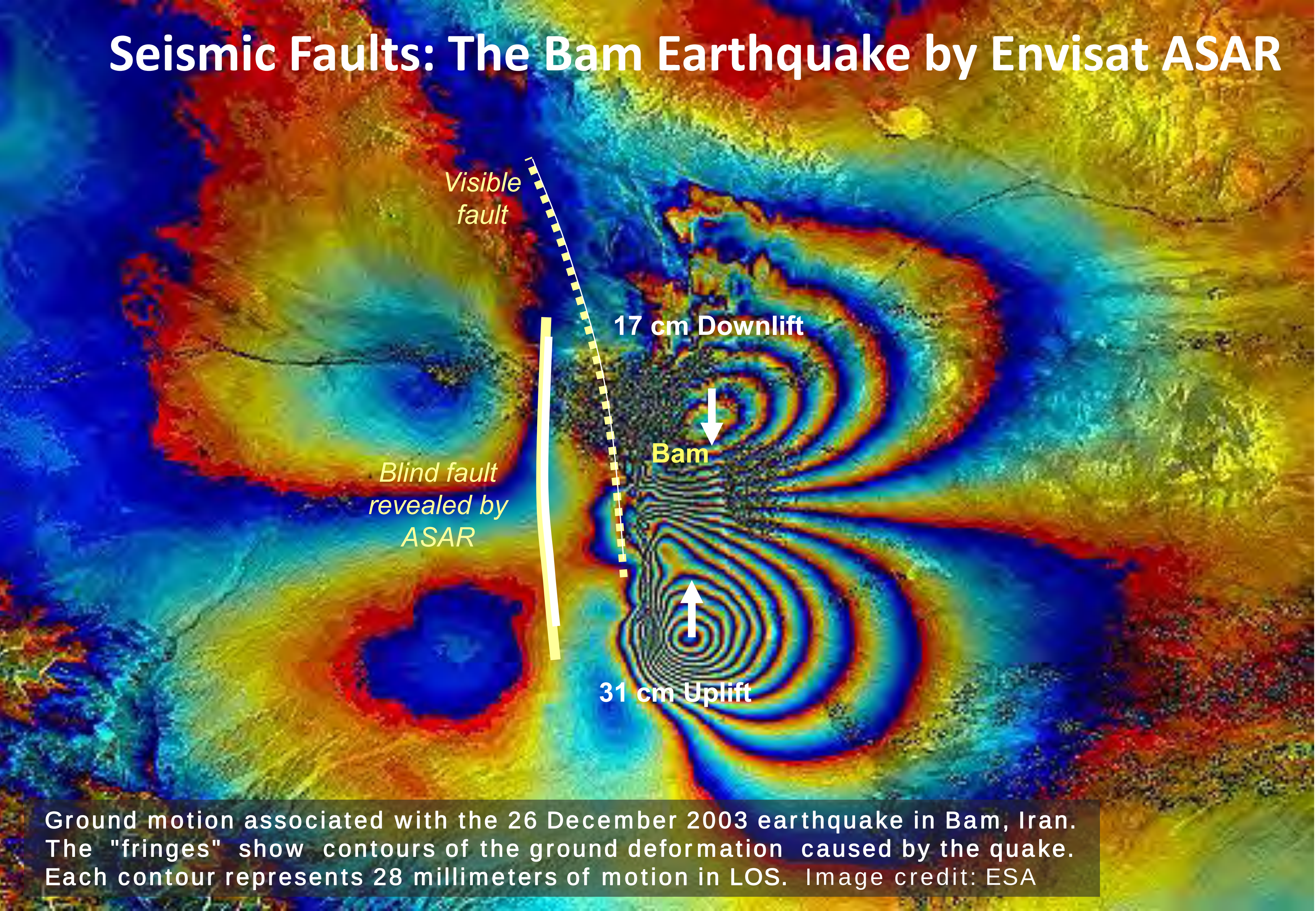

Ground motion associated with the 26 December 2003 earthquake in Bam, Iran. The "fringes" show contours of the ground deformation caused by the quake. Each contour represents 28 millimeters of motion in LOS. Image credit: ESA

Ice motion of fast moving glaciers

The combination of **short repeat pass times** and a **systematic acquisition scenario** and a low SAR frequency (**L-band**) is optimum for fast ice motion.

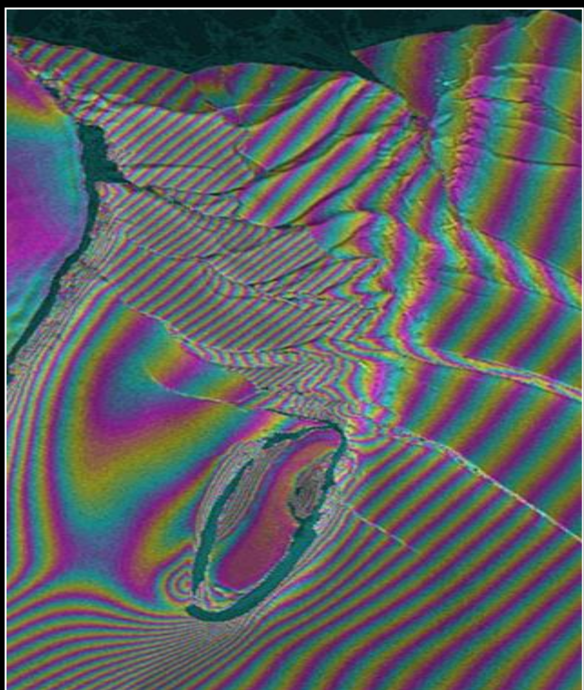

ERS Tandem 1-Day RP Time

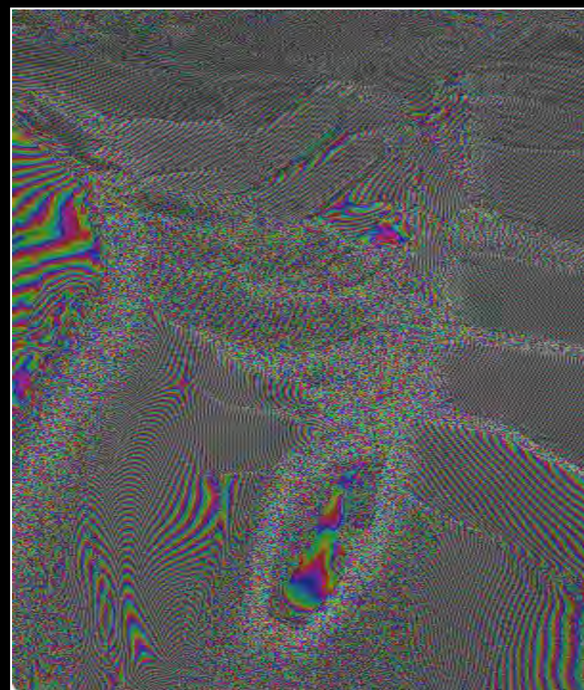

RADARSAT 24-Days RP Time

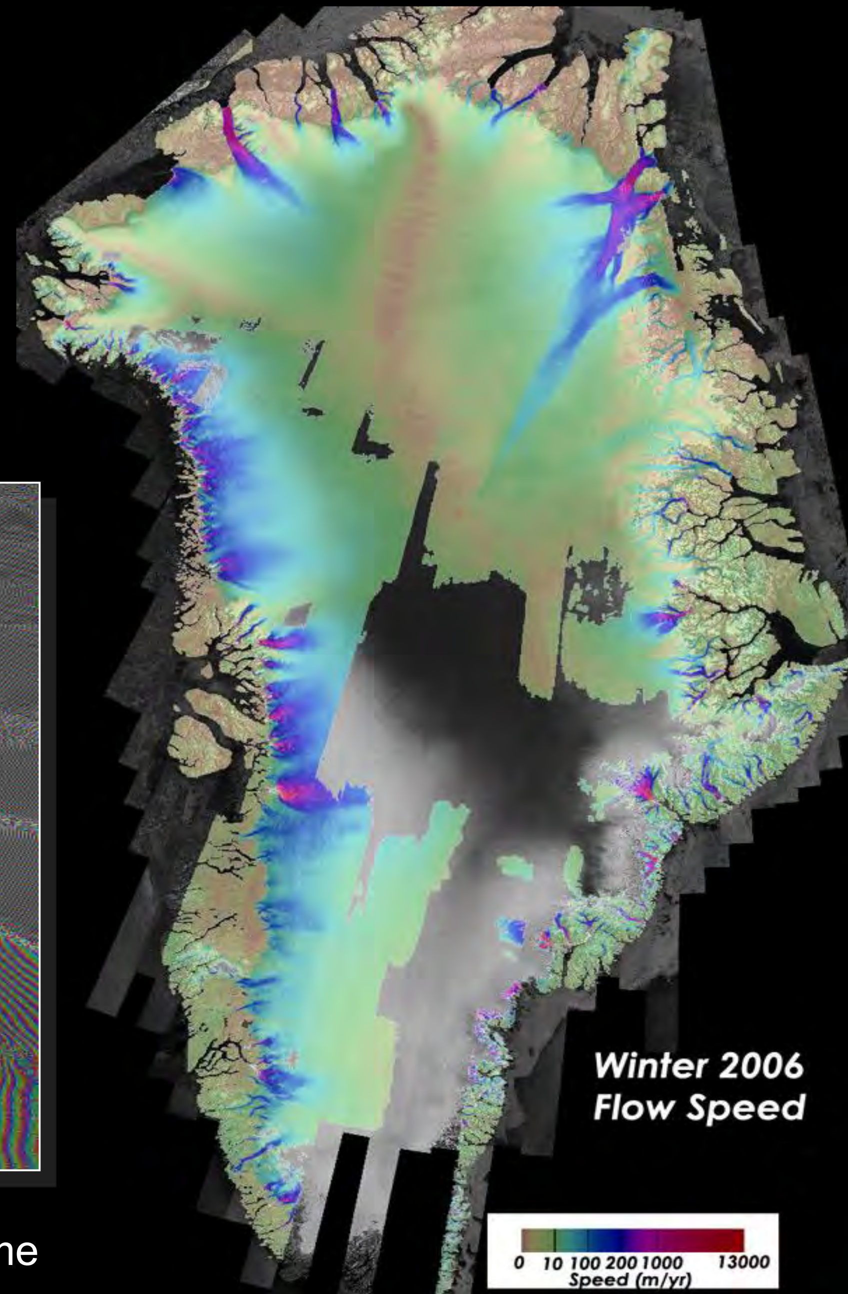

Image credit: NASA/JPL

Ice Surface Velocity from TerraSAR-X: Nimrod Glacier

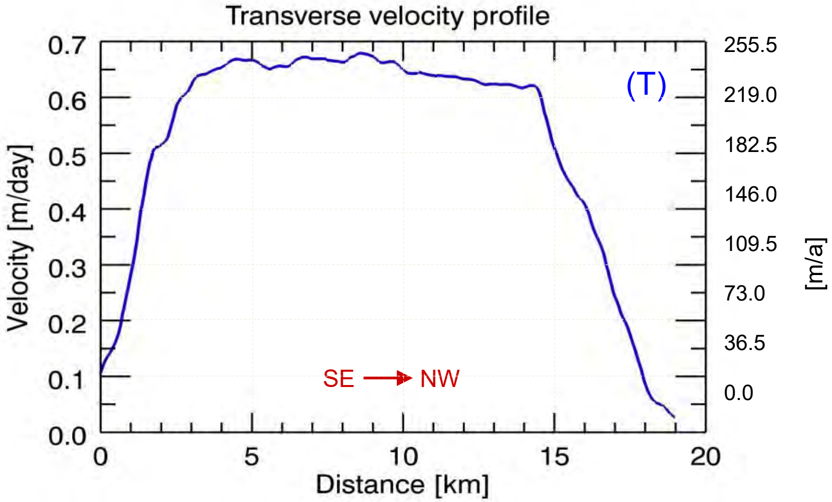

Plug-like shape: strong side drag

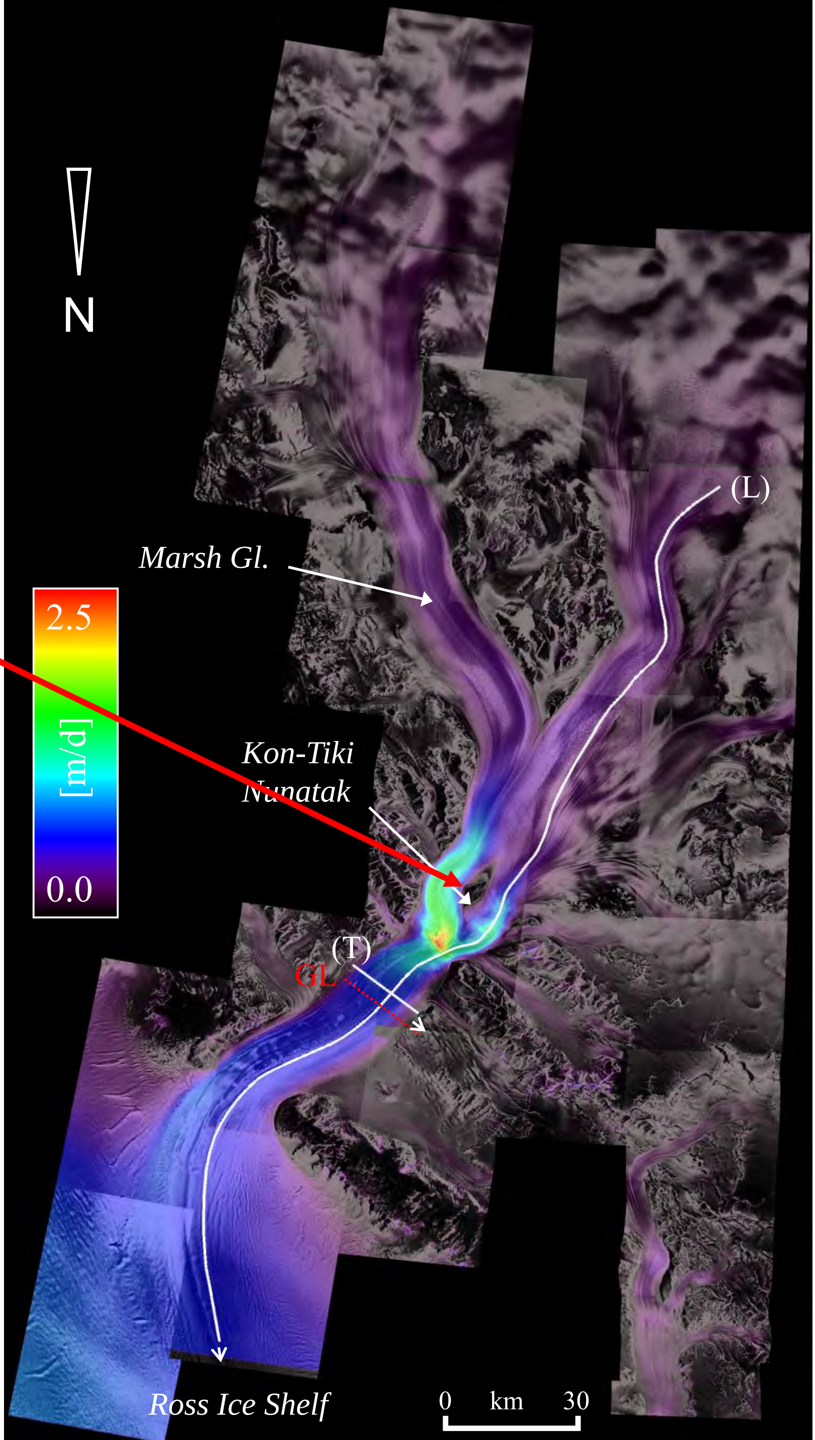

hajnsek@ifu.baug.ethz.ch
irena.hajnsek@dlr.de

Thermal Dilation: Berlin Main Train Station

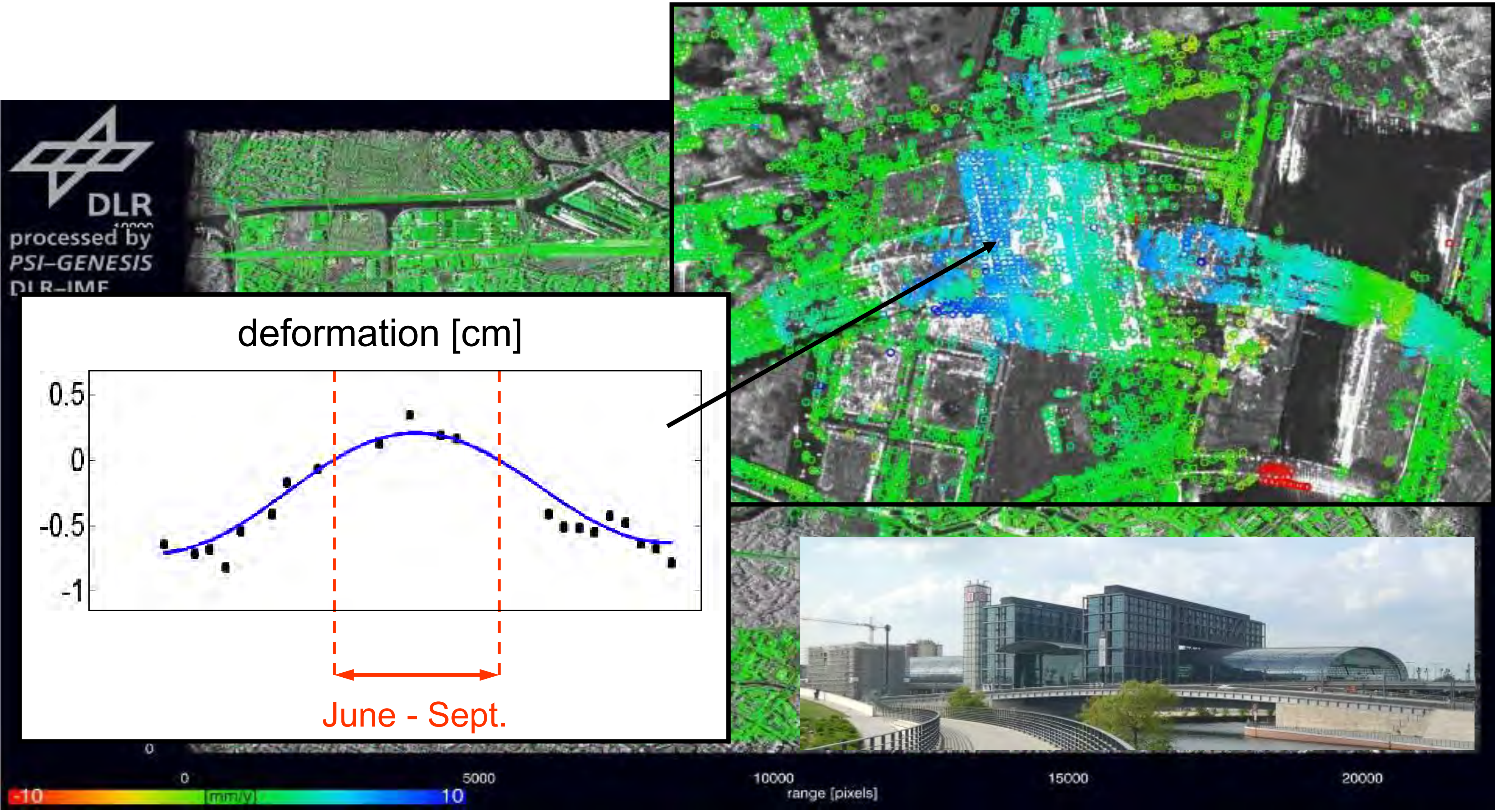

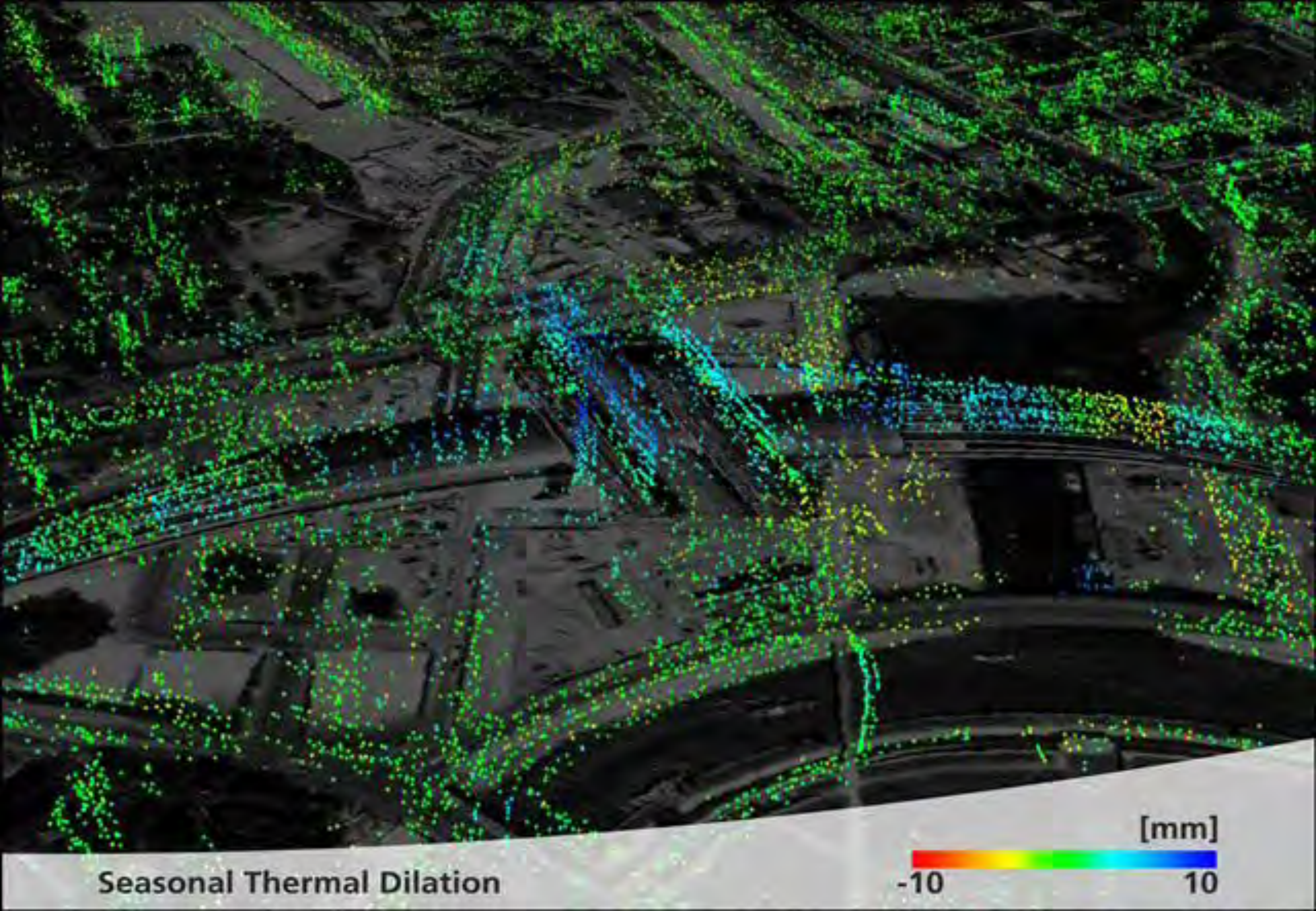
[mm]
-10
10
Seasonal Thermal Dilation

PSI Land Subsidence Monitoring

Semarang - Indonesia

27/12/02 to 23/08/06

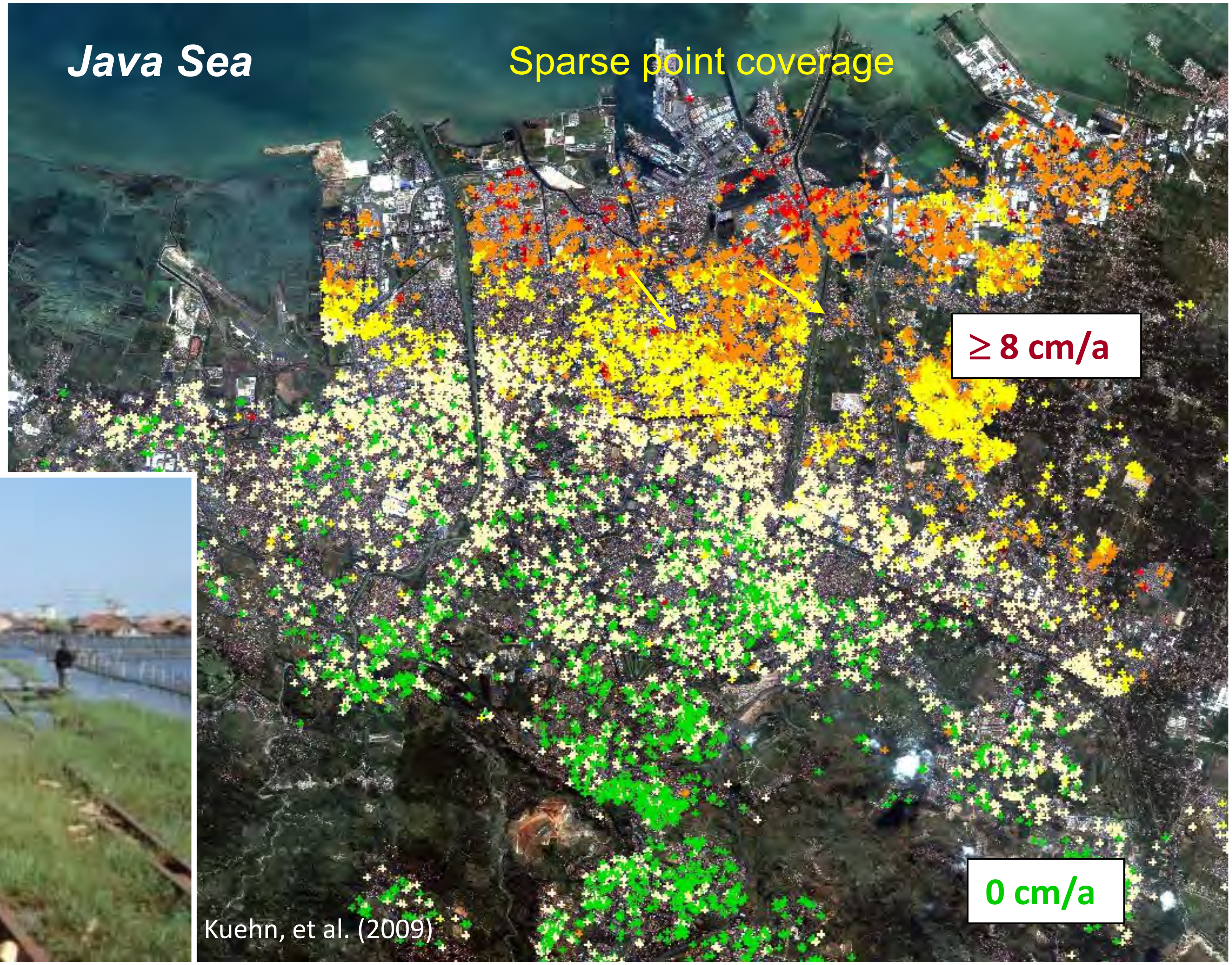

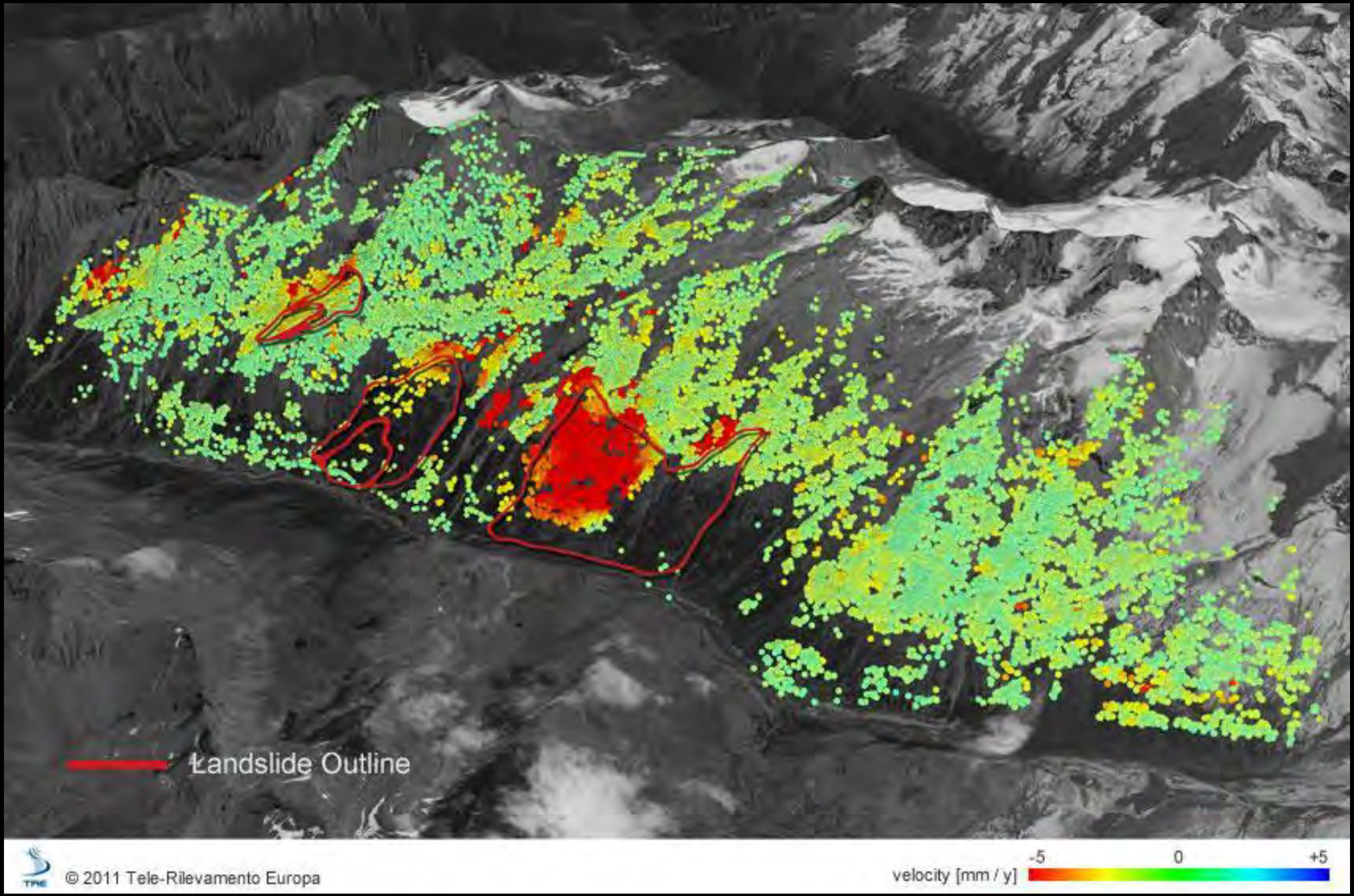

Active landslide in Valsavarenche, Italy. For each ground point identified a time-series of its deformation can be reconstructed to show its movement over the time period analyzed.
Image credit: Treuropa / Sensor: Radarsat

Principles and Basics of Pol-InSAR

Irena Hajnsek
*Earth Observation and Remote Sensing,
Institute of Environmental Engineering, ETH Zürich
*Microwaves and Radar Institut,
German Aerospace Center, Oberpfaffenhofen

Earth Observation and Remote Sensing

hajnsek@ifu.baug.ethz.ch
irena.hajnsek@dlr.de

ETH
Eidgenössische Technische Hochschule Zürich
Swiss Federal Institute of Technology Zurich

SAR Polarimetry (PolSAR)

Allows the identification / decomposition of different scattering processes occurring inside the resolution cell

SAR Interferometry (InSAR)

Allows the location of the effective scattering center inside the resolution cell

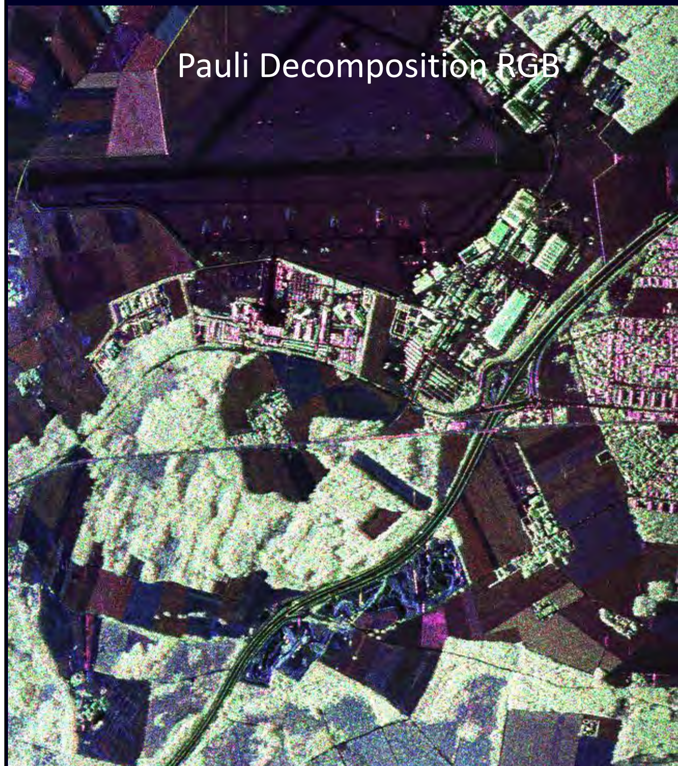

Polarimetric SAR Interferometry (Pol-InSAR)

Potential to separate in height different scattering processes occurring inside the resolution cell

Interferometry vs. Polarimetry

$$S^{1}_{HH} = A^{1}_{D} + A^{1}_{S}$$

$$S^{2}_{HH} = A^{2}_{D} + A^{2}_{S}$$

$$\varphi = \arg\{\, S^{1}_{HH} \; S^{2*}_{HH} \,\}$$

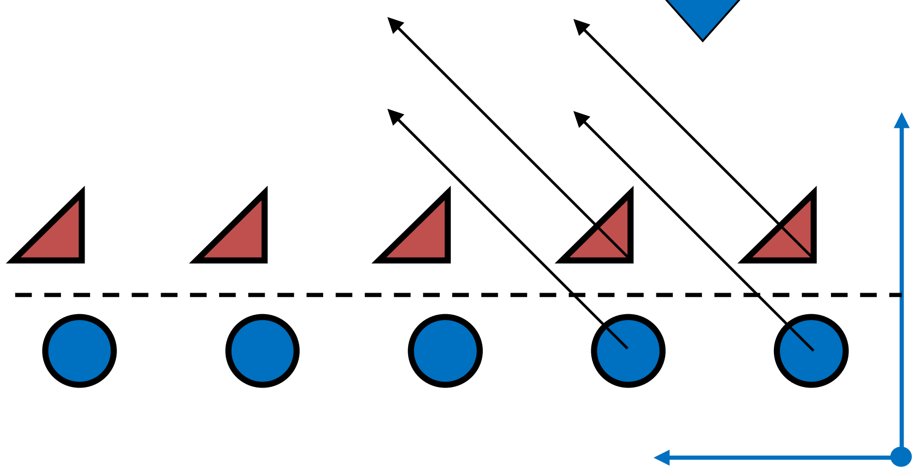

$$S_{HH} + S_{VV} = 2A_{S}$$

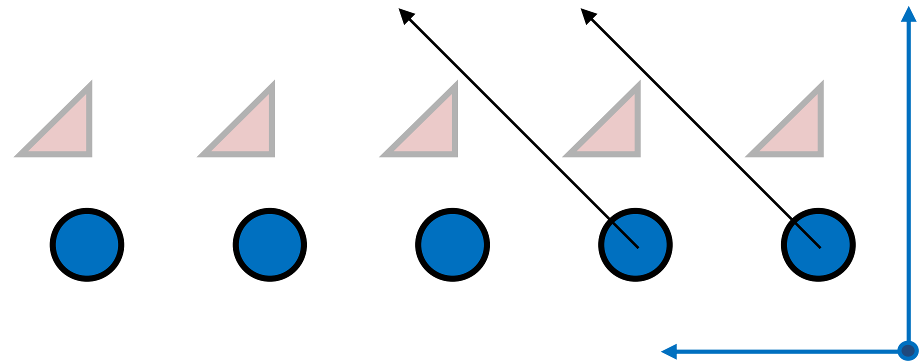

$$S_{HH} - S_{VV} = 2A_{D}$$

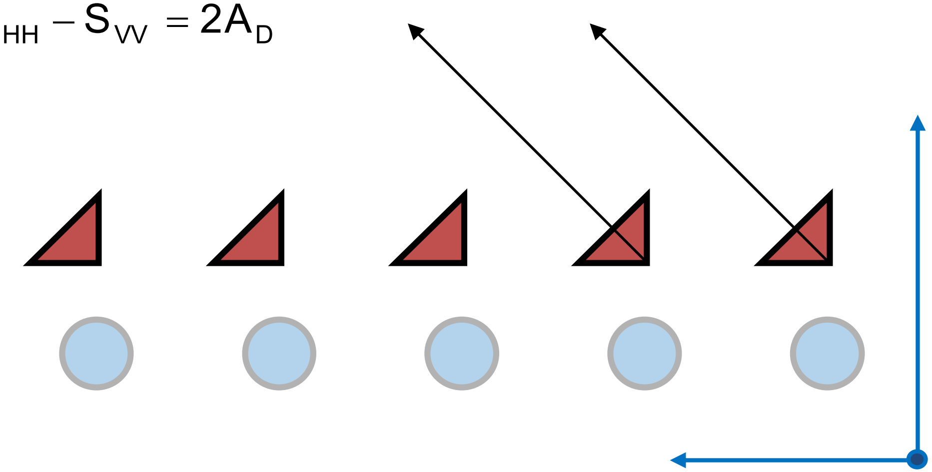

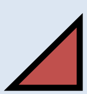 $[S_D] = A_D \begin{bmatrix} 1 & 0 \\ 0 & -1 \end{bmatrix}$ Dihedral Reflector

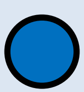 $[S_S] = A_S \begin{bmatrix} 1 & 0 \\ 0 & 1 \end{bmatrix}$ Sphere or Triedral Reflector

Polarimetric Interferometry

$$i_{1S} = S^1_{HH} + S^1_{VV} = 2A^1_S$$

$$i_{2S} = S^2_{HH} + S^2_{VV} = 2A^2_S$$

$$\varphi_S = \arg\{\, i_{1S} \; i^*_{2S} \,\}$$

$$i_{1D} = S^1_{HH} - S^1_{VV} = 2A^1_D$$

$$i_{2D} = S^2_{HH} - S^2_{VV} = 2A^2_D$$

$$\varphi_D = \arg\{\, i_{1D} \; i^*_{2D} \,\}$$

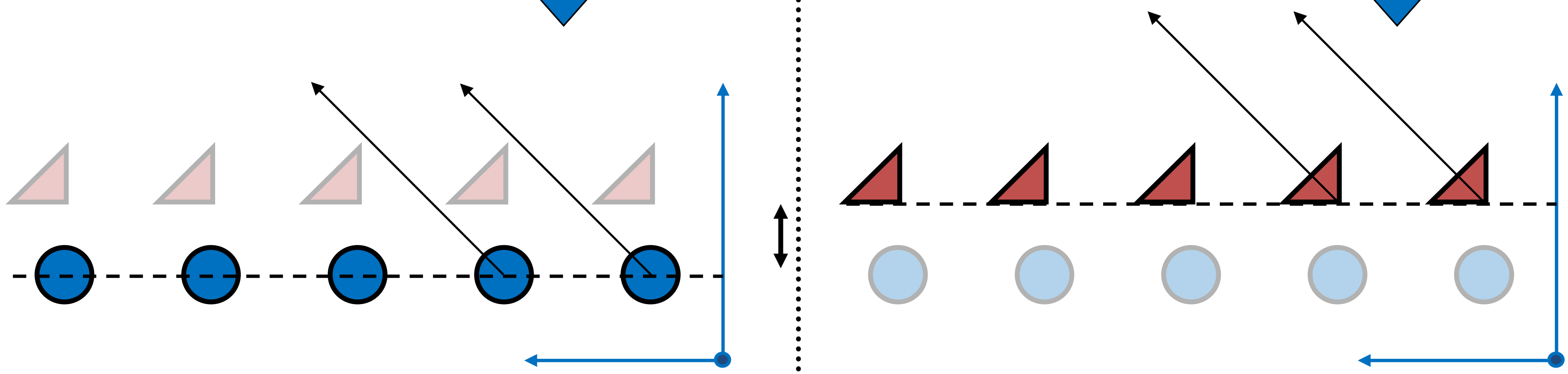

$$[S_D] = A_D \begin{bmatrix} 1 & 0 \\ 0 & -1 \end{bmatrix}$$ Dihedral Reflector

$$[S_S] = A_S \begin{bmatrix} 1 & 0 \\ 0 & 1 \end{bmatrix}$$ Sphere or Triedral Reflector

hajnsek@ifu.baug.ethz.ch
irena.hajnsek@dlr.de

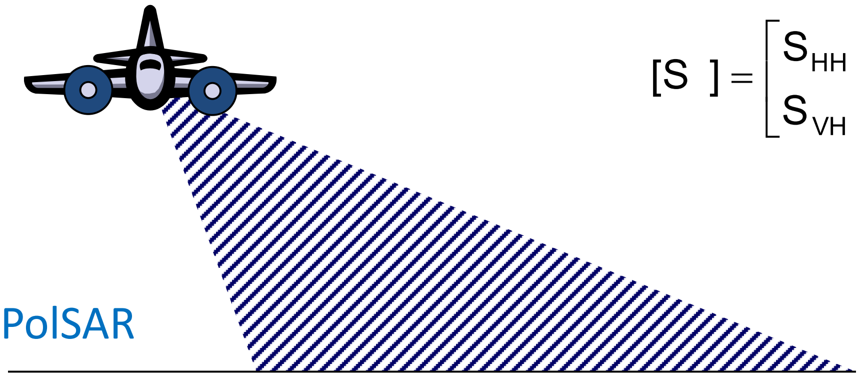

PolSAR

$$[S] = \begin{bmatrix} S_{HH} & S_{HV} \\ S_{VH} & S_{VV} \end{bmatrix}$$

Polarimetric Coherences

$$\tilde{\gamma}(S_{ij}\ S_{mn}) = \frac{\langle S_{ij}\ S_{mn}^{*} \rangle}{\sqrt{\langle S_{ij}\ S_{ij}^{*} \rangle \langle S_{mn}\ S_{mn}^{*} \rangle}}$$

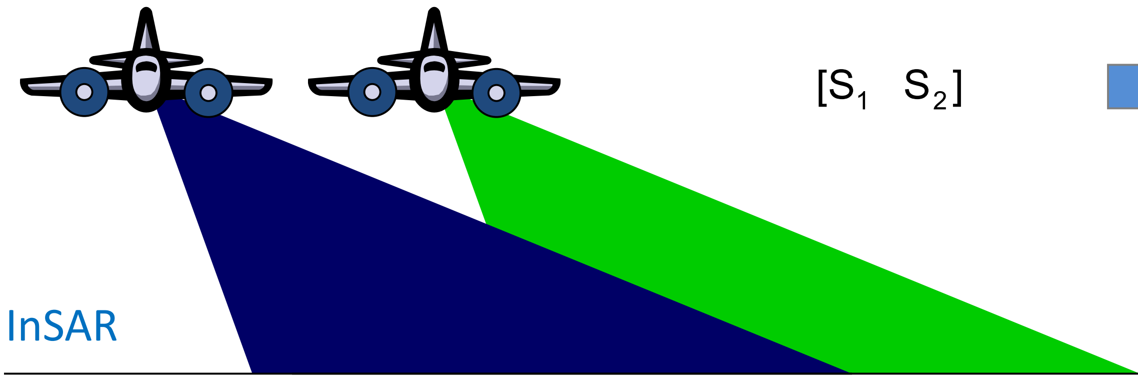

InSAR

$$[S_1\ \ S_2]$$

Interferometric Coherences

$$\tilde{\gamma}(S_1\ S_2) = \frac{\langle S_1\ S_2^{*} \rangle}{\sqrt{\langle S_1\ S_1^{*} \rangle \langle S_2\ S_2^{*} \rangle}}$$

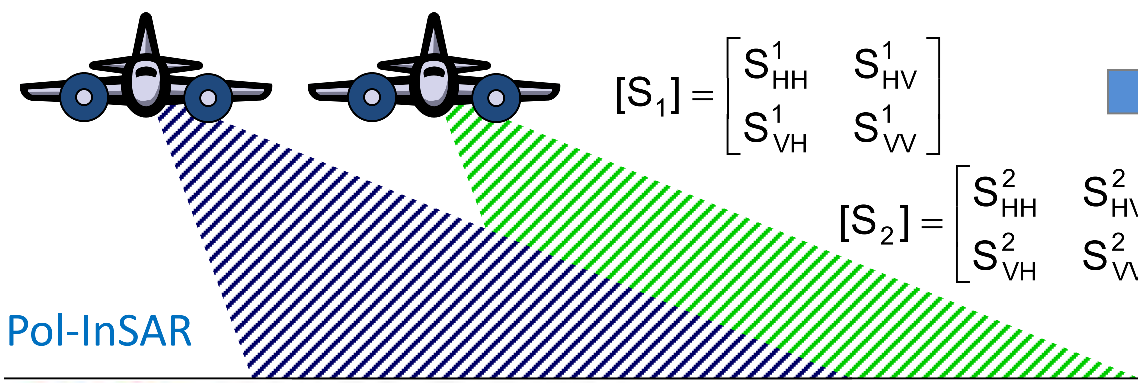

Pol-InSAR

$$[S_1] = \begin{bmatrix} S_{HH}^{1} & S_{HV}^{1} \\ S_{VH}^{1} & S_{VV}^{1} \end{bmatrix}$$

$$[S_2] = \begin{bmatrix} S_{HH}^{2} & S_{HV}^{2} \\ S_{VH}^{2} & S_{VV}^{2} \end{bmatrix}$$

Polarimetric / Interferometric Coherences

$$\tilde{\gamma}(S_{ij}^{1}\ S_{mn}^{2}) = \frac{\langle S_{ij}^{1}\ S_{mn}^{2\,*} \rangle}{\sqrt{\langle S_{ij}^{1}\ S_{ij}^{1*} \rangle \langle S_{mn}^{2}\ S_{mn}^{2\,*} \rangle}}$$

Complex Coherences on the Unit Circle

$$\tilde{\gamma} := \frac{\sum_{k=1}^{N} S_1(k) S_2^*(k)}{\sqrt{\sum_{k=1}^{N} S_1(k) S_1^*(k) \sum_{k=1}^{N} S_2(k) S_2^*(k) >}} = \exp(i \ \mathrm{Arg}(\tilde{\gamma})\ ) \cdot |\tilde{\gamma}|$$

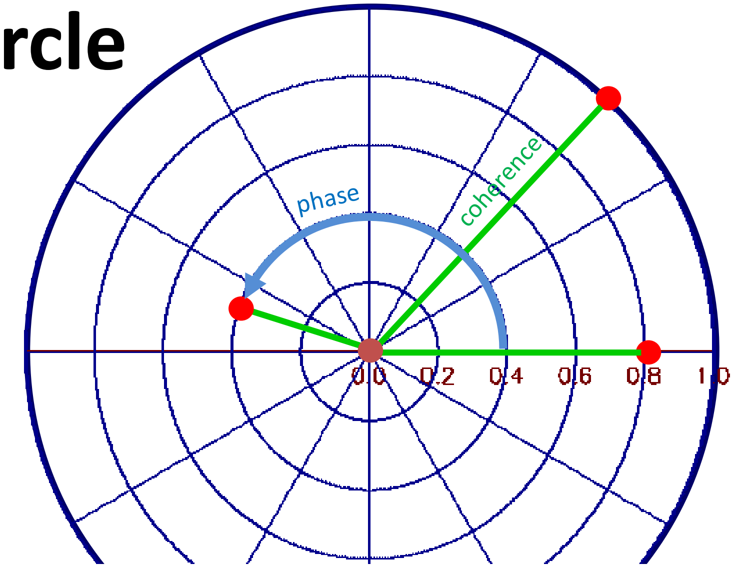

Correlation Coefficient	$0 \leq |\tilde{\gamma}| = \gamma \leq 1$

Interferometric Phase	$0 \leq \mathrm{Arg}(\tilde{\gamma}) = \varphi \leq 2\pi$

Cramer Rao Bounds:

(expresses the lower bound on the variance of the estimator):

Correlation Coefficient $\quad \mathrm{VAR}(|\tilde{\gamma}|)_{CR} = \dfrac{(1-|\gamma|^2)^2}{2N}$

Interferometric Phase $\quad \mathrm{VAR}(\varphi)_{CR} = \dfrac{1-|\gamma|^2}{2N|\gamma|^2}$

$\varphi = \arg(\tilde{\gamma})$ and N is the number of Looks

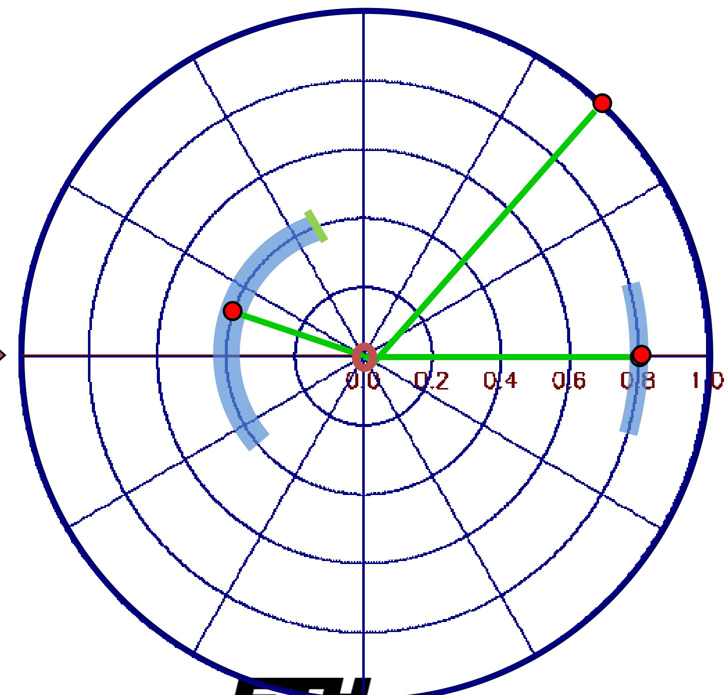

Why is Interferometry important for Volume Scatterers?

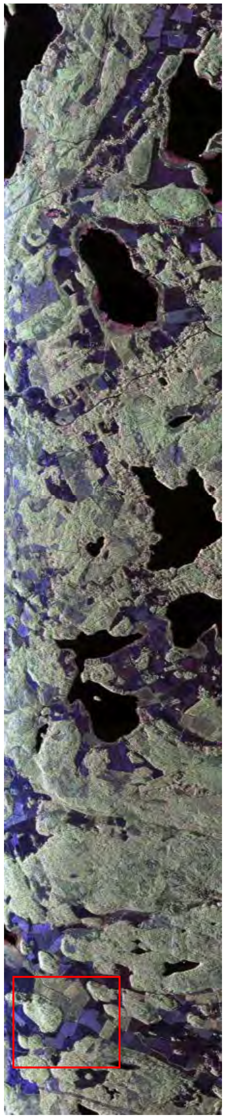

E-SAR / Test Site: Helsinki, Finland

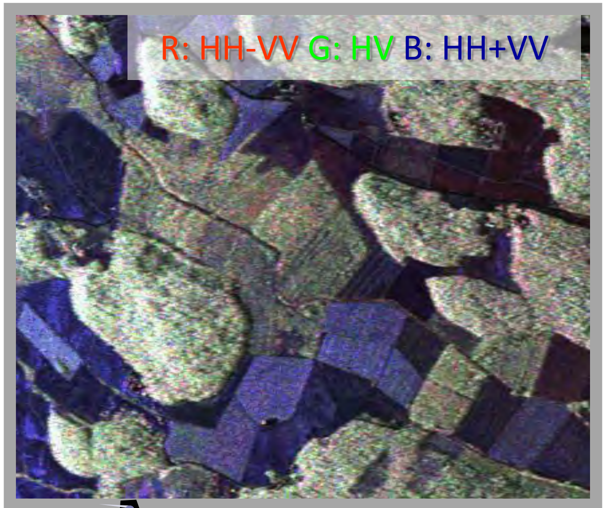

HH-VV Coherence

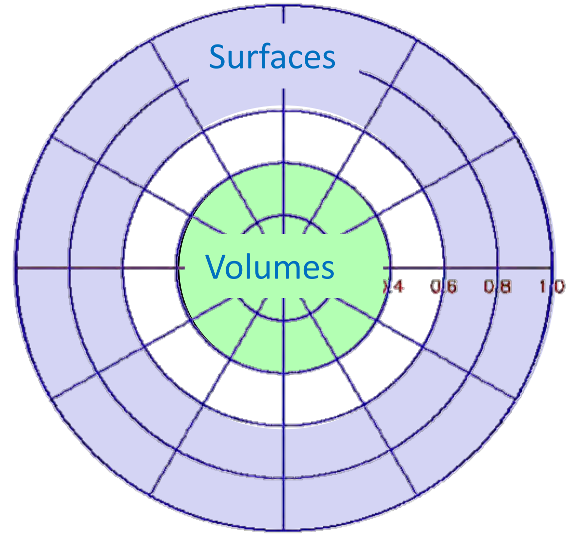

HH-HH Coherence

HH-HH Coherence

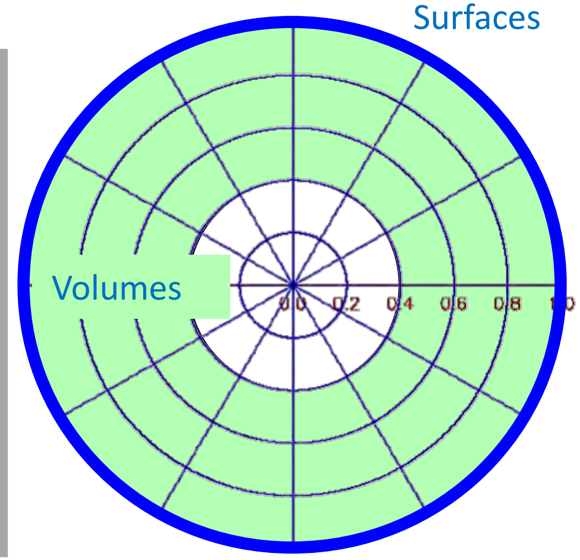

hajnsek@ifu.baug.ethz.ch
irena.hajnsek@dlr.de

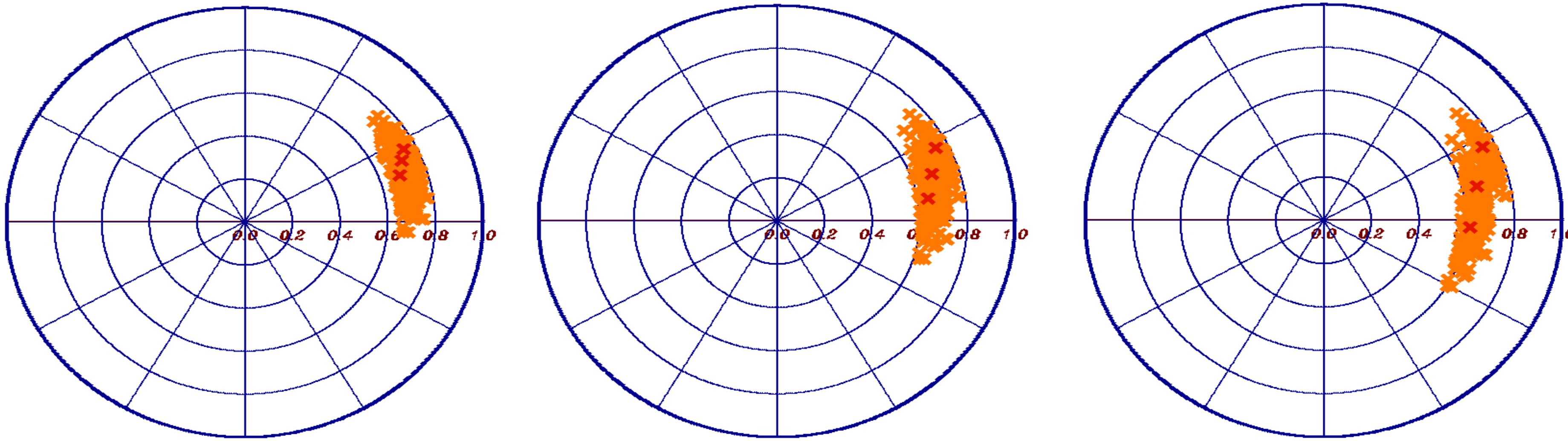

Pol-InSAR: Basic Principles & Ideas

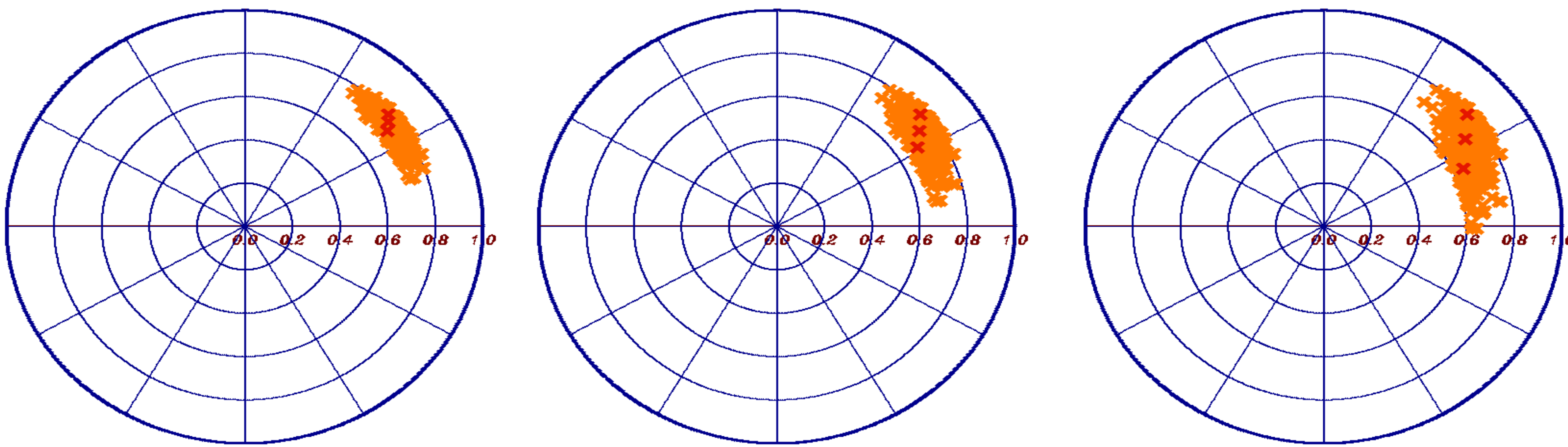

SAR Interferometry for Volume Structure

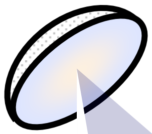

S_1 S_2

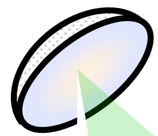

Interferometric Coherence

$$\tilde{\gamma}(S_1\ S_2) = \frac{\langle S_1\ S_2^* \rangle}{\sqrt{\langle S_1\ S_1^* \rangle \langle S_2\ S_2^* \rangle}}$$

Volume Coherence

$$\tilde{\gamma}_{Vol}(f(z),k_z) = e^{ik_z z_o} \frac{\int_o^{h_v} f(z)\ e^{ik_z z} dz}{\int_o^{h_v} f(z)\ dz}$$

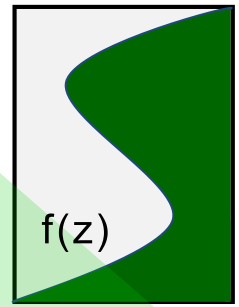

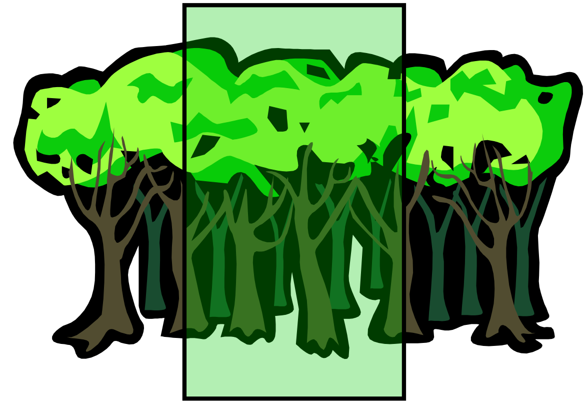

$f(z)$ ... vertical reflectivity function

Vertical Wavenumber: $\kappa_z = \dfrac{\kappa \Delta\theta}{\sin(\theta_0)}$

$$\tilde{\gamma} = \tilde{\gamma}_{Temporal}\ \gamma_{SNR}\ \tilde{\gamma}_{Vol}$$

- $\tilde{\gamma}_{Temporal}$ ... temporal decorrelation
- γ_{SNR} ... additive noise decorrelation
- $\tilde{\gamma}_{Volume}$ ... geometric decorrelation

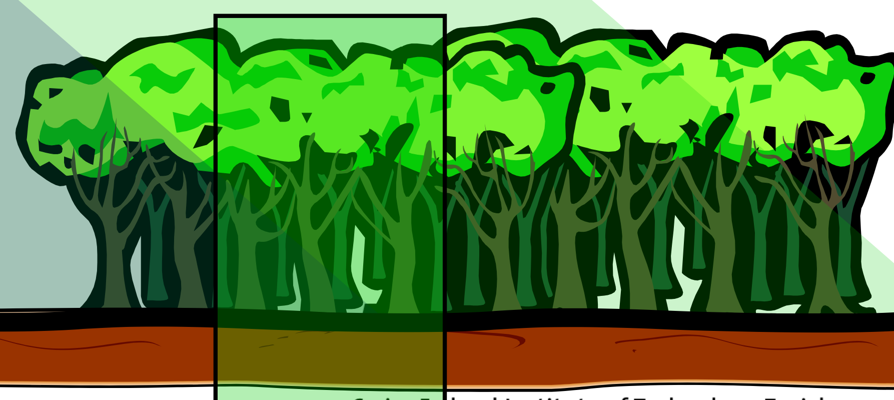

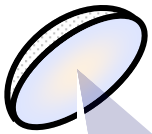

S_1 S_2

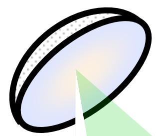

Interferometric Coherence

$$\tilde{\gamma}(S_1\ S_2) = \frac{< S_1\ S_2^* >}{\sqrt{< S_1\ S_1^* > < S_2\ S_2^* >}}$$

SAR Interferometry for Volume Structure

Volume Coherence

$$\tilde{\gamma}_{Vol}(f(z),k_z) = e^{ik_z z_o} \frac{\int_o^{h_v} f(z)\ e^{ik_z z} dz}{\int_o^{h_v} f(z)\ dz}$$

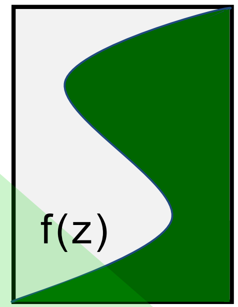

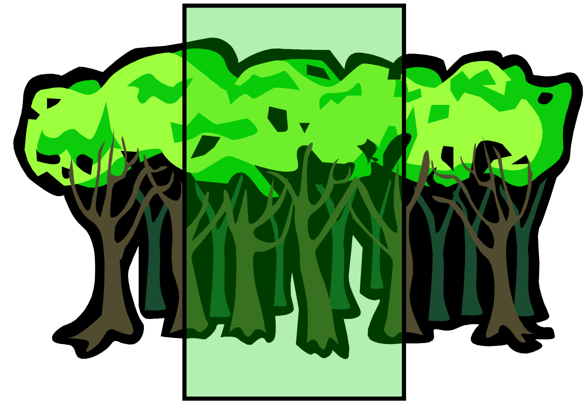

$f(z)$ … vertical reflectivity function

Vertical Wavenumber: $\kappa_z = \dfrac{\kappa \Delta\theta}{\sin(\theta_0)}$

$$\tilde{\gamma} = \tilde{\gamma}_{Temporal}\ \gamma_{SNR}\ \tilde{\gamma}_{Vol}$$

- $\tilde{\gamma}_{Temporal}$ … temporal decorrelation
- γ_{SNR} … additive noise decorrelation
- $\tilde{\gamma}_{Volume}$ … geometric decorrelation

SAR interferometry allows to reconstruct the vertical reflectivity function f(z) of a volume scatterer by means of interferometric (volume) coherence measurements at different vertical wavenumbers κ_Z, i.e. at different spatial baselines.

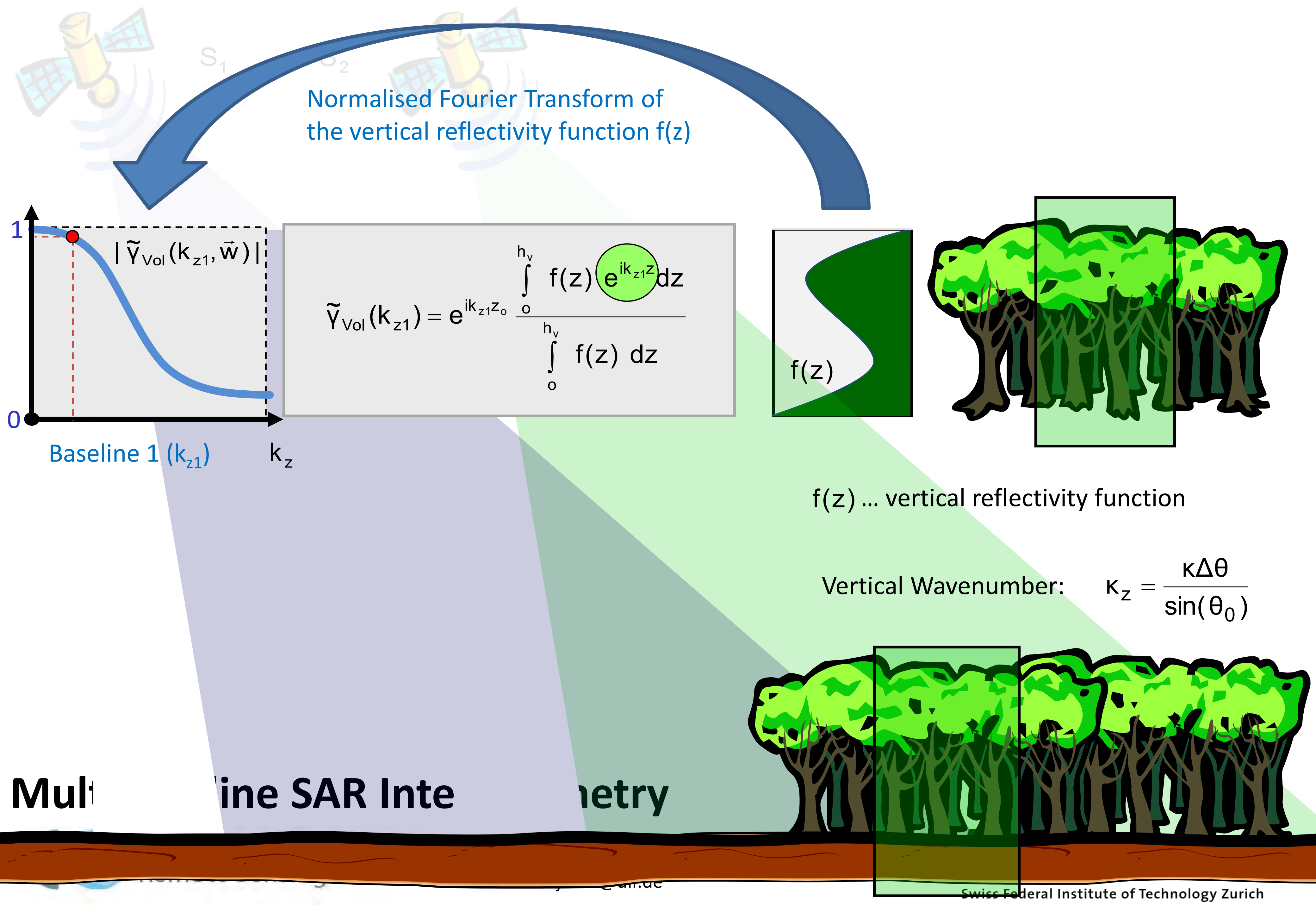
Normalised Fourier Transform of
the vertical reflectivity function f(z)
1
0
$|\tilde{\gamma}_{Vol}(k_{z1}, \vec{w})|$
Baseline 1 (k_{z1})
k_z
$$\tilde{\gamma}_{Vol}(k_{z1}) = e^{ik_{z1}z_o}\frac{\int_o^{h_v} f(z)\, e^{ik_{z1}z}\, dz}{\int_o^{h_v} f(z)\, dz}$$
f(z)
f(z) … vertical reflectivity function
Vertical Wavenumber: $\kappa_z = \frac{\kappa\Delta\theta}{\sin(\theta_0)}$
Mult
ine SAR Inte
etry
Swiss Federal Institute of Technology Zurich

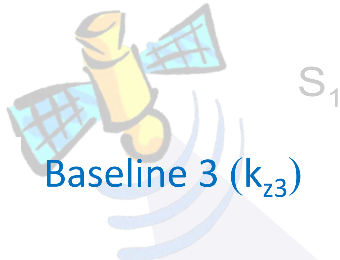

Baseline 3 (k_{z3})

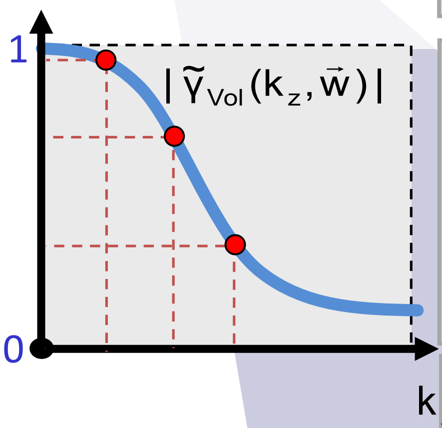

$$\tilde{\gamma}_{Vol}(k_{z3}) = e^{ik_z z_0} \frac{\int_0^{h_v} f(z)\, e^{ik_{z3} z} dz}{\int_0^{h_v} f(z)\, dz}$$

$$\tilde{\gamma}_{Vol}(k_{z1}) = e^{ik_{z1} z_0} \frac{\int_0^{h_v} f(z)\, e^{ik_{z1} z} dz}{\int_0^{h_v} f(z)\, dz}$$

$$\tilde{\gamma}_{Vol}(k_{z2}) = e^{ik_z z_0} \frac{\int_0^{h_v} f(z)\, e^{ik_{z2} z} dz}{\int_0^{h_v} f(z)\, dz}$$

Baseline 2 (k_{z2})

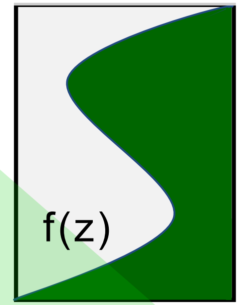

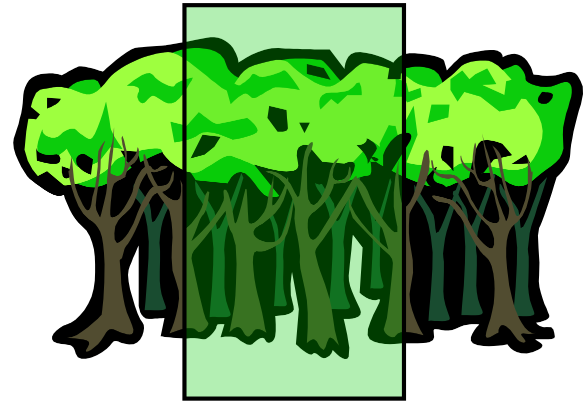

$f(z)$ … vertical reflectivity function

Vertical Wavenumber: $\kappa_z = \dfrac{\kappa \Delta\theta}{\sin(\theta_0)}$

Multi-baseline measurements allow to sample the spectrum of the vertical reflectivity FT{f(z)} @ different spatial baselines (i.e. spatial frequencies) k_z.

Multibaseline SAR Interferometry

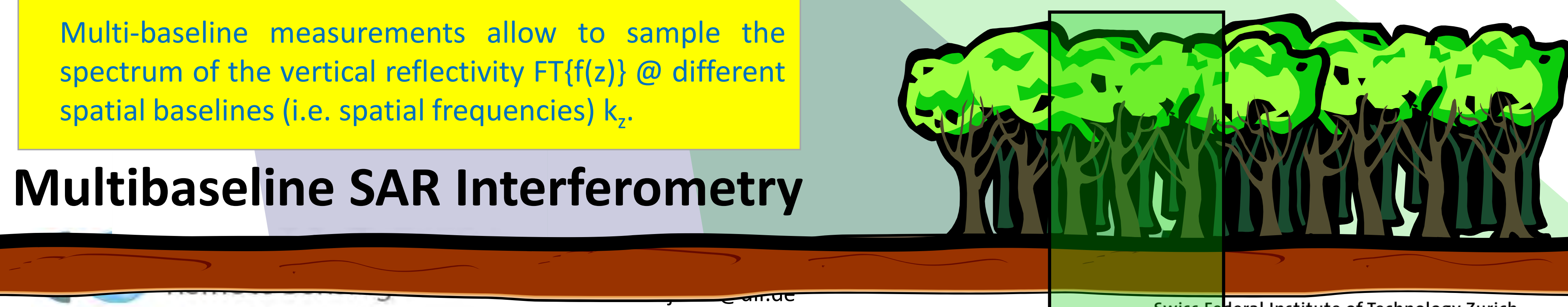

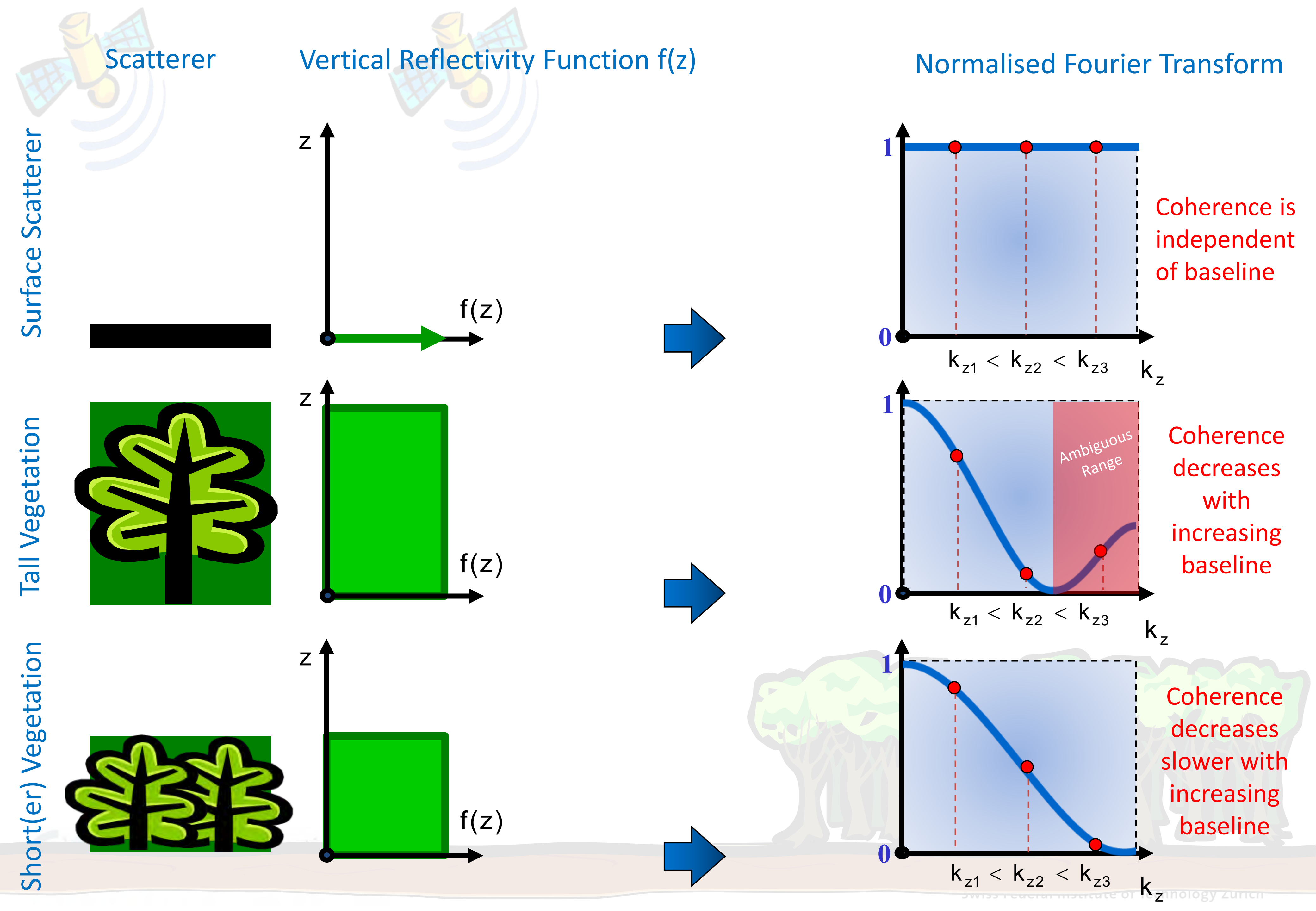

Scatterer
Vertical Reflectivity Function f(z)
Normalised Fourier Transform
Surface Scatterer
Tall Vegetation
Short(er) Vegetation
z
f(z)
1
0
$k_{z1} < k_{z2} < k_{z3}$
k_z
Coherence is independent of baseline
Ambiguous Range
Coherence decreases with increasing baseline
Coherence decreases slower with increasing baseline

Amplitude Image

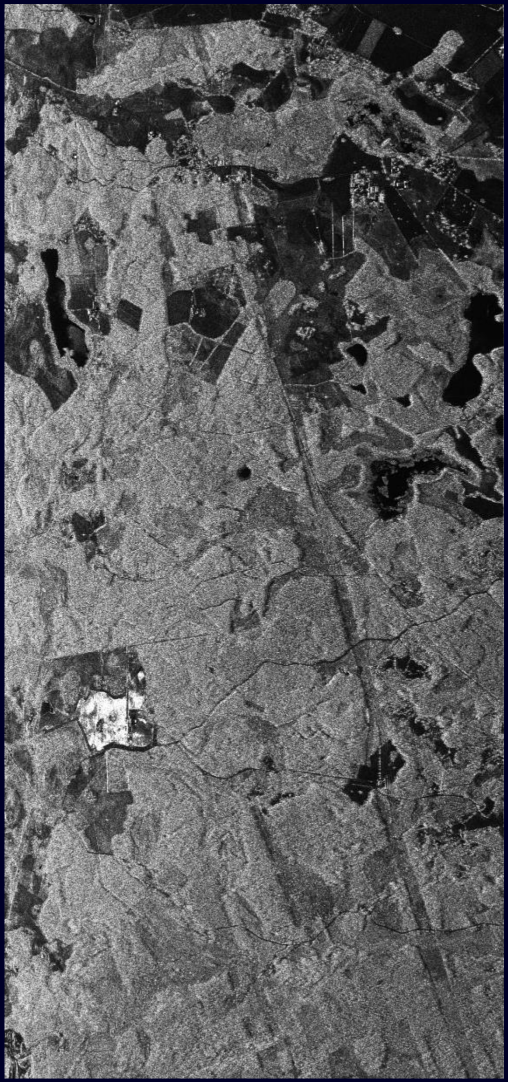

Interferometric Coherence: Volume Decorrelation

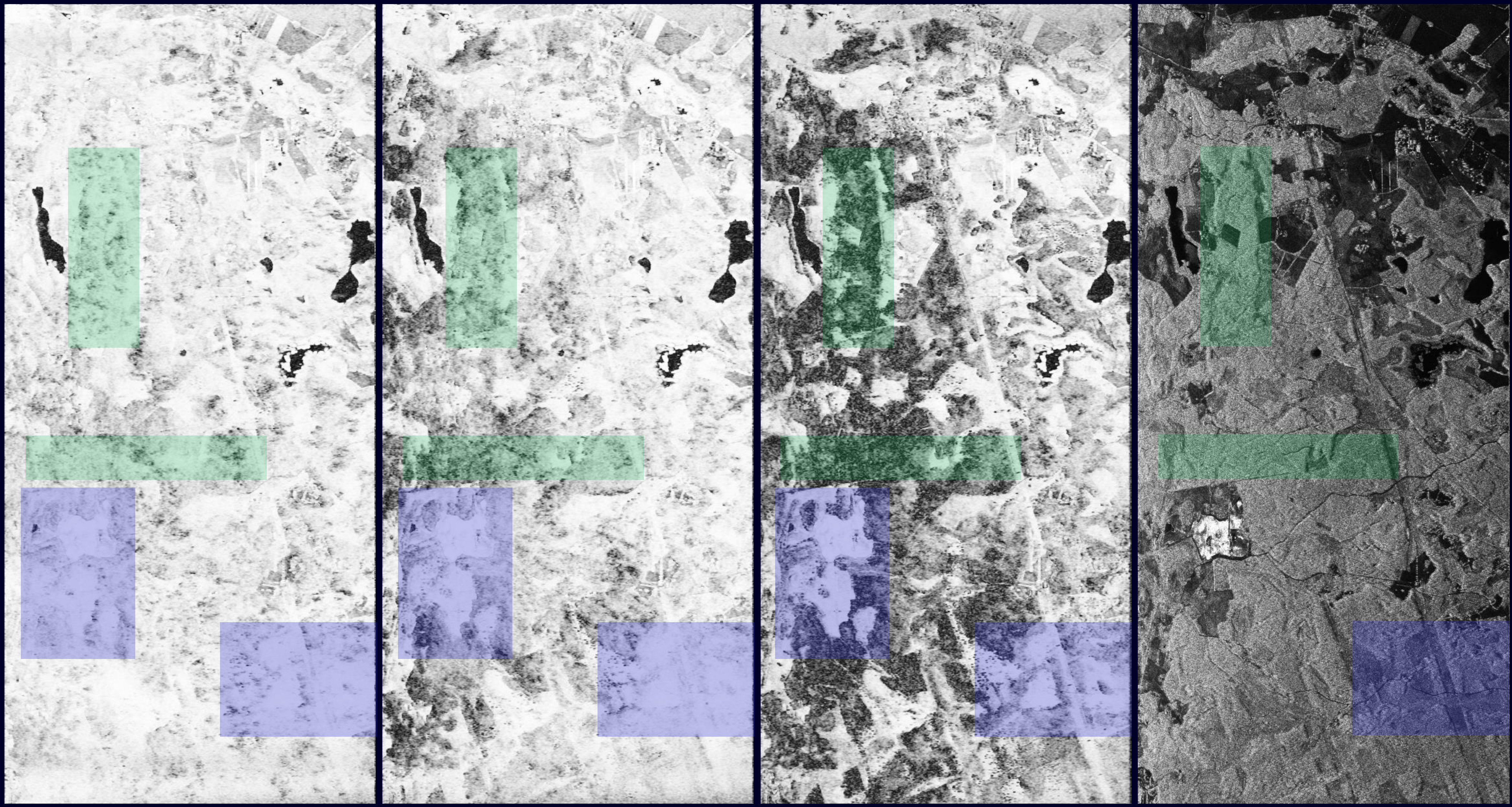

Spatial Baseline 3m   8m   16m   24m

hajnsek@ifu.baug.ethz.ch
irena.hajnsek@dlr.de

Polarimetric SAR Interferometry

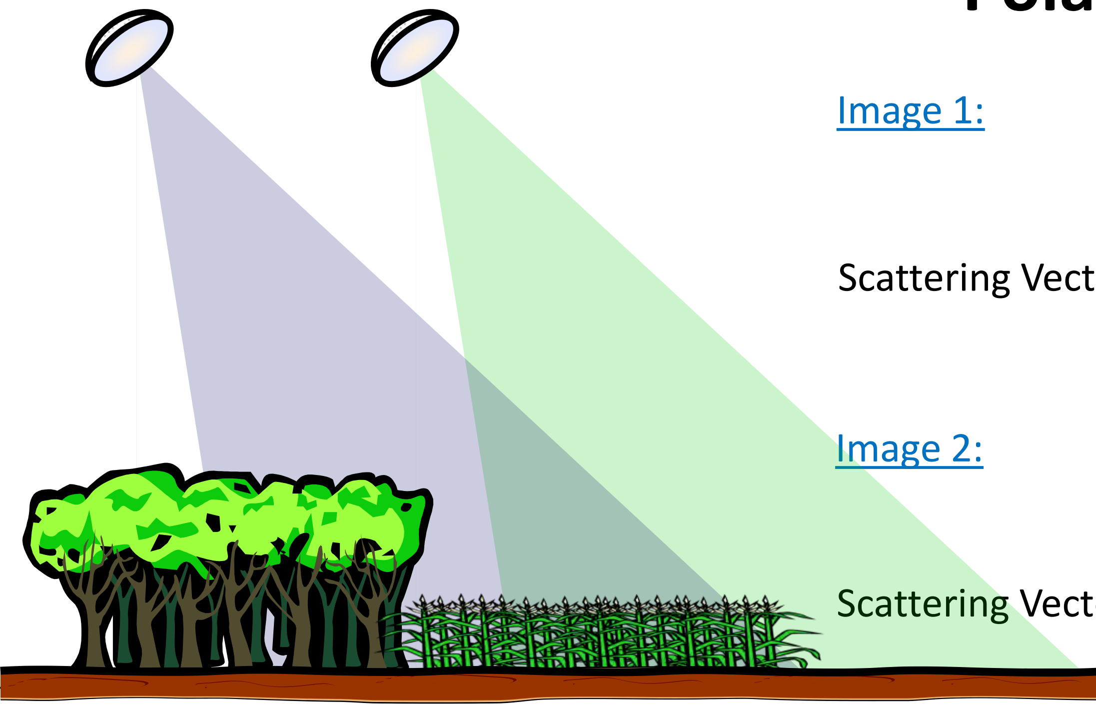

Image 1: Scattering Matrix: $[S_1] = \begin{bmatrix} S^1_{HH} & S^1_{HV} \\ S^1_{VH} & S^1_{VV} \end{bmatrix}$

Scattering Vector 1: $\vec{k}_1 = \frac{1}{\sqrt{2}}[S^1_{HH} + S^1_{VV} \quad S^1_{HH} - S^1_{VV} \quad 2S^1_{HV}]^T$

Image 2: Scattering Matrix: $[S_2] = \begin{bmatrix} S^2_{HH} & S^2_{HV} \\ S^2_{VH} & S^2_{VV} \end{bmatrix}$

Scattering Vector 2: $\vec{k}_2 = \frac{1}{\sqrt{2}}[S^2_{HH} + S^2_{VV} \quad S^2_{HH} - S^2_{VV} \quad 2S^2_{HV}]^T$

Image formation: $i_1 = \vec{w}_1^{+} \cdot \vec{k}_1$ and $i_2 = \vec{w}_2^{+} \cdot \vec{k}_2$ ... projection of the scattering vector on a (complex) unitary vector $\vec{w}_i$

$\vec{w}_i$ used to select a given polarisation out of all possible polarisations provided by the scattering matrix [S]

Example: $S_{HH} + S_{VV}$ image: $\vec{w} = [1 \quad 0 \quad 0]^T \rightarrow i = \vec{w}^{+} \cdot \vec{k}_j = \frac{1}{\sqrt{2}}(S^j_{HH} + S^j_{VV})$

S_{HH} image: $\vec{w}_1 = [1/\sqrt{2} \quad 1/\sqrt{2} \quad 0]^T \rightarrow i_j = \vec{w}^{+} \cdot \vec{k}_j = S^j_{HH}$

Polarimetric SAR Interferometry

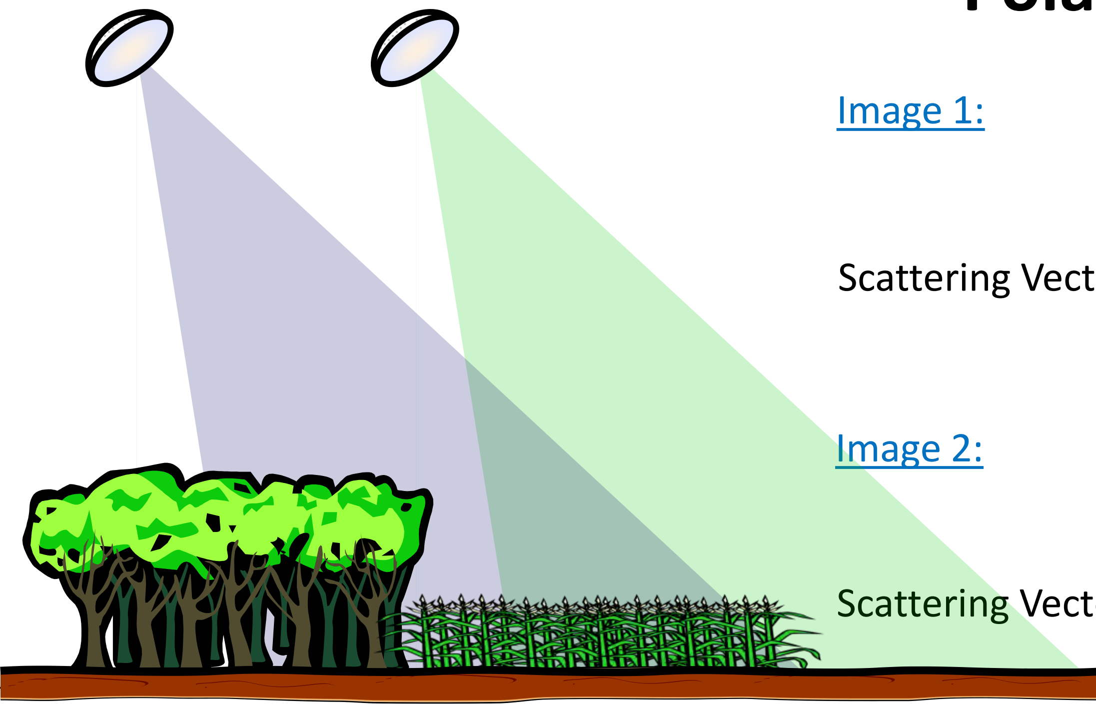

Image 1: Scattering Matrix: $[S_1] = \begin{bmatrix} S^1_{HH} & S^1_{HV} \\ S^1_{VH} & S^1_{VV} \end{bmatrix}$

Scattering Vector 1: $\vec{k}_1 = \frac{1}{\sqrt{2}}[S^1_{HH} + S^1_{VV} \quad S^1_{HH} - S^1_{VV} \quad 2S^1_{HV}]^T$

Image 2: Scattering Matrix: $[S_2] = \begin{bmatrix} S^2_{HH} & S^2_{HV} \\ S^2_{VH} & S^2_{VV} \end{bmatrix}$

Scattering Vector 2: $\vec{k}_2 = \frac{1}{\sqrt{2}}[S^2_{HH} + S^2_{VV} \quad S^2_{HH} - S^2_{VV} \quad 2S^2_{HV}]^T$

Image formation: $i_1 = \vec{w}_1^+ \cdot \vec{k}_1$ and $i_2 = \vec{w}_2^+ \cdot \vec{k}_2$ where $\vec{w}_i$ are complex unitary vectors*

Interferogram formation: $i_1 \; i_2^* = (\vec{w}_1^+ \cdot \vec{k}_1)(\vec{w}_2^+ \cdot \vec{k}_2)^+ = \vec{w}_1^+(\vec{k}_1 \cdot \vec{k}_2^+)\vec{w}_2 = \vec{w}_1^+[\Omega]\vec{w}_2$

Interferometric Coherence: $\tilde{\gamma}(\vec{w}_1, \vec{w}_2) = \frac{< i_1 \; i_2^* >}{\sqrt{< i_1 \; i_1^* > \; < i_2 \; i_2^* >}} = \frac{< \vec{w}_1^+[\Omega]\vec{w}_2 >}{\sqrt{< (\vec{w}_1^+[T_{11}]\vec{w}_1) > \; < (\vec{w}_2^+[T_{22}]\vec{w}_2) >}}$

where $[T_{11}] = < \vec{\kappa}_1 \cdot \vec{\kappa}_1^+ >$ $[T_{22}] = < \vec{\kappa}_2 \cdot \vec{\kappa}_2^+ >$ and $[\Omega] = < \vec{\kappa}_1 \cdot \vec{\kappa}_2^+ >$

$\vec{w}_i$ used to select a polarisation state out of all possible polarisations provided by the scattering matrix [S]

Polarisation 3

$$\tilde{\gamma}_{Vol}(f(z)) = e^{ik_z z_o}\frac{\int_o^{h_v} f(z)\, e^{ik_z z}\,dz}{\int_o^{h_v} f(z)\;dz}$$

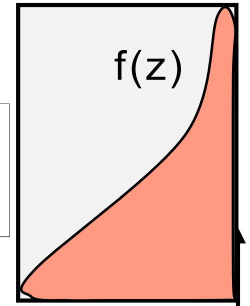

Polarisation 1

$$\tilde{\gamma}_{Vol}(f(z)) = e^{ik_z z_o}\frac{\int_o^{h_v} f(z)\, e^{ik_z z}\,dz}{\int_o^{h_v} f(z)\;dz}$$

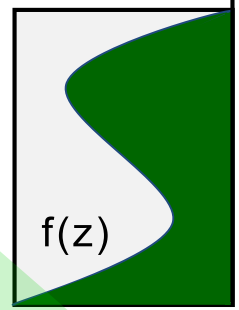

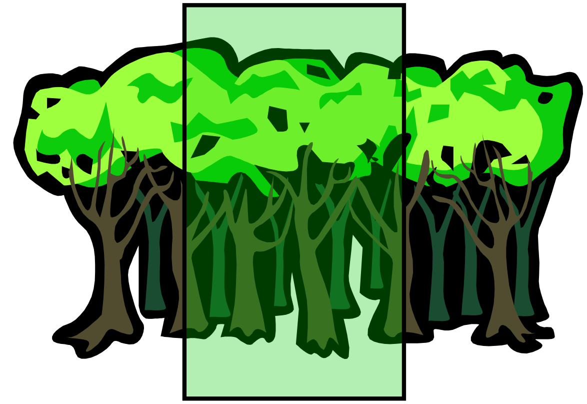

Polarisation 2

$$\tilde{\gamma}_{Vol}(f(z)) = e^{ik_z z_o}\frac{\int_o^{h_v} f(z)\, e^{ik_z z}\,dz}{\int_o^{h_v} f(z)\;dz}$$

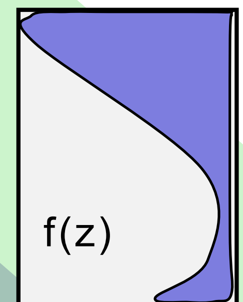

f(z) … vertical reflectivity function

Polarimetric SAR Interferometry

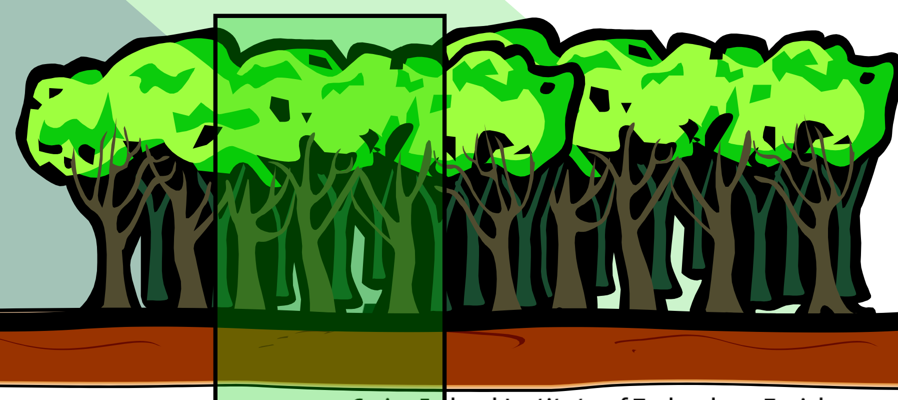

Interferometric Coherence: Volume Decorrelation

Amplitude Image HH | Sp. Baseline 16m Pol 1 | Pol2 | Pol 3

Geometrical Representation

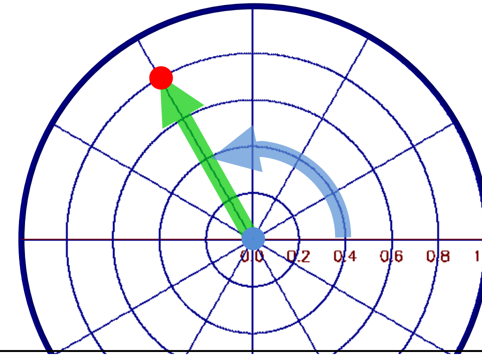

Interferometric Coherence:

$$\tilde{\gamma}(\vec{w}_i,\vec{w}_i) = \underbrace{|\tilde{\gamma}(\vec{w}_i,\vec{w}_i)|}_{\text{Radius}} \cdot \exp\left(i\, \underbrace{\mathrm{Arg}\{\tilde{\gamma}(\vec{w}_i,\vec{w}_i)\}}_{\text{Angle}}\right)$$

► can be represented by a single point on the unit circle

Coherence Region:

$$\tilde{\gamma}(\vec{w}_i,\vec{w}_i) \quad \forall \quad \vec{w}_i = \begin{bmatrix} \cos\alpha \exp(i\varphi_1) \\ \sin\alpha\cos\beta\exp(i\varphi_2) \\ \sin\alpha\sin\beta\exp(i\varphi_3) \end{bmatrix} \quad 0 \le \alpha \le \frac{\pi}{2} \quad -\pi \le \beta \le \pi \quad \in C$$

Shape and size depend on acquisition parameters and the structure of the underlying scatterer.

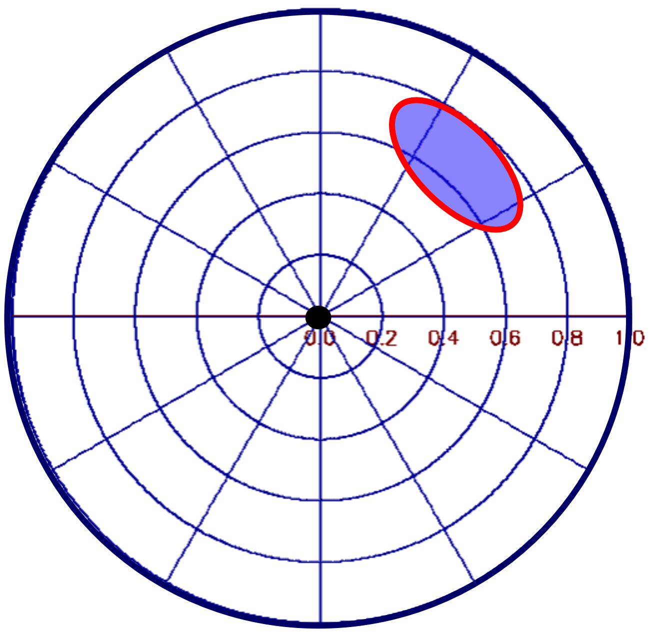

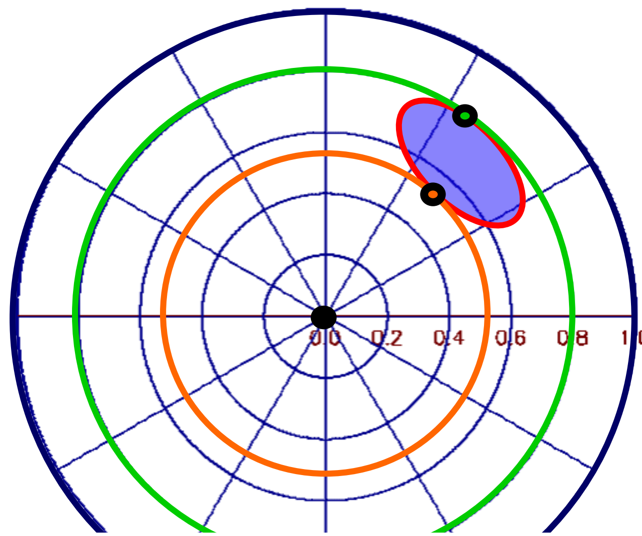

Max./ Min. Interferometric Coherence as function of the polarisation used to form the interferogram

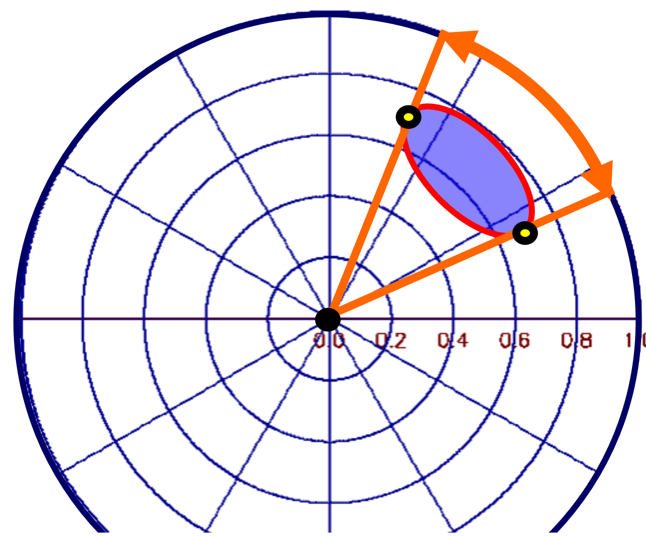

Max. Phase Difference between interferograms formed at different polarisations

Coherence Region Interpretation

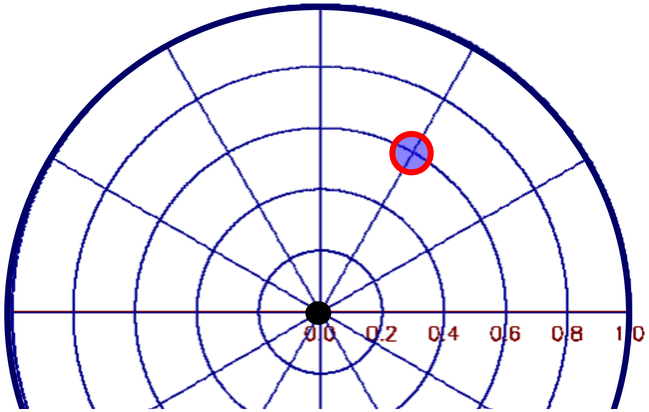

<u>Point Like Coherence Region</u>
i.e. InSAR Coherence and Phase are independent of polarisation.

Pol-InSAR does not provide any additional information compared to InSAR !!!

<u>(Random) Volume scattering</u>

hajnsek@ifu.baug.ethz.ch
irena.hajnsek@dlr.de

Coherence Region Interpretation

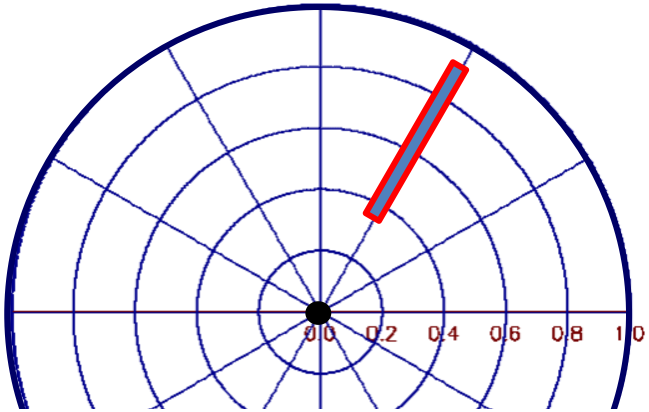

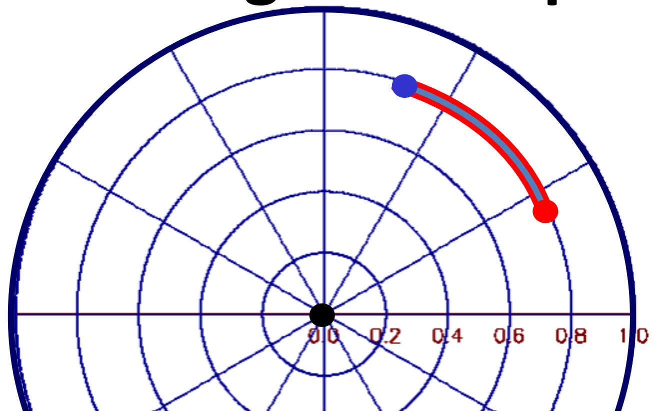

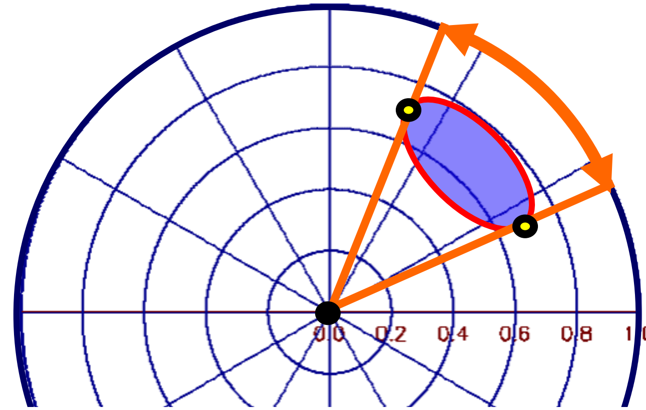

Radial Coherence Region
i.e. InSAR Coherence changes with polarisation but not the location of the phase center.

Radial Coherence Region
i.e. InSAR Phase changes, but not the InSAR coherence with polarisation

Elliptical Coherence Region
i.e. InSAR Coherence and Phase changes with polarisation.

Surface Scattering

$$\tilde{\gamma}(\vec{w}) = \gamma_{SNR}(\vec{w})\ \tilde{\gamma}_{Vol} \overset{\tilde{\gamma}_{Vol}:=1}{=} \gamma_{SNR}(\vec{w})$$

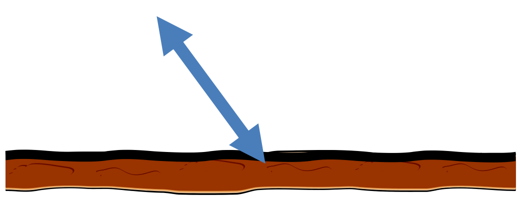

(Polarised) Coherent scaterrers at different heights

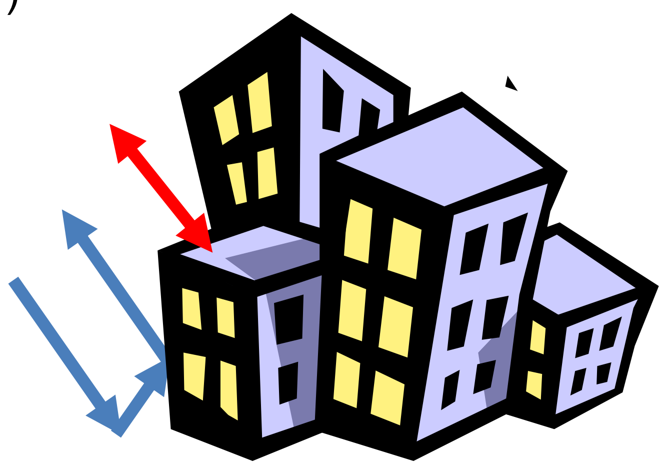

(Depolarising) Scaterrers at different heights

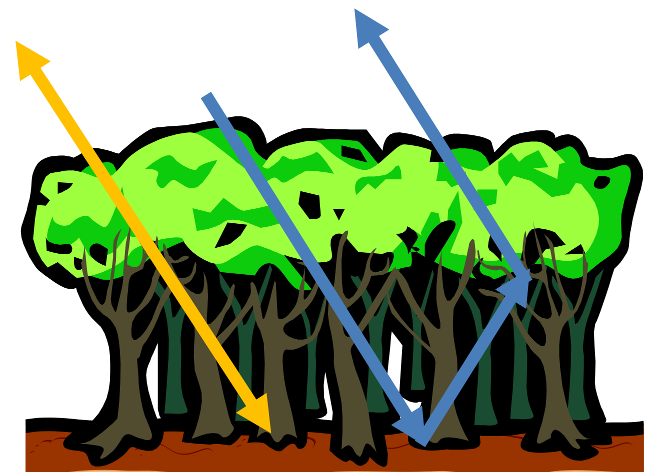

Coherence Region (CR)

Interferometric Coherence:

$$\tilde{\gamma}(\vec{w}_1,\vec{w}_2)=\frac{<\vec{w}_1[\Omega]\vec{w}_2^{\,+}>}{\sqrt{<\vec{w}_1[T_{11}]\vec{w}_1^{\,+}><\vec{w}_2[T_{22}]\vec{w}_2^{\,+}>}}$$

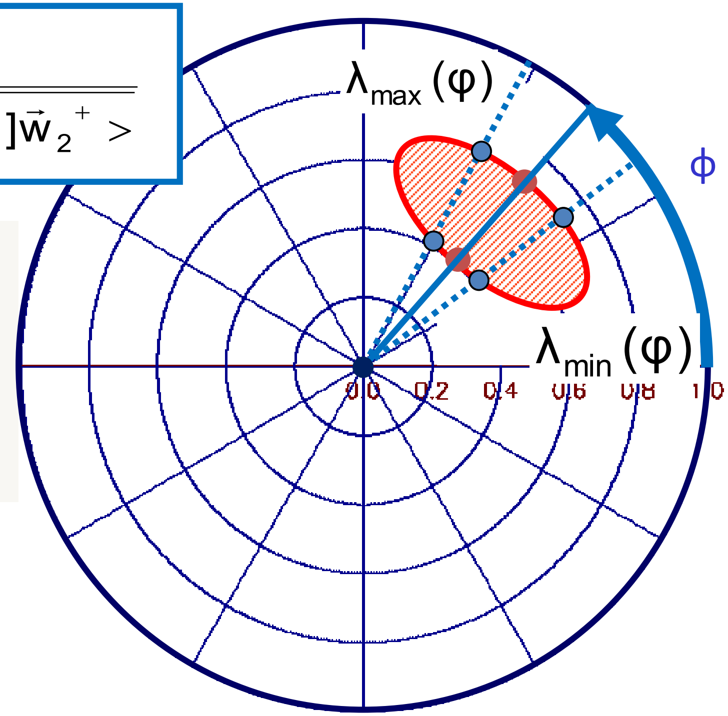

The boundary of the coherence region can be reconstructed by estimating for each angle ϕ the max (λ_1) and min (λ_2) coherences:

Optimisation Problem ($\vec{w}_1=\vec{w}_2$):

$$\boxed{[T]^{-1}[\Omega_\varphi]\ \vec{w}=\lambda\ \vec{w}}$$

where $[T]=\frac{1}{2}([T_{11}]+[T_{22}])$, $\lambda=-(\lambda_1+\lambda_2^*)$ $[\Omega_\varphi]=\frac{1}{2}(\exp(i\varphi)[\Omega]+\exp(-i\varphi)[\Omega]^+)$

and $[T_{11}]:=<\vec{k}_1\cdot\vec{k}_1^+>$ $[T_{22}]:=<\vec{k}_2\cdot\vec{k}_2^+>$ $[\Omega]:=<\vec{k}_1\cdot\vec{k}_2^+>$

Coherence Region: $\forall\varphi\rightarrow\lambda_{max},\lambda_{min}$ that have to be connected to provide the boundary of the CR

Shape and size are characterised by the acquisition and scattering parameters

hajnsek@ifu.baug.ethz.ch
irena.hajnsek@dlr.de

Structure Parameters & Applications

Forest

- Forest Height
- Forest (Vertical) Structure
- Forest Biomass
- Underlying Topography

→

- Forest Ecology
- Forest Management
- Ecosystem Modeling
- Climate Change

Agriculture

- Underlying Soil Moisture
- Moisture of Vegetation Layer
- Height of Vegetation Layer
- Soil Roughness

→

- Farming Management
- Ecosystem Modeling
- Water Cycle / CC
- Desertification

Snow & Ice

- Ice Layer Structure
- Penetration Depth (Ice)
- Snow Layer Thickness
- Snow Water Equivalent

→

- Ecosystem Change
- Water Cycle
- Water Management

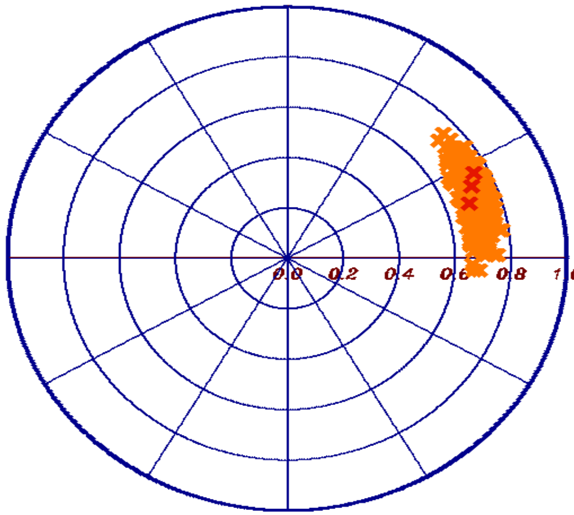

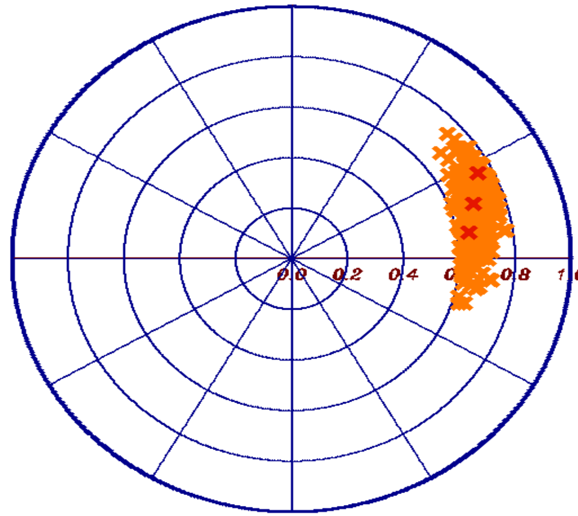

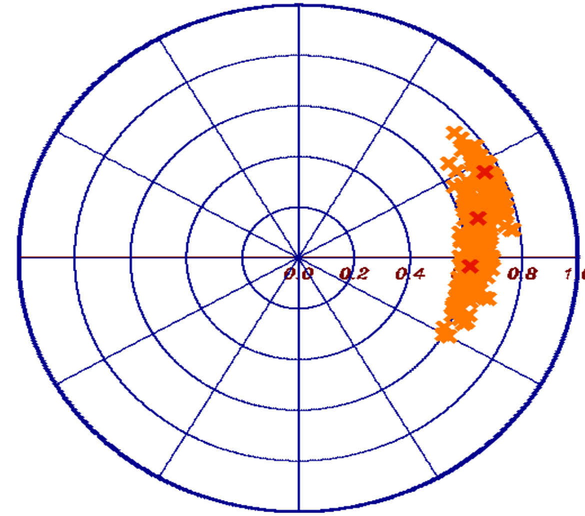

Model-Based Parameter Inversion

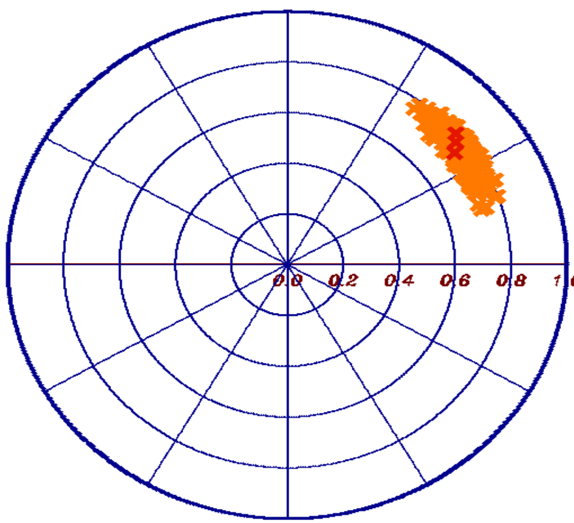

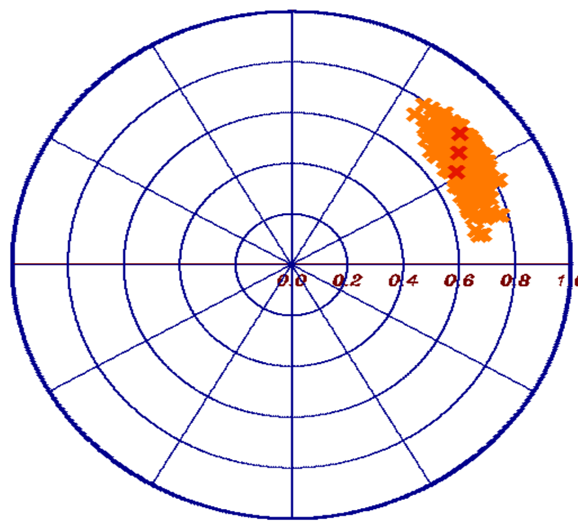

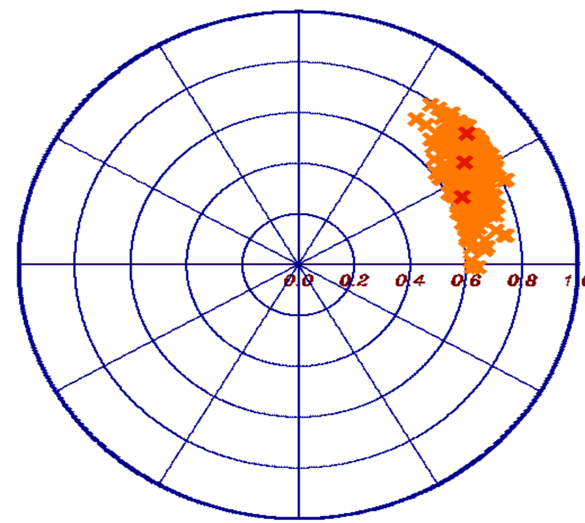

hajnsek@ifu.baug.ethz.ch
irena.hajnsek@dlr.de

Interferometric Coherence

$$\tilde{\gamma}(S_1\ S_2) = \frac{< S_1\ S_2^* >}{\sqrt{< S_1\ S_1^* >\ < S_2\ S_2^* >}}$$

Volume Coherence

$$\tilde{\gamma}_{Vol}(f(z)) = e^{ik_z z_o} \frac{\int_o^{h_v} f(z)\, e^{ik_z z} dz}{\int_o^{h_v} f(z)\ dz}$$

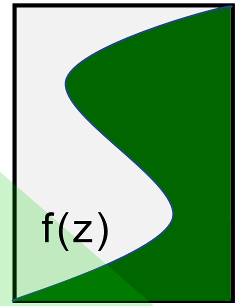

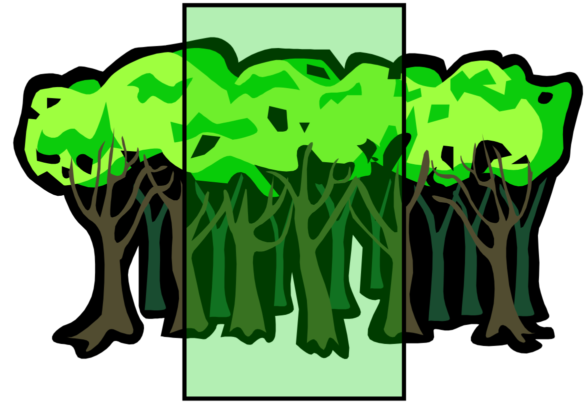

2 Layer Inversion Model

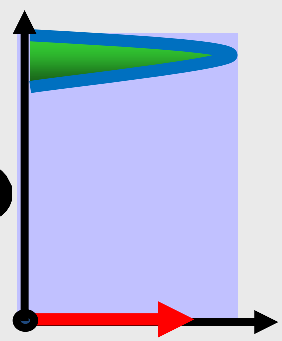

Volume Layer Ground Layer

$$f(z) = m_V f_V(z) + m_G \delta(z - z_0)$$

$$\tilde{\gamma}_{Vol}(\vec{w}) = \exp(i\varphi_0) \frac{\tilde{\gamma}_V + m(\vec{w})}{1 + m(\vec{w})}$$

$f_V(z)$ … volume reflectivity function

Volume Coherence

$$\tilde{\gamma}_V = \frac{I}{I_0} \quad \begin{cases} I = \int_0^{h_V} \exp(i\kappa_z z') f_V(z') dz' & m(\vec{w}) = \dfrac{m_G(\vec{w})}{m_V(\vec{w}) I_0} \\ I_0 = \int_0^{h_V} f_V(z') dz' & \kappa_z = \dfrac{\kappa \Delta\theta}{\sin(\theta_0)} \end{cases}$$

$f_V(z)$ has to be parameterised (N param)

Volume Height	h_V
Topography	φ_0
G/V Ratio	$m(\vec{w})$

3+N Unknowns

S_1 S_2

Interferometric Coherence

$$\tilde{\gamma}(S_1\ S_2) = \frac{< S_1\ S_2^* >}{\sqrt{< S_1\ S_1^* > < S_2\ S_2^* >}}$$

Volume Coherence

$$\tilde{\gamma}_{Vol}(f(z)) = e^{ik_z z_o} \frac{\int_o^{h_v} f(z) e^{ik_z z} dz}{\int_o^{h_v} f(z)\ dz}$$

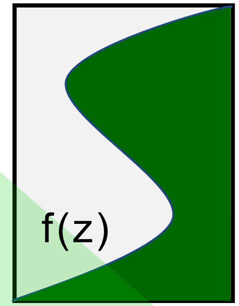

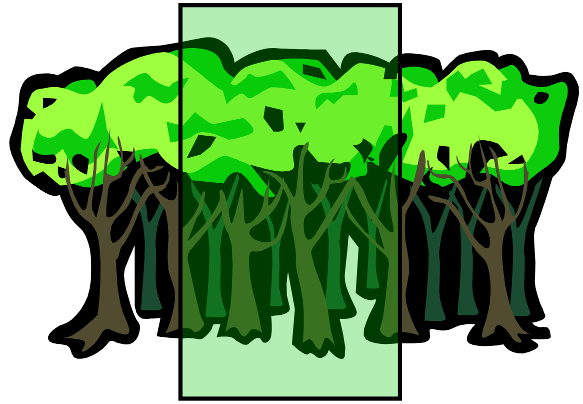

2 Layer Inversion Model

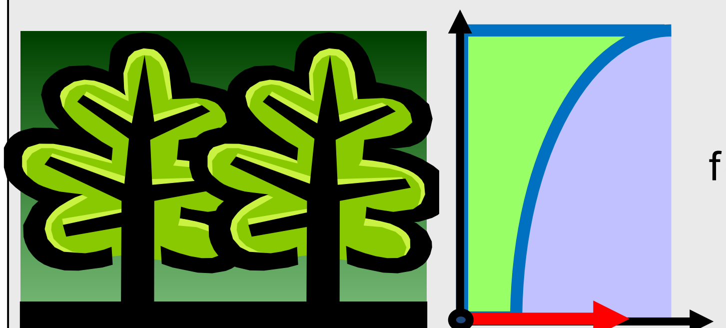

Volume Layer Ground Layer

$$f(z) = m'_V e^{\left(\frac{2\ \sigma\ z}{\cos\theta_0}\right)} + m'_G \delta(z - z_0)$$

$$\tilde{\gamma}_{Vol}(\vec{w}) = \exp(i\varphi_0) \frac{\tilde{\gamma}_V + m(\vec{w})}{1 + m(\vec{w})}$$

$$f_V(z) = e^{\left(\frac{2\ \sigma\ z}{\cos\theta_0}\right)}$$ ... volume reflectivity function = exponential function

Volume Coherence

$$\tilde{\gamma}_V = \frac{I}{I_0} \quad \begin{cases} I = \int_0^{h_V} \exp(i\kappa_z z')\ m_V \exp\left(\frac{2\ \sigma\ z'}{\cos\theta_0}\right) dz' \\ I_0 = \int_0^{h_V} m_V \exp\left(\frac{2\ \sigma\ z'}{\cos\theta_0}\right) dz' \end{cases}$$

$$m(\vec{w}) = \frac{m_G(\vec{w})}{m_V(\vec{w}) I_0}$$

$$\kappa_z = \frac{\kappa\Delta\theta}{\sin(\theta_0)}$$

σ	"Volume Extinction"
Volume Height	h_V
Topography	φ_0
G/V Ratio	$m(\vec{w})$

4 Unknowns

Modeling approaches for $f_V(z)$

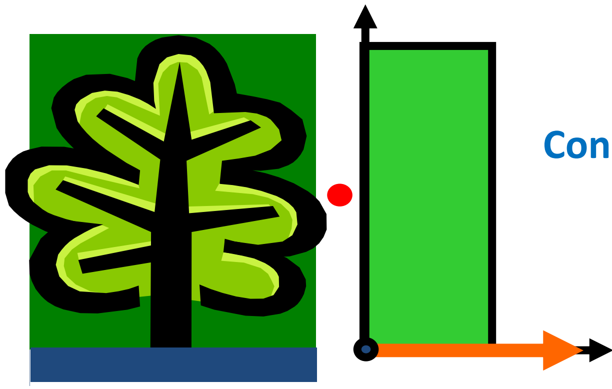

Constant Profile

$$f_V(z) = ct.$$

Linear Profile $f(h_V,\sigma)$

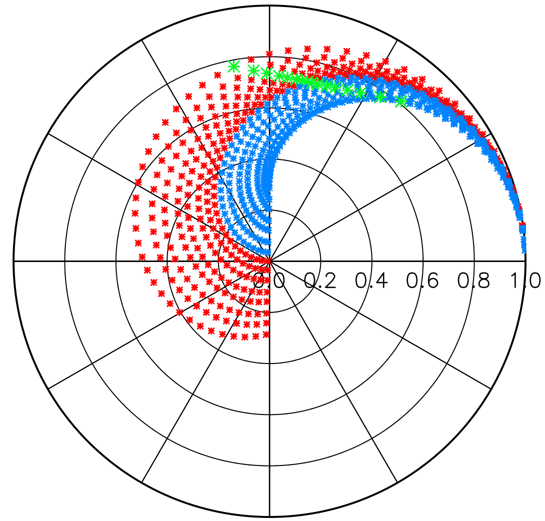

Exp. Profile $f(h_V, \sigma)$

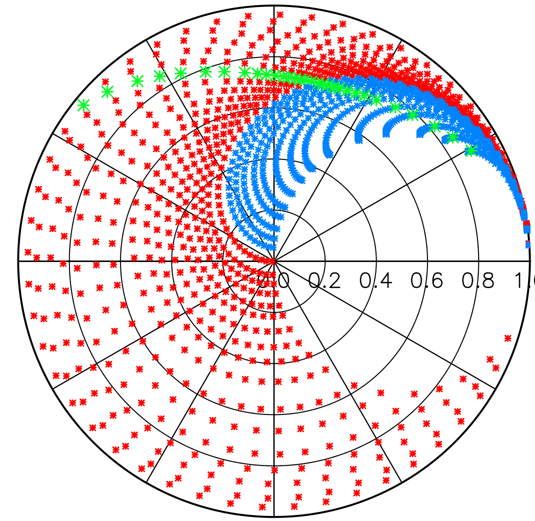

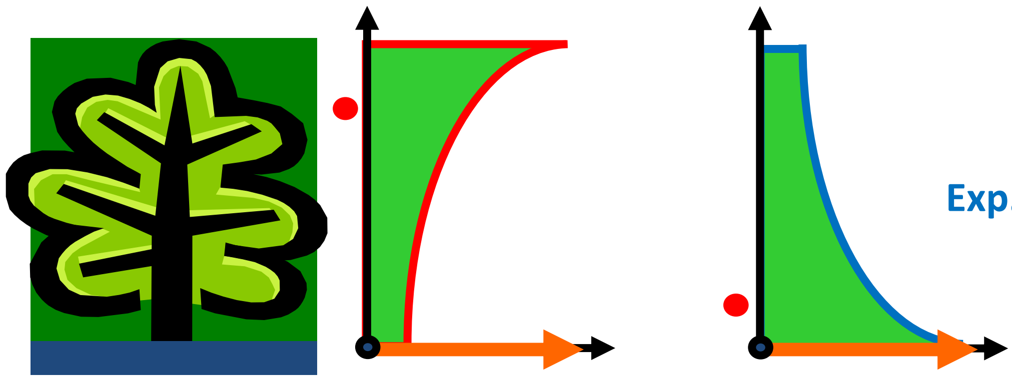

Exp. Profile

$$f_V(z) = \exp\left(\pm \frac{2\ \sigma\ z}{\cos\theta_0}\right)$$

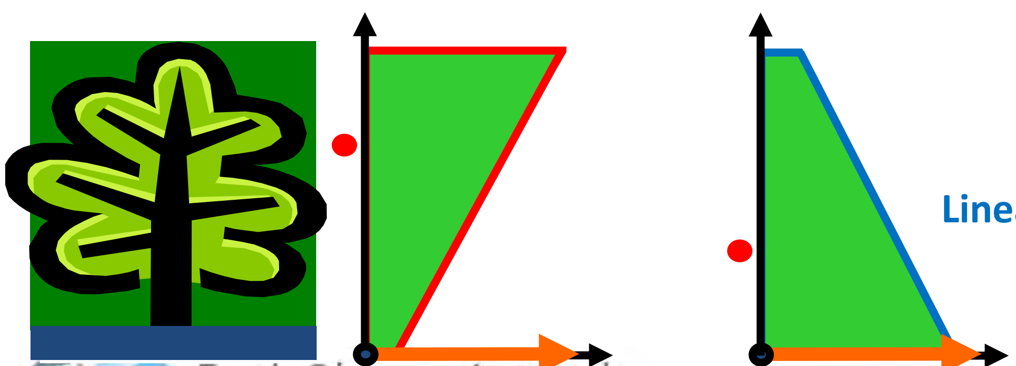

Linear Profile

$$f_V(z) = (\pm \frac{2\ \sigma\ z}{\cos\theta_0} + 1)$$

hajnsek@ifu.baug.ethz.ch
irena.hajnsek@dlr.de

Polarimetric Behaviour: Random vs. Oriented Volume

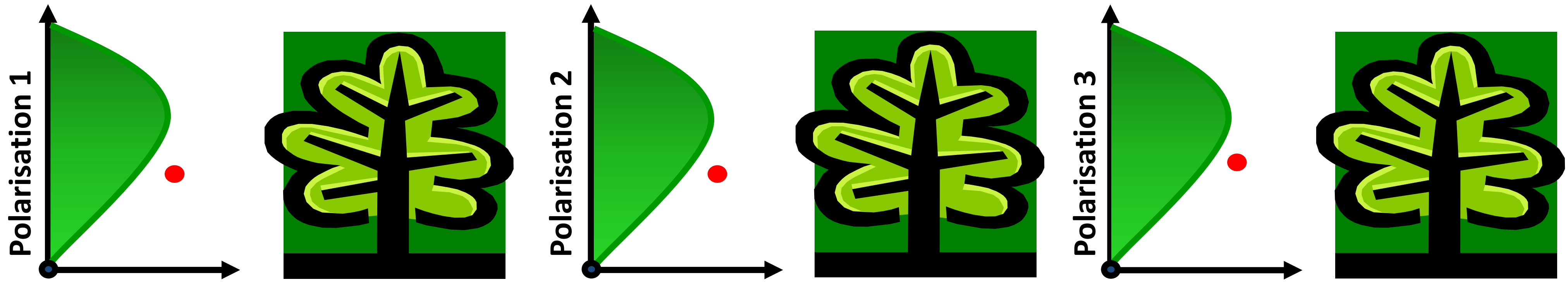

Random Volume: The vertical reflectivity function is independent of polarisation (or each polarisation sees the same volume vertical reflectivity $f_v(z)$)

$$f_v := f_v(z) \mapsto \tilde{\gamma}_V(\kappa_z)$$

Oriented Volume: The vertical reflectivity function changes with polarisation (or each polarisation sees a different volume vertical reflectivity $f_v(z)$)

$$f_v := f_v(z,\vec{w}) \mapsto \tilde{\gamma}_V(\kappa_z,\vec{w})$$

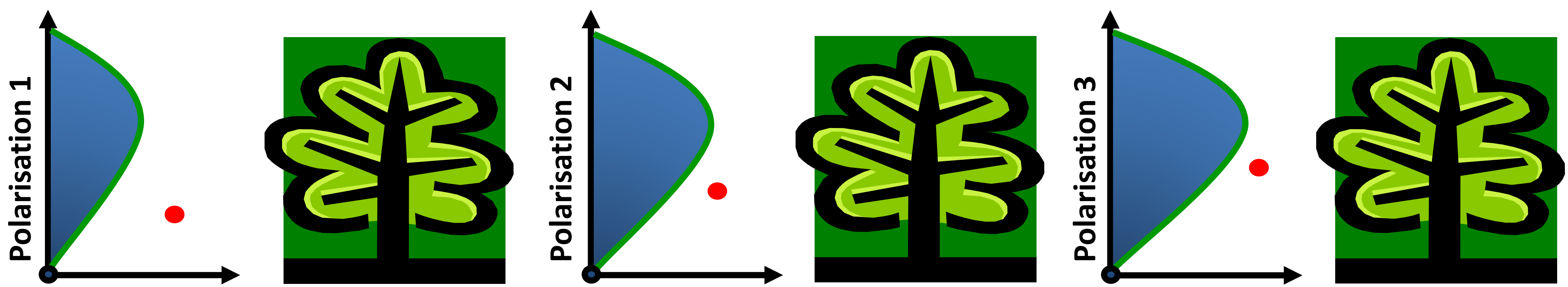

hajnsek@ifu.baug.ethz.ch
irena.hajnsek@dlr.de

Polarimetric Behaviour: 3-dim vs 2-dim Ground Scatterer

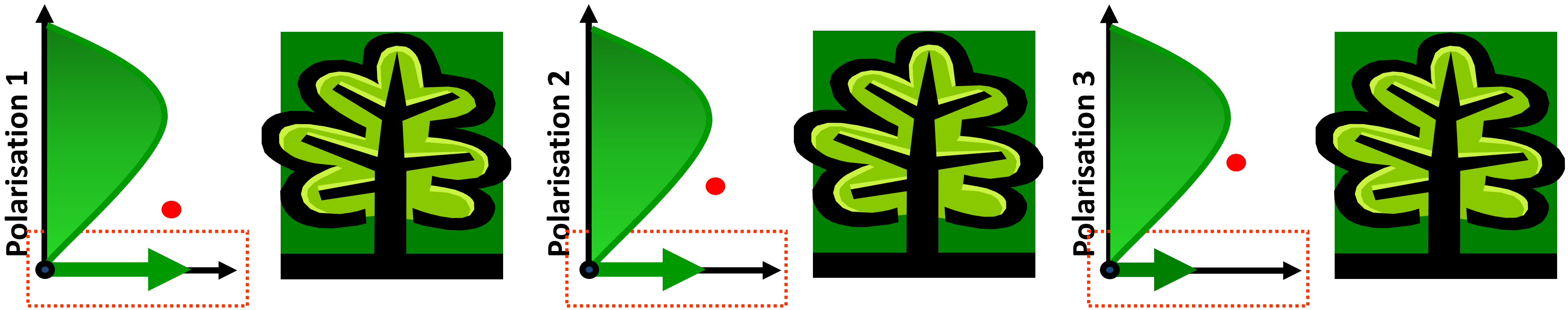

3-dim ground scatterer: A ground scattering component is visible in all polarisations (or there is no polarisation that "switches-off" the ground)

$$\forall\ \vec{w} \quad m(\vec{w}) \neq 0$$

2-dim ground scatterer: There is (at least) one polarisation in which the ground disappears

$$\exists\ \vec{w} \mapsto m(\vec{w}) = 0$$

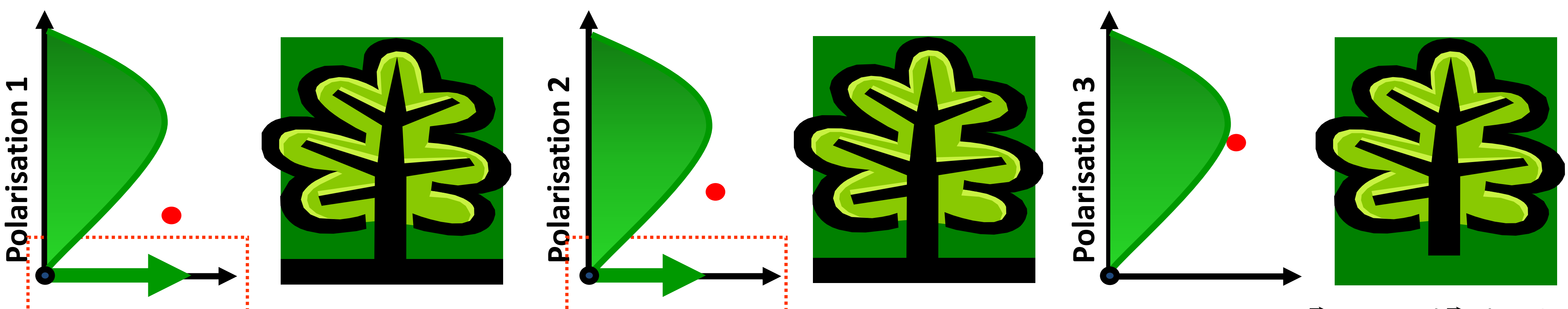

$$\exists \vec{w}_x \mapsto m(\vec{w}_x) = 0$$

hajnsek@ifu.baug.ethz.ch
irena.hajnsek@dlr.de

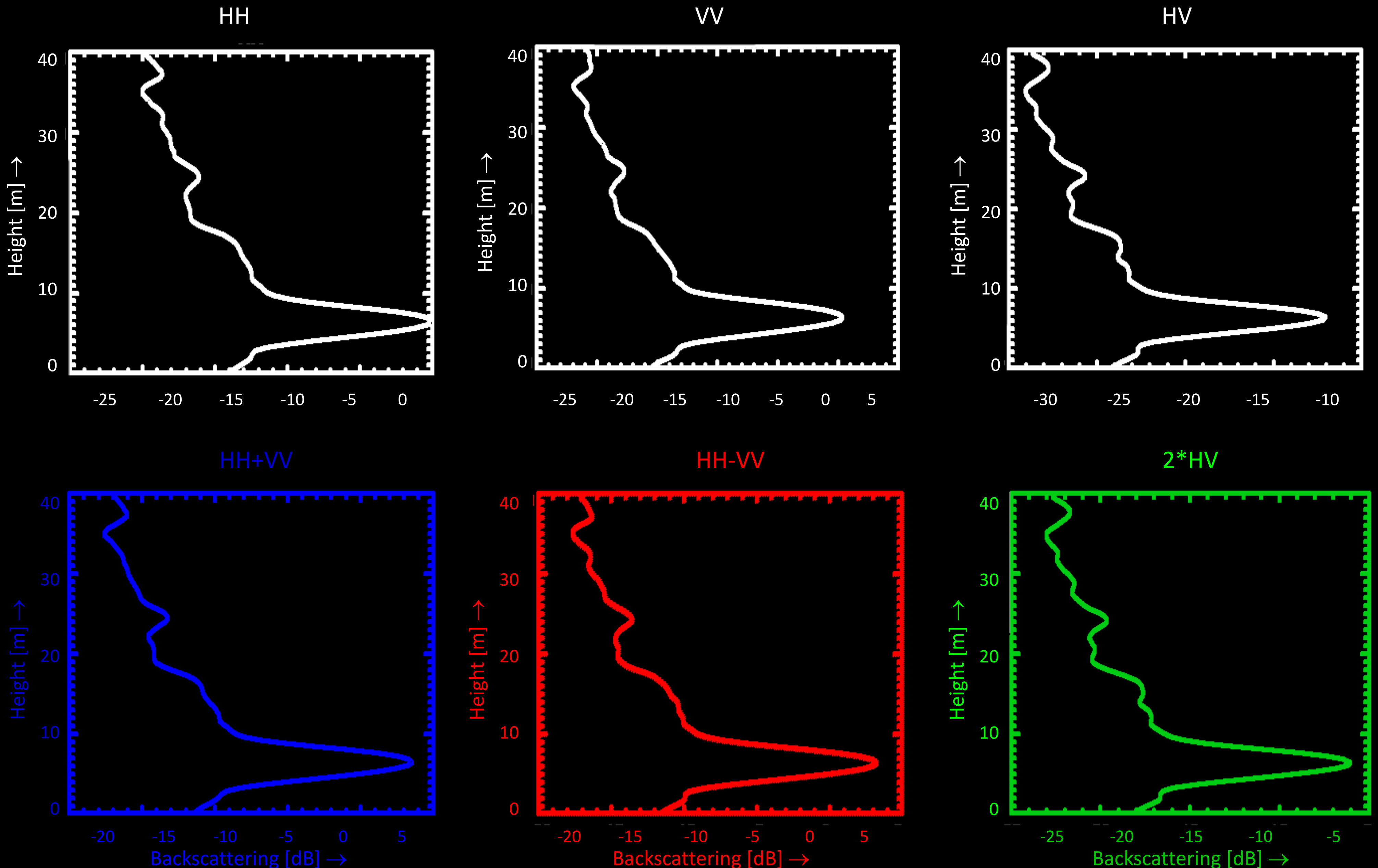

Bare Surface Backscattering Profiles

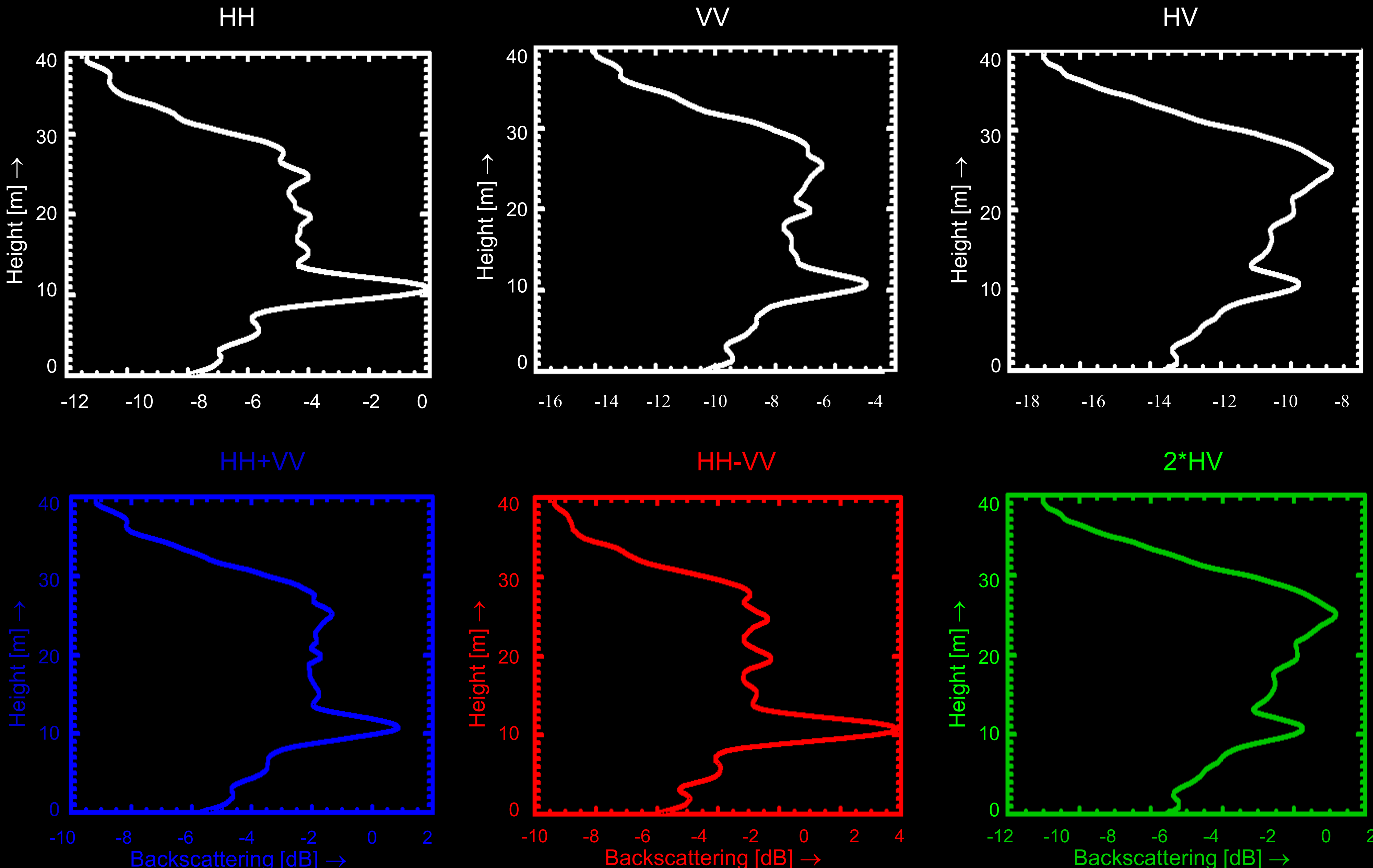

Mixed Forest Backscattering Profiles (12-20 m height)

RVoG Scattering Model: Geometrical Interpretation

Interferometric Coherence:
(2 Layer Random Volume)

$$\tilde{\gamma}(\vec{w}) = \exp(i\varphi_0)\frac{\tilde{\gamma}_V + m(\vec{w})}{1+m(\vec{w})}$$

$$\boxed{\tilde{\gamma}(\vec{w}) = \exp(i\varphi_0)\left[\tilde{\gamma}_V + \frac{m(\vec{w})}{1+m(\vec{w})}(1-\tilde{\gamma}_V)\right]}$$

$$\tilde{\gamma}(\vec{w}) = \exp(i\varphi_0)[\ B \ + \ X(\vec{w})\ \ A\ ]$$

Equation of a straight line in the complex plane ▶

The coherence region of the RVoG model is a line segment !!!

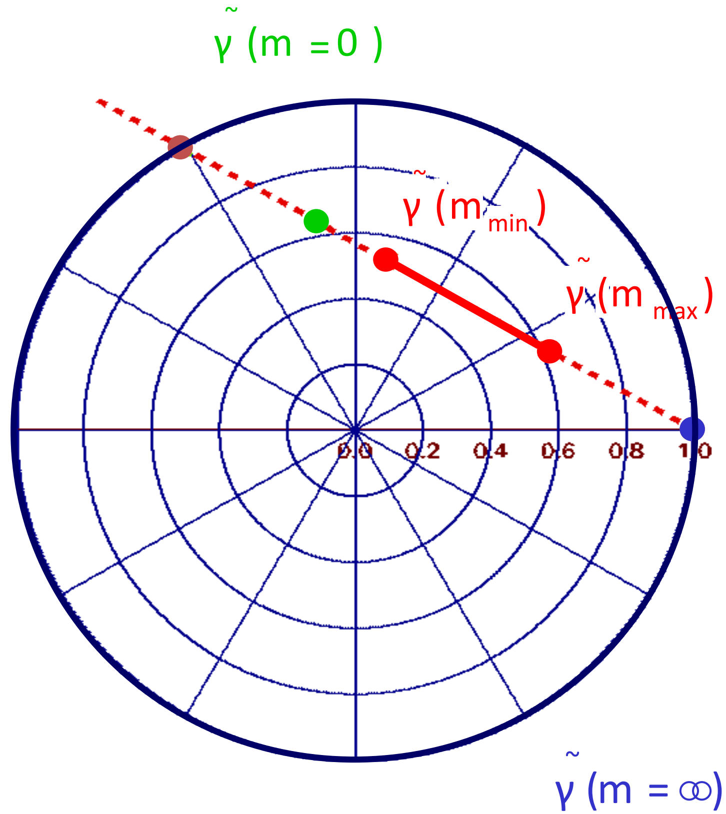

- The ends of the segment correspond to the coherences given by the max / min G-V Ratio: $\tilde{\gamma}(m_{max})$ and $\tilde{\gamma}(m_{min})$
- One of the line-unit circle intersection points correspond to the “Ground only” point, i.e. $\tilde{\gamma}(m=\infty) = \exp(i\varphi_0)$
- The second line-unit circle intersection points is non-physical
- The “Volume only” point (i.e. $\tilde{\gamma}(m(\vec{w})=0) = \exp(i\varphi_0)\tilde{\gamma}_V$) lies on the line but (in general) not on the coherence region segment

hajnsek@ifu.baug.ethz.ch
irena.hajnsek@dlr.de

Eidgenössische Technische Hochschule Zürich
Swiss Federal Institute of Technology Zurich

RVoG Solution on the Unit Circle

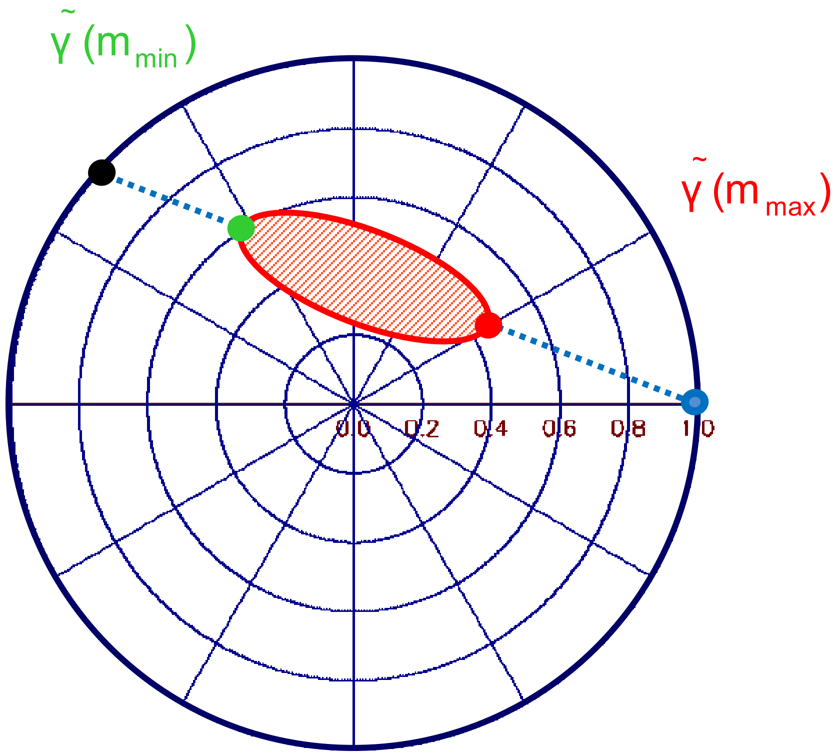

1. Estimation of the Coherence Region (CR);
2. Line fit through the extreme points of the CR

   $\tilde{\gamma}(m_{min})$ and $\tilde{\gamma}(m_{max})$

3. Estimation of the line-circle intersection point that corresponds to the underlying ground, i.e.:

   $$\tilde{\gamma}(m = \infty) = \exp(i\varphi_0)$$

RVoG Solution on the Unit Circle

Curve of constant extinction σ and variable height h_V

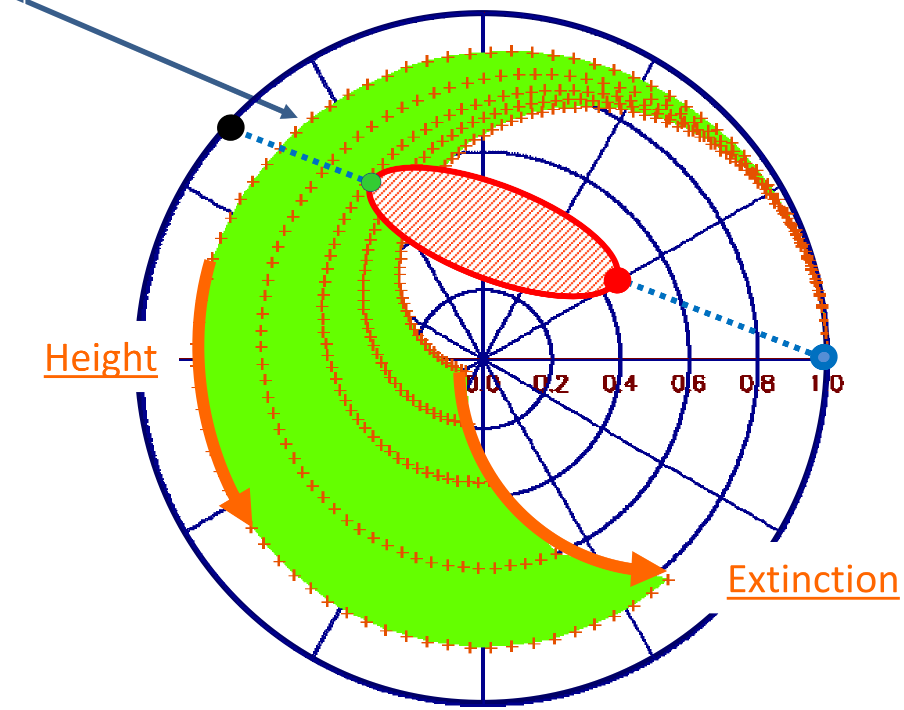

$$\tilde{\gamma}(m=0) = \exp(i\phi_0)\frac{\int_0^{h_V} \exp(i\kappa_z z')\exp\left(\frac{2\sigma z'}{\cos\theta_0}\right)dz'}{\int_0^{h_V} \exp\left(\frac{2\sigma z'}{\cos\theta_0}\right)dz'}$$

4. From the underlying ground point $\tilde{\gamma} = \exp(i\varphi_0)$ a Volume Height–Extinction Look-Up Table (LUT) is initialised that provides at every intersection with the line a solution couple (h_V, σ)

There is no unique solution of the RVoG model in the context of a single baseline !!!

5. Regularisation: Assuming a 2-dim ground, i.e. $\tilde{\gamma}(m_{min}) = \tilde{\gamma}(m=0)$ leads to a unique (h_V, σ) solution through the intersection of $\tilde{\gamma}(m_{min})$ with the LUT

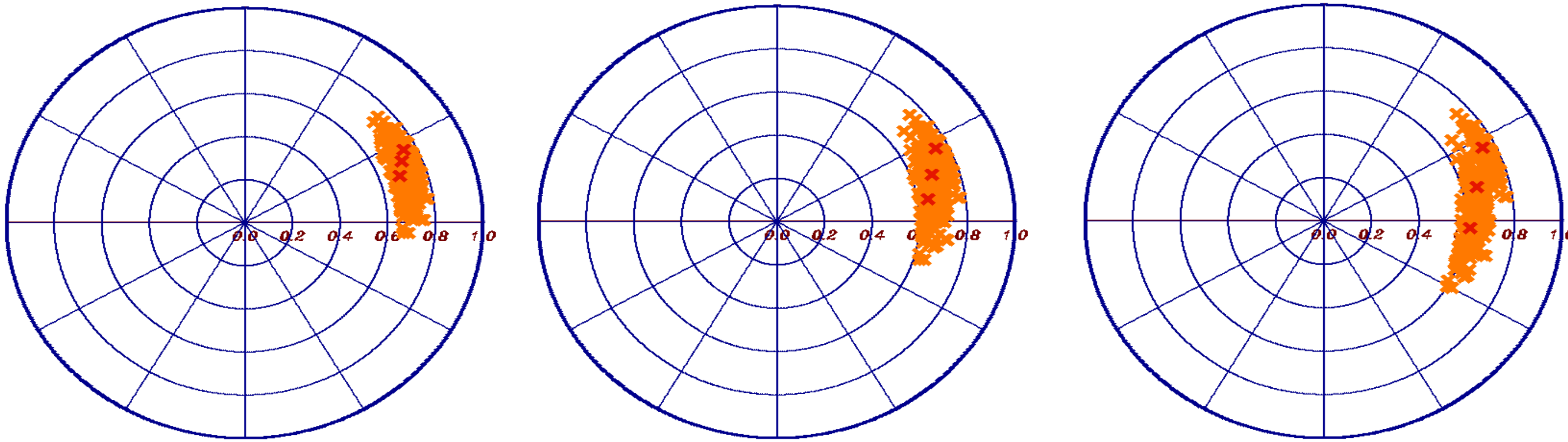

RVoG Inversion: Validation

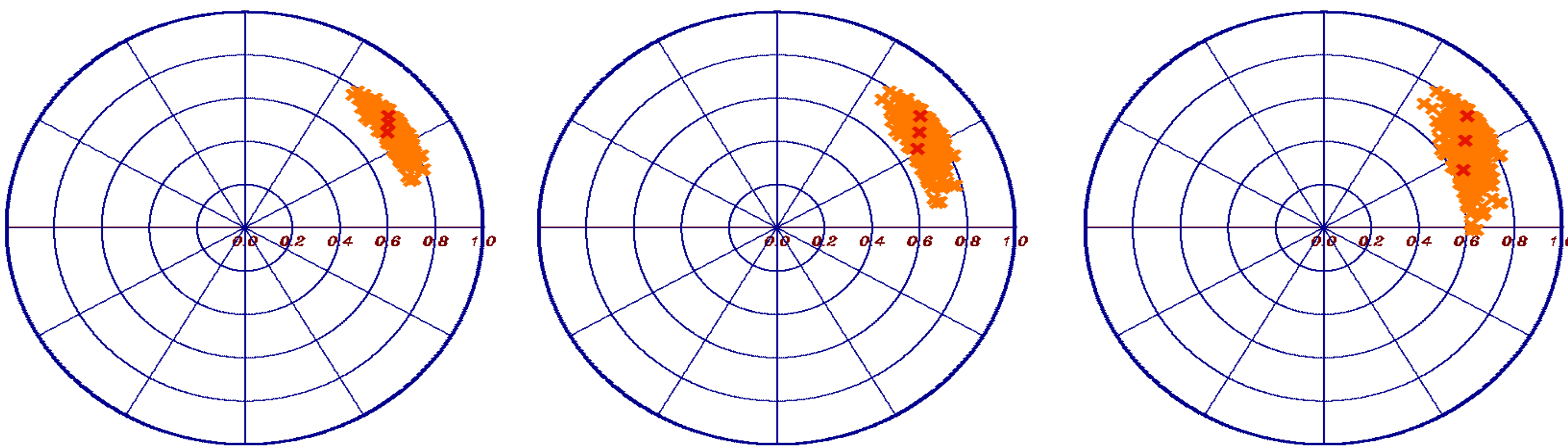

Structure Parameters & Applications

Forest

- Forest Height
- Forest (Vertical) Structure
- Forest Biomass
- Underlying Topography

→

- Forest Ecology
- Forest Management
- Ecosystem Modeling
- Climate Change

Agriculture

- Underlying Soil Moisture
- Moisture of Vegetation Layer
- Height of Vegetation Layer
- Soil Roughness

→

- Farming Management
- Ecosystem Modeling
- Water Cycle / CC
- Desertification

Snow & Ice

- Ice Layer Structure
- Penetration Depth (Ice)
- Snow Layer Thickness
- Snow Water Equivalent

→

- Ecosystem Change
- Water Cycle
- Water Management

Forest: The beginning of Pol-InSAR

SIR-C/X-SAR / Test Site: Kudara, Russia

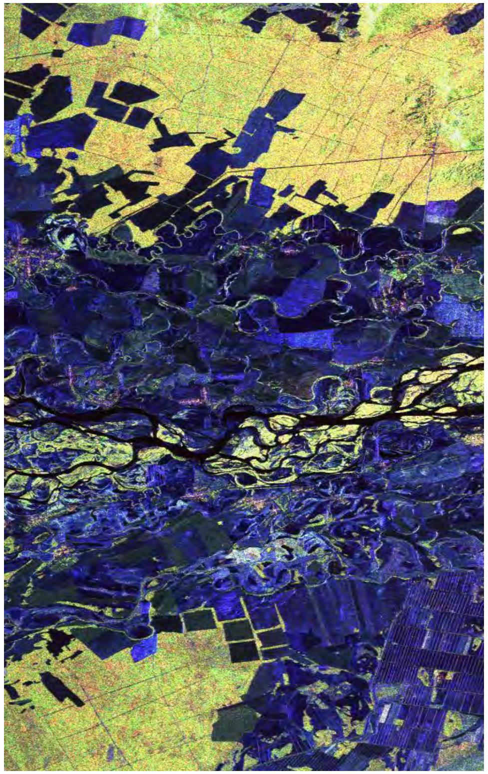

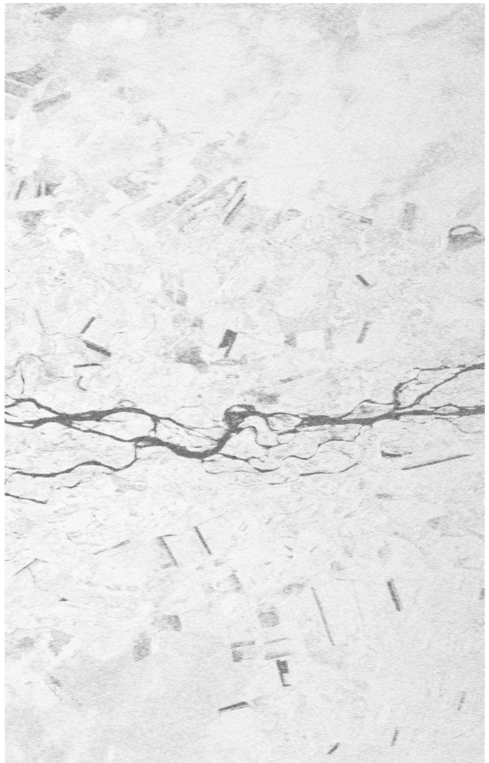

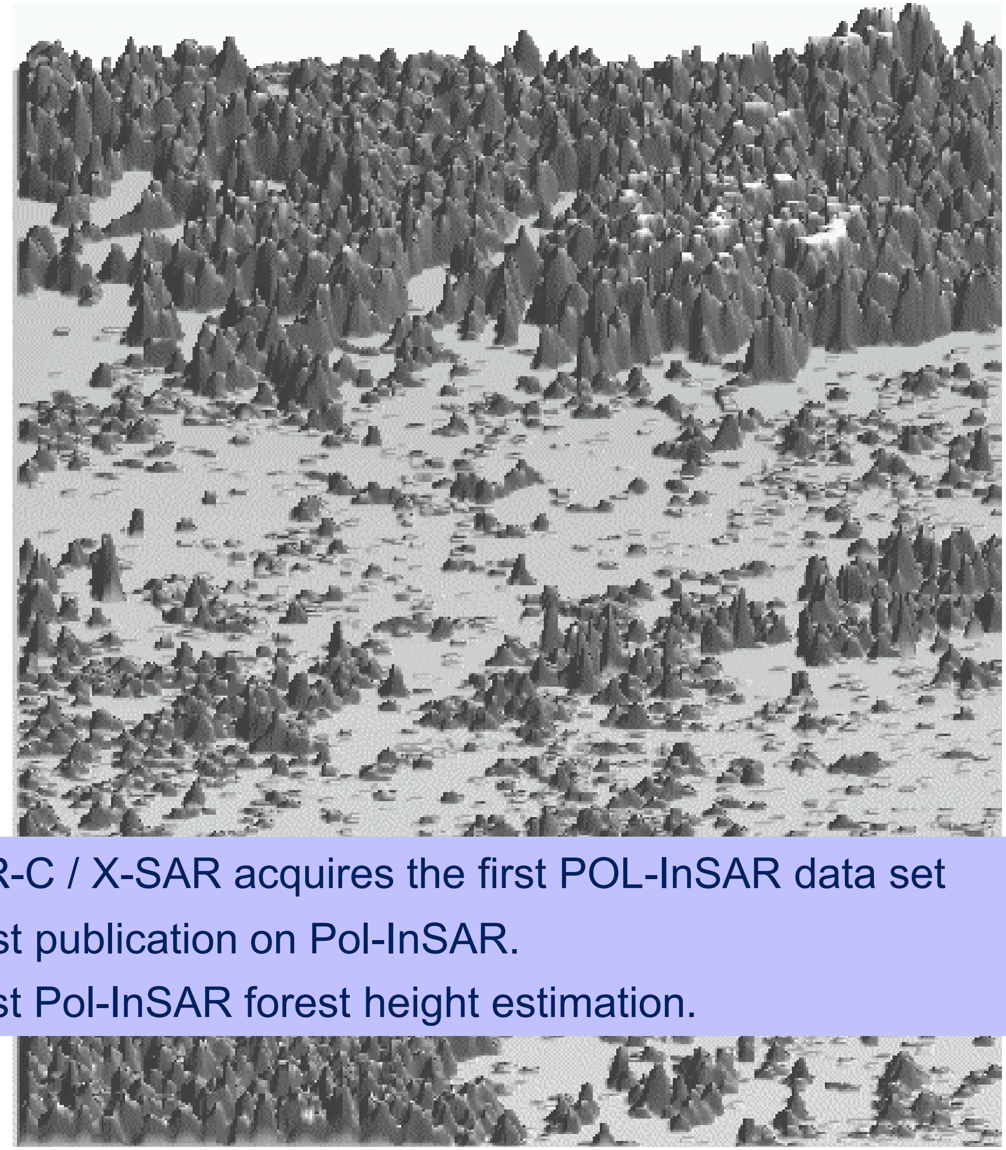

L-band / Pauli RGB

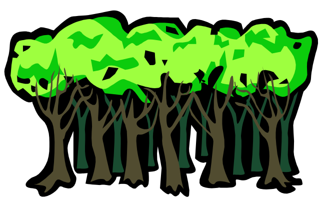

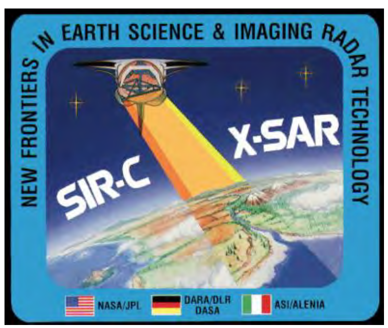

1994: SIR-C / X-SAR acquires the first POL-InSAR data set

1996: First publication on Pol-InSAR.

1998: First Pol-InSAR forest height estimation.

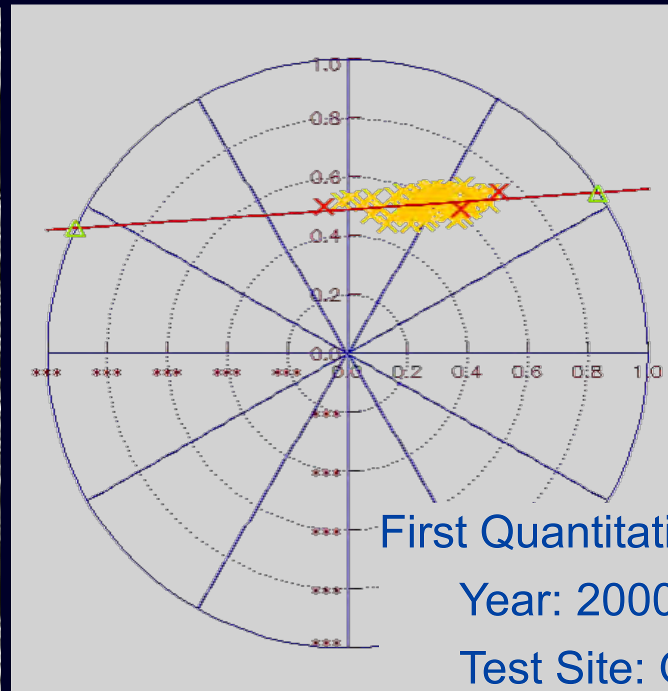

First Quantitative Pol-InSAR Demonstration:

Year: 2000 Sensor: E-SAR (DLR)

Test Site: Oberpfaffenhofen / Germany

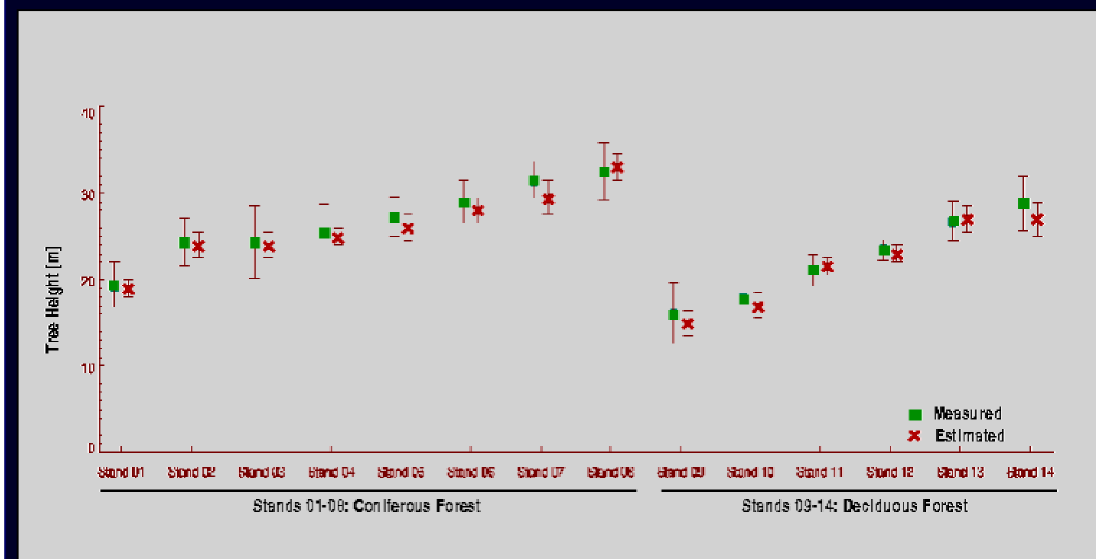

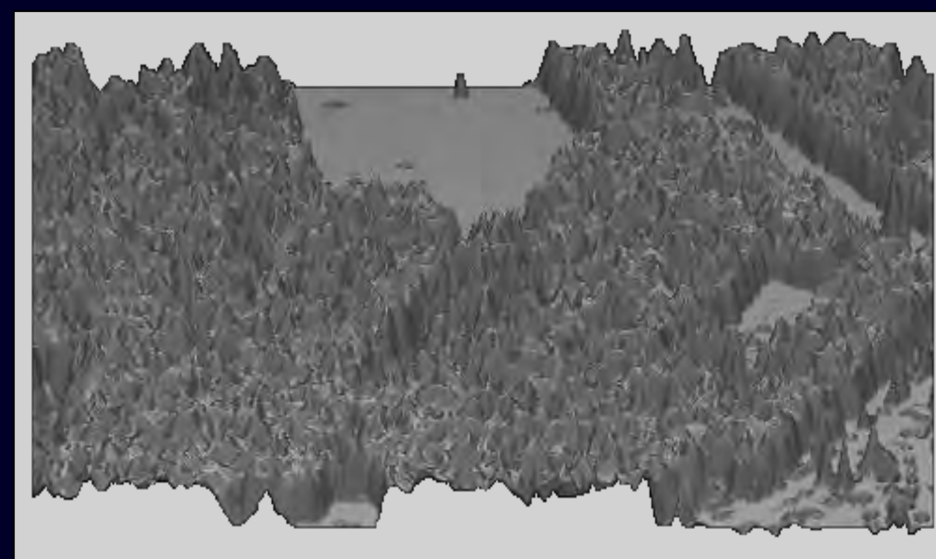

Traunstein Test Site

Forest type	Temperate
Topography	Moderate slopes
Height	25 ~ 35m
Species	N. Spruce, E. Beech, White Fir
Biomass	40 ~ 450 t/ha

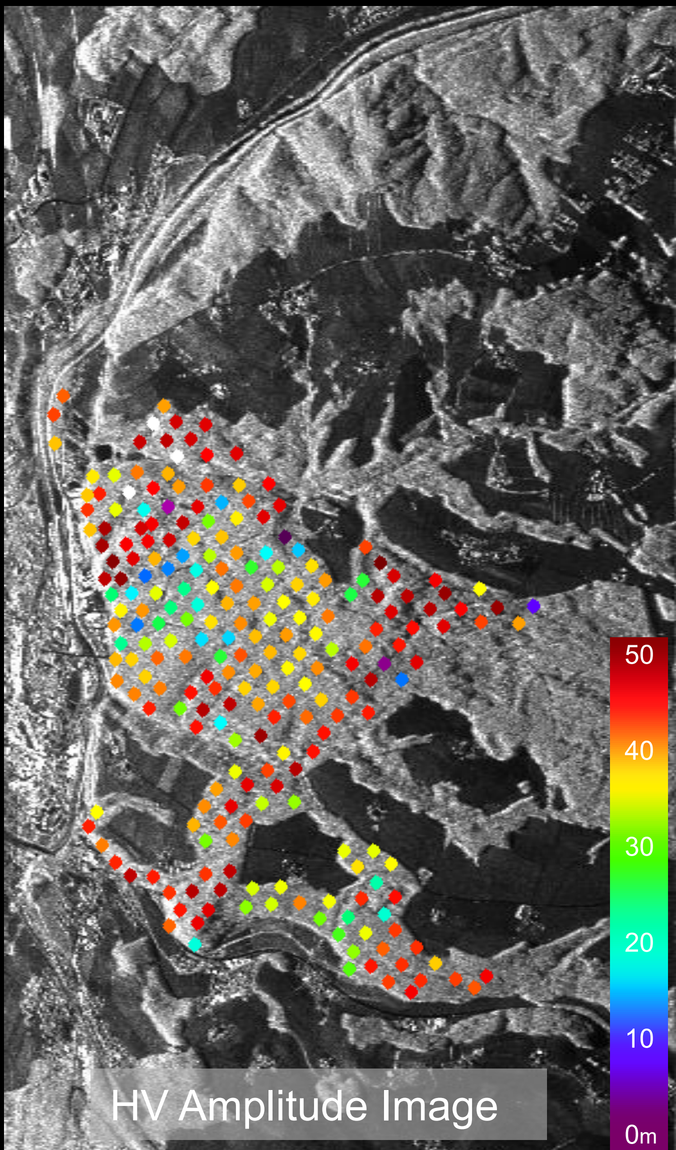

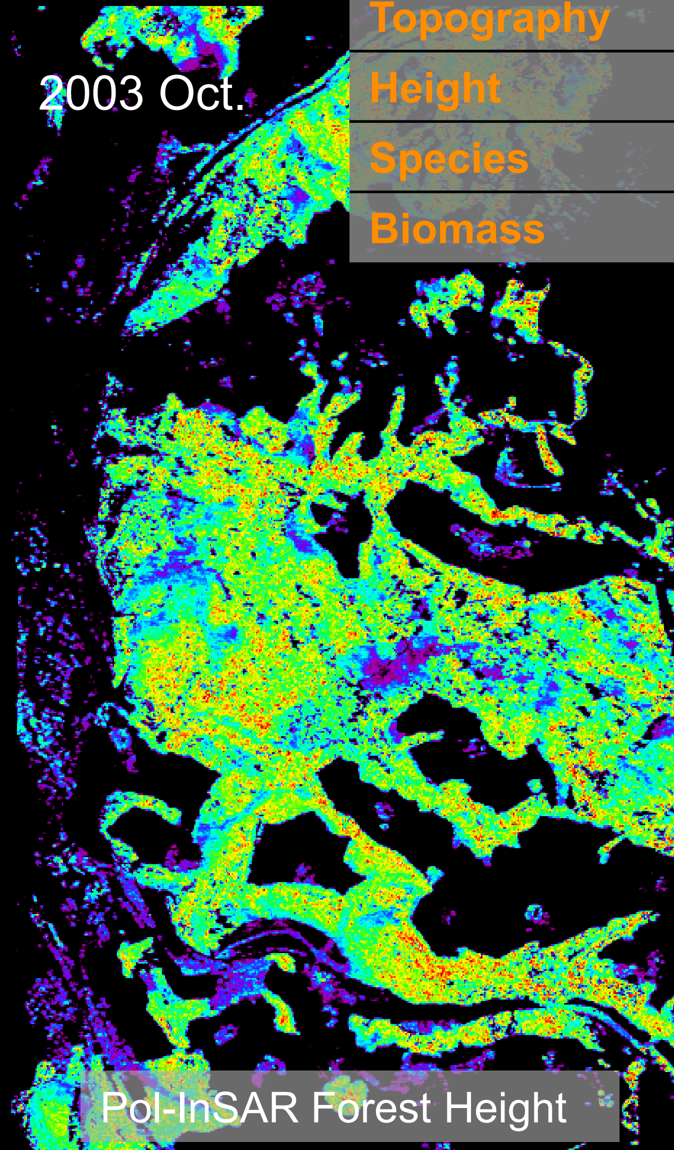

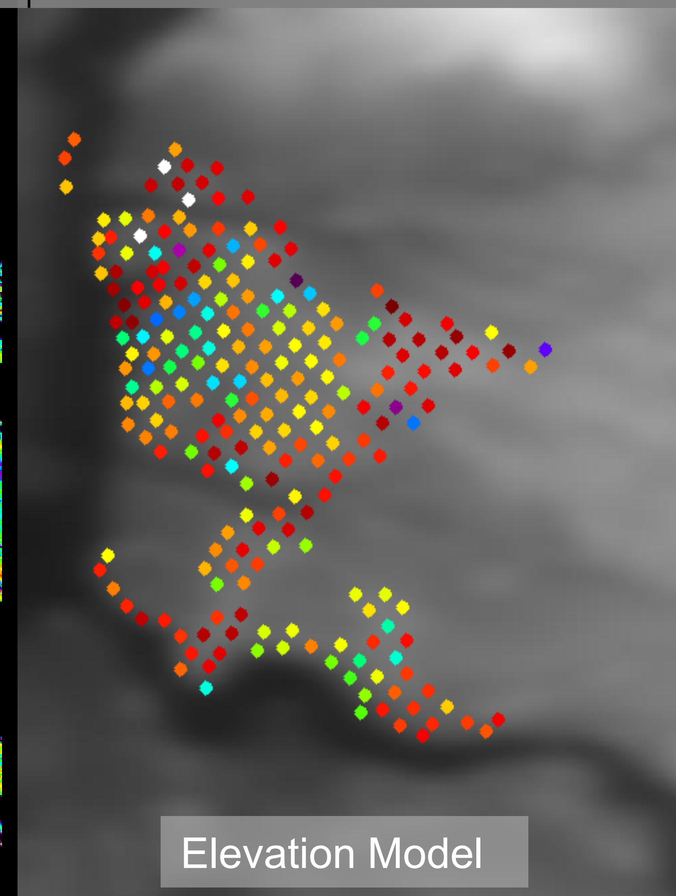

Traunstein Test Site

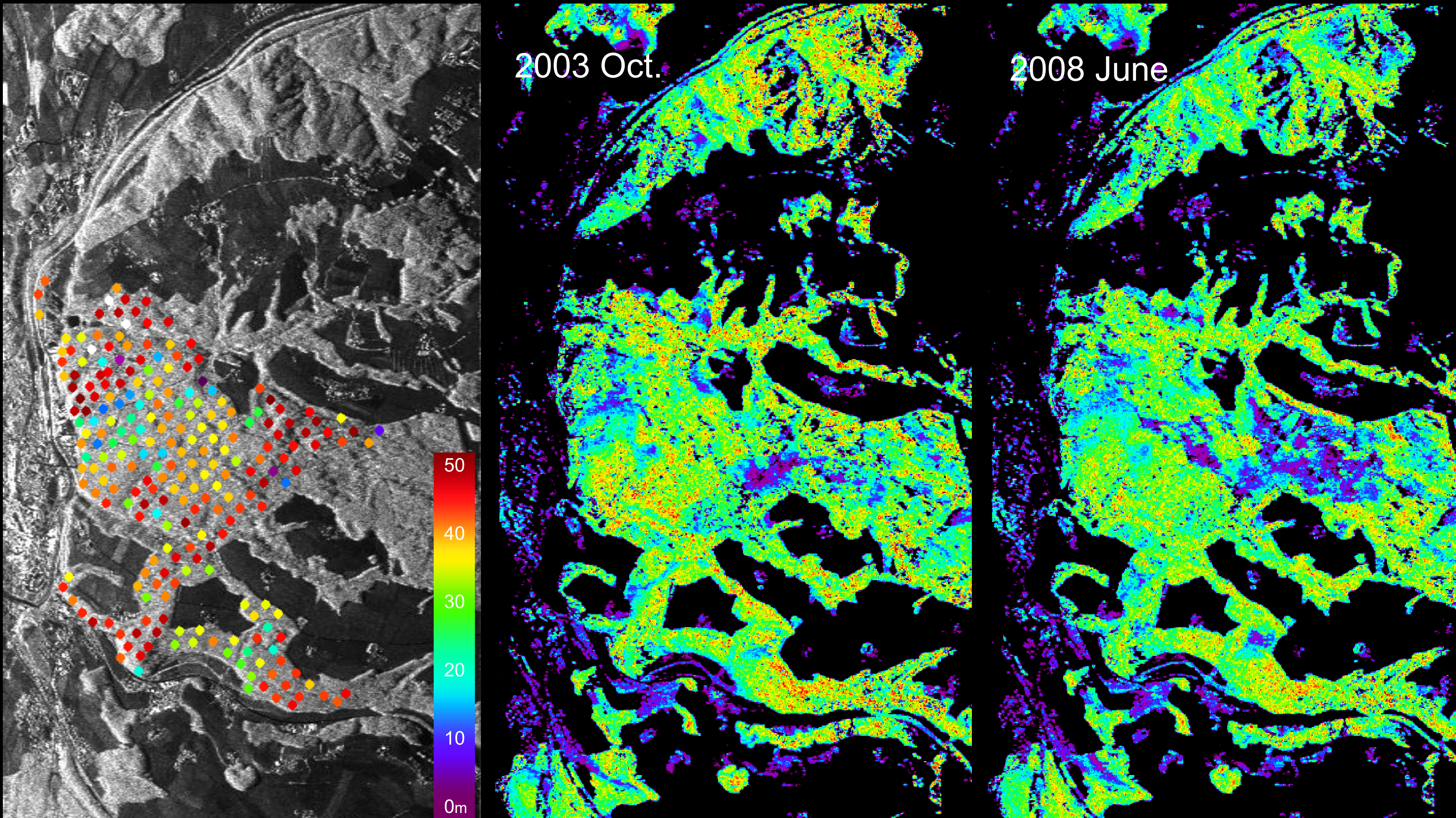

Traunstein Test Site

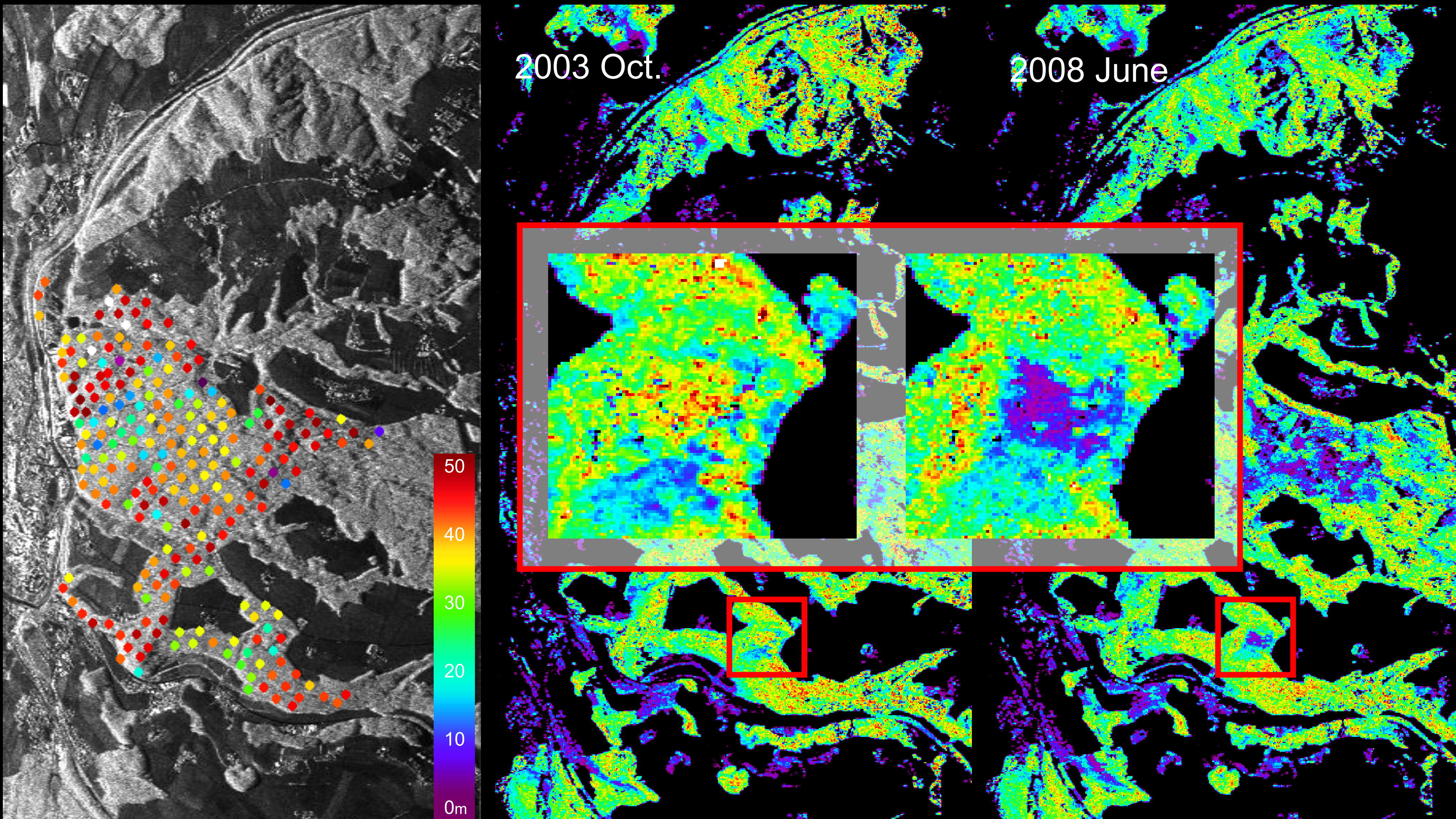

hajnsek@ifu.baug.ethz.ch
irena.hajnsek@dlr.de

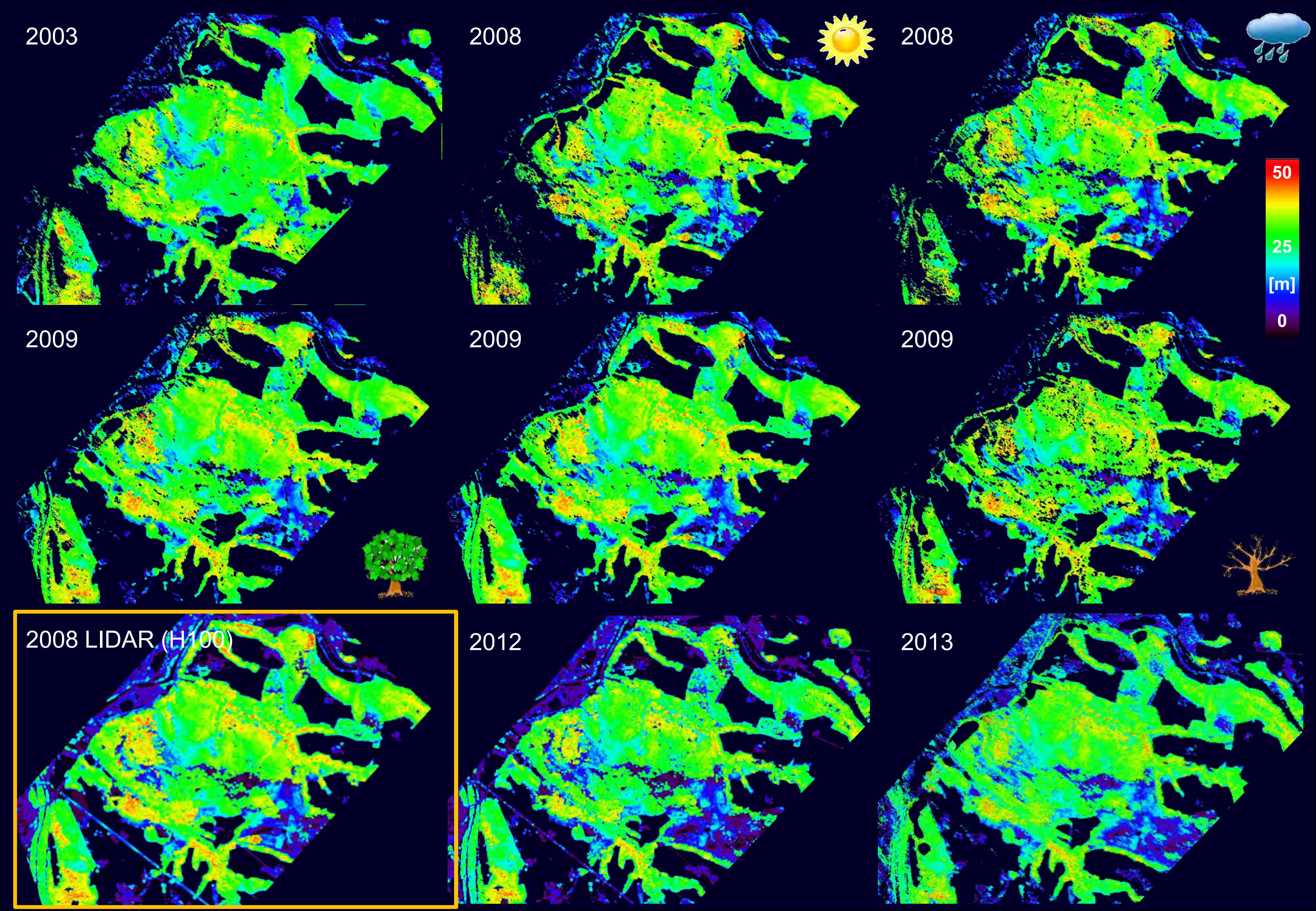

2003
2008
2008
50
25
[m]
0
2009
2009
2009
2008 LIDAR (H100)
2012
2013

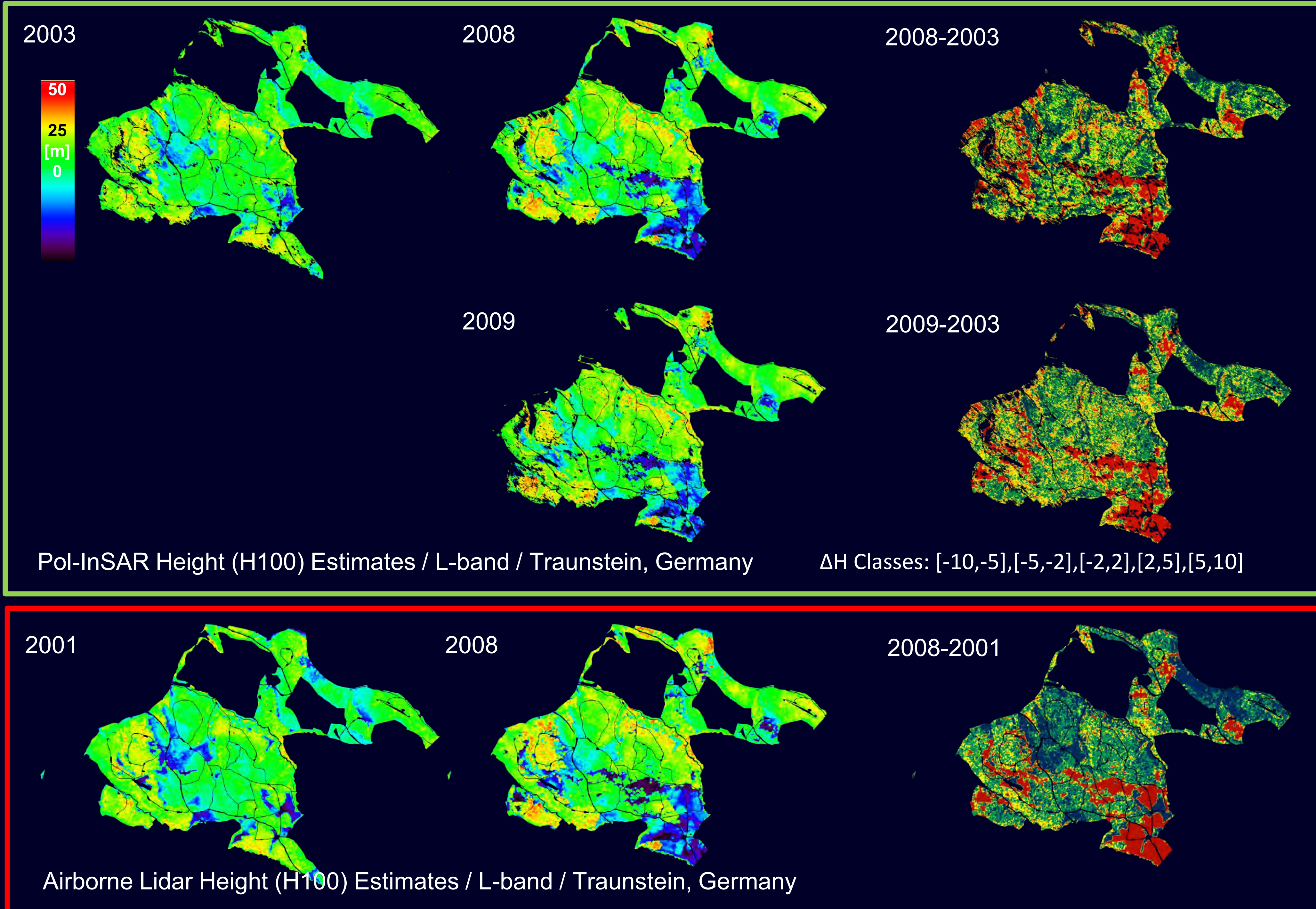
2003
50
25
[m]
0
2008
2008-2003
2009
2009-2003
Pol-InSAR Height (H100) Estimates / L-band / Traunstein, Germany
ΔH Classes: [-10,-5],[-5,-2],[-2,2],[2,5],[5,10]
2001
2008
2008-2001
Airborne Lidar Height (H100) Estimates / L-band / Traunstein, Germany

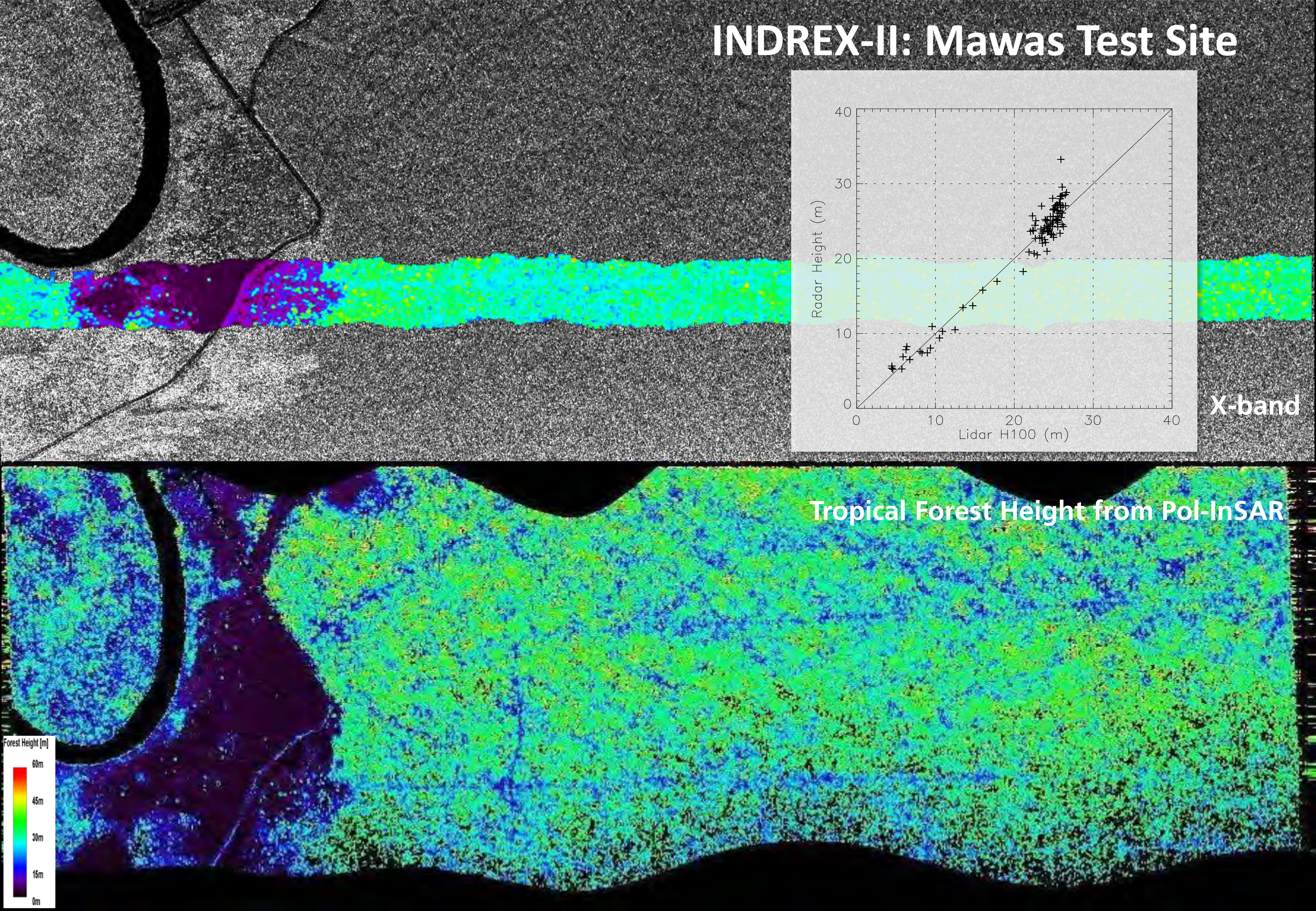
INDREX-II: Mawas Test Site
Radar Height (m)
Lidar H100 (m)
0
10
20
30
40
X-band
Tropical Forest Height from Pol-InSAR
Forest Height [m]
60m
45m
30m
15m
0m

Bangladesh Mangrove Height

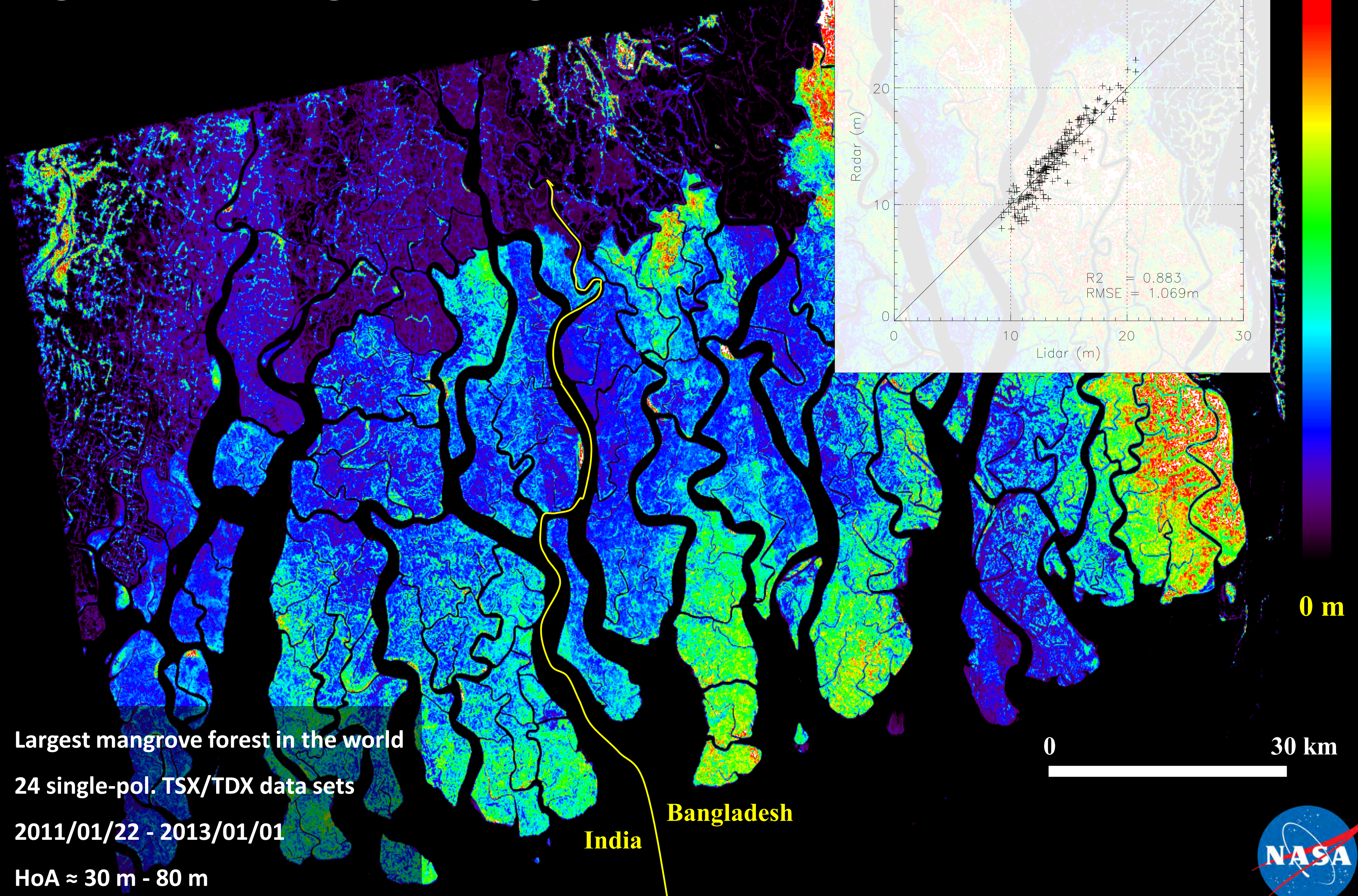

- Largest mangrove forest in the world
- 24 single-pol. TSX/TDX data sets
- 2011/01/22 - 2013/01/01
- HoA ≈ 30 m - 80 m

Polarimetric Coherence Tomography (PCT)

f(z) … vertical reflectivity function

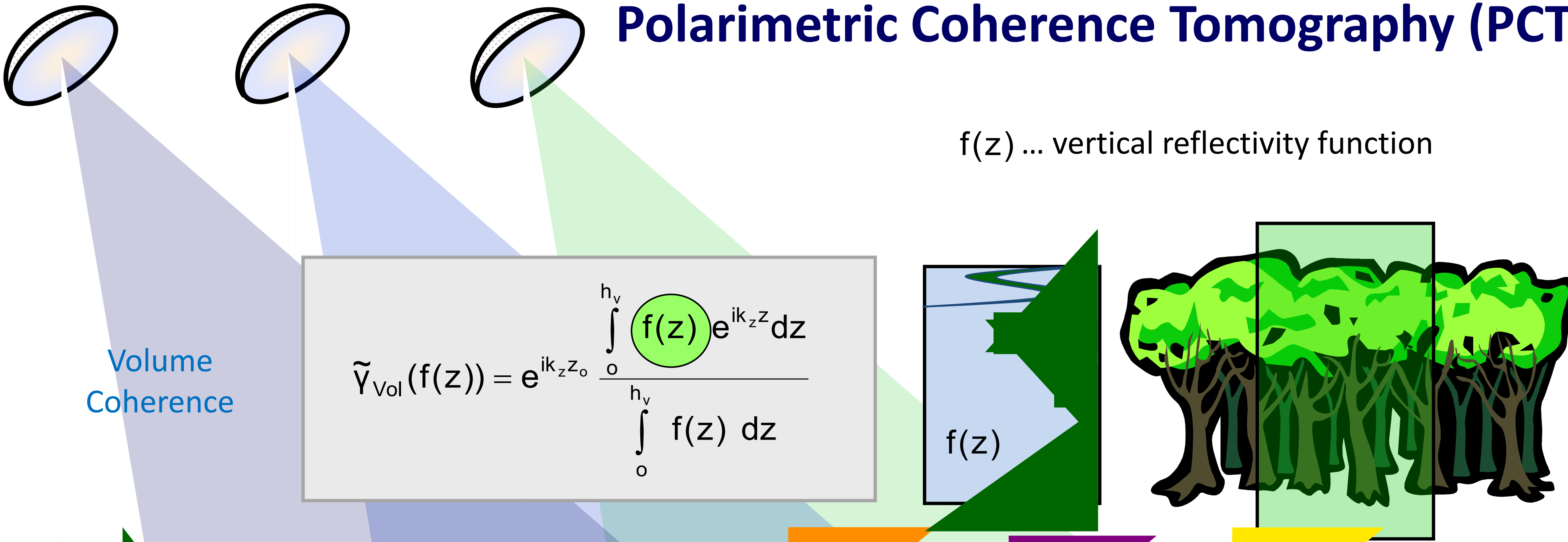

$$\tilde{\gamma}_{Vol}(f(z)) = e^{ik_z z_o}\,\frac{\int_o^{h_v} f(z)\, e^{ik_z z}\,dz}{\int_o^{h_v} f(z)\; dz}$$

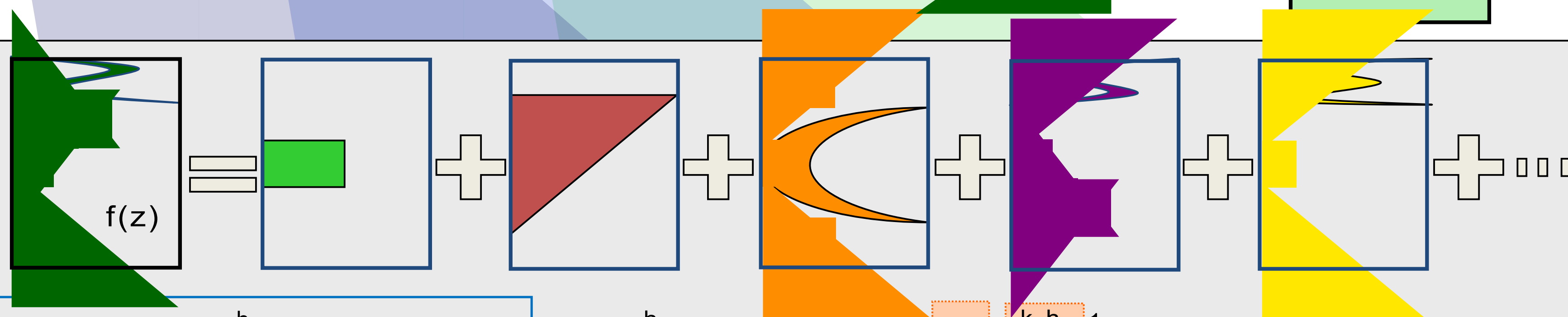

$$\tilde{\gamma}_{Vol}(f(z)) = e^{ik_z z_o}\,\frac{\int_o^{h_v} f(z)\, e^{ik_z z}\,dz}{\int_o^{h_v} f(z)\, dz}$$

$$\int_0^{h_v} f(z)\; e^{ik_z z}\,dz = \frac{h_v}{2}\, e^{i\frac{k_z h_v}{2}} \int_{-1}^{1} (1+f(z'))\; e^{i\frac{k_z h_v}{2} z'}\, dz'$$

$$\int_0^{h_v} f(z)\; dz = \frac{h_v}{2} \int_{-1}^{1} (1+f(z'))\; dz'$$

Fourier Legendre Series: $f(z') = \sum_n a_n P_n(z')$ where $a_n = \frac{2n+1}{2}\int_{-1}^{1} f(z') P_n(z')\,dz'$

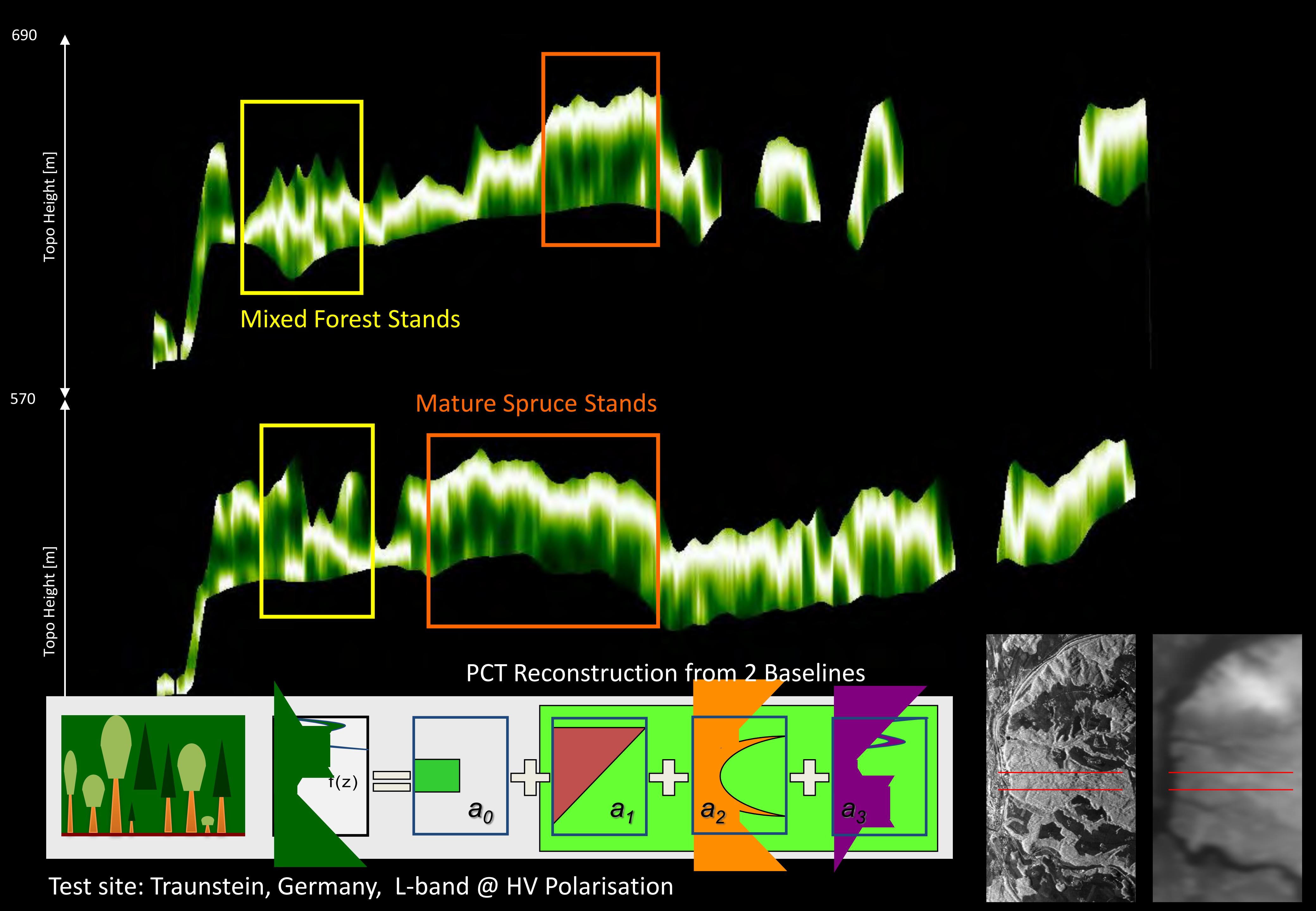
690
Topo Height [m]
Mixed Forest Stands
570
Mature Spruce Stands
Topo Height [m]
PCT Reconstruction from 2 Baselines
f(z)
a_0
a_1
a_2
a_3
Test site: Traunstein, Germany, L-band @ HV Polarisation

Agriculture Pol-InSAR Applications

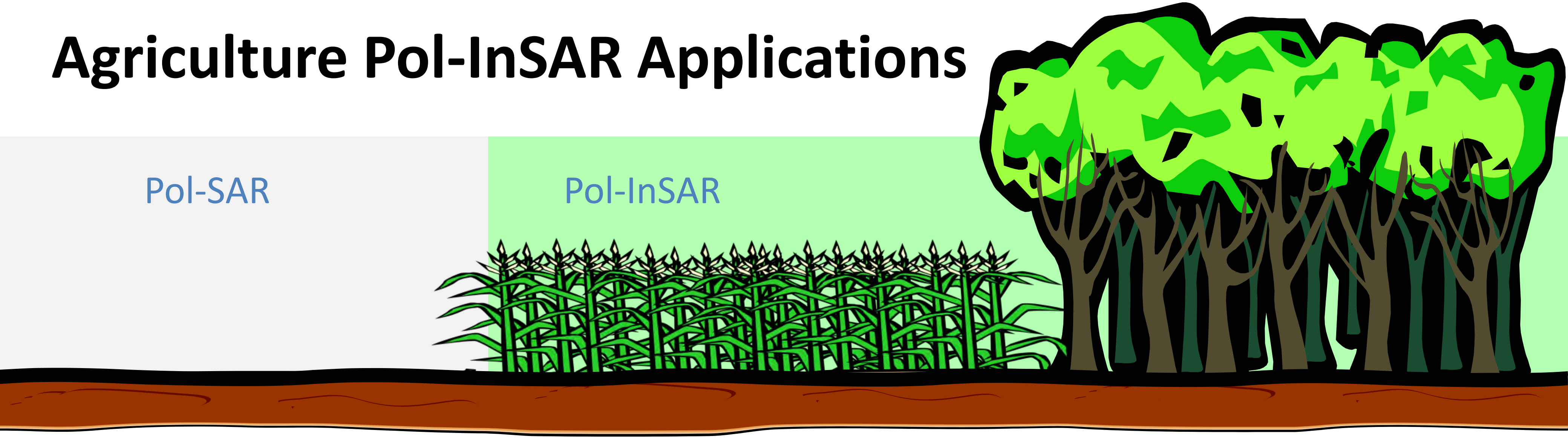

<u>Bare Surfaces:</u> Isolated Scattering Center
- Low Entropy scatterers -> High polarimetric coherence
- The interferometric coherence is baseline independent

<u>Vegetated Surfaces:</u> Volume Scatterers
- High Entropy scatterers -> Low polarimetric coherence
- The interferometric coherence depends on the baseline

Forest vs Agricultural Vegetation	**Impact**
Orientation effects in the vegetation layer	Anisotropic Propagation
Thinner / shorter vegetation layer	Increased importance of ground scattering
Short crop / plant phenological cycle	Short spatial / large temporal baseline
Variety of crop / plant structure	Abstract modelling

Agriculture Vegetation @ Alling/Germany 2000

Test Site: Kuettighoffen, Switzerland

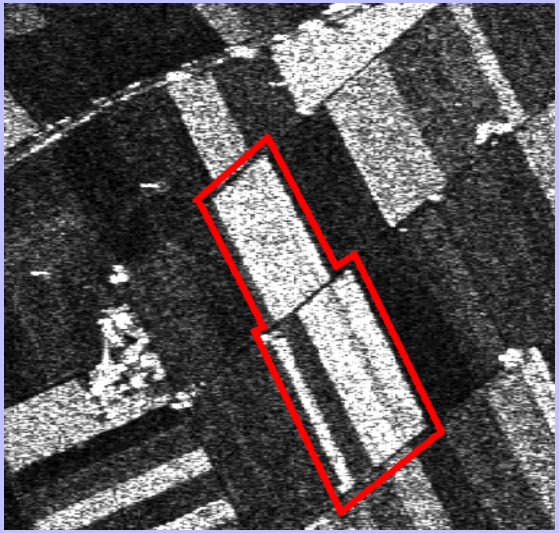

SAR Image @ L-band

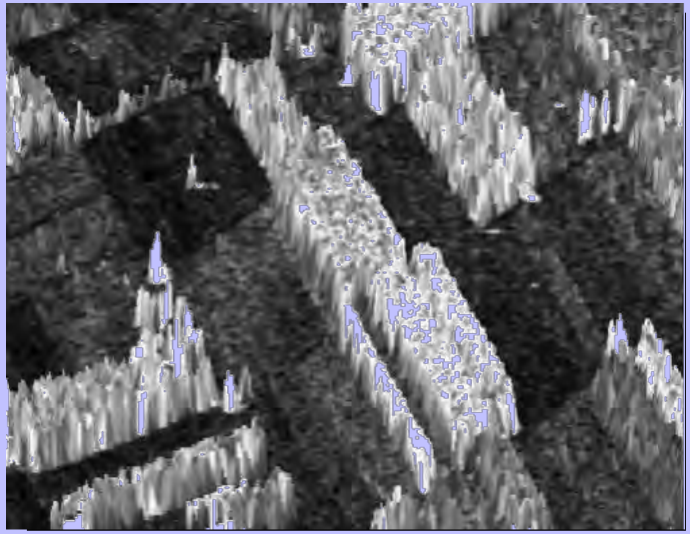

3-D Height Map

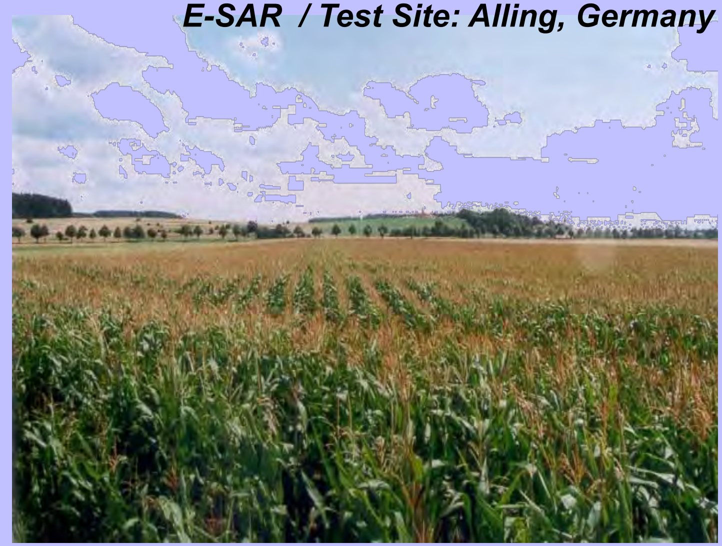

Interferometric Coherence:

$$\boxed{\tilde{\gamma}(\vec{w}) = \exp(i\varphi_0)\frac{\tilde{\gamma}_V(\vec{w}) + m(\vec{w})}{1 + m(\vec{w})}}$$

$$\tilde{\gamma}_V(\vec{w}) = \frac{I}{I_0} \qquad I = \int_0^{h_V} \exp(i\kappa_z z')\exp\left(\frac{2\ \sigma(\vec{w})\ z'}{\cos\theta_0}\right)dz'$$

$$I_0 = \int_0^{h_V} \exp\left(\frac{2\ \sigma(\vec{w})\ z'}{\cos\theta_0}\right)dz'$$

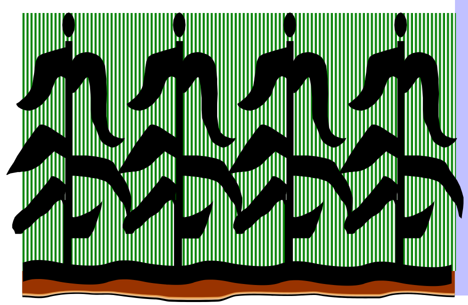

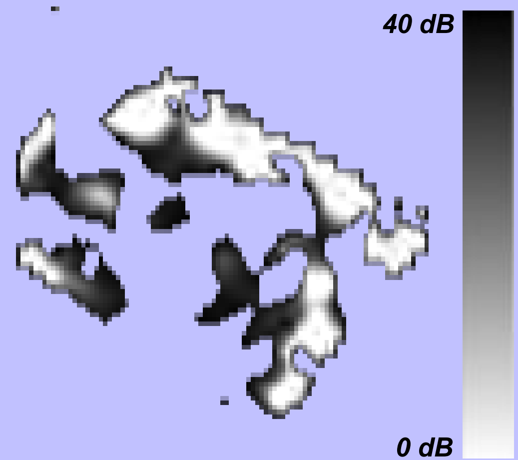

Differential Extinction

hajnsek@ifu.baug.ethz.ch
irena.hajnsek@dlr.de

AGRISAR @ L-band in April 2006

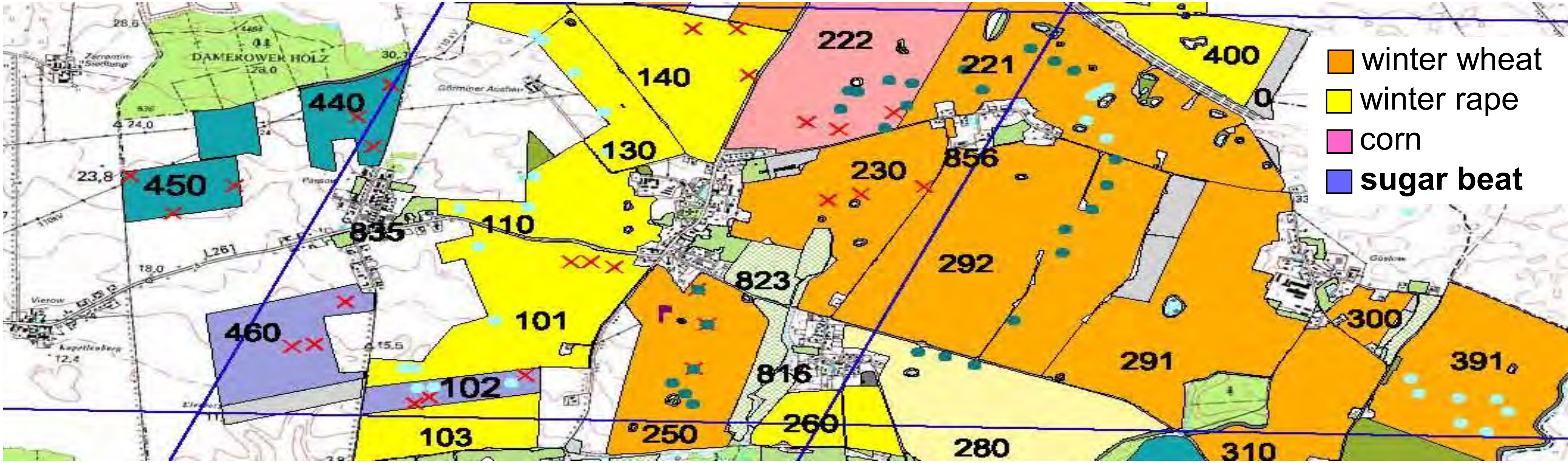

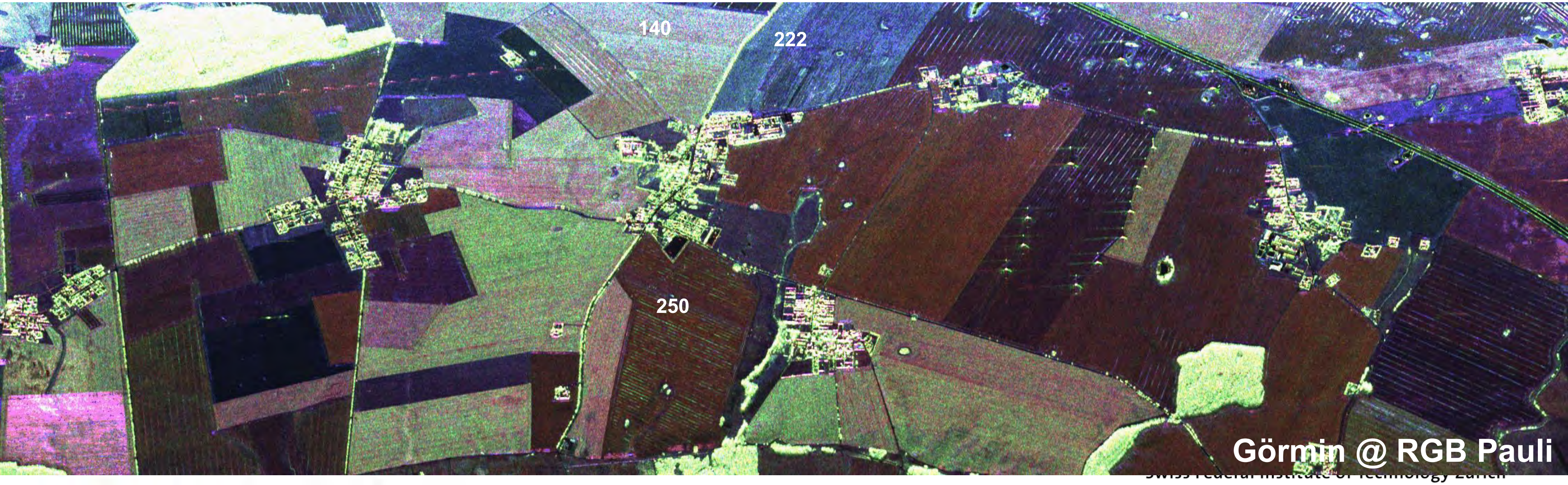

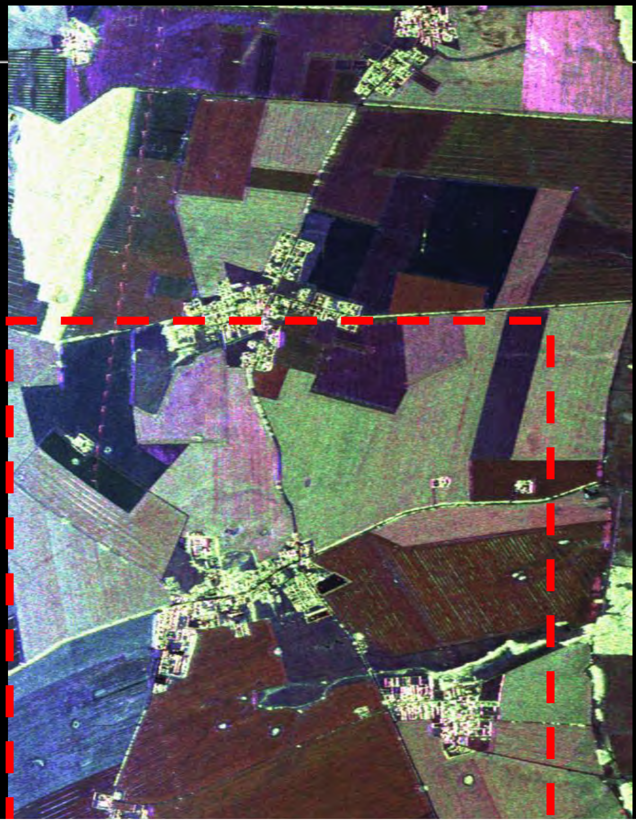

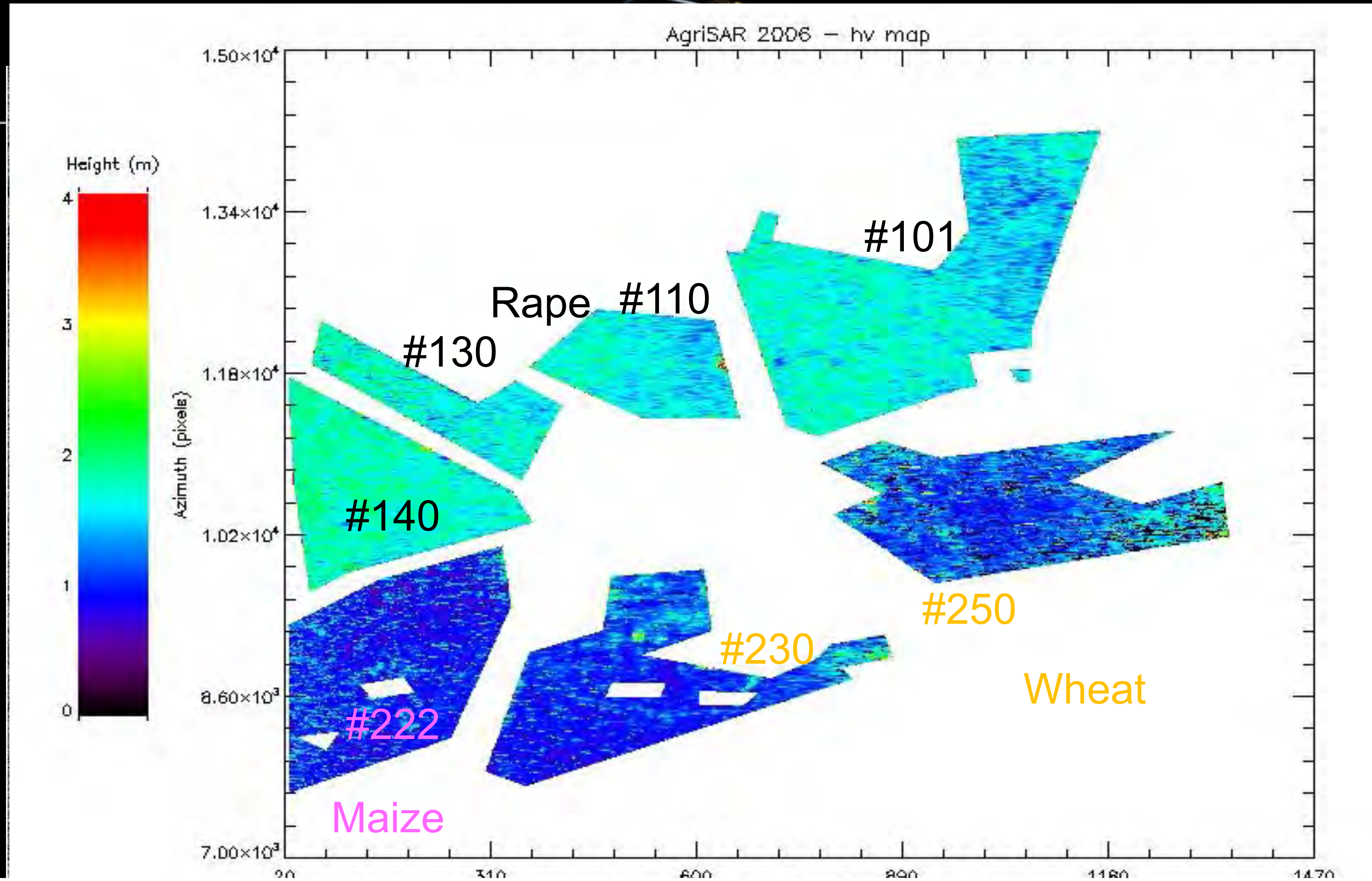
AgriSAR 2006 – hv map
Height (m)
Azimuth (pixels)
#101
Rape #110
#130
#140
#250
#230
Wheat
#222
Maize

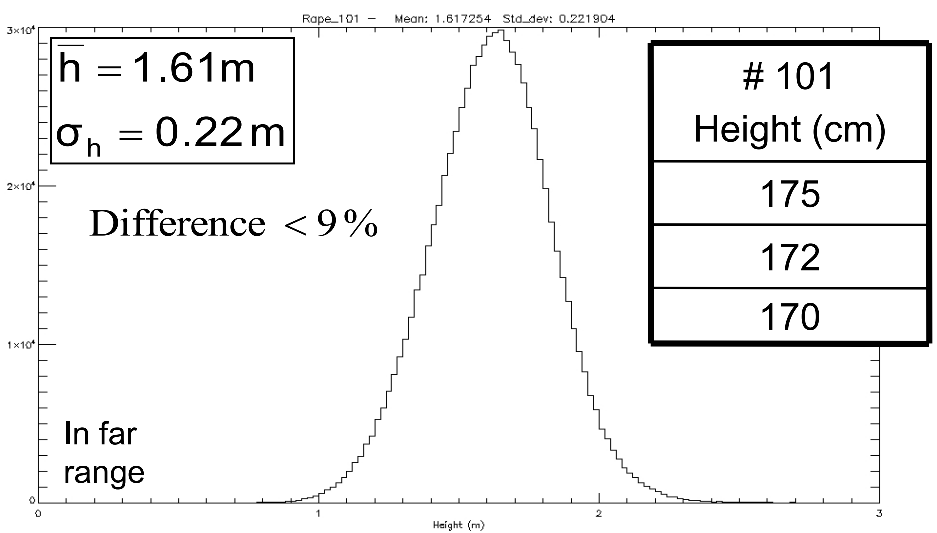
Rape_101 – Mean: 1.617254 Std_dev: 0.221904
$\overline{h} = 1.61$m
$\sigma_h = 0.22$ m
Difference < 9 %
101
Height (cm)
175
172
170
In far range
Height (m)

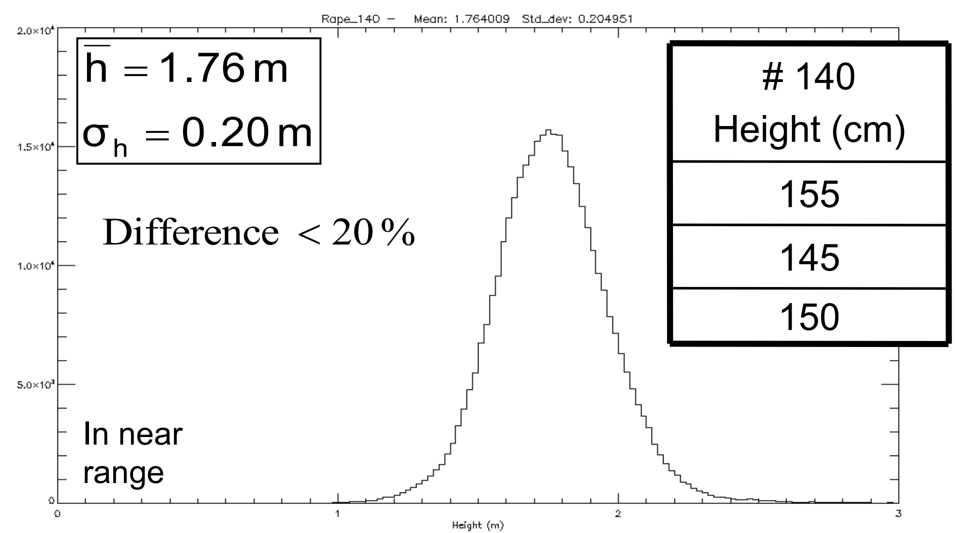
Rape_140 – Mean: 1.764009 Std_dev: 0.204951
$\overline{h} = 1.76$ m
$\sigma_h = 0.20$ m
Difference < 20 %
140
Height (cm)
155
145
150
In near range
Height (m)

CROP-EX 2014: Crop height estimation from Pol-InSAR data

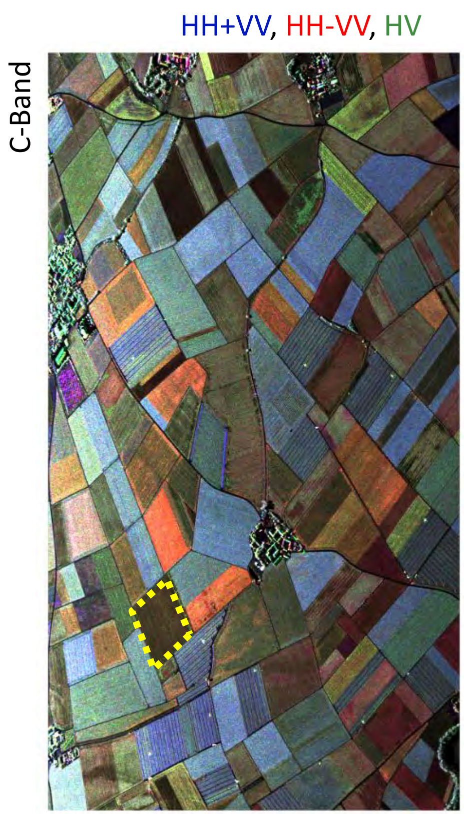

Wheat

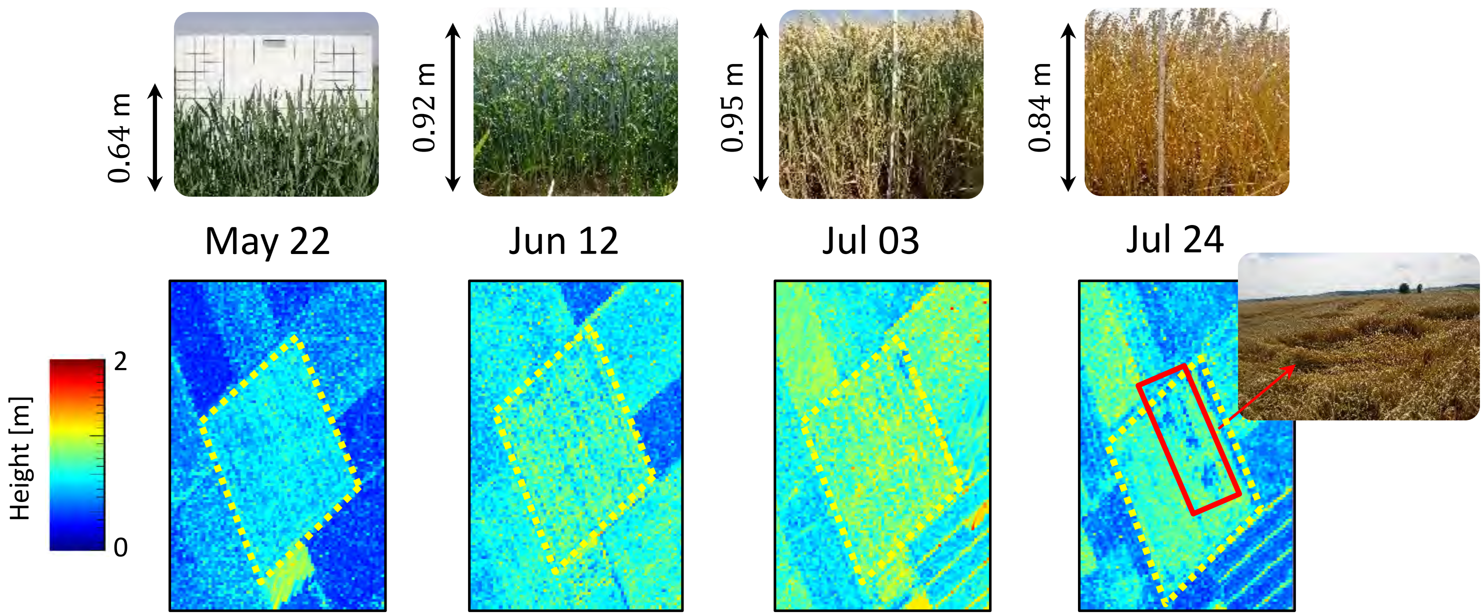

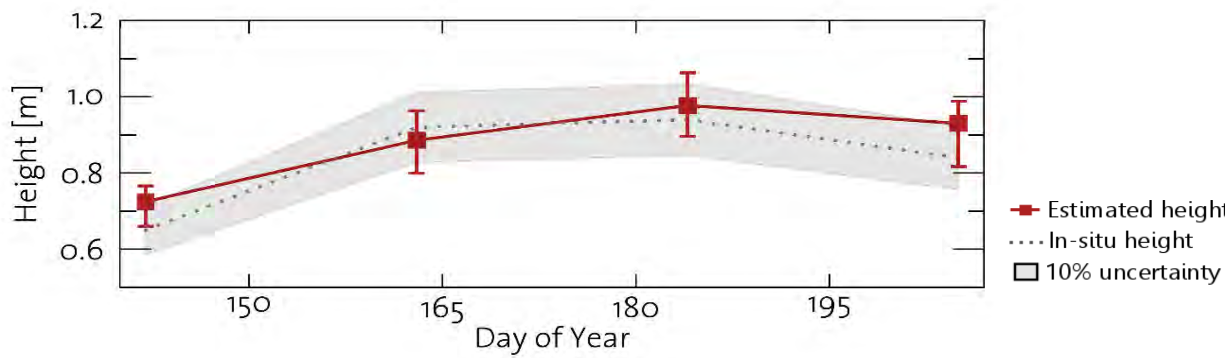

Sensor: DLR's F-SAR (airborne)
Frequency: C-Band (≈5 GHz)
Number of spatial baselines: 2 (k_V between 2 rad and 4 rad)
Max. temporal baseline: 90 minutes
Equivalent Number of Looks: 100

CROP-EX 2014: Crop height estimation from Pol-InSAR data

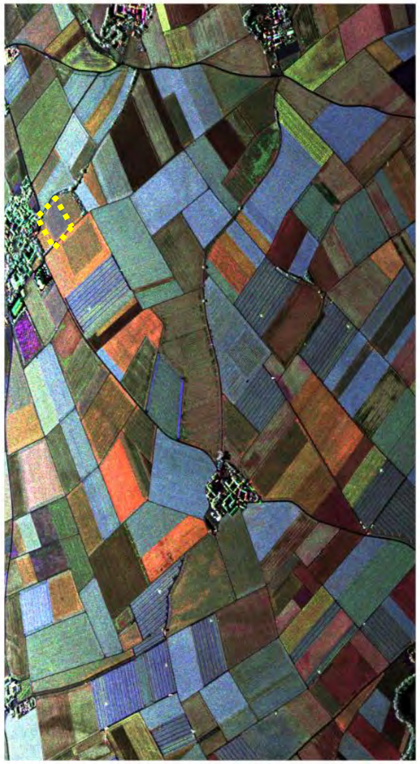

Maize

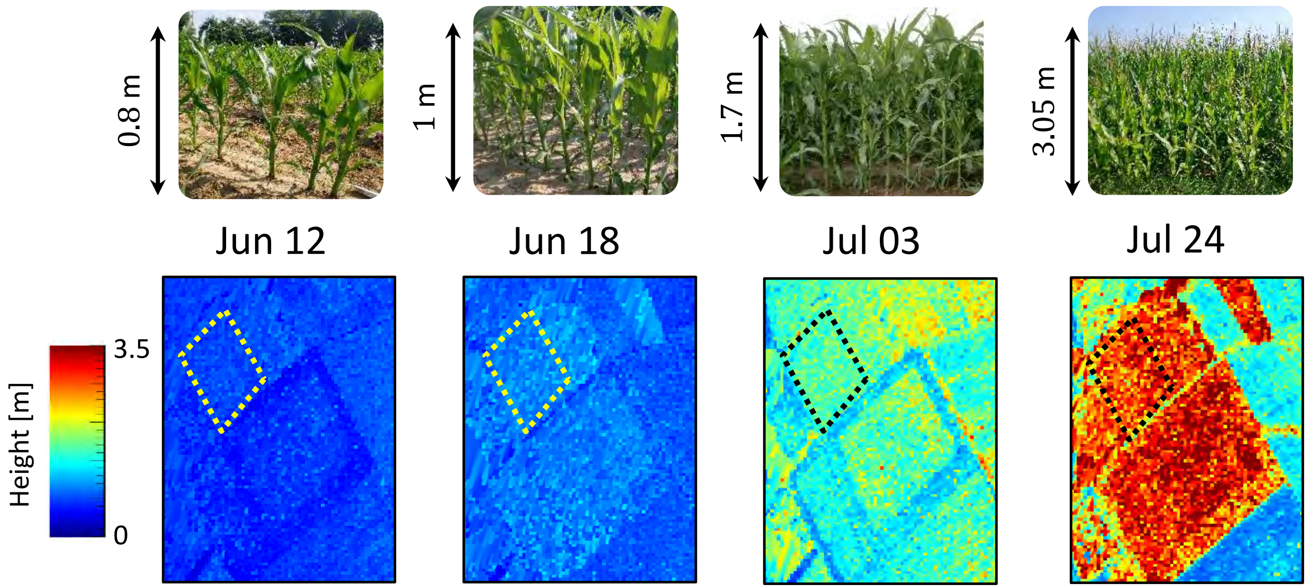

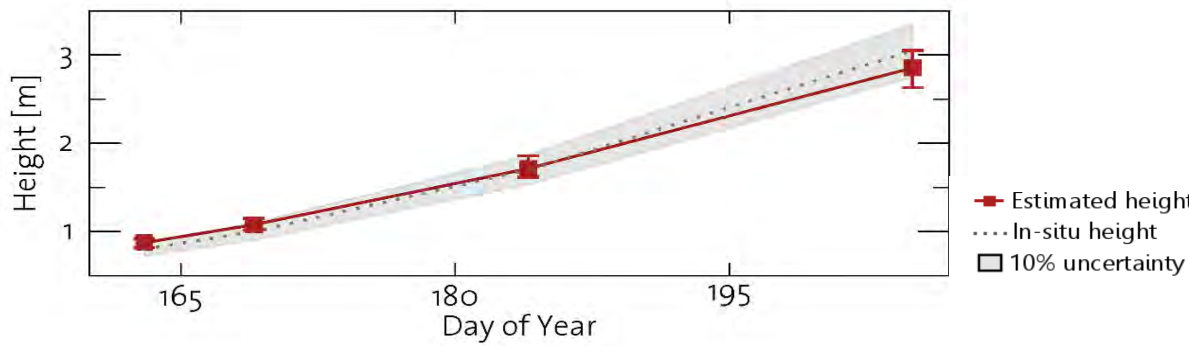

Sensor: DLR's F-SAR (airborne)
Frequency: C-Band (≈5 GHz)
Number of spatial baselines: 2 (k_V between 2 rad and 4 rad)
Max. temporal baseline: 90 minutes
Equivalent Number of Looks: 100

D-InSAR Soil Mapping @ different Polarisation and L-band

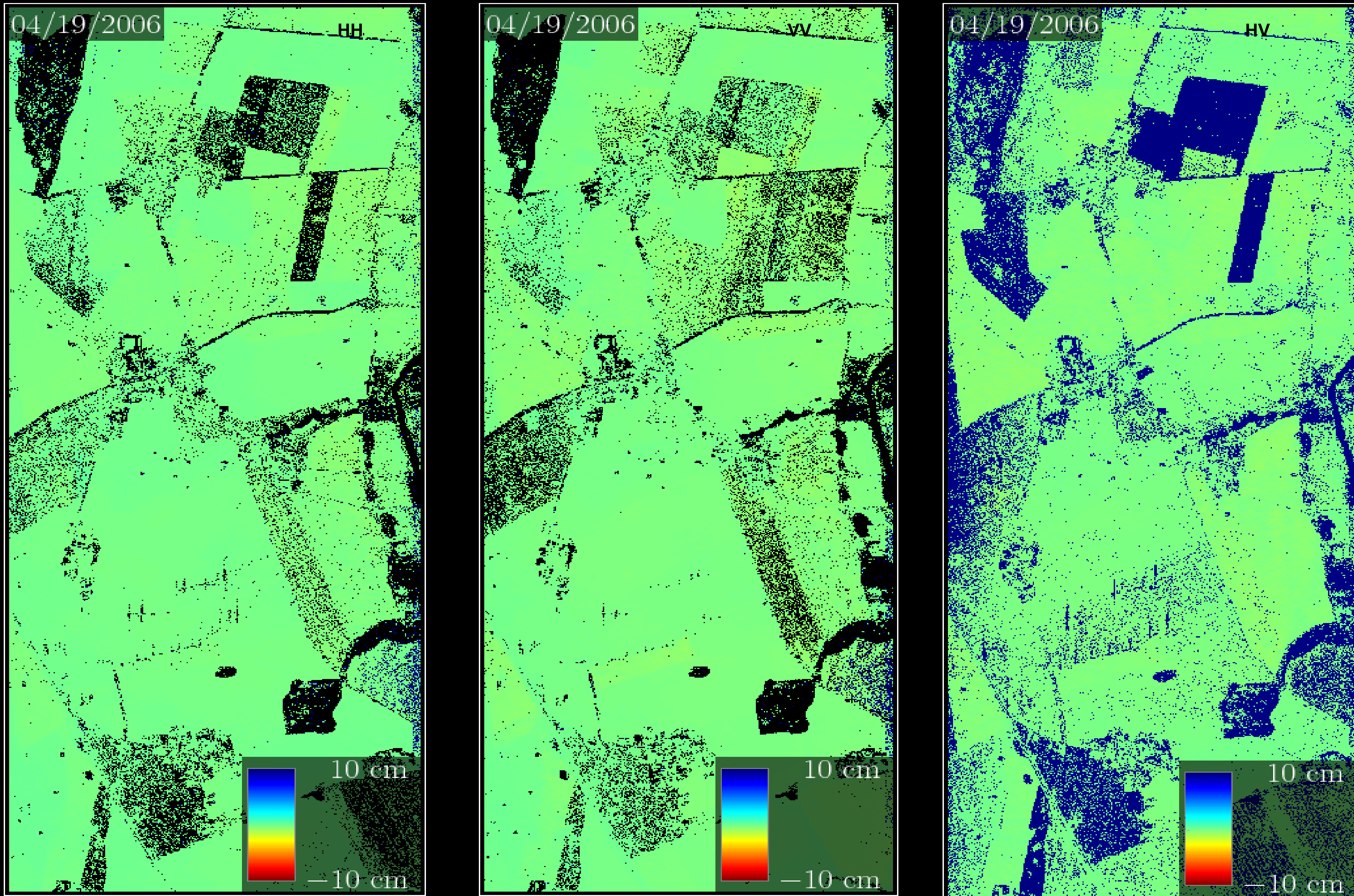

Deformation Change in Time @ Winter Rape (101-1)

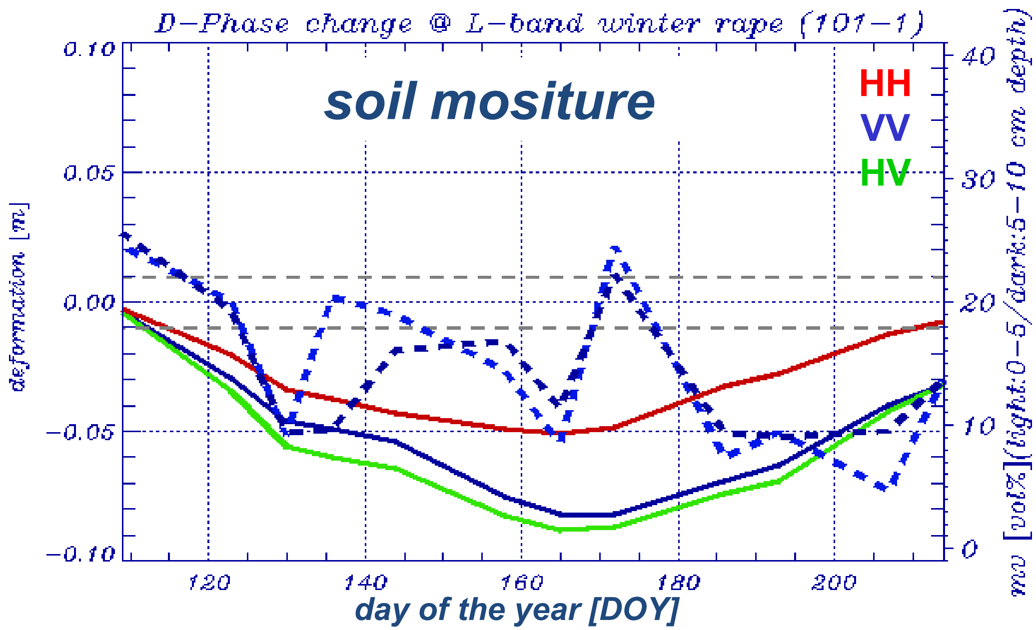

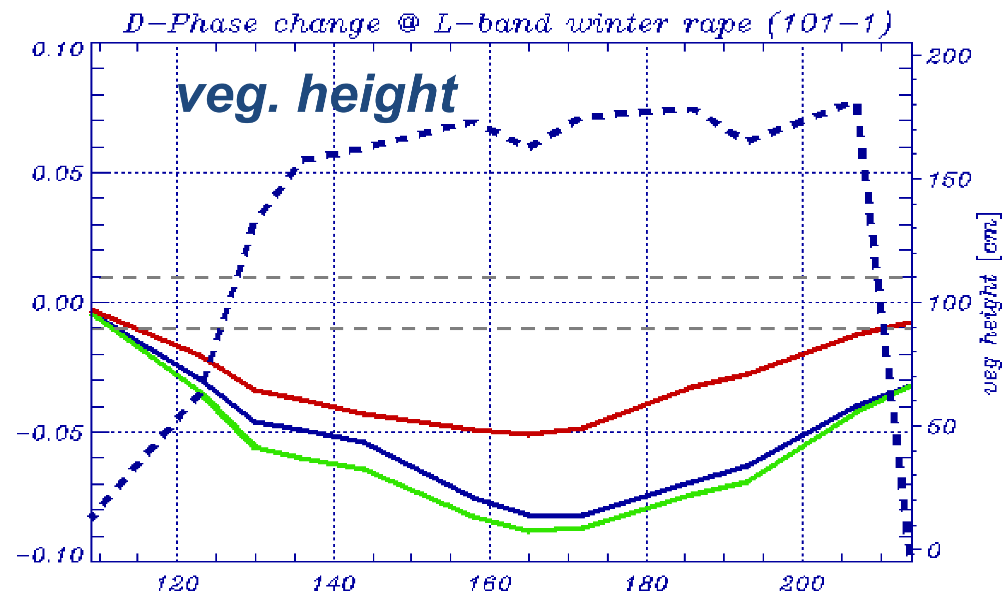

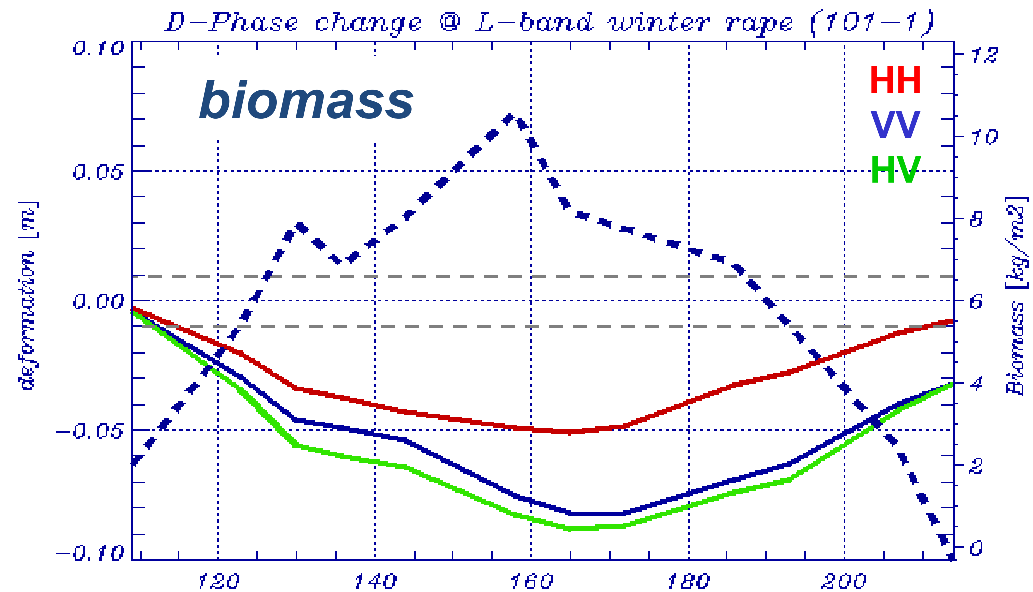

- Deformation up to 9 mm in VV & HV and up to 5 mm for HH
- Soil moisture: slight correlation over time – no correlation with local variation
- Veg. height: slight correlation in the beginning and no sensitivity in time
- Biomass: best correlation results over time

Structure Parameters & Applications

	Parameters		Applications
Forest	• Forest Height • Forest (Vertical) Structure • Forest Biomass • Underlying Topography	⇨	• Forest Ecology • Forest Management • Ecosystem Modeling • Climate Change
Agriculture	• Underlying Soil Moisture • Moisture of Vegetation Layer • Height of Vegetation Layer • Soil Roughness	⇨	• Farming Management • Ecosystem Modeling • Water Cycle / CC • Desertification
Snow & Ice	• Ice Layer Structure • Penetration Depth (Ice) • Snow Layer Thickness • Snow Water Equivalent	⇨	• Ecosystem Change • Water Cycle • Water Management

Snow

First Pol-InSAR Snow Experiment in Austria 2004

E-SAR: Kuehtai / Austria 2004 Cooperation with University of Innsbruck

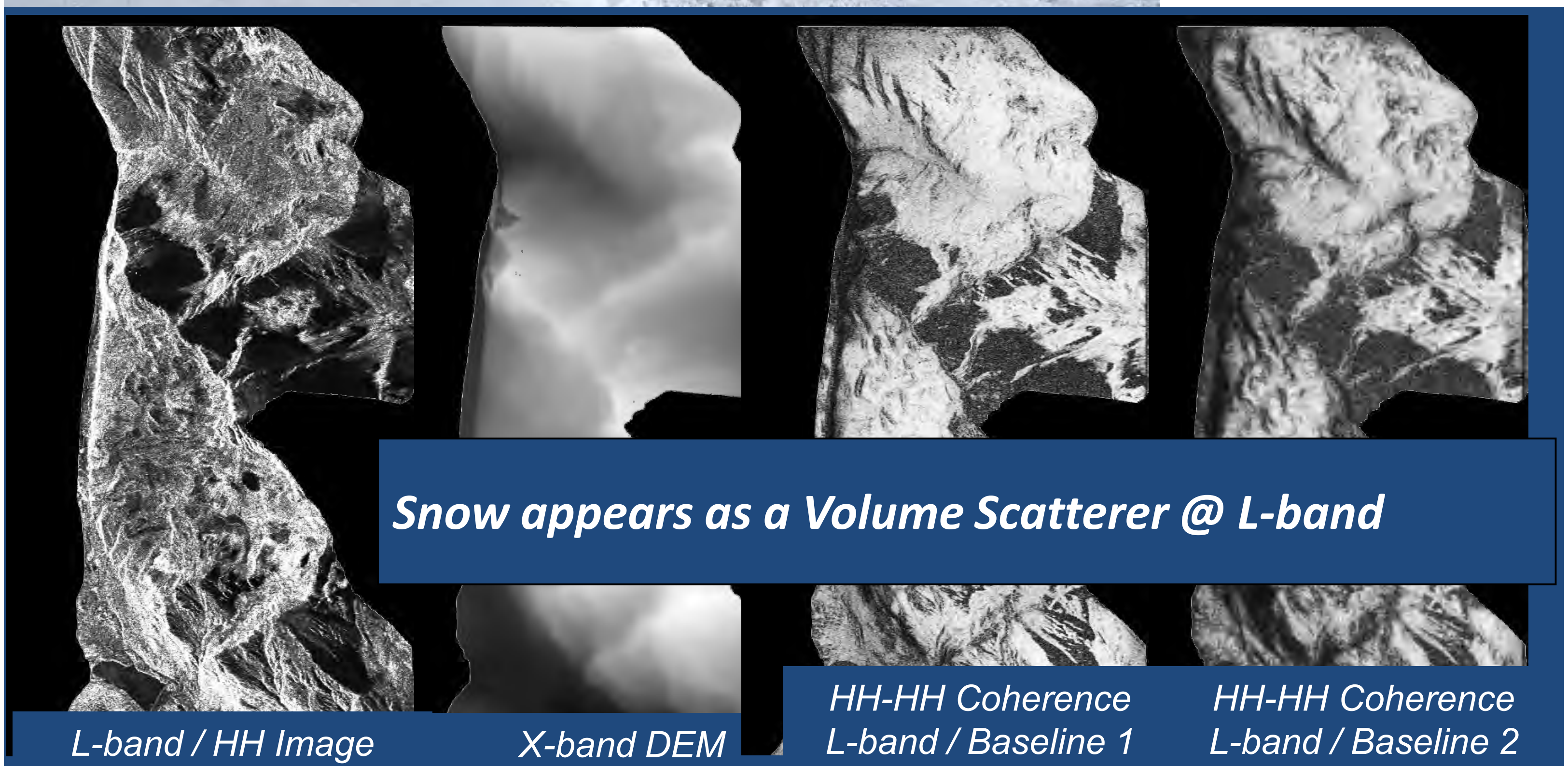

Campaign Objectives:

Investigation of Pol-InSAR for snow characterisation

Snow Depth Estimation

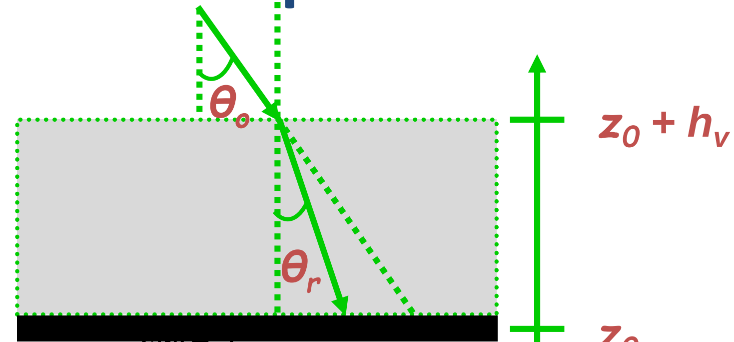

$$n' = \frac{\sin(\theta_o)}{\sin(\theta_r)}$$

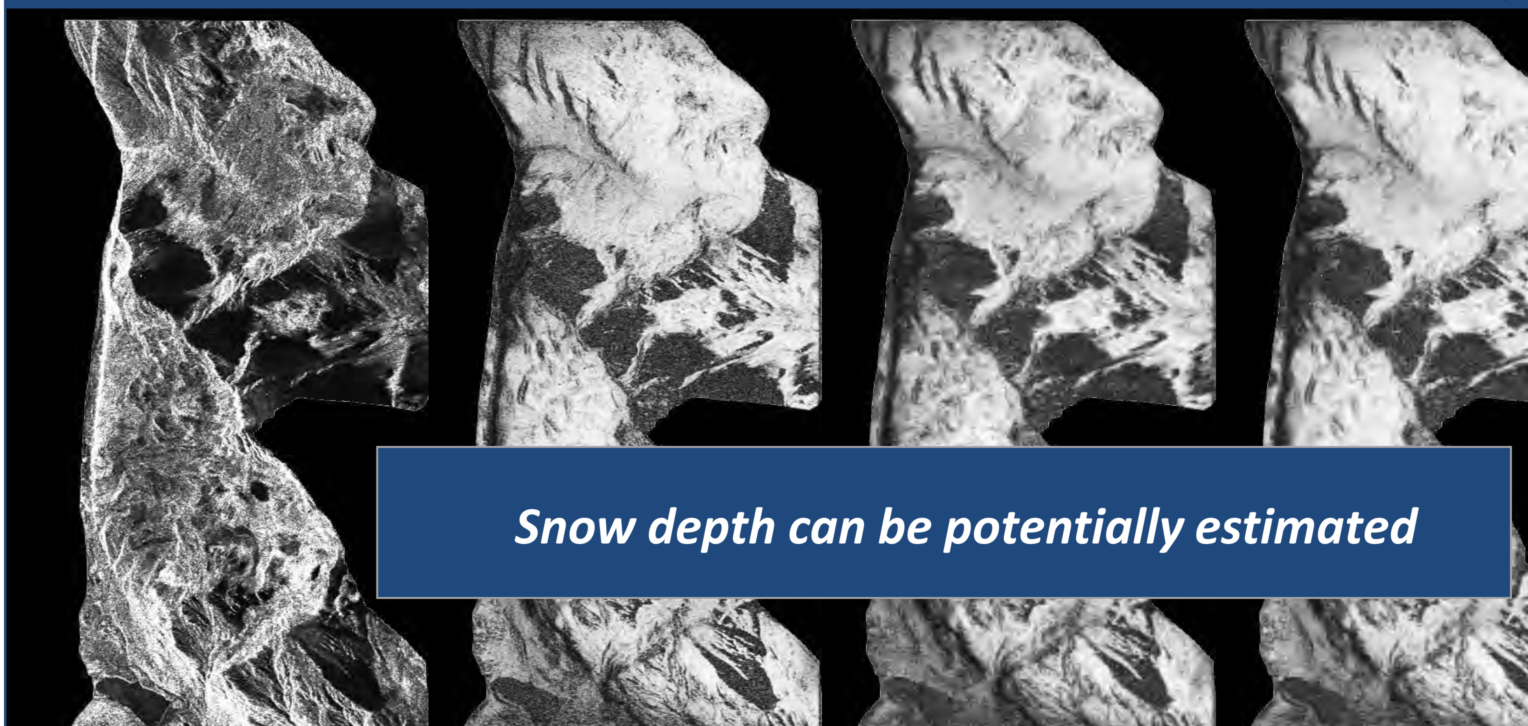

Snow depth can be potentially estimated

L-band / HH Image | *HH-HH Coherence* | *XX-XX Coherence* | *VV-VV Coherence*

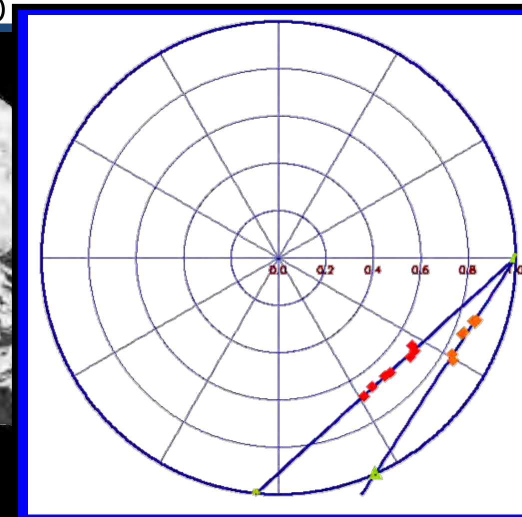

Baseline 1 (20M): $\Delta\varphi$=17° -> Δz=1.48m

Baseline 2 (40M): $\Delta\varphi$=28° -> Δz=1.22m

hajnsek@ifu.baug.ethz.ch
irena.hajnsek@dlr.de

IceSAR Campaign 2007 @ ~80°N

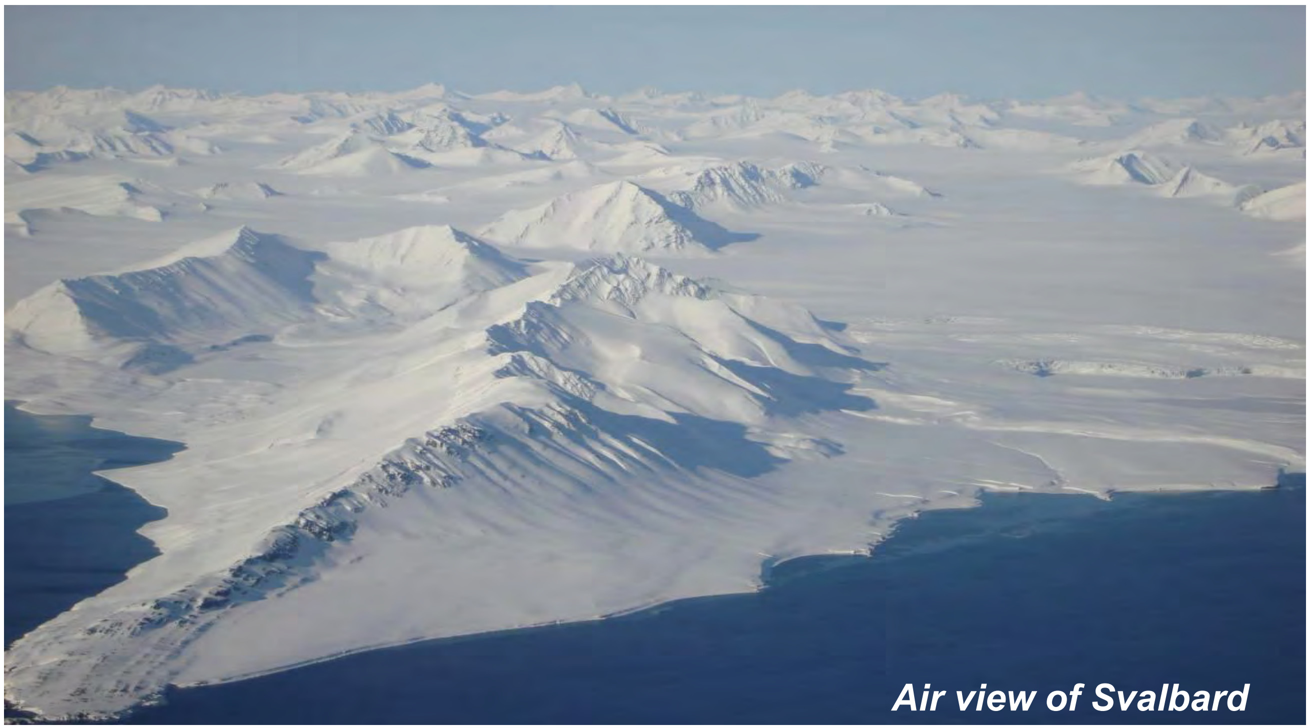

Air view of Svalbard

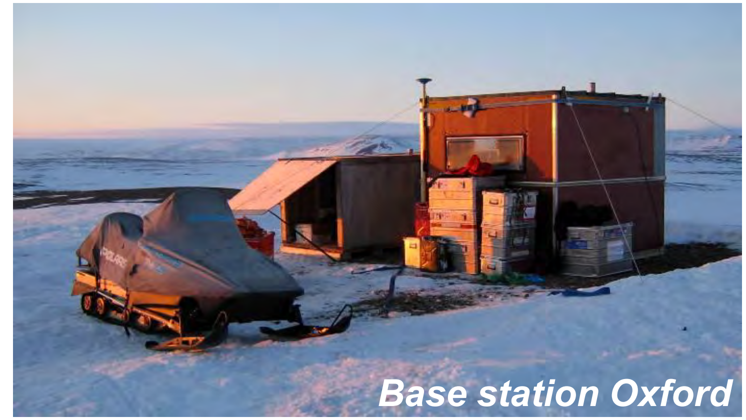

Base station Oxford

CR Installation

ICESAR Team

hajnsek@ifu.baug.ethz.ch
irena.hajnsek@dlr.de

Austfonna: 2 Flight Tracks (~ 10km) @ CryoSAT

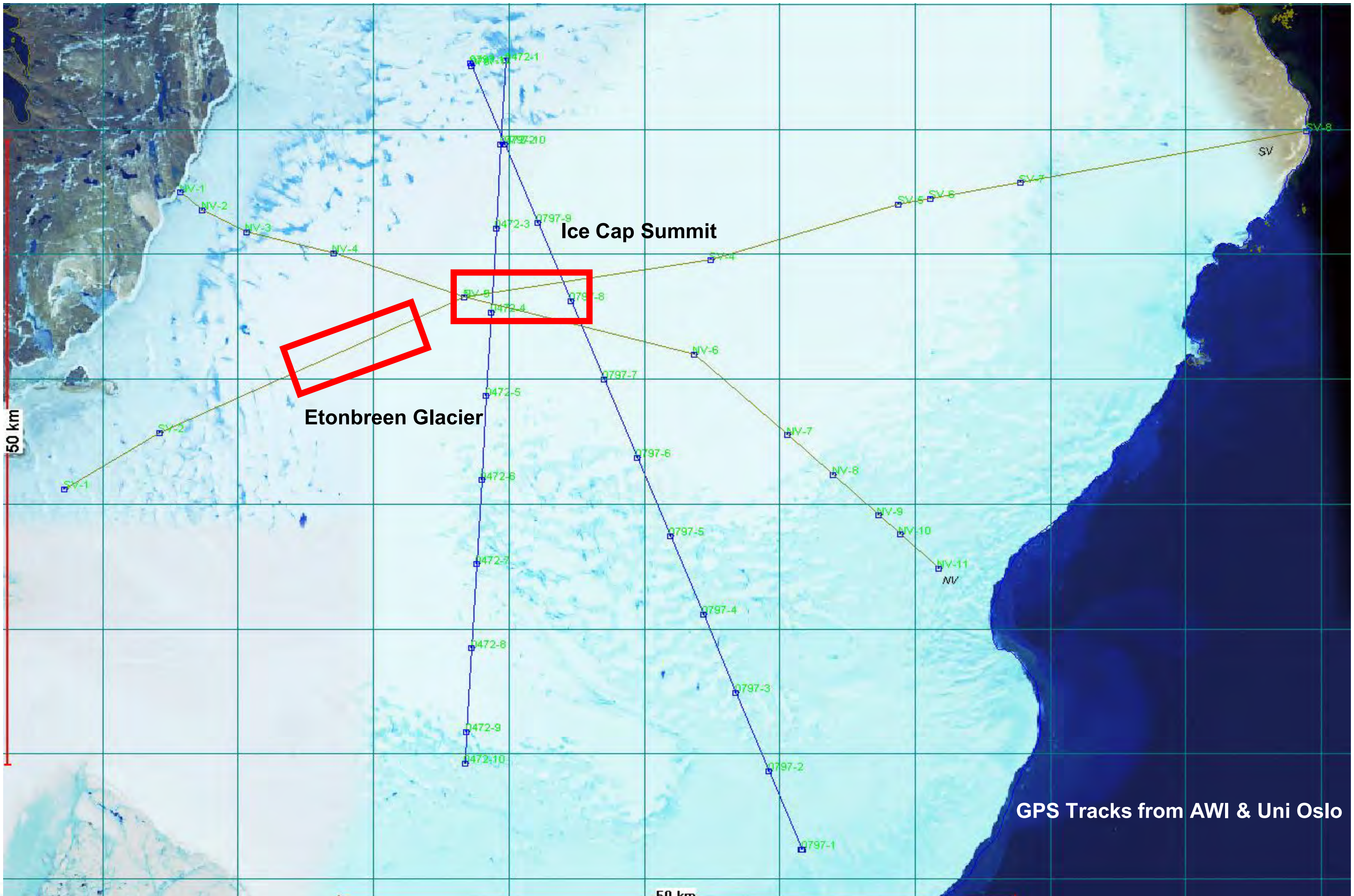

ICESAR Campaign 2007: InSAR Coherences

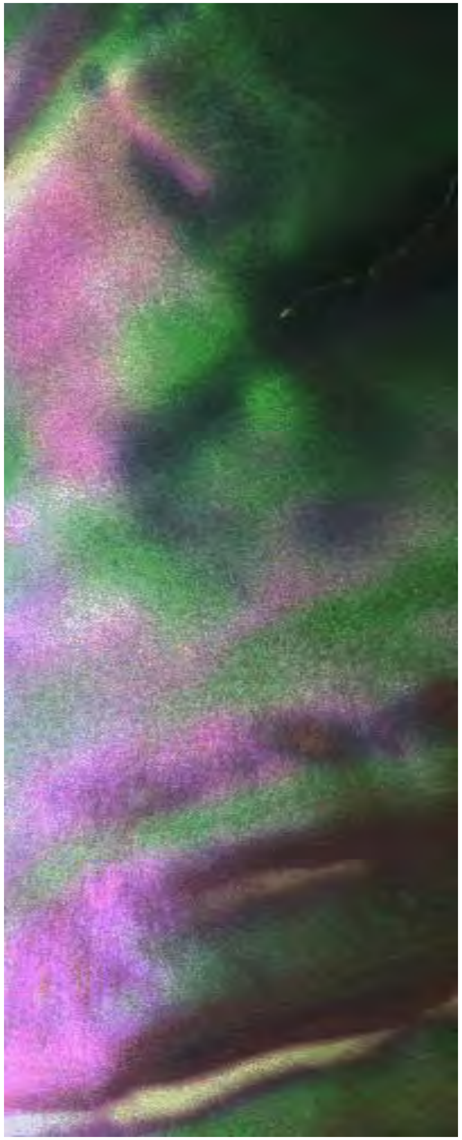

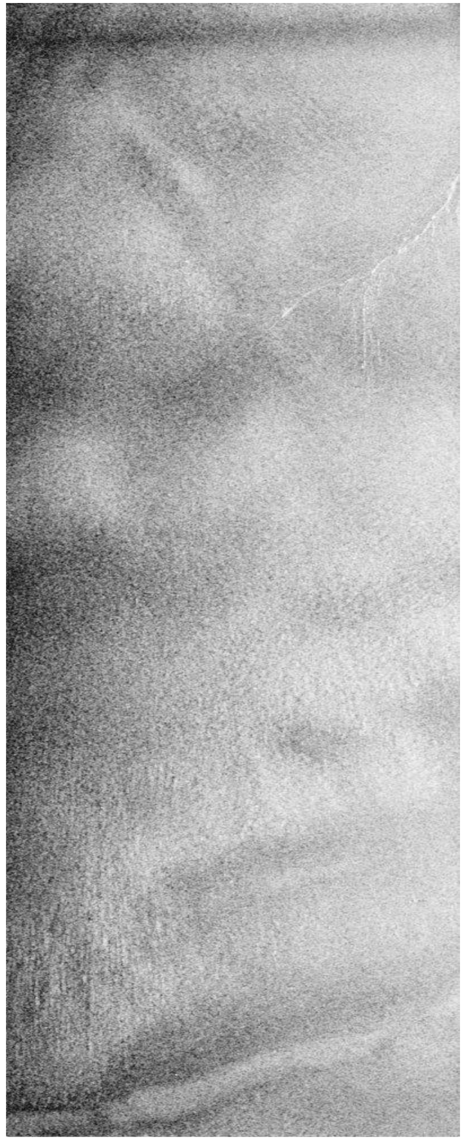

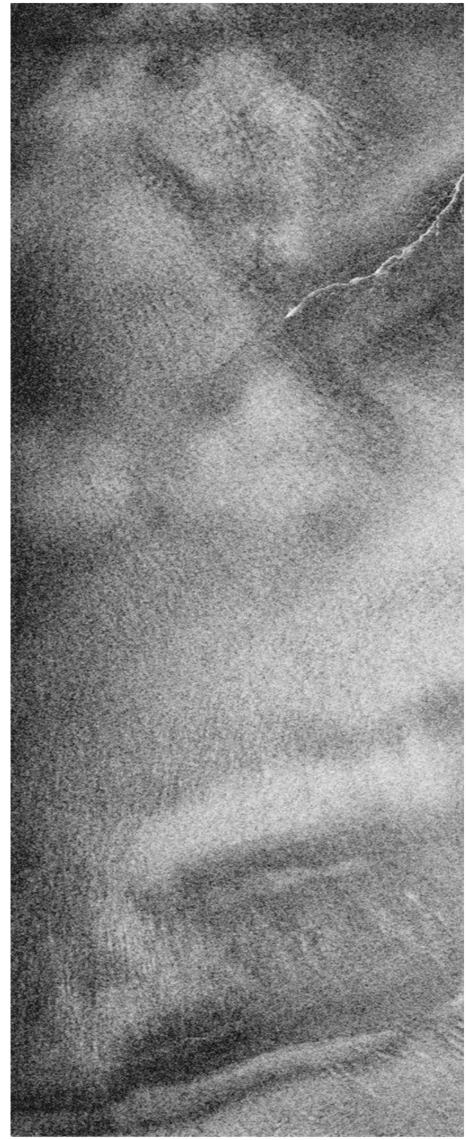

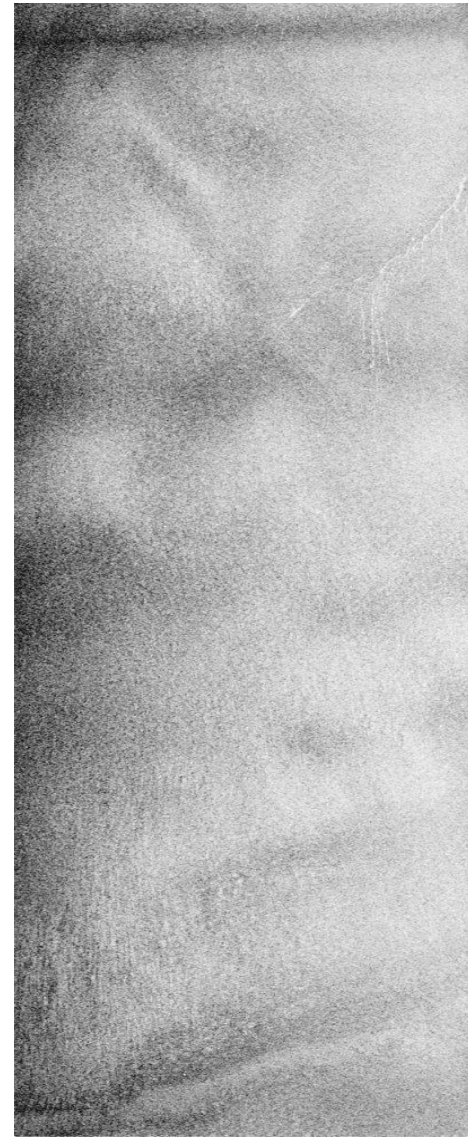

Two Layer Ice Model: Ground + Infinite Volume

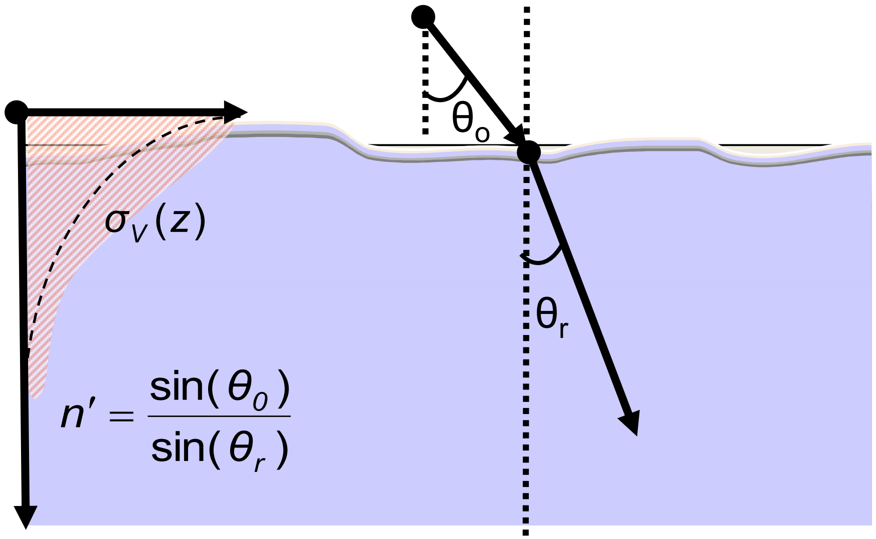

Interferometric (Volume) Coherence:

$$\tilde{\gamma}(\vec{w}) = \exp(i\varphi_0)\frac{\tilde{\gamma}_V + m(\vec{w})}{1 + m(\vec{w})}$$

$$\tilde{\gamma}_V = \frac{I}{I_0} = \frac{2\sigma}{2\sigma - i\kappa_z\cos(\theta_r)} = \frac{1}{1 - i\kappa_z d_{2z}}$$

$$\left\{\begin{aligned} I &= \int_0^\infty \exp(i\kappa_z z')\exp\left(\frac{2\ \sigma\ z'}{\cos\theta_0}\right)dz' \\ I_0 &= \int_0^\infty \exp\left(\frac{2\ \sigma\ z'}{\cos\theta_0}\right)dz' \end{aligned}\right.$$

Penetration Depth: $$d_{2z} = \frac{1}{2\sigma}\cos(\theta_r)$$

G/V R: $$m(\vec{w}) = \frac{m_G(\vec{w})}{m_V(\vec{w})T_{a-v}(\vec{w})}$$

Vertical Wavenumber: $$\kappa_z = \frac{\kappa\Delta\theta_r}{\sin(\theta_r)}$$

Wavenumber: $$\kappa = \frac{4\pi n'}{\lambda}$$

4 Parameters:

Extinction	σ
Ref. Index	n'
Topography	φ_0
G/V Ratio	$m(\vec{w})$

Extinction Inversion Results

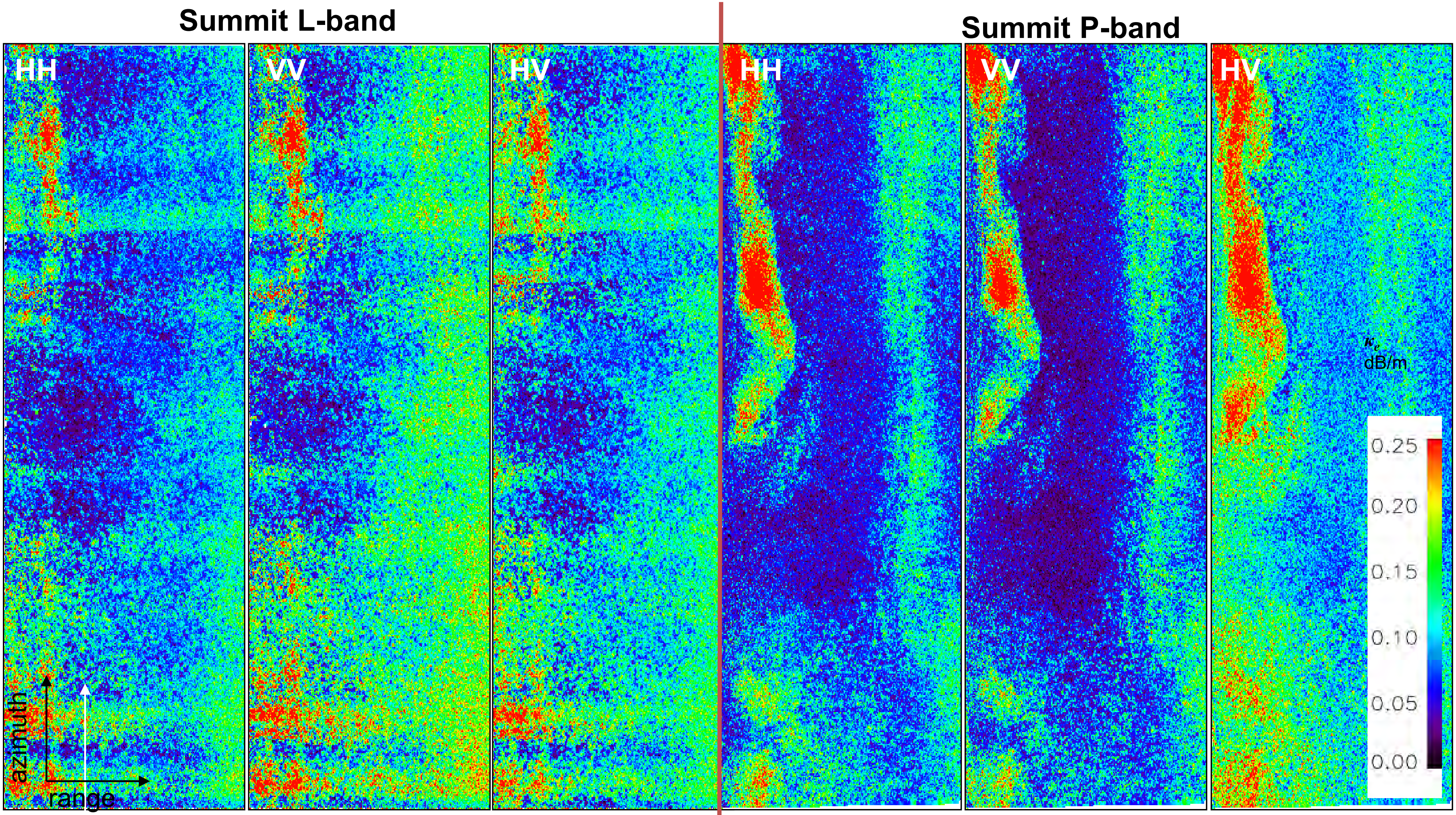

Extinction Inversion Stability

L-band $\sigma°$

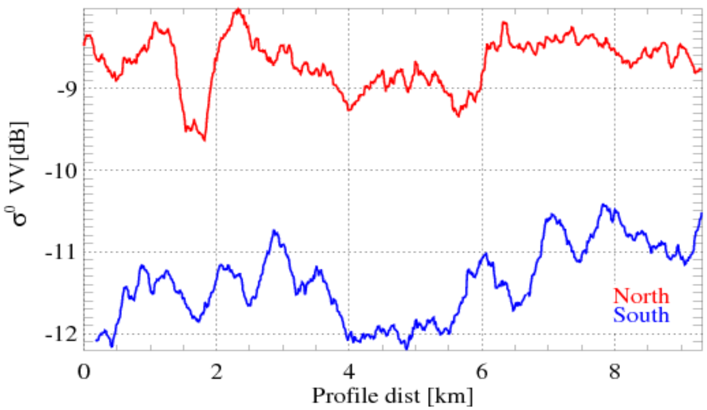

L-band κ_e

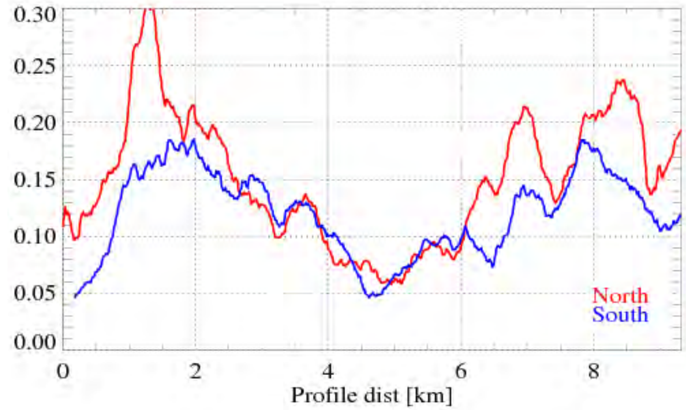

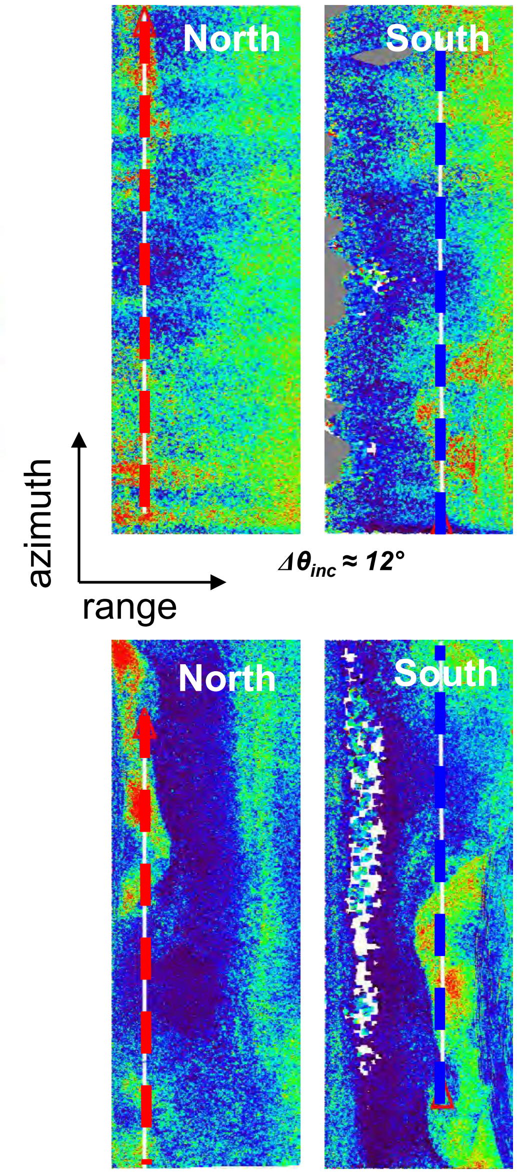

P-band $\sigma°$

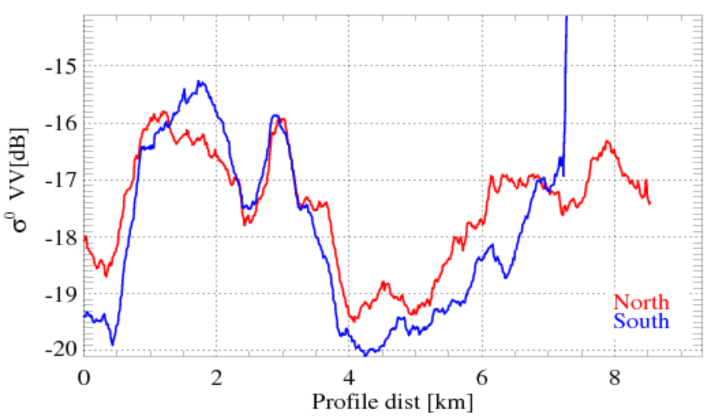

P-band κ_e

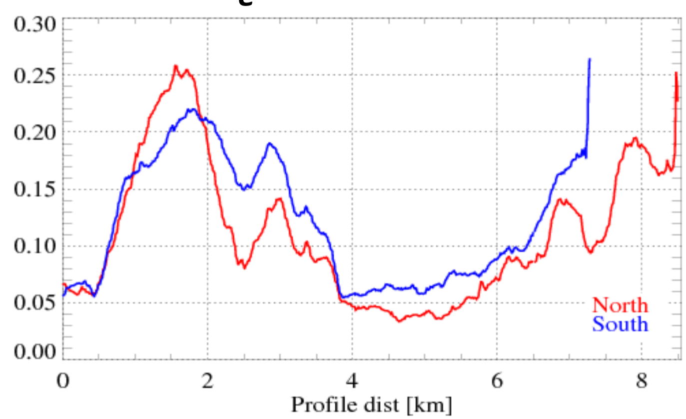

First Validations of the Estimated Extinction Parameter

P-band Sounder vs. P-band Pol-InSAR (Summit)

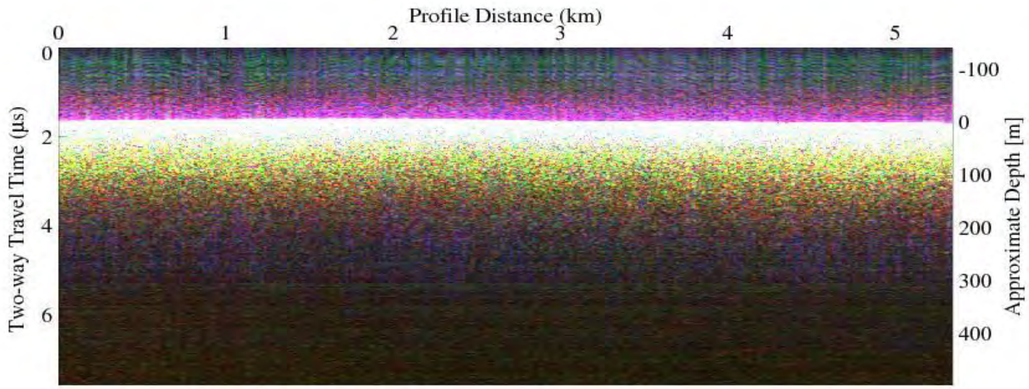

- σ^0_{SND} ***(sounder summed over depth)***
- κ_e ***(P-band Pol-InSAR extinctions)***

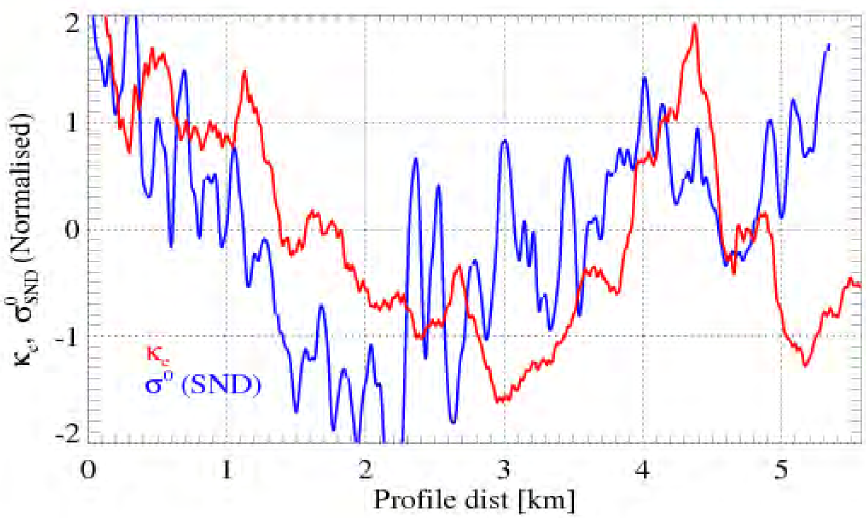

GPR (800 MHz) vs. L-band Pol-InSAR (Etonbreen)

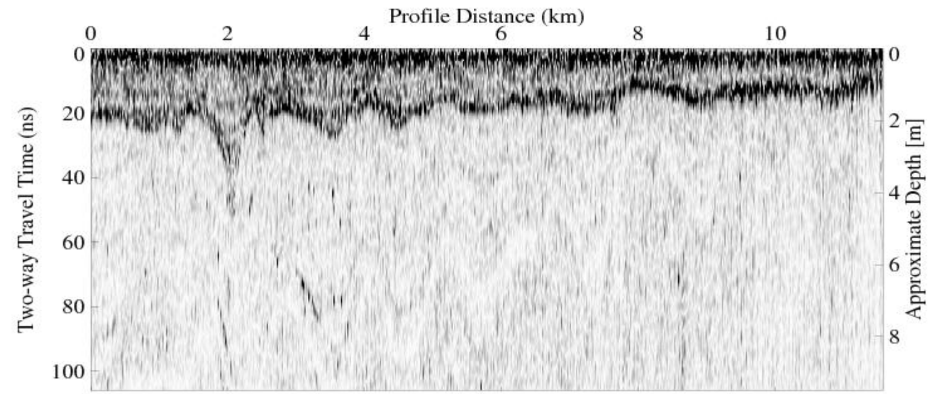

- σ^0_{GPR} ***(volume summed over depth)***
- κ_e ***(L-band Pol-InSAR extinctions)***

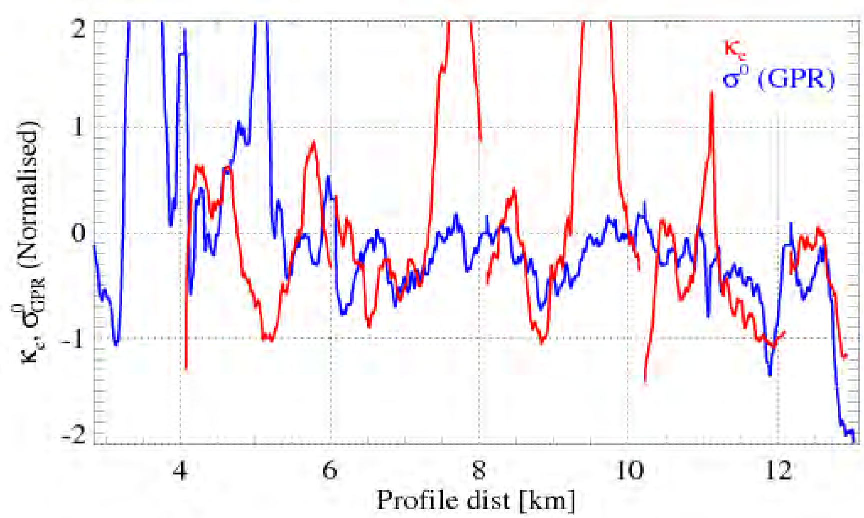

Books: Suggested Further Readings

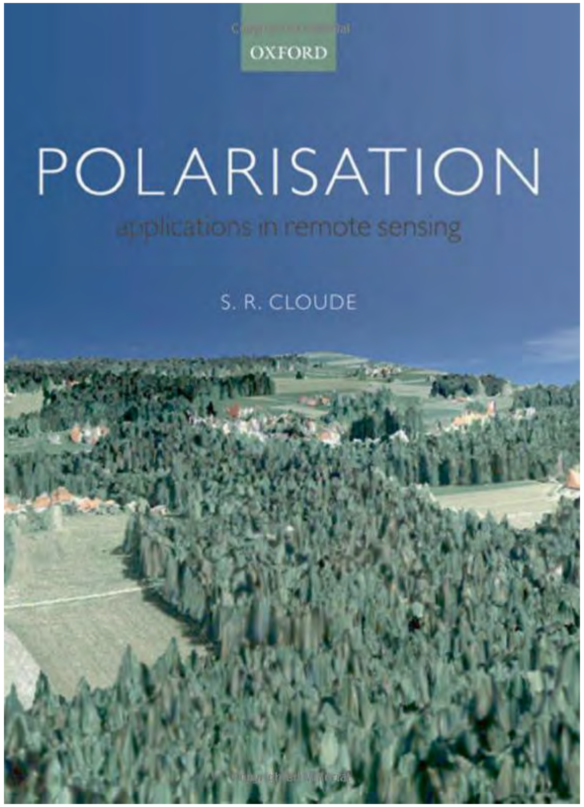

Polarisation: Applications in Remote Sensing

Shane R. Cloude
Oxford University Press
October 2009

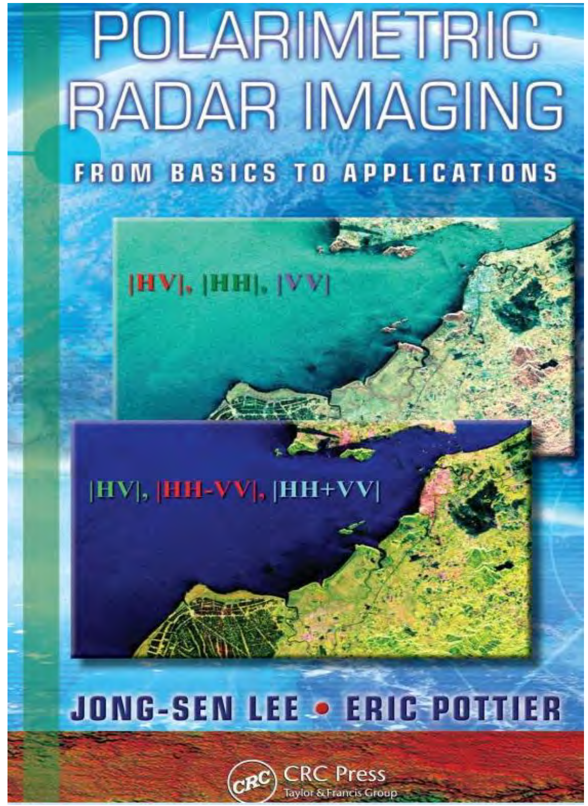

Polarimetric Radar Imaging: From basics to applications

J.-S. Lee & E. Pottier
CRC Press
February 2009

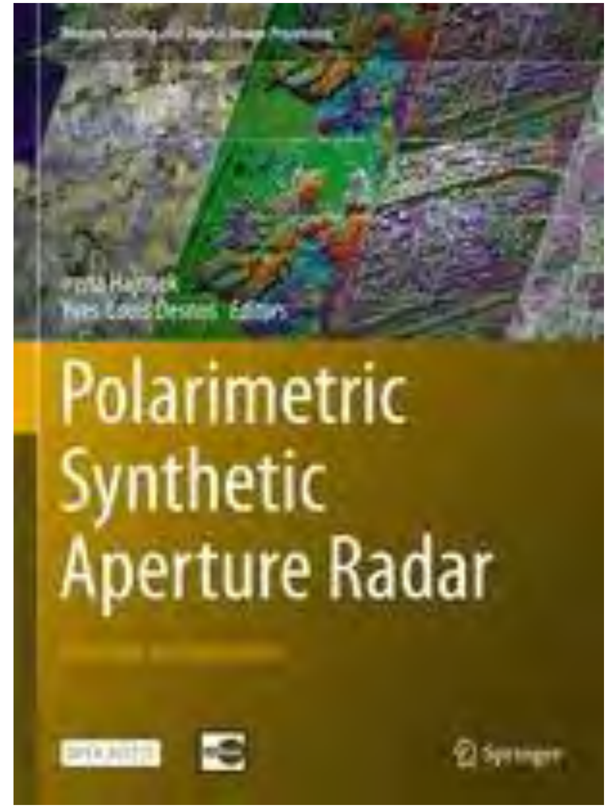

Polarimetric Synthetic Aperture Radar

Irena Hajnsek &
Yves-Louis Desnos
Springer
March 2021